College of Aeronautics
Cranfield University

S. C. Blank

Passive Techniques for Controlling the Flow in Supersonic Wing - Body Junctions

Ph.D. Thesis

ProQuest Number: 10832253

All rights reserved

INFORMATION TO ALL USERS
The quality of this reproduction is dependent upon the quality of the copy submitted.

In the unlikely event that the author did not send a complete manuscript
and there are missing pages, these will be noted. Also, if material had to be removed,
a note will indicate the deletion.



ProQuest 10832253

Published by ProQuest LLC (2019). Copyright of the Dissertation is held by Cranfield University.

All rights reserved.
This work is protected against unauthorized copying under Title 17, United States Code
Microform Edition © ProQuest LLC.

ProQuest LLC.
789 East Eisenhower Parkway
P.O. Box 1346
Ann Arbor, MI 48106 – 1346

Cranfield University
College of Aeronautics

Ph. D. Thesis

S. C. Blank

Passive Techniques for Controlling the Flow in Supersonic Wing - Body Junctions

Supervisor : Prof. J. L. Stollery

March 1994

Executive Summary

Junction flows are common to all flight speeds and they are associated with undesirable features such as increases in drag, limitations on performance and at supersonic speeds high heat transfer rates. Junction flows are associated with performance losses in turbomachinery (around 30% of the total pressure losses in an axial turbine) and they can lead to premature detection of military underwater vessels. Junction fairings are widely used at subsonic speeds and correct fairing of the C-141 wing alone, could have resulted in potential fuel savings of approximately US $ 40,000 per year per aircraft which can be roughly translated into a $ 600,000 saving during the lifetime of each airframe. Typically, for a modern transport type of aircraft the wing juncture accounts for between 1 and 2 % of cruise drag and therefore, careful design of the wing junction is necessary.

At supersonic speeds, by far the most disadvantageous feature associated with juncture design is high heat transfer rates due to shock / shock interaction. These heat transfer rates are sufficient to cause severe structural damage leading to component burn-off. Typical leading edge temperatures during re-entry for an aerospaceplane, like HOTOL, are around 2000 K, exclusive of increases in temperature caused by the interaction. Although drag reduction may not be so relatively critical at these flight speeds, the potential loss of control components, like stabilising fins, needs to be carefully examined and some configuration re-design may be necessary as a consequence.

This research project is aimed at developing a technique through which the disadvantageous features associated with supersonic junction designs can be alleviated. It was found that through re-design of the wing / body junction the maximum mean static pressure local to the fin leading edge could be halved, the strength of the junction vortices could be lowered and the amount of separated flow reduced. The applications of the technology span all vehicles operating within the supersonic flight regime and therefore, the markets to which the technology is applicable are military aircraft, defence systems, aerospaceplanes and commercial supersonic transports. As the technology is, in principle, applicable to the design of commercial supersonic transport aircraft (HSCT) and the market for these vehicles is forecast to be worth up to $ 200 billion (FY 1987) an examination of the issues behind marketing this type of vehicle is presented in the non-technical section. The presently available data produced by the major manufacturers were found to be lacking in the following areas (a) evaluations of market elasticity, (b) distribution techniques, (c) the availability of acquisition finance and financing techniques, (d) political sensitivity analysis (d) product life cycle analysis and (f) the relationship marketing of the venture.

Technical Summary

An experimental investigation of glancing shock wave / turbulent boundary layer interaction produced by hemi-cylindrically blunted fins was conducted in two test facilities. The majority of the tests were made in the large 9" x 9" continuous supersonic wind tunnel at a Mach number of 2.45 and at a Reynolds number ($R_{e\delta}$) of 4.1 x 10^4. Additionally some flow visualisation tests, in which blunt leading edge strake design parameters were investigated, were conducted at a Mach number of 2.43 and $R_{e\delta}$ of 5.8 x 10^4 in the smaller 2.5" x 2.5" short duration facility. The investigation's primary aim was to assess the potential of using passive techniques, namely fillets and strakes, to eliminate or alleviate the amount of separated flow and the flow field's unsteadiness, and to reduce the pressure levels experienced around the fin.

Swept (45°) and unswept fins of $D/\delta = 1.6$ and unswept fins of $D/\delta = 0.6$ were tested in the larger wind tunnel, and straight models of $D/\delta = 0.682$ were used in the smaller facility. A number of different types of modification were investigated including ramp-type fillets, sharp leading edge strakes and blunt leading edge strakes.

The study involved mean static pressures measured on the side wall, surface oil flow pictures taken over the side wall and the fin, and schlieren pictures taken in two planes normal to each other. In addition, laser light sheet flow visualisation and high speed ciné films were taken of the shock systems produced by some of the models.

It was found that filleting the junction did not improve the flow field characteristics whilst the addition of a sharp leading edge strake to the junction showed some beneficial effects on the mean surface static pressure distributions. The blunt leading edge strakes were found to possess the greatest potential for minimising the interaction. The incorporation of either blunt or sharp strakes into the junction helped to minimise the unsteadiness of the interaction.

Acknowledgements

This thesis is dedicated to my family.

The author owes a debt of gratitude to his supervisor, Professor John L. Stollery and Dr. Kevin Garry of the College of Aeronautics for all of their help over the past few years.

During the 18th Congress of the International Council of the Aeronautical Sciences (ICAS) the author presented a paper based upon some of the material contained within this doctoral thesis. The author's paper won the ICAS-McCarthy first prize and the author would like to thank Mrs. Camille D. McCarthy and Professor Paolo Santini for instigating the award. The generosity of Captain "Jock" Lowe of British Airways, the Royal Aeronautical Society, the Fellowship of Engineering (now the Royal Academy of Engineering) and the Science and Engineering Research Council enabled the author to have the opportunity to travel to Beijing, P. R. of China, to present his paper. I would like to thank them for their support.

Contents

Page No.

Executive Summary i
Technical Summary ii
Acknowledgements iii
Contents iv
Notation vi
List of Tables and Figures vii

1. Introduction 1
1.1 Junction Flows - Reasons for Their Control 1
1.2 Review of Previous Research 3
1.2.1 Overview 3
1.2.2 Flow Field Models for Blunt Fins in Supersonic Flows 4
1.2.2.1 The Unsteady Aspects of the Flow Field 6
1.2.3 Practical Junction Vortex Control Methods 8
1.2.3.1 The Effects of Changes in the Leading Edge Shape and Sweep Angle 8
1.2.3.2 The Effects of Filleting the Junction 10
1.2.3.3 The Effects of Adding Strakes to the Junction 13
1.3 The Scope of the Present Research 16
1.4 The Economic Justification for the Research 16

2. The Experimental Programme 19
2.1 The 9" x 9" Continuous Supersonic Wind Tunnel 19
2.1.1 The Flow in the Working Section 19
2.1.2 The Shock Generators 20
2.1.3 The Test Techniques Employed 20
2.1.3.1 Surface Oil Flow Visualisation 20
2.1.3.2 Schlieren Photography 21
2.1.3.3 Mean Static Pressure Surveys 21
2.1.3.4 High Speed Ciné Photography 21
2.1.3.5 Laser Light Sheet Flow Visualisation 22
2.1.3.5.1 The Optical System 22
2.1.3.5.2 The Seeding Mechanism 22
2.2 The 2.5" x 2.5" Intermittent Supersonic Tunnel. 23
2.2.1 The Flow in the Working Section 23
2.2.2 The Shock Generators 24
2.2.3 The Testing Techniques Employed 24
2.2.3.1 Surface Oil Flow Visualisation 24
2.2.3.2 Schlieren Photography 24
2.3 Errors 24

3. Results and Discussion *26*
3.1 The Effects of Filleting the Junction 26
3.1.1 The Unswept Shock Generators 26
Case 1 : The Blunt Unswept Fin of D/δ = 1.6 26
Case 2 : The Blunt Filleted Unswept Fin of D/δ = 1.6 30
3.1.2 The Swept Shock Generators 35
Case 3 : The Blunt Swept Fin of D/δ=1.6 35
Case 4 : The Blunt Filleted Swept Fin of D/δ=1.6 36
3.2 The Effects of Incorporating Strakes 39
3.2.1 The Incorporation of Sharp Leading Edge Strakes 39
Case 5 : The Blunt Unswept Fin of D/δ = 1.6 with a Sharp 70° Swept Strake of h/δ=1.6. 39
3.2.2 The Incorporation of Blunt Leading Edge Strakes 42
Case 6 : The Blunt Unswept Fin of D/δ = 0.6 42
Case 7 : The Blunt Unswept Fin of D/δ = 0.6 with a Blunt 45° Swept Strake of h/δ=1.6. 43
3.3 Investigations into the Importance of the Height of a Blunt Strake 47
Case 8 : The Independent Blunt 45° Swept Strake of h/δ=1.6. 47
Case 9 : The Blunt Unswept Fin of D/δ = 0.682 with a Blunt 45° Swept Strake of h/δ =1.6. 48
Case 10 : The Independent Blunt 45° Swept Strake of h/δ=3.2. 50
Case 11: The Blunt Unswept Fin of D/δ=0.682 with a Blunt 45° Swept Strake of h/δ=3.2. 51

4. Conclusions *56*

Recommendations for Future Work *58*

References *59*

Appendix A : The YNU Ray Tracing Method *67*

Tables and Figures *71*

Notation

Symbol	Physical Significance	Unit
Roman		
A	Attachment line	
C_D	Coefficient of drag	
C_L	Coefficient of lift	
C_P	Coefficient of pressure	
D	Fin leading edge diameter measured normal to the leading edge	m
H	Boundary layer shape parameter	
I.R.	Infra-red	
L	Length from the fin leading edge to the first point of fin influence on the flow field (for strake models - see fig. 44)	m
LEX	Leading edge extension	
M	Mach number	
Re	Reynolds number	
S	Separation line	
U	Upstream influence line	
USAF	United States Air Force	
V	Vortex	
Y	Lateral length	m
c	Model chord	m
h	Strake height	m
t	Thickness (of a wing etc.)	m
x	Longitudinal length	m
Greek		
Δ	Change in	
α	Angle of incidence	°
δ	Boundary layer thickness (99.5%)	m
δ^*	Boundary layer displacement thickness	m
ε	Propagation angle of the fin's influence on the flow field (see Section 3.3)	°
μ	Mach angle	°
θ	Boundary layer displacement thickness	m
λ	Sweep back angle	°
Subscripts		
MAX	Maximum	
∞	Freestream conditions	
s	Strake	

List of Tables and Figures

Tables

1. Applications of longitudinal vortex control.
2. Wind tunnel tests.
3. YNU Ray Tracing method results for the LFV system used in the 9"x9" wind tunnel.
4. The Interactions' length scales.
5. Data table for the strake / fin combinations.
6. Disturbance propagation angles for the strake / fin combinations.

Figures

1. Flight corridors for typical high speed vehicles with indications of the equilibrium stagnation temperature and the onset of air dissociation encountered at high speed (Poisson-Quinton (1978)).
2. Practical examples of shock-impingement heating (Edney (1968) and Kaufman et al (1974)).
3. Combined schlieren and phase-change coating techniques revealing shock-on-shock interactions and aerodynamic interference heating (Peake and Tobak (1980)).
4. Damage to ventral fin on NASA X-15A-2 aircraft from shock impingement (Peake and Tobak (1980)).
5. Effect of shock impingement on fin leading edge heat transfer at M_{∞}= 14 (Hiers and Loubsky (1967)).
6. General characteristics of blunt fin induced shock wave turbulent boundary layer interaction.
7. Flow field models for straight blunt fins.
8. Sharp generator flow field models (Kubota (1980)).
9. Effect of leading edge sweep (Stollery et al (1986) and Price and Stallings (1967)).
10. Side view oil flow pattern for a swept fin of D/δ=1.6 (Hussain (1985)).
11. The effects of circular cross sectional fillets around blunt fins (Lakshmanan et al (1986) and Haq (1993)).
12. Contours of mean surface pressure coefficient C_P on the test wall with the thin approach boundary layer (Devenport et al (1991)).
13. Wall pressure distributions for a modified sharp leading edge fin (Koide and Stollery (1993)).
14. The effects of including a cone like extension at the wing leading edge root (Fulker et al (1993)).
15. Reduction of parasitic drag (Poisson-Quinton (1980)).
16. Wing root fillets as used on the A 310 (Jupp (1980)).
17. Correlation of fillet size and pressure distribution (Krenz (1983)).
18. Effect of wing fuselage fillet on drag for a research wing of Airbus-type (Krenz (1983)).
19. Wing-body fairing research : High wing subsonic transport (Haines (1983)).
20. Experimental arrangement in the 9" x 9" (23 cm x 23 cm) wind tunnel.

21. Models used in the 9" x 9" wind tunnel.
22. The mounting methods used in the 9" x 9" wind tunnel for the schlieren tests.
23. The pressure tapped disc used to gather the pressure measurements.
24. The arrangement of the LFV system.
25. The models used in the 2.5" x 2.5" wind tunnel (D/δ=0.682).
26. Oil flow photographs for the straight model of D/δ=1.6 and its derivatives.
27. The location of the shock waves for the straight fin of D/δ = 1.6 and its derivatives.
28. Individually exposed side view schlieren photographs for the straight fin of D/δ=1.6 and its derivatives.
29. Selected frames from a high speed cine film taken at 4 kHz of a straight blunt fin, leading edge diameter = 1".
30. Flow field model for the straight fin of D/δ=1.6 with a fillet.
31. Pressure plots for the straight fin of D/δ=1.6 with and without a fillet.
32. The effects of filleting at subsonic speeds (Devenport et al (1989)).
33. The effects of sweep on the wall pressure distributions generated by a blunt fin (Hussain (1985)).
34. Oil flow photographs for the swept model of D/δ=1.6 and its derivative.
35. Flow field models for a blunt swept fin of 45° sweep and D/δ=1.6.
36. Flow field model for the swept fin of D/δ = 1.6 with a fillet.
37. Side view schlieren images for the swept fin of D/δ=1.6 and its derivative.
38. The plan view schlieren images of the unmodified swept fin, the filleted fin and a 45° delta wing.
39. Pressure plots for the 45° swept fin of D/δ=1.6 with and without a fillet.
40. Laser Flow Visualisation images of the flow fields for the unswept fin of D/δ=1.6 with and without a sharp leading edge strake.
41. Pressure plots for the fin of D/δ=1.6 with and without a sharp leading edge strake.
42. Pressure contour plot with the separation lines for the D/δ=1.6 fin with a sharp leading edge strake.
43. Flow field model for the unswept fin of D/δ=1.6 with a sharp leading edge strake.
44. Plan view oil flow photographs for the D/δ=0.6 fin with and without a blunt leading edge strake.
45. Side view oil flow photographs for the D/δ=0.6 fin with and without a blunt strake.
46. Flow field model for the D/δ=0.6 fin.
47. Plan view schlieren images for the D/δ=0.6 fin with and without a blunt strake.
48. Side view schlieren photographs for the straight fin of D/δ=0.6 with and without a blunt strake.
49. Flow field model for the D/δ=0.6 fin with a blunt 45° swept strake.
50. Pressure plots for the fin of D/δ=0.6 with and without a blunt leading edge strake.
51. Flow visualisation results for straight hemi-cylindrically blunted fin and straight fin with a blunt strake (Kleifges (1993)).
52. Mean and RMS pressure distribution for a plain fin with and without a blunt leading edge strake (Kleifges (1993)).
53. Plan view oil flow photographs for the blunt 45° swept strakes of h/δ=1.6.
54. Side view oil flow photographs for the blunt 45° swept strakes of h/δ=1.6.
55. Schlieren pictures for the blunt 45° swept strakes of h/δ=1.6.

56. Flow field model for the blunt unswept fin of $D/\delta=0.682$ with a blunt 45° swept strake of $h/\delta=1.6$.
57. The variation in "jet" path with increasing h/δ.
58. A comparison of the location of the "jet" paths.
59. Oil flow photographs for the blunt 45° swept strakes of $h/\delta=3.2$.
60. Schlieren pictures for the blunt 45° swept strakes of $h/\delta=3.2$.
61. Primary separation line location of straight blunt fins at zero incidence (Fomison (1986) and Saida and Hattori (1984)).
62. Flow field model for the blunt unswept fin of $D/\delta=0.682$ with a blunt 45° swept strake of $h/\delta=3.2$.
63. A comparison of the oil flow patterns produced by selected strake modifications.

1. Introduction

1.1 Junction Flows - Reasons for Their Control

Across each of the three flight regimes (sub-, super- and hypersonic) blunt leading edge / body junction flows are associated with undesirable flow features such as increases in drag, unsteady flow, and at super- and hypersonic speeds inviscid-viscous interactions occur. The range of applications is immense (see Table 1) and most of them constitute an overwhelming rationale for the study of vortex physics and vortex control. Compressibility appears to alter the quantitative, but not the qualitative features of three-dimensionally separated flows occurring in blunt wing / body junctions (Peake and Tobak (1980)).

When an incoming boundary layer flow encounters the large pressure gradient in front of a bluff airfoil / flat plate junction, a horseshoe vortex or system of horseshoe vortices is generated (Sung and Lin (1989)). Subsonic blunt fin intersection region vortex control has been the subject of relatively intense research during the last decade, prompted primarily by the many problems associated with the conning-tower / hull necklace vortices on submarines (Bushnell (1992)).

Submarine stealth has necessitated research into junction flows as the longitudinal vorticity produced by the submarines' conning tower / hull interface exacerbates various phenomena which can increase the chances of the submarine being detected (Wettern (1987), Partala (1985) & McConnell (1985)). Depending upon the submarine's depth, the strength and configuration of these vorticity fields, and the conditions in the ambient water column, the resulting disturbances can possibly be detected by, for example, infra-red, optical, radar, microwave, or laser sensors. In addition, to the non-acoustic detection issues, vorticity generated by the conning-tower / hull junction and other similar junctions, such as the stabiliser / hull junction, can also severely impact other important figures of merit such as controllability and manoeuvrability (Stone and Polhamus (1957)), passive acoustic signature, body drag, and propulsor efficiency and vibration.

Juncture flows are also very important in the design of turbomachinery in which the juncture flow occurring at the turbine / compressor blades' roots and tips are termed blade end-wall flows. An understanding of blade-end wall flows is particularly important

because the total pressure losses associated with the end-wall flows are much larger than the blade profile losses. The available literature (Bhargava and Rishi (1989)) shows that pressure losses due to the secondary flow caused by the juncture flow form approximately half the losses in axial turbines.

Kinetic heating which is a major problem of high-speed (super- and hypersonic) flight arises from two processes : compression through shock waves or compression fans, and shear in the boundary layer (Peake and Tobak (1980)). The first is predominant at stagnation points and leads to very high local surface temperatures. To demonstrate this, the equilibrium stagnation temperatures at the vehicle nose are plotted in fig. 1 as dashed lines over the flight domains. These temperatures reach about 150 °C for Concorde cruising at about Mach 2, and higher than 7,000 °C for the Apollo capsule during its re-entry phase (Poisson-Quinton (1978)). Temperatures less severe than these stagnation conditions are produced by viscous shear forces and they are usually experienced over the remainder of the airframe. Uncontrolled separations produced by shock boundary layer interactions may not always have significant effects on drag but, high local heat transfer rates in reattachment zones, the unsteadiness of the interaction and the potentially destabilizing effects of the vortex motions upon downstream control surfaces may be important (Korkegi (1971) & Nielson (1978)).

The most serious surface heating problems encountered in hypersonic vehicle design are the result of shock / shock interactions in proximity to the vehicle skin which are often produced by junction flows. Extremely high heat transfer rates, many times the ordinary stagnation point values, may occur in relatively small regions on the vehicle surface accompanied by high pressure peaks that complicate the design of the thermal protective skin (Keyes and Hains (1973), & Hains and Keyes (1972)). Unlike an ordinary stagnation point, the location of the region of peak heat transfer is not well defined and the interaction region will move about the body depending on Mach number, altitude and attitude. Figure 2 (a)-(c) shows some practical examples of shock-impingement heating (Edney (1968)). The interactions shown in figure 2 (a)-(c) are "inviscid". The inviscid interactions in fig. 2 (a)-(c) are examples of shock / shock interaction rather than shock wave / boundary layer interaction. However, both forms of interaction have much in common with one another. The major difference is that the impinging shock in an inviscid interaction is a bow shock wave (e.g. the fuselage bow shock in fig. 2 (b)) whilst in viscous interactions (fig. 2 (d)) the impinging shock is formed through boundary layer separation. In viscous interactions, the adverse pressure gradient across the bow shock wave causes the boundary layer to separate and the bow shock wave bifurcates (fig. 2

(d)). Within the separated region the flow recirculates and a number of horseshoe vortices can be formed.

Figure 3 reveals the shock wave shapes and aerodynamic interference heating about a model of the Space Shuttle matched to its external hydrogen-oxygen tank (Creel and Hunt (1972)). Probably, the first in-flight confirmation of the severity of shock impingement heating was the damage to the ventral fin of the NASA X-15A-2 rocket driven airplane during a high altitude flight at Mach 6.7. The unswept ventral fin supported a ramjet test model (fig. 4 (a)) that came adrift from the airplane during flight as a result of the catastrophic shock-impingement heating damage (figs. 4 (b) & (c)).

Leading-edge sweep was found to have a marked influence on shock-impingement heating. For unswept or moderately swept cylinders (fig. 5), high local heating is noted at the leading edge in the vicinity of the intersection of the external shock with the cylinder bow wave (Newlander (1961), Bushnell (1968), Hiers and Loubsky (1967) & Gulbran et al (1967)). Heat peaks as high as 10 times stagnation values have been observed, as shown in fig. 5(b). The very localised nature of the heat peak due to shock impingement is illustrated by the relatively narrow "burn through" on the fin in fig. 4. For highly swept cylinders or fins, near 45° or more, no local increases in heating were observed (Hiers and Loubsky (1967), Gulbran et al (1967), Beckwith (1964) & Bushnell (1965)) and leading-edge heating rates are found to be reasonably well predicted by simple infinite swept cylinder theories using local flow conditions.

1.2 Review of Previous Research

1.2.1 Overview

Longitudinal vortex initiation is a part of the general subject of 3D flow separation and therefore, the control of vortex formation relates directly to flow separation control. Vortex control has been, and still is, ad-hoc/empirical and an inventor's "playing field". Contemporary CFD is able to solve the juncture problem numerically and provide estimates of the general flow phenomena (Chen and Hung (1991), Visbal (1989), Sung et al (1991), Burke (1987), Baker (1982), Lakshmanan et al (1988), McMaster and Shang (1988), Ohring (1989) & Levy (1988)). However, the detailed transition and turbulence physics required for accurate predictions are not yet in hand, but the codes have been

used (Sung and Lin (1989), Sung et al (1991)) to investigate vortex control approaches for juncture regions and to investigate parametric effects.

Rao and Campbell (1987) and Skow and Erickson (1982) have produced excellent review papers concerning the control of subsonic wing-body junction flows and the basic flow structure has been studied in considerable detail (Woo et al (1977), Niedoroda and Dalton (1992), Baker (1979) & Chen and Hung (1991)). At both subsonic and supersonic speeds the main feature of the flow field is a horseshoe vortex which normally forms around the nose of the protuberance and trails downstream. The main vortex usually engenders subsidiary vortex systems which can dynamically interact. The number and relative strengths of the vortices is a function of protuberance geometry, Mach number, Reynolds number etc.

1.2.2 Flow Field Models for Blunt Fins in Supersonic Flows

Attempts as early as 1960 were made into modelling the flow field around protuberances at supersonic speeds. Green's 1970 summary is a good description of the state of the research effort to that date and it presented numerous questions for further investigations. Surface flow visualisation techniques dominated these early attempts at modelling the flow field. Qualitatively, the subsonic fins of Sutton (1987), East and Hoxley (1968), and Mehta (1984) generated flow fields similar to those created at supersonic speeds but quantitatively the subsonic and supersonic flows varied. This ability to compare the two flows qualitatively is not surprising because behind the bow shock wave, in the locality of the generator's nose, a pocket of subsonic flow exists.

The late 1960's saw a major expansion of research into three dimensional separation and the practical need to predict surface pressures and heat transfer rates provided the stimulus. Price and Stallings (1967) and, Young et al (1968) undertook serious studies of the flow field with hemi-cylindrically blunted generators, in turbulent boundary layers, at zero degrees incidence. The former found that the pressure distribution along the centre-line bore a resemblance to that beneath a "two-dimensional" compression step and the differences were hypothesised to be due to lateral escape of fluid from the plane of symmetry. The pressure levels were found to increase with Mach number and insensitivity to Reynolds number was discovered. Young et al (1968) found that the surface pressure data varied with generator diameter and Mach number, whilst freestream Reynolds number and boundary layer thickness had little significance. In contrast to the work by Young et al (1968), 1977 saw Sedney and Kitchens (1977)

discovering that 2, 4 or 6 vortices could exist around the leading edge of a blunt generator depending upon the Reynolds number. As the Reynolds number was increased the number of vortices decreased. The position of the primary separation and attachment positions varied slightly but the structure between them was determined to be Reynolds number dependent.

Dolling and Bogdonoff, (1982) showed that the scaling length for the centreline pressure distribution over a wide range of D/δ and M was D provided that the incoming boundary layer was turbulent. Fomison (1986) later confirmed the influence of D/δ for Mach 2.45. Dolling and Rodi (1988) tried to correlate the length scales produced by fins with wedge-shaped, hemi-cylindrical and elliptic leading edges. They found that to a first approximation the normalised centreline length scales correlate with the leading edge drag coefficient. They also included data from previous studies at M = 1.98 & 2.48 and they obtained a reasonable correlation for the upstream influence line. However, the separation lines' length scales showed a clear Mach number influence when plotted against leading edge drag coefficient.

For a blunt fin the near-field or nose region is bluntness dominated whilst the downstream far-field is similar to that for a sharp fin (Stollery et al (1986)). Currently, two slightly different flow field models exist for blunt fins. Both of the models agree upon the general characteristics of the flow field, as shown in fig. 6, but they differ on particular details. Fomison (1986) investigated the effects of bluntness and sweep on glancing interaction and his flow field model (fig. 7 (b)) included a "jet" of high pressure air escaping up the side of the fin. Hussain (1985) who concentrated upon the effects of sweep disputed Fomsion's flow field model as he believed that a vortex was responsible for the "jet" like pattern on the side of Fomsion's and his own fins (fig. 7 (a)). Except for their varying interpretations of the flow along the side of the fin their flow field models were in excellent agreement. The data obtained in the present study supports Fomsion's interpretation of the streak line patterns, rather than Hussain's (1985), and further discussion upon this point is given later (see Section 3.1.1)

Since the mid-1980's a number of numerical studies have been undertaken. Their number is constrained due to the early stage of development of Navier-Stokes codes which is the type of code required to predict the flow field in its entirety. Hung and Buning (1984), using a Reynolds averaged Navier-Stokes code, achieved good agreement with the experimental data of Dolling and Bogdonoff (1982). Only one horseshoe vortex pair was found but the surface pressure distributions agreed well. Chen and Hung (1991)

investigated cylindrical protuberances in sub- and supersonic flows with laminar and turbulent boundary layers. However, for the supersonic flow they only examined the turbulent boundary layer case. They used the unsteady three-dimensional Reynolds averaged compressible Navier-Stokes equations with an algebraic turbulence model. For the supersonic turbulent boundary layer calculation the Baldwin-Lomax turbulence model was applied and the results were compared to earlier experiments (Sedney and Kitchens (1975)). The streamline paths when compared to experiment were very encouraging and the code predicted all of the major features of the flow field.

1.2.2.1 The Unsteady Aspects of the Flow Field.

High speed schlieren, shadow cinematography and series of individually exposed photographic frames taken at random time intervals, all show that the shock wave / boundary layer interaction occurring about a blunt wing / body junction is unsteady (Dolling (1989)). In practice, such photographs represent an integration of the light beam across the width of the tunnel, and as the bow shock wave exhibits rippling (in plan view), the data are usually only qualitative.

Most of the quantitative work on flow field unsteadiness (for "two-dimensional" flows, sharp or blunt fins and circular cylinders) comes from wall pressure fluctuation measurement and a small amount of additional data has been contributed through hot wire anemometry. In the majority of these studies the emphasis has been on the separation shock's dynamics whilst less stress has been placed on the reattachment process and the motion of the outgoing boundary layer. Investigations into the unsteadiness of shock wave / turbulent boundary layer interactions have been concentrated around the frequency of the motion and the length scales associated with it. Nominally two-dimensional step or ramp flow has formed the flow field for the majority of these studies but a small number have been made with three-dimensional flows. The data from three-dimensional flows are invariably much harder to interpret as the boundary layer can be highly skewed (Dolling (1989)). The bulk of the three-dimensional interaction studies have considered sharp fin flow and the supply of data for blunt fins / cylinders is somewhat limited.

The first paper of major importance concerning the unsteadiness of blunt fin induced interaction was by Dolling and Bogdonoff (1981). They tested a range of fins with different diameters in a number of boundary layers of varying thickness. Measurements were made along the centreline and up to four diameters outboard of it. Their findings

indicated that the RMS pressure levels were up to two orders of magnitude above that of the incoming boundary layer.

Gramann and Dolling (1986) investigated the relevance of surface tracer techniques (e.g. oil flow) which have zero frequency response to an unsteady flow field. They used a "semi-infinite" cylinder at Mach 5 and they concluded that the separation line indicated by the surface tracers was the downstream boundary of a region of intermittent separation.

Dolling and Narlo (1987) re-examined the earlier work in Dolling and Bogdonoff (1981) (Mach 2.95) and conducted further experiments with circular cylinders at Mach 5. Their results confirmed the findings of Dolling and Bogdonoff (1981) and they found that both blunt fins and circular cylinders exhibited the same general trends namely, the mean shock frequency is dependent upon the body's diameter and it decreases with increasing D. They only tested models of 0.5" and 0.75" diameter. Thus, the range of diameters under investigation was severely constrained and this must be noted when considering their statements about the effects of diameter. However, they did correlate their work to other authors in order to expand the range of diameters over which their statements are based. Additionally, they discovered that the results for both blunt fins and circular cylinders could be correlated using a Strouhal number (using D and the freestream velocity) for the limited database available.

Dolling (1993) states that between the upstream influence line, U, and the primary separation line, S_1, the wall pressure signal is intermittent and the RMS of the pressure fluctuations decreases rapidly, with the maximum just upstream of S_1. At a given Mach number, the magnitude of the maximum RMS of the wall pressure fluctuations *along the centreline* depends on the ratio D/δ. Thus, the centreline flow is unaffected by the cylinder wake (Dolling (1993)).

Gonsalez and Dolling (1993) examined the effects of the sweepback angle of the shock wave generated by a series of blunt fins. Their fins covered the range D/δ from 0.42 to 1.27 and the fins had 0 and 18 ° leading edge sweep. Their work was correlated to Erengil and Dolling's (1992) compression ramp data and Schmisseur and Dolling's (1992) sharp fin data (see below). All three sets of experiments were conducted at Mach 4.95. For blunt fins it was found that the maximum RMS of the pressure fluctuations near separation did not occur on the centreline but a small distance away from the centreline. For moderate interaction sweepback angles (<20-30°) the difference between the maximum RMS value and the centreline's RMS value was small. Gonsalez and

Dolling's (1993) work confirmed Dolling's (1993) statement (above) about the maximum RMS of the pressure fluctuations being dependent upon the fin's diameter but Gonsalez and Dolling (1993) found that for large D/δ an asymptotic value exists.

Schmisseur and Dolling (1992) investigated the wall pressure signal near separation for sharp fins over a range of interaction sweepback angles (25-55°). They found that the shock frequencies at high angles of incidence were about 5 kHz whilst those for zero incidence were in the range of 0.5-1 kHz. When the results were compared to Erengil and Dolling's (1992) swept compression ramp data. It was shown that the maximum RMS in the intermittent region correlates with the sweep of the interaction and *not* with the inviscid pressure rise as had previously been suggested.

Gonsalez and Dolling (1993) discovered that for all three model configurations (those of Schmisseur and Dolling (1992), Erengil and Dolling (1992) & Gonsalez and Dolling (1993)) the maximum of the RMS pressure fluctuations was equivalent to one half of the separation shock's strength and that the mean up- and downstream shock speeds were approximately constant at 3% of the freestream velocity. Furthermore, they were able to define a Strouhal number based upon the intermittent region length (the distance between the upstream influence line and the mean primary separation line as denoted by the oil flow method), the maximum zero crossing frequency (the zero crossing frequency is calculated through taking the mean value of the probability distribution of the time between consecutive passages of the shock over a transducer) and the freestream velocity. This Strouhal number was found to remain essentially constant, at 0.022, for all of the model geometries used by Schmisseur and Dolling (1992), Erengil and Dolling (1992) & Gonsalez and Dolling (1993) regardless of the local interaction sweepback angle.

1.2.3 Practical Junction Vortex Control Methods

1.2.3.1 The Effects of Changes in the Leading Edge Shape and Sweep Angle

Sharp Fins in Supersonic Flows

Near the root of the fin, the fin penetrates the boundary layer whose local Mach number decreases as the wall is approached. At some point the wedge angle, of the sharp fin, will reach the shock detachment angle. Between this point and the sonic line within the boundary layer the shock will be detached. At low wedge angles the "surface flow" turns towards the plane of the shock wave, the angle turned through can equal or exceed the

wedge angle and the influence of the shock is felt well ahead of its "inviscid position". Even at low wedge angles there is evidence of a small corner vortex as the higher pressure on the wedge attempts to escape up the wall surface (Stollery (1989)). Kubota (1980) has produced a complete flow field model of the supersonic sharp fin case for various shock strengths (fig. 8). Fomison's (1986) blunt fin flow field model is similar to Kubota's (1980) sharp fin flow field model except in the vicinity of the leading edge where the effects of bluntness cause the bow shock wave to detach. The characteristics of the nose region flow depend upon the geometry of the body (blunt or sharp) whilst the far field is dependent upon the wedge angle.

Blunt Fins in Supersonic Flows

Blunting the leading edge changes the local pressure distribution dramatically. The bow shock bifurcates to create a lambda foot and separation on the side wall occurs (fig. 6). A characteristic double peak is formed in the pressure distribution on the side wall and in the vicinity of the nose. The nature of the horseshoe vortex in wing / body junction is strongly dependent upon the wing nose shape as the size and strength of the vortex increases with nose bluntness (Mehta (1984), Fomison (1986) & Stollery et al (1986)). Thus, the most effective appendage vortex control technique is to reduce the magnitude and extent of the perturbation by reducing the appendage leading edge diameter (Kubendran et al (1988 (a)) & Fomison (1986)) or by increasing the leading edge sweep angle (Lakshmanan et al (1988) & McMaster and Shang (1988)).

Hussain (1985) investigated the effects of sweep using a series of swept hemi-cylindrically blunted models. As the sweep angle of his fins was increased the shape of the leading edge in the freestream direction became a slender ellipse. This caused the stand-off distance of the bow shock and the distance between the fin's leading edge and the upstream influence line to decrease as the sweep angle was increased (fig. 9). Thus, the effects of bluntness were muted and compressed, into a smaller zone. Nevertheless, many of the features occurring for the unswept case are still visible even with 75 ° of sweep. Figure 10 shows Hussain's (1985) oil flow results for a series of swept fins. Note that the separated region of flow decreases as the leading edge sweep of the fin is increased.

Fulker et al (1993) used both experimental results and numerical calculations in an investigation centred around reducing the overall drag of a 45° swept wing / body configuration at M = 1.56. They tried to reduce the leading edge nose radius of their wing in the root region, such that the sweep of the inviscid shock would remain constant.

The reasoning behind this approach was that in inviscid flow, the bow shock wave must be normal to the body at the wing root and therefore, has zero sweep (fig. 14 (a)). Hence, in the root region the shock strength is significantly higher than further outboard, giving rise to a large increase in local wave drag and, in a real viscous flow, leading to a local separation of the fuselage's boundary layer. No results are illustrated for this method in Fulker et al (1993) but the paper does report that the authors' attempts to reduce the configuration's drag using this method were unsuccessful.

1.2.3.2 The Effects of Filleting the Junction

Blunt Fins in Subsonic Flows

Fillets have long been used on an empirical basis and much of the early work is described in Hoerner's (1965) book. Hoerner indicates that increasing the fillet radius is favourable (for drag reduction) as is extending the fillet beyond the trailing edge of the appendage (Boatwright (1960) & Sung et al (1988)). Recent work (Sung and Lin (1989), Sung et al (1991), Ohring (1989), Kubendran (1983), Sung et al (1988), Kubendran and Harvey (1985), Hubbart et al (1976) & Guta (1987)) has included detailed flow field studies aimed at determining the influence of such junction modifications upon vortex generation and behaviour. However the work reported here for *supersonic flows* indicates that *simple leading edge extensions* (the term "strake" is used to denote this type of fairing in this thesis) can have significant mitigation effects upon the vortex strength and size and that they may yield better results than fillets.

Devenport et al (1989) discovered adverse effects when they introduced a circular cross section fillet with a radius equivalent to 0.53 times the maximum thickness of the wing. They found that the fillet :

- displaced the separated flow structure away from the wing surface,
- expanded the spectral level of the surface pressure fluctuations under the horseshoe vortices,
- increased the distortion of the time-averaged boundary layer structure produced by the horseshoe vortex and,
- increased the area over which the vortex occurred.

Devenport et al (1989) suggest that the fillet could increase the size and the strength of the horseshoe vortex and they conclude by stating "in applications where elimination or attenuation of the horseshoe vortex or its unsteady motions are required, this type of

device clearly should not be used". However, they acknowledge that the effects of the fillet on interference drag were outside of the scope of their investigation. They conclude that apart from any possible beneficial effects on the interference drag of the junction, the fillet did not modify the flow field in any desirable way. Furthermore, Sung et al's (1991) subsonic computations indicated that the small fillets of 0.13c did not reduce the pressure build-up close to the wing's leading edge and that his fillet did not affect the flow field in a positive manner.

Jacobs and Ward (1935) investigated 209 subsonic wing-fuselage combinations and concluded that fillets slightly reduced the maximum lift coefficient of a wing / fuselage combination except, for certain well-shaped fillets that increased the maximum lift coefficient with increasing fillet size. The differences between the maximum lift coefficients for filleted and unmodified combinations were found to be very small if the wing junction itself produced large amounts of drag (Jacobs and Ward (1935)). Straight plan-form fillets improved the maximum lift coefficients relative to the unmodified mid-wing combination, owing to the increase in area due to the fillets. Washed-in and washed-out fillets affected maximum lift coefficients in a manner similar to that to be expected with corresponding changes in the camber of the section (Jacobs and Ward (1935)).

The majority of the available data indicates that fillets do not have any significant mitigation effects on horseshoe vortex strength but Jacobs and Wards' (1935) $C_{L_{MAX}}$ data for filleted wing body junctions indicate that higher lift coefficients can be obtained relative to the unmodified wing-body combinations for certain well shaped fillets.

Blunt Fins in Supersonic Flows

Lakshmanan et al (1988) suggest that very large circular fillets of three and one-half body diameters would be required to achieve any worthwhile mitigation effects on the horseshoe vortices residing around the base of the fin. The 3-D Navier Stokes equations with the Baldwin - Loxmax turbulence model were used to compute the pressure profile in the interaction region, the particle paths and the limiting streamlines. Computed results for an unswept blunt fin at M=2.96 with a laminar boundary layer were compared to experimental data from Young et al (1968). The code was also validated against the turbulent interactions of Stollery et al (1986) for low Reynolds number interactions and against Price and Stallings (1967) for higher Reynolds number flows around swept fins. For all of the validation computations the code agreed with the available experimental data.

The authors then examined the effects of filleting the fin. The Mach number considered was 2.4 and Re_δ was 1.3×10^5. Filleting the fin resulted in :

- a reduction in the pressure trough between the two peaks (fig. 11 (a)), indicating a reduction in the velocity of the reversed flow. Note that for a fillet of radius 3.5D only a small pressure drop was calculated,

- the initial pressure rise generated by the model moves upstream as the size of the fillet is increased,

- the computed particle paths indicated the presence of a single vortex residing on the filleted portion of the fin. The streamlines downstream of the leading edge lost most of their vortical character and the computed surface limiting streamline indicated that no separation occurred on the surface of the fin.

Haq (1993) investigated experimentally the effects of incorporating a fillet of circular cross-section (R = 3.5D) around a fin of $D/\delta = 1.11$ at $M_\infty = 6.2$ and $Re = 4 \times 10^7$. His model was similar to Lakshmanan et al's (1988) and his investigation centred around heat transfer measurements and schlieren photography of the interaction. The schlieren images indicated that a separation shock was formed ahead of the fillet such that it followed the contours of the fillet. This separation shock wave merged with the fin's bow shock wave, about half way up the fillet, to form an Edney type IV interaction.
Haq (1993) discovered that the effects of filleting the junction were that :

- the fillet pushed the primary separation line upstream by 0.8D,

- a shock / shock interaction is "thought to take place" between the bow shock wave and the separation shock and a supersonic jet is generated, similar to the unmodified fin. However, this jet does not impinge directly onto the fin leading edge, as for the unmodified case, but is deflected upwards and grazes the leading edge. Thus, the localised heat transfer rates are reduced (compare fig. 11 (b) to (c)).

- the flow formed a small separation bubble on the fillet and a high heat transfer rate occurred at the attachment point. The flow in the separation bubble escaped laterally and downstream forming a thin horseshoe vortex which approximately followed the contours of the fillet (fig. 11 (d)).

- the majority of the flow passing onto the fillet remained attached and high pressures in the vicinity of the leading edge and the side of the fin merely caused the flow to pass to lower pressure regions on the plate.

Haq (1993) concluded that filleting the fin reduced the overall severity of the interaction, decreased the size of the interaction region (the lateral extent of the disturbed flow was reduced by 20% at the trailing edge), lowered the heating rates within the interaction region and that the vast majority of the flow remained attached. Hence, Haq's (1993) results and conclusions support those of Lakshmanan et al's (1988) computational study.

The available subsonic data indicates that small fillets ($R < 2D$) do not have any significant weakening effects upon the horseshoe vortices. Lakshmanan et al's (1988) and Haq's (1993) supersonic data suggests that large fillets ($R > 2$) are required in order to weaken the vortex. Blunt fins in supersonic flow have a small pocket of subsonic flow ahead of the leading edge and this enables a qualitative comparison of the flow fields generated by blunt fins in sub- and supersonic flows. One could therefore, expect to be able to draw qualitative comparisons between the effects of fillets at sub- and supersonic speeds in a similar manner to a qualitative comparison of unmodified fin's in sub- and supersonic flows. The subsonic investigations, to date, have concentrated on small fillets and this may explain why no beneficial effects have been discovered at subsonic speeds.

Sharp Fins in Supersonic Flows

The only known paper concerning the use of fillets around sharp fins is Koide and Stollery (1993). They investigated the effects of placing a fillet of circular cross section such that the radius of the fillet increased in proportion to the distance from the leading edge. Their fillet was a minor alteration relative to the unmodified condition and it was not in a similar category to the large scale junction modifications suggested by Lakshmanan et al (1988) for blunt fins. The experiments were conducted at M=2.45 and they concluded that the presence of that type of fillet worsened the juncture flow.

1.2.3.3 The Effects of Adding Strakes to the Junction

The addition of a strake (herein defined as a fairing which starts ahead of the unmodified fin's leading edge and whose thickness does not exceed the maximum thickness of the wing) to the wing planform is similar to the incorporation of leading edge extensions (LEX) in the design of the wing. Strakes can be used to either negate or promote vortex

production depending upon the angle of attack. In the case of LEXs at moderate α they are used to improve the overall flow through the use of "control vortices" whereas at low α they can be used to provide partial cancellation. A number of laboratory investigations into the effects of strakes have been conducted and most of the papers have a bias towards subsonic blunt fins.

Blunt Fins in Subsonic Flows

A number of researchers (Sung and Lin (1989), Devenport (1992) & Kubendran et al (1988 (b))) have considered strakes applied to bodies at subsonic speeds. Devenport et al (1992) tested a strake ("a large fairing in the corner between the wing nose and body surface") through a range of incidences and at various boundary layer thicknesses in a subsonic facility. At zero degrees angle of attack the results indicated that the strake eliminated leading edge separation and thus, the formation of a horseshoe vortex around the wing nose. The large drawback of adding the strake to the junction was that at non-zero incidences it became less effective and separation occurred on the windward side of the strake. However, the strake still eliminated much of the flow field unsteadiness and flow non-uniformity associated with the horseshoe vortex.

Sung et al (1991) computed the flow around a strake identical to Devenport et al's (1992). Sung et al (1991) considered the effects of the strake over 0 to 6° incidence and he found that the strake's performance was not dramatically affected by small angle of attack changes. Devenport et al (1992) considered a much larger range of incidences than Sung et al (1991) and for small angles of incidence their results are in agreement.

Devenport et al (1992) discovered that the strake caused important modifications to the pressure distribution around the junction relative to the unmodified condition. Firstly, the strake greatly reduced the magnitude of the adverse pressure gradient experienced by the test wall boundary layer upstream of the nose and secondly, the magnitude of the pressure minimum found on the wall close to the maximum thickness of the wing was also greatly reduced (fig. 12).

Kubendran et al (1988 (b)) tested a similar configuration to Devenport et al (1992) but the strake's leading edge was straight not curved as in Devenport et al (1992) (see fig. 12 (f)). Kubendran et al tested two strakes with sweepback angles of 63 and 45°. They found that the 63° strake eliminated separation and that it generally performed better than the 45° strake. Sung and Lin's (1989) computational study supported Kubendran et

al's experimental results regarding the benefits of sweeping the leading edge of the strake.

Sharp Fins in Supersonic Flows

Koide and Stollery (1993) considered the effects of employing strakes about a sharp fin at supersonic speeds. Their experimental data indicate that strakes can be used to modify the shock structure and that the impingement of the rear part of the shock structure on the wall must be delayed in order to maximise the beneficial effects of the junction modification (fig. 13).

Blunt Fins in Supersonic Flows

The only known study is that by Fulker et al (1993) who investigated various ways of improving the flow around a blunt 45° swept wing at M = 1.56. The investigation was conducted using both computational and experimental means. The theoretical calculations utilised an explicit time marching, finite volume code developed for solving the Euler equations for complete configurations known as SAUNA. Identical configuration's to those used for the computational study were tested in the 8 ft x 8 ft wind tunnel at DRA Bedford. An Euler code was used because the authors had greater experience of Euler codes, than fledgling Navier-Stokes codes. Euler methods have to be restricted to situations where there are thin shear layers. Most of the flows considered by Fulker et al (1993) were of this category but they note that the wing junction flow produced by such codes must be treated with extreme caution.

Fulker et al (1993) tried to create a pocket of conical flow at the wing root through the employment of a cone-like extension to the wing leading edge root (compare figs. 14 (a) & (b)). They used a cone-like extension of sufficient length to enable the cone's bow shock and the wing's bow shock wave to merge. This cone-like extension produced a weak shock of the same sweep as the main part of the wing's bow shock wave. It is apparent that, without root treatment, the bow shock wave is normal at the root (fig. 14 (c)). The addition of the leading edge cone gives rise to the Mach number contours shown in fig. 14 (d). Comparison between figs. 14 (c) & (d) shows that the addition of the cone has had the desired effect. The result of this modification was a 6 drag counts reduction in the wing drag (from $C_D = 0.00792$ to $C_D = 0.00729$) whilst the body's drag remained constant (Fulker et al (1993)).

1.3 The Scope of the Present Research

The present research is aimed at investigating the effects of filleting and incorporating strakes into supersonic wing / body junctions. The emphasis of the programme is placed upon assessing the potential that fillets and strakes possess with regards to improving the flow around blunt supersonic wing / body junctions.

The objectives of the programme were to minimise or preferably, eliminate :

- the pressure rise experienced ahead of and around the junction,
- the amount of separated flow generated by the junction and,
- the shock system's unsteadiness.

Both swept (45°) and unswept fins were considered during the early phase of the investigation. Efforts were concentrated upon the straight blunt fin interaction as the research progressed because of the severity of the unswept interaction. Initially, triangular ramp-type fillets were tested but this avenue was discarded in favour of strakes due to negative results. Both sharp and blunt leading edge strakes were tested and the final stages of the investigation focused upon blunt leading edge strake design parameters.

The thesis stresses the effects of the junction modifications and how the modifications have affected the flow field models developed by previous researchers, such as Hussain (1985) and Fomison (1986).

1.4 The Economic Justification for the Research

The use of fillets and strakes is quite common at subsonic speeds but little is known about their effects on supersonic juncture flows. A number of examples of the economic benefits associated with modifying subsonic wing / body junctions with various fairings are given below. The economic benefits of introducing fillets or strakes into junctions at supersonic speeds are unknown and further development of the concepts contained in this thesis are required prior to being able to establish such relationships.

- Wind-tunnel tests of the USAF's C-141 showed that redesign of the wing-fuselage fillet would improve the vortex flow pattern around the junction giving a 5%

reduction in cruise drag and, thanks to a better lift distribution, it would be possible to add a 6 ft wing-tip extension without increasing the wing stress enabling an additional 3% drag reduction. Performance calculations illustrated that this 8% drag reduction could be translated into a 8% fuel saving for each C-141 (fig. 15), i.e. a total saving of 82,000,000 gallons of fuel per year for a fleet of 277 C-141. On the other hand, the modification was estimated to cost about $ 11m which was roughly equivalent to one year's fuel saving. Unfortunately, this improved wing fillet was not developed, because it was proposed too late in the programme (Poisson-Quinton (1978)).

- The thicker wing section employed on the A 310 compared to the A300 made the achievement of a low interference drag junction much harder than on the A300. The increase in the wing root section's t/c between the A300 and the A310 worsened the separation occurring towards the rear of the wing. This resulted in the A310's wing root trailing edge fairing being increased in size and the improvement in cruise drag as illustrated in fig. 16 (a). The cruise drag improvements quoted in fig. 16 (a) are relative to A 300 type fillets applied to the A 310 wing. Thus, the improvements are from a comparison of the A300 type fillet applied to the A310 and the A310 with the fillets used on the A310.

  The importance of minimising leading edge separation was appreciated during the design of the A 300 as a strake aimed at suppressing this vortex was developed. However, the gain for suppressing the horseshoe vortex on the A 300 was fairly modest, about 0.5% of cruise drag, due to the relatively small leading edge radius whilst as the A 310 wing had a much thicker root section the potential improvement for suppressing this vortex was significantly higher, about 1.33% of cruise drag (Jupp (1980)). Figure 16 (b) shows the smooth flow around the A 310 wing root leading edge strake that was eventually achieved and no separation zones are visible.

- NLR-HST tested a modern transport (an Airbus type of aircraft - the exact type is not specified in the literature (Krenz (1983))) and they found that the size of the fillet required to suppress the wing junction vortex was dependent upon the relative root thickness, the setting angle of the wing, the leading edge radius and the wing height position at the fuselage. The type of fairing depended upon the aerodynamic lay-out of the entire inner wing, where the root section is one dominant part. Figure 17 simplifies the correlation of the wing root pressure distribution and fairing size. The size of the fairing required for drag reduction was found to increase as the velocity over the upper side of the wing root and size of the suction peak at the leading edge

increased. The drag reduction was normally of the order of 1 to 2 % of the total aircraft drag and hence quite important to the overall performance of the aircraft. Figure 18 illustrates the drag polars of a wing of the type of the one shown on the right hand side of fig. 17, (i.e. without high velocity at the front of the inner wing leading edge) and figure 18 presents drag measurements at a typical cruise Mach number for two wing-fuselage fairing sizes compared to the configuration without fairing. A 5 counts improvement was gained through the usage of the smaller fairing whilst the larger fillet does not improve the drag any further.

- In 1964 ARA examined the effects of placing fairings in a high wing / fuselage junction in order to minimise the large adverse pressure gradients occurring when no fairing was employed (Haines (1983)). For the without fairing case, the wing was simply added to the top of the fuselage with a small 0.03" radius (R/t = 0.6) in the underwing junction. Fairing A was designed as an envelope of the local wing flow streamlines except that for practical reasons, the full waisting could not be adopted below the rear of the wing. Figure 19 (b) shows that fairing A, although small, was successful in reducing C_D by as much as 0.0010 under certain conditions. Oil flow patterns showed that the flow was still separating on top of the fuselage just ahead of the wing leading edge and as a result, a relatively strong pair of vortices trailed back along the side of the fuselage as shown in fig. 19 (c). A larger fillet was developed, culminating in Fairing B, fig. 19 (a), which virtually converts the configuration into a shoulder layout and eliminates the re-entrant corners in the junctions below the wing. The oil flow pattern in the lower photograph of fig. 19 (c) indicates that the flow along the side of the fuselage is significantly different from that in the upper picture. The dividing streamline between the flow and the forward fuselage and the flow around the immediate wing leading edge can be discerned but there is no sign of a herring bone pattern under a vortex. The improved flow is reflected in the sizeable reductions in drag evident in fig. 19 (b) typically, ΔC_D = -0.0010 at C_L = 0.2 or -0.0025 at C_L = 0.5, relative to the values for the original wing-body combination. The reduction in the interference drag must be even greater since the configuration without Fairing B clearly has a larger surface area.

2. The Experimental Programme

The experimental data presented in this thesis were obtained from two different test facilities, the 9" x 9" continuous supersonic wind tunnel and the intermittent 2.5" x 2.5" supersonic facility. The vast bulk of the work was conducted in the former whilst qualitative flow visualisation experiments concerning blunt strake design parameters were conducted in the latter.

2.1 The 9" x 9" Continuous Supersonic Wind Tunnel

A two dimensional asymmetric nozzle of the type shown in fig. 20 was used to establish the required Mach number in the test section. For the present series of tests the nominal Mach 2.5 liner was employed. A water cooling system in the settling chamber allows the stagnation temperature to be kept roughly constant and equal to around 293 K. During tunnel running an automatic pressure regulator enables the maintenance of a pre-selected stagnation pressure in the range of 13.8 to 82.7 kPa (2 to 12 psi).
The flow properties maintained throughout the test programme were :

Total pressure, P_0	$248 \pm 4 \times 10^2$ Pa
Total temperature, T_0	293 ± 2 K
Mach number, M_∞	2.45 ± 0.03
Unit Reynolds number	$2.62 \pm 0.09 \times 10^6$ / m

2.1.1 The Flow in the Working Section

Schlieren photographs taken of the test section flow, by Fomison (1986), showed that no spurious wave systems existed. The test section boundary layer was surveyed by Kubota (1980) at three different stations across the test section. If the measured boundary layer velocity profile is transformed using the van Driest (1957) transformation and compared to an incompressible equilibrium profile from Bradshaw (1977) it is suggested by Fomison (1986) that the turbulent boundary layer profile on the side wall is close to equilibrium.

The 99.5% boundary layer thickness (δ) measured 1.6 cm and the corresponding displacement and momentum thicknesses were 0.38 and 0.10 cm respectively.

2.1.2 The Shock Generators

Two plain hemi-cylindrically blunted fins of one inch diameter were manufactured from plain aluminium. One of these fins was swept back 45 degrees whilst the other was unswept. These models are illustrated in fig. 21 (a) & (b). Two ramp type fillets were manufactured for each of these plain fin models from aluminium as shown in fig. 21 (a) & (b). The fillets were designed so that they could be placed between the side wall and the plain fin and this resulted in the aspect ratio of the combination fins being greater than that for the plain models.

After the results for the fillets had been obtained, it was decided to investigate the effects of incorporating a sharp edged strake into the junction design. The bow shock was strongest for the straight fin so this model was selected as the candidate for the initial strake tests. The strake had a very large sweep back angle (70°) and had a h/δ ratio of 1.6 (fig. 21 (a)).

Finally, two straight models of $D/\delta = 0.6$ were tested in the continuous facility. One of these models was kept plain whilst the other had a blunted strake attached to its leading edge (fig. 21 (c)). The strake had a circular cross-sectional profile in the direction normal to its leading edge and was swept back by 45°.

A summary of the tests conducted for each of the models is provided in Table 2.

2.1.3 The Test Techniques Employed

2.1.3.1 Surface Oil Flow Visualisation

For the purposes of the oil flow tests the shock generators were painted matt black in order to give good photographic contrast with the white oil streaks. The surface oil flow patterns were obtained using a mixture consisting of titanium dioxide and motor oil with a few drops of oleic acid added to avoid coagulation. The oil patterns on the side wall were photographed whilst the tunnel was running but the fin side view patterns had to be captured after tunnel shut down because there was no clear view of the model's surface and this, occasionally, resulted in some slight smearing.

2.1.3.2 Schlieren Photography

Single pass schlieren tests were conducted with the model mounted vertically in contact with the upper working section liner, and horizontally, with the fin base almost touching the glass window (fig. 22). During the horizontal tests a gap of 0.2 mm was left between the glass window and the model base at atmospheric conditions to allow for any window deflections resulting from the differential pressure loading occurring from tunnel running. A microsecond spark source was used to generate the light beam and the flow pictures were recorded on HP 5 400 ASA film loaded in an Olympus camera.

Two 10" diameter parabolic mirrors of focal length 10 feet were used to create a single pass schlieren system and various lenses were used to produce different magnifications of the image which were focused on the shutter plane of the camera.

2.1.3.3 Mean Static Pressure Surveys

Detailed surveys of the mean surface static pressure distribution in the interaction region were made by means of an array of pressure ports drilled in a turn-table (fig. 23). Each of the ports were connected in turn via a scanivalve to a Druck PDCE 22 (15 psia) pressure transducer. The ports were scanned slowly with one second being allocated for the settling time. The pressure transducer signals were amplified, digitised and displayed by an on-line computer which also stored the data onto floppy discs. Ten readings were taken for each port and the average value was calculated and downloaded from a MINC minicomputer via a VAX 750 to a UNIX work-station.

2.1.3.4 High Speed Ciné Photography

A standard single pass schlieren system was used for the high speed photography, the same 10" diameter parabolic mirrors of focal length 10 feet were used as in Section 2.1.3.2. However, the Olympus camera was replaced by a Hadland Hyspeed ciné camera loaded with Kodak RAR 2479 400 ASA film running at 4000 frames per second and the spark source was replaced by a 650 Watt over-head projector bulb.

2.1.3.5 Laser Light Sheet Flow Visualisation

2.1.3.5.1 The Optical System

A laser light sheet flow visualisation system was developed using a Coherent Innova 70-4 (4 Watt maximum output) Argon Ion laser. A diagrammatic sketch of the optical system is in fig. 24 (a) and the properties of the lenses are listed in Table 3. Appendix A explains the YNU Ray Tracing method that was used to develop the lens system.

A combination of two spherical and cylindrical lenses was used to enable a number of different model configurations to be investigated. The conceptual idea of using a system involving these two types of lenses was gained from the laser light sheet flow visualisation study conducted by Alvi and Settles (1991).

The laser beam was first focused in the centre of the wind tunnel test section using the two spherical lenses S_1 and S_2 (fig. 24 (b)). The output of S_2 was then expanded into a sheet using a combination of two cylindrical lenses C_1 and C_2. The two spherical lenses, S_1 & S_2, allow the focus of the laser beam to be changed by varying the spacing t_{12} between them. Similarly the semi-height of the sheet, y, could be controlled by adjusting t_{56}. The shock images produced by this technique were recorded by a 35 mm Olympus camera using Kodak TRI-X Pan film (ASA 400).

2.1.3.5.2 The Seeding Mechanism

Under normal operating conditions the air used within the tunnel is passed through a silica gel dryer but this system was partially bypassed in order to seed the flow. Steam was passed from an urn, via insulated tubing, through two dispensers mounted in the roof and floor of the tunnel's stagnation chamber. Upon passing through the nozzle the water vapour condensed to form miniature ice crystals.

The resulting ice crystals in the flow field reveal the shock structure by scattering the laser light from the light screen described earlier. The brightness of a flow feature in the laser light sheet flow visualisation technique is determined by the ice crystal density. High density zones appear to be very bright whilst darker zones indicate low density regions. An exception to this rule can occur in the case of boundary layer flow because the static temperature of the flow is high enough to melt the ice particles. On account of this boundary layers generally appear to be dark in the images of the interaction.

2.2 The 2.5" x 2.5" Intermittent Supersonic Tunnel.

The blunt strake design parameter flow visualisation study was conducted in the intermittent suck-down supersonic wind tunnel. This tunnel has a working cross section of 2.5" x 2.5" and it is driven by air at ambient conditions. Stagnation conditions were slightly below atmospheric because of the small pressure drop across the silica gel drying system.

The vacuum tank has an internal volume of 46 cubic metres (approximately 1600 cubic feet) and it is evacuated continually by a 25 kilowatt (33.5 horsepower) electrically driven pump. For the present tests a Mach 2.5 asymmetric two-dimensional nozzle section was used. Subsequent calibration tests revealed that the true Mach number was slightly lower at 2.43.

The run time of the facility was around twenty seconds and this enabled the use of several standard intermittent tunnel techniques to obtain data. Further information about the tunnel and calibration methods can be found in Blank (1991). In summary, the test conditions were :

Total pressure, P_0	$100.4 \pm 0.84 \times 10^3$ Pa
Total temperature, T_0	293 ± 4 K
Mach number, M_∞	2.43 ± 0.04
Unit Reynolds number	$1.02 \pm 0.1 \times 10^7$ / m

2.2.1 The Flow in the Working Section

The test section boundary layer is a turbulent boundary layer growing under an almost zero pressure gradient. The optical boundary layer thickness is about 0.2" (5 mm) which is equivalent to the figure quoted by Kubota (1979). The actual (velocity) thickness of the boundary layer (defined by the point at which the local velocity is 99.5% of the external velocity) is 0.23" (5.85 mm) (Dickman (1977)), and the corresponding displacement thickness is 0.07".

2.2.2 The Shock Generators

Four models, of the same D/δ ratio to that used in Blank (1991), were tested (fig. 25) in order to determine the influence of the fin on the modified junction's flow and to investigate the effects of strake height. The strake-wing-body models spanned half the tunnel whilst the cut-off models' span was only the strake height (fig. 25 (i) & (ii) - also note the comments on (iii) & (iv)).

2.2.3 The Testing Techniques Employed

2.2.3.1 Surface Oil Flow Visualisation

A solution of titanium dioxide in paraffin was used to obtain the mean positions of the separation and attachment lines. The oil flow mixture for the 2.5" x 2.5" tunnel was different to that used in the 9" x 9" tunnel because the 9" x 9" wind tunnel requires a significant period of time before the test speed can be attained unlike the case for the 2.5" x 2.5" wind tunnel in which the test speed is obtained very quickly. Thus, the oil flow mixture for use in the 9" x 9" wind tunnel has to be more dense than that used in the 2.5" x 2.5" tunnel. All photographing of the model had to be conducted once the oil flow mixture had dried and the tunnel had been shut-down because of the lack of a clear view of the model.

2.2.3.2 Schlieren Photography

A single pass schlieren system was constructed with the model mounted in the vertical plane. Two parabolic mirrors of 8" diameter with a focal length of 10 feet were used instead of lenses and illumination was provided by a microsecond spark source. The resultant flow pictures were captured on the same photographic equipment as mentioned in Section 2.1.3.2.

2.3 Errors

The calibration of the transducers and the resolution of the A/D converter represent sources of potential errors. The transducers were regularly checked and they were found to be consistent to within a reasonable percentage band. The equation used to link the measured voltages to the known pressures was of the form

$$\mathbf{v} = A\,\mathbf{p} + B$$

where **v** represents the transducer's output voltage, **p** represents the known pressure and A & B are constants.

The maximum percentage differences based around the average in the calibration factors were contained within the following bands :

	A Percentage change	B Percentage change
P_0	0.18	9.9
P_∞	0.39	5.7
P_{local}	0.13	14.7

The percentage differences for the B values are much greater than those for the A values because small variations in the transducer's output voltage and small variations in the gradient caused relatively large percentage changes in the B values. The largest of which was $o(10^{-4})$ V / bar.

The A/D converter has a resolution of 0.0025 V which relates to a potential error of 0.2 % and 3.4 % in P_0 and P_∞ respectively and a maximum error of 4.4% in P_{local}. The latter figure is stated as a maximum error because P_{local} is generally above P_∞ and as such a 0.0025 V change in the voltage output produced by a larger pressure than P_∞ will cause the measurement error when expressed as a percentage to reduce. Therefore, the percentage error for P_{local} is based on the freestream conditions.

3. Results and Discussion

3.1 The Effects of Filleting the Junction

3.1.1 The Unswept Shock Generators

Case 1 : The Blunt Unswept Fin of $D/\delta = 1.6$

Numerous previous investigators (Fomison (1986), Stollery (1989), Hussain (1985) & Sedney and Kitchens (1977)) have described in some considerable detail the development of glancing interaction. Leading edge bluntness causes the bow shock wave to detach and hence the two sides of the fin can communicate more easily than in the sharp fin case. A strong curved shock wave will be generated and local separation at the root is almost inevitable. Local separation will, in turn, feed forward through the subsonic section of the boundary layer and modify the shape of the bow shock creating a lambda foot (fig. 6).

Some indication of the complexity of the flow field can be gained from the oil flow photograph, fig. 26 (i). The pattern generated by the oil flow mixture is sketched in fig. 7 (b). There are three separation lines marked S_1, S_2 and S_3 and two attachment lines on the wall. The first two pairs of separation and attachment lines, S_1, A_1, S_2 & A_2, lie in a horseshoe manner around the fin. This suggests that there are four horseshoe vortices residing around the fin in a manner similar to that suggested by Sedney and Kitchens (1977) and the vortex skeletons are drawn in fig. 7 (c).

The pattern on the side of the fin (fig. 26 (iv)) is similar to those recorded in (Fomison (1986), Stollery (1989) & Hussain (1985)). In fig. 7 (a), taken from Hussain (1985), the vortex V_4 is seen to climb up the side of the fin yet in the oil flow photographs taken during the present and Fomison's (1986) study the attachment line A_2 does not ascend the fin but remains on the side wall indicating the presence of a vortex, V_4, close to the wall (fig. 7 (b) & (c)). The distinctive region of flow passing around the model's shoulder and climbing up the fin's side is therefore believed to represent an attached high pressure "jet" type of flow as in Fomison's (1986) flow field model (fig. 7 (b) & (c)) not a vortical flow as expressed by Hussain (1985). The boundaries of this flow are denoted by lines of entrainment in the oil flow photographs and there is no visible evidence, in either Hussain's (1985), Fomison's (1986) or the present study, of the presence of any

attachment lines which would accompany the separation lines denoted by S_4 & S_5 in Hussain's (1985) flow field model (see figs. 10 (b) & 26 (iv)). Thus, the author disputes Hussain's (1985) interpretation of the flow along the side of the fin. For the above mentioned reasons, Fomison's (1986) flow field model will be used and the term "jet" will be used to denote the type of flow occurring between the two lines of entrainment on the side of the fin.

Schlieren Images and Shock Wave Unsteadiness

The schlieren photograph taken normal to the wall, fig. 27 (a) (i), indicates the existence of a "double bow" shock system as opposed to a single shock wave. The upstream shock's position was found to correspond to the stand-off distance of the bow shock wave in the vicinity of the triple point and the rear image was found to relate to the lambda foot. The stand-off distance of the upstream shock wave was compared to the table for the stand-off distances in Liepman and Roshko (1957). The value given for an one inch diameter cylinder at Mach 2.5 in Liepman and Roshko (1957) was 0.42" and the distance measured off the photographs was 0.46". It must be noted that the stand-off distance of the shock wave varied over the height of the model (fig. 28 (i)) and the figure quoted above is for the bow shock wave in the vicinity of the triple point.

Details of the flow in the root region are shown in fig. 28 (i). These schlieren images clearly indicate the gross local unsteadiness of the separation shock structure and the movement of the triple point. Note that there are a considerable number of compression waves coming from the separated region. The triple point undergoes a vertical motion of about 0.6D (0.6D = δ).

The author working in a different wind tunnel at M = 2.3, δ = 6 mm and Re /m = 10^7 on a hemi-cylindrically blunted strut of D/δ = 0.7 found that the triple point underwent a height change of 0.3D (or 0.2δ). Clearly, D/δ is a parameter of great importance to this motion as it appears that an increase in D/δ increases the triple point's amplitude (see Table 4(b)).

Further observations of the shock structure reveal that the separation shock's amplitude is about D and that the lambda foot undergoes a similar curling motion to that mentioned in Dolling and Bogdonoff (1981). Both Dolling and Bogdonoff (1981) (at M = 2.95) and Blank (1991), have found that the distance between the most upstream and downstream locations of their separation shock waves has been D. Furthermore, Dolling and Bogdonoff (1981) tested a number of different diameter "semi-infinite" fins in a variety

of boundary layers (δ = 0.3, 0.42, 0.52 and 1.6 cm) with a freestream unit Re of 6.3 x 10^7 /m. They found that the streamwise excursions of the shock structure traversed a distance of D regardless of the thickness of the boundary layer. Thus, the separation shock's amplitude when expressed in terms of D appears to be independent of Re_δ (for $0.12 \leq D/\delta \leq 1.6$) and Mach number changes over the limited data range in Table 4(b). More data is required to be able to extend this relationship over larger ranges of M and Re_δ.

A high speed cine film was taken of the shock motion in order to observe the fluctuation of the shocks. Often the image of the separation shock wave was blurred (fig. 29) and this is believed to be due to the shock wave moving at a very high speed relative to the framing rate of the camera. A bubble type region could be discerned in the fin / wall corner and its motion appears to be connected to the motion of the separation shock wave. It is further believed that the expansion / contraction of this bubble type region (fig. 29) is related to the separation of the boundary layer.

The majority of the shock system's motion, on the high speed film, appears to be localised as shown in the top two diagrams of fig. 29. This motion is extremely energetic (jittery) and consists of high velocity movement. It is not periodic in the sense of a single frequency motion. For ease of reference this motion will be referred to as the normal oscillatory pattern. The shock system's motion also contains some motion during which the distance between the fin leading edge and the separation shock increases rapidly to an extreme condition. This motion is a gross excursion from the normal oscillatory pattern and it is sketched in the lower two diagrams in fig. 29. The gross excursion motion occurs about 3 to 4 times per second, although the interval between the gross excursions is irregular. Superimposed upon the gross excursion motion is a high velocity, small amplitude motion similar to that entertained during the normal oscillatory motion. It should be noted that the gross excursion motion is also recorded on the high speed cine film for the Case 5 fin but it does not occur on the films for Cases 6 & 7. In summary, the film for the Case 1 model indicates that the shock motion has two distinct components. One is the low frequency, large amplitude motion (occurring 3-4 times per second) whilst the other component has a much higher frequency and smaller amplitude.

Over the period of a micro-second the motion induced by the low frequency component will cause the shock's foot to move a distance of 8 x 10^{-6} inches. Due to the short duration of the spark source images (one micro-second) the shock's motion has effectively been "frozen". However, for the cine film the distance over which the gross

excursion motion will have caused the shock's foot to move during the exposure time is 2 x 10^{-3} inches. Although this distance is much larger, it is unlikely to cause any significant blurring of the image and this explains why the low frequency motion is so easily recognised. The blurred shock images in the high speed film must be caused by significantly higher velocity motion. With the present data it is not possible to estimate the higher frequencies causing the shock to vibrate but it is possible to recognise its existence.

Dolling (1993) notes that the separation shock's foot responds to pressure fluctuations under the incoming flow which convect into the interaction and that the separation shock's motion is influenced by pressure variations under the separated flow. Furthermore, he argues that events under the separated flow precede the shock motion and this indicates that the shock motion is affected twice by the incoming turbulent structures - firstly, when they pass through the separation shock and secondly, when they recirculate upstream of the fin root. Cross correlations of the shock motion to various pressure signals have indicated that the separation shock's motion can be attributed to both perturbations in the instantaneous ratio of static quantities across the separation shock (incoming turbulence) and the expansion / contraction (pulsation) of the separation bubble (Dolling (1993)). High frequency perturbations of the shock are driven by both upstream and downstream turbulence but the low frequency perturbations come only from the downstream fluctuations (Dolling (1993)). Based upon Dolling's (1993) statements, it is believed that the energetic high velocity motion recorded on the film is induced by the up- and downstream turbulence.

The low frequency, large amplitude motion that Dolling refers to has a frequency of a few hundred Hertz (Dolling (1993)). The lowest frequency noted by Dolling is around 200 Hz. Dolling and Smith's (1989) investigation revealed that fins of $D/\delta = 0.78$ and 1.17 had distinct frequency peaks of 0.5 and 0.8 kHz respectively. Dolling (1993) and Dolling and Smith (1989) have stated, based upon this data, that for a given δ an increase in D decreases the frequency of the motion. Dolling (1993) amplifies the above by pronouncing that "the separation shock frequencies are also influenced by the downstream separated flow, since the incoming conditions are fixed and only D is altered". Given that the current programme is interested in the frequencies for a larger value of D/δ than the values of D/δ examined by Dolling and Smith (1989), one could expect that the low frequency component of the motion would be about a few hundred Hz.

The freestream velocity is 567 m/s and the corresponding characteristic mean shock speed equates to 17 m/s (3% of the freestream velocity - see Section 1.2.2.1). The frequency corresponding to the mean shock speed, given that the length scale of the motion is D, equates to around 300 Hz. The estimated shock velocity for a gross excursion, ignoring the superimposed high frequency motion, is estimated at being less than 0.5 m/s. Clearly, there is a difference of two orders of magnitude between the low frequencies (and the corresponding shock velocities) that Dolling refers to and the frequency of the gross excursions recorded on the film. Unfortunately, there is no data to the best of the author's knowledge indicating how the shock motion is influenced by Mach number and Reynolds number changes.

The author has been unable to discover any plausible explanation for the difference in the shock velocities noted by Dolling and the gross excursion velocity. It has been suggested that the downstream flow maybe feeding through the return circuit of the wind tunnel and affecting the freestream flow. These gross excursions also occur for the Case 5 fin (equivalent to the Case 1 fin plus a sharp strake) but they do not occur on the films taken for Cases 6 & 7. Thus, it has been advanced that wind tunnel effects occur when the tunnel is loaded with essentially the Case 1 model. Given the available data and the discussion regarding the difference in frequency / velocity between the gross excursions and Dolling's "low frequencies" one cannot rule out this argument. The available data does not conclusively indicate whether the gross excursions recorded on the films for Cases 1 & 5 are due to wind tunnel effects or flow field effects. This issue has to remain open and it is recommended that further research is conducted (see Recommendations for Future Work).

Case 2 : The Blunt Filleted Unswept Fin of $D/\delta = 1.6$

The side wall oil flow pattern, fig. 26 (ii), indicates that the fillet induces an upstream movement of the primary separation line, S_1, (of around 0.8 D) and the upstream influence line, U, (of about 1.2 D) relative to the fin alone case. This movement is clearly indicated by comparing the position of the primary separation lines for the unmodified and the model with a fillet in fig. 26 (i) & (ii) to the location of the turn-table joint, T.

Figure 30 comprises of a sketch of the streak lines and a vortex skeleton representation of the flow field. The separation lines S_1 & S_2 and the attachment line A_1 pass around the leading edge of the fin in a horseshoe manner (figs. 26 (ii) & 30 (a)). This suggests that the vortices V_1, V_2 and V_3 are horseshoe vortices (fig. 30 (b)). The attachment line

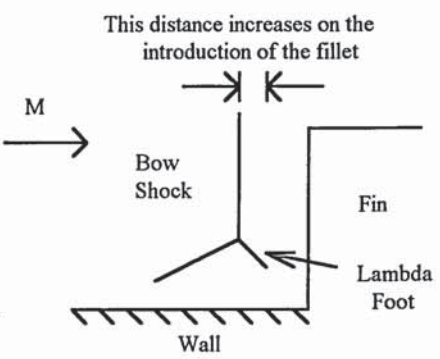
A_2 initially follows the contours of the base of the fillet but eventually it moves away from the base of the fillet and approaches S_2. A third separation line, S_3, is easily distinguished around the fillet / wall interface and close scrutiny will reveal a black line near the fin / fillet interface which represents its accompanying attachment line, A_3. The separation line S_3 leaves the fillet / side wall interface when it's past the curved portion of the fillet and it gradually climbs the fillet in an elongated "S" like manner. One would normally expect to find a small vortex rotating in the opposite sense to the primary vortex between A_2 and S_3 in the plane of symmetry. This expectation is supported by the close proximity of the two lines (A_2 and S_3) whilst in the vicinity of the curved portion of the fillet and for a small distance afterwards, but once past a certain point a sudden increase in the distance between these two lines occurs (figs. 26 (ii) & 30 (a)). A possible explanation for this is that V_5 moves up the side of the fin and V_4 expands to fill the gap left between V_3 and V_5 in the plan view. Hence, the increase in the magnitude of V_4's footprint on the wall (fig. 30 (b)).

The nodal point of attachment (NPA) for the non-filleted fin reported in Stollery et al (1986) is still present, in the same position, on the fin leading edge. Also, the "jet" like flow appears to be relatively unaffected by the introduction of the fillet, fig. 26 (iv) & (v).

A comparison of the side view schlieren pictures to those for the Case 1 fin indicates that the fillet has little effect upon the structure of the shock system (compare fig. 28 (i) & (ii)). The introduction of the fillet has increased the amplitude of the triple point to 0.69D from 0.6D.

The fillet does not affect the separation shock's amplitude which remains at about D. The approximate up- and downstream bounds of the motion correspond to the location of the mean (or time averaged) primary and secondary separation lines obtained through the oil flow technique. Interestingly, this region in the oil flow pictures suffers from poor resolution in comparison to the other areas, and this maybe linked to the unsteady shock motion.

The fillet has a number of effects upon the bow shock wave which the superimposing of the shocks (fig. 27 (b)) shows. The bow shock is pushed slightly upstream and the distance between the lambda foot and the bow shock wave has been



increased relative to the unmodified example (see sketch).

Indeed most of the data indicates that the fillet affects the separated flow area in a similar manner to an increase in diameter. The fillet increases the frontal projected area of the fin within and close to the boundary layer, hence the fillet might be expected to have a similar effect upon the shock structure to that of an increase in D/δ. Due to the scarcity of experimental data the relationship between fillet area and its distribution, and the ratio of effective D/δ cannot be derived. The data does not however, scale directly with either the ratio of fillet area to total fin area or to the fin area presented to the undisturbed boundary layer.

The centreline (Y=0.0") pressure distributions (fig. 31 (i) & (ii)) show that the pressure rise for the filleted fin starts upstream of the pressure rise for the plain fin. The height of the pressure plateaux are similar but there is no dip in the pressure distribution near the fin root for the filleted case. This difference is due to the majority of the flow on the fillet being entrained in the vortex, V_5 (see fig. 26 (ii) & 30 (b)).

The pressure distribution for the filleted fin at Y = 0.5" (fig. 31 (iv)) does not posses the characteristic double hump pressure distribution of the plain fin (fig. 31 (iii)). Instead, the pressure distribution indicates that the pressure rapidly rises to form a plateau which is created through the presence of V_1 to V_4. Thereafter, the pressure gradually decreases as the suction exerted by V_5 on the fillet decreases (see figs. 26 (ii) & 30).

A comparison of the unmodified fin's and the filleted fin's pressure distributions at Y = 1.5" (fig. 31 (v) & (vi)) reveals that the two distributions are qualitatively similar, unlike the distributions at Y = 0.0" and 1.0". This can be explained by considering the oil flow patterns for the unmodified and the filleted fins in fig. 26 (i) & (ii). The vortices that are encountered at Y = 1.5" for both the unmodified fin and the modified fin are V_1 to V_4 (fig. 7 (c) & 30 (b)). The vortices V_1, V_2 and V_3 for both fins (see figs. 7 (c) & 30 (b)) lie in a horseshoe manner around the fin. Hence, as the qualitative flow fields are similar at Y = 1.5" one can expect that the pressure fields for the two models will also be similar and this has been proven to be the case.

Note the variation in the pressure gradient between S_2 and A_2 in figs. 31 (iv) & (vi). At Y = 1.0" the pressure curve between S_2 and A_2 for the modified fin is reasonably smooth and this implies that the suction induced by the vortex V_3 on the wall is not very large. However, at Y = 1.5" the suction induced by the same vortex on the wall is

significantly larger and this implies that the strength of V_3 has grown considerably. At Y = 1.5" the modified and the unmodified fin's pressure plots and the oil flow pictures start to look similar and the effects of the fillet on the modified fin's flow field fade away. Clearly, one of the effects of the fillet has been to suppress the vortex V_3.

Although the pressure tapping density for the filleted fin appears to be rather coarse (see fig. 31), the pressure gradients generated by the filleted fin in the region directly ahead of the leading edge (Y= 0.0"), are steeper than those for the fin alone. Towards the outer edge of the fillet and beyond the fillet ($Y \geq 1.5$) the pressure gradients generated by the filleted fin and the unmodified fin are similar. This variation in the gradients of the pressure plots is probably due to the alteration in projected area that the introduction of the fillet has caused. The flow close to the centreline of the model has to negotiate the curvature of the fillet which is considerable whilst the flow encountering the outer edges of the fillet has to negotiate a smaller change in direction relative to the unmodified condition.

The flow field model that is suggested by the results for this fin is similar to that for the fin alone but a third vortex pair is present on the fillet and the second vortex pair climbs up the downstream region of the fillet (fig. 30). The majority of the flow on the fillet is dominated by V_5 and this vortex is responsible for the lack of a dip in the pressure distributions at Y = 0.0" and Y = 1.0". In the region ahead of the fillet two pairs of vortices exist which are similar in strength to those created by the plain fin. Based upon the pressure distributions the strength of the vortex V_3 increases as one progresses from the centreline until it reaches a similar strength to that possessed by V_3 for the unmodified fin (figs. 30 & 31).

Five investigations into the effects of filleting unswept wing / body junctions were identified by the author (Lakshmanan et al (1988), Devenport et al (1989), Koide and Stollery (1993), Sung et al (1991) and Haq (1993)). The papers are useful, in the main, for a qualitative comparison but not quantitative correlation.

Devenport et al (1989) and Koide and Stollery (1993) concluded that their fillets displaced the flow in a manner suggestive of an increase in the projected frontal area. The results of Devenport et al's (1989) experimental subsonic investigation are summarised above (Section 1.2.3.2). He noted that the addition of the fillet caused the pressure levels on the wall to increase (fig. 32) and that the primary separation line moved upstream. In the present study, the addition of the fillet did not produce any

perceivable increases in the pressure levels experienced around the model. However, Devenport et al's (1989) data and the present data do agree on the upstream movement of the primary separation line and the apparent displacement of the unmodified fin's flow field. With hindsight one could have expected the primary separation line to move upstream upon the addition of the fillet.

Koide and Stollery's (1993) experimental sharp fin results indicated that the pressure plateau was lengthened and that the pressure gradient was made steeper by the introduction of a fillet (fig. 13). Furthermore, the fillet produced a similar shock structure to the unmodified fin but the dimensions of the shock structure were larger. Thus, the present results in a qualitative manner, agree with Koide and Stollery's (1993).

Lakshmanan et al (1988) considered the effects of filleting wing / body junctions using Navier-Stokes computations at supersonic speeds. Lakshmanan et al's (1988) results are summarised in Section 1.2.3.2. Haq (1993) investigated experimentally a similar configuration to Lakshmanan et al (1988).

A qualitative comparison of Lakshmanan et al's (1988) and Haq's (1993) results to the present programme's data yields the following,

- Lakshmanan et al (1988) predicted that the pressure drop following the pressure plateau would decrease as the radius of the fillet was increased and that the pressure drop would disappear with correct filleting (fig. 11 (a)). As there is no pressure drop in the present results between $0.0 \leq Y < 1.5$" (fig. 31) both sets of data agree that the pressure drop can be eliminated through filleting.

- Both sets of data are in agreement regarding the upstream movement of the initial pressure rise upon the introduction of a fillet.

- The data differ with regards to separation on the fin surface. Separation is evident in the present data but Lakshmanan et al's (1988) results indicate that it can be prevented.

As no vorticity or heat transfer measurements were taken, no comment can be given upon the issue of vortex deformation or heat transfer.

Lakshmanan et al (1988) and Haq (1993) have both found that fillets of R = 3.5D reduced the strength of the horseshoe vortex and Sung et al (1991) have suggested that fillets of radius in excess of 0.53t would be required in order for there to be significant mitigation effects on the horseshoe vortex strength. The present results show that the fillet used did not reduce the magnitude of the pressure rise ahead of the fin's leading edge but the pressure drop, following the usual plateau, could be eliminated. Thus, we can conclude that the fillet reduced the strength of the vortices close to the fin's centreline and that it did not lower the level of the pressure plateaux. To a large degree the fillet can be considered to have been ineffective in a manner similar to that experienced with Sung et al's (1991) circular cross-section fillet as neither fillet reduced the upstream pressure rise. Vorticity was not measured during the present programme so no comment can be voiced with respect to the effects of the fillet on the vorticity generated by filleted fins.

3.1.2 The Swept Shock Generators

Case 3 : The Blunt Swept Fin of D/δ=1.6

Price and Stallings (1967) reported the effects of sweep on glancing interaction as long ago as 1967. Upon the introduction of sweep the centre-line pressure distribution collapses (fig. 33) and the disturbed area (defined by the primary separation line) contracts (fig. 9 (b)) (Price and Stallings (1967)). Hussain (1985) examined blunted fins at various sweep angles up to 75° and incidence angles from 0 to 24° at the same test conditions as the present study. He confirmed the benefits of sweep in greatly reducing the level and extent of the disturbed pressure field. The characteristic double peaked pressure signature is reduced dramatically in scale as the sweep is increased (Stollery (1989)) and the effects of sweep on the whole flow field for the non-filleted models is quite significant. However, Hussain's (1985) and the present author's oil flow pictures (fig. 34 (i)) indicate that separation still occurs at 45° of sweep and Hussain's (1985) results show that separation is present up to 75° of sweep (fig. 10) although the size and the effect of the separated flow region is greatly reduced.

The fin side view oil flow photograph (fig. 34 (iii)) indicates the existence of a region of flow which initially passes around the curved leading edge and then rises up the side of the fin. This region of flow is believed to be the swept fin version of the "jet" experienced by the Case 1 fin. Hussain (1985) noted the connection between the unswept and the swept versions of this flow but his flow field model (fig. 35 (a)) indicates that this flow is

vortical. Similar arguments to those used in Section 3.1.1 for the straight fin's flow field model can be advanced with regards to invalidity of Hussain's (1985) swept fin flow field model. Thus, the flow field model proposed in fig. 35 (b) will be adopted. Moreover the flows are unsteady and it is to this we shall now turn.

The triple point appears to undergo a height variation of about δ whilst the separation shock is located roughly 0.5D upstream of the fin root (fig. 37 (i)). The shock structure is still locally unsteady but the separation shock's length scale has been reduced relative to the straight fin. The separation shock and the lambda foot appear to be considerably weaker than their unswept counterparts in fig. 28 (i). In brief, not only does sweep reduce the mean properties of the interaction it also reduces the unsteadiness of the shock / shock interaction, limiting it to within about a diameter vertically and approximately half a diameter ahead of the fin root.

The schlieren image of the bow shock wave (fig. 38 (i)) indicates that the bow shock is diffuse in the neighbourhood of the leading edge. Hussain (1985) conducted a series of experiments with delta wings placed in the freestream but none of his results indicate any similar effects in the locality of the leading edge. During the present series of tests an examination of the inviscid shock produced by a 45° delta wing was conducted (fig. 38 (iii)) and the obtained image was identical to Hussain's (1985). The images produced by the 45° swept fin and the delta wing differ due to the presence of the wall boundary layer and the resulting shock / boundary layer interaction. The location of the shock wave in the outer portions of figs. 38 (i) & (iii) are identical and this implies that in the outer regions the strength of the two shocks are identical. The diffuse nature of the shock wave in fig. 38 (i) can be explained by the weak shock images that are produced by the same wing, fig. 37 (i), in the vicinity of the triple point.

Case 4 : The Blunt Filleted Swept Fin of D/δ=1.6

The oil flow patterns for the filleted swept fin (fig. 34 (ii) & (iv)) are much more complex than those without the fillet (fig 34 (i) & (iii)). The primary separation line, S_1, is extremely well-defined but the corresponding attachment line, A_1, has poor resolution. Secondary separation, S_2, also occurs and the attachment line A_2 appears in the vicinity of the fillet / wall interface. The oil flow pattern on the *side wall* is akin to the unmodified fin's (compare the photos in fig. 34). Thus, one may assume that there are four vortices residing around the base of the fillet (fig. 36 (b)) in a similar manner to V_1 to V_4 in fig. 35 (b).

The patterns on the fillet and fin are very complex (figs. 34 (ii) & (iv) and 36) and the interpretation of the lines in certain regions, notably the front of the fillet, is exceedingly difficult (fig. 36). Hence, the flow on the leading edge of the fillet is not sketched in fig. 36 (b). Certain distinctive features are easily identified, and one of these, is the nodal point of attachment (NPA) (fig. 34 (iv)). Sweep causes the NPA to approach the fin root and the introduction of the fillet produces a single NPA located close to the root of the fillet (fig. 34 (iv)).

A distinctive separation line, S_4, and an accompanying attachment line, A_4, appear in front of the fin's leading edge. The separation line, S_4, gradually descends the fillet as it passes around the fin leading edge. Another separation line, S_3, leaves the fillet / wall interface where it is located whilst in the curvature zone, and climbs up the side of the fillet (at a much faster rate than in unswept filleted example above). Eventually, S_3 and S_4 intersect but only a single separation line can be seen emerging from the intersection point (fig. 34 & 36). It is believed that two weak vortices exist in the leading edge portion of the fin / fillet interface, V_5 & V_6 (fig. 36 (b)), and that as they pass around the fin they start to dissipate. The vortex V_4 is dominant and this vortex climbs up the fillet to cause the intersection of S_3 & S_4.

The path of the "jet" on the side of the fin is altered considerably by the introduction of the fillet (fig. 34 (iv)). It no longer climbs up the fin along the edge of the fin's curvature, as in fig. 34 (iii), but it passes, instead, initially along the fin / fillet interface, for about 0.5D, before ascending the fin. This results in a reduction in the disturbed fin flow area (compare the two photographs in figs. 34 (iii) & (iv)).

The side view schlieren images indicate that a substantial change in the shock structure occurs upon the introduction of the fillet (fig. 37 (a)). The main effect of the fillet is that it has altered the inviscid shock structure and that the flow in the modified case undergoes compression through two oblique shock waves (fig. 37 (a) (ii)). The downstream oblique shock is reasonably steady whilst the lower part of the upstream oblique shock suffers from local unsteadiness due to turbulent fluctuations in the separated shear layer and / or boundary layer flow, fig. 37 (a). A large number of individually exposed photographs were taken of the shock structure and a small selection of them are shown in fig. 37 (a). Weak compression waves could only occasionally be seen ahead of the fillet's leading edge and the combined streamwise length scales for the oblique shock waves' unsteadiness appeared to be much smaller than the corresponding

value for the unmodified condition. A visual examination of the randomly exposed photographs indicates that the unsteadiness of the oblique shocks is concentrated on the fillet and at the fin / fillet interface. The reflected shock from the intersection of the two oblique shock waves is also present on the photographs, fig. 37 (a) (ii).

The location of the shock waves produced by the swept fin with and without a fillet are compared in fig. 37 (b). The shocks for the unmodified fin have been plotted with respect to their position relative to the fin alone whilst the shocks for the modified fin have been drawn relative to the combination fin. The bow shock for the unmodified fin diverges from the inviscid shock location along the majority of the length of the wing whereas the path of the bow shock for the modified fin (until the intersection point with the upstream oblique shock) is identical to that of the inviscid shock. The base of the shock structure for the modified fin consists of two inviscid shocks interacting rather than a lambda foot as for the unmodified fin.

The pressure plots, figs. 39 (i) to (xii), indicate that the fillet has considerably altered the pressure distribution around the model. From Y = 0.0" to Y = 2.0" (figs. 39 (i) to (viii)) the introduction of the fillet has caused the vortices between S_1 and A_2 to strengthen. The vortices between S_1 and A_1 are stronger than those downstream of S_2. Across the whole of the flow field the pressure rises earlier for the modified model than for the unmodified model. This is believed to be a direct result of the presence of the fillet generating a greater disturbance within the flow field than that generated by the unmodified model. For both Y = 3.0" and Y = 3.5" (figs. 39 (ix) to (xii)) the pressure plateaux start much earlier than for the unmodified model but the level to which the pressure rises is about the same as for the unmodified model.

In summary, the introduction of the fillet has caused the vortices on the wall to be pushed upstream, the primary vortex pair to strengthen (V_1 & V_2) and the separated flow area to increase.

3.2 The Effects of Incorporating Strakes

3.2.1 The Incorporation of Sharp Leading Edge Strakes

Case 5 : The Blunt Unswept Fin of $D/\delta = 1.6$ with a Sharp 70^c Swept Strake of $h/\delta = 1.6$.

The oil flow pattern indicates that the small region of the flow near the leading edge root of the strake is characteristic of normal swept sharp fin flow (fig. 26 (iii)). This region of flow, bounded by the incomplete separation lines either side of the strake, will be termed "strake dominated". The vast majority of the flow field is similar to the flow field generated in Case 1 above (fig. 26 (i)), so this region of flow will be termed either "bluntness dominated" or "fin dominated".

Analysis of the side view schlieren photographs (examples of which are in fig. 28 (iii)), reveals that the separation shock's maximum location upstream of the fin's leading edge is 2.6D and that the closest the separation shock gets to the fin's leading edge is 0.6D. These two values indicate that the length scale of the separation shock's horizontal motion is two diameters. Thus, the incorporation of the strake into the junction has increased the length scale by one diameter.

However, the high speed cine film for this model reveals that the above is an oversimplification of the situation regarding the effects of incorporating the strake on the shock system's unsteadiness. The film indicates that, in general, the shock system produced by the strake is more stable than that produced by the unmodified fin. More specifically, the normal oscillatory pattern is more stable for the Case 5 fin than for the Case 1 fin. The cine films for the strake and for the unmodified fin show that the shock systems posses an unsteady intermittent motion which has a large amplitude (i.e. gross excursions from the normal oscillatory pattern). Further analysis of the strake's cine film shows that it is the low frequency large amplitude component that has caused the increase in the motion's length scale and that for the majority of the film the modified fin's shock system is very stable and it is almost stationary. Hence, the individually exposed photographs are likely to look relatively similar because the amount of time that the separation shock spends undergoing large amplitude motion is small relative to the amount of time that the shock spends undergoing small amplitude local motion. Thus, a comparison of the two individually exposed photographs in fig. 28 reveals that the two photographs are very similar as would be expected from an examination of the cine film.

Using Dolling's (1993) work (see Section 3.1.1) it is possible to conclude that the strake attenuates the high frequency motion (which implies that it altered the characteristics of the high frequency component of the downstream flow) and that it amplifies the effects of the gross excursions noted in Case 1 (see Section 3.1.1).

The bounds of the triple point's vertical motion are 1.14" and 1.6" from the base of the fin. When expressed in terms of δ, the length scale of the triple point is 0.8δ. The amplitude of the triple point generated by the unmodified fin (see Table 4) was δ and the strake appears to have slightly attenuated this motion at the expense of the separation shock's horizontal movement.

The schlieren photographs of the present and the unmodified models (fig. 27 & 28) indicate that the strake reduces the stand-off distance of the bow shock by a very small amount. This effect of the strake diminishes as one proceeds away from the fin's centreline (fig. 27 (c)). The effect of the strake upon the flow field is very small and the characteristics of the blunt fin are dominant. The laser light sheet pictures also indicate that the shocks associated with the modified configuration are generally in the same position as those created by the unmodified fin (fig. 40). Except for fig. 40 (iii) the schlieren images and the LFV images correlate exceptionally well. It is quite possible that fig. 40 (iii) was photographed whilst the unmodified fin's shock was undergoing a large amplitude low frequency motion as this could cause the disparity between the location of the two shock structures.

The pressure data reveals a number of intriguing effects of the strake. The centre line pressure distribution (Y=0.0") has two very sharp peaks (fig. 41 (ii)). The first peak encountered when travelling in the streamwise direction corresponds to the first attachment line, A_1, and its accompanying separation line, S_1, occurs near the foot of the pressure rise. The secondary separation line, S_2, lies in a region of steep rising pressure (based on the freestream direction), and its attachment line, A_2, is the probable cause of the second peak. The position of S_2 in a region of rising pressure (fig. 41 (ii)) indicates that the majority of the flow around S_2 must be in the direction A_1 to A_2 which contrasts to the location of S_2 for the unmodified fin (fig. 41 (i)).

The pressure distribution at Y = 0.75" for the fin with a sharp strake (fig. 41 (iv)) indicates that the gradient of the pressure rise encountered by the flow between S_2 and A_2 at Y=0.0" (fig. 41 (ii)) is significantly reduced. The size of the second pressure peak

for the fin with a sharp strake is much smaller than that for the plain fin (compare fig. 41 (iii) & (iv)). The reduction in the gradient of the pressure rise between S_2 and A_2 has resulted in the formation of a region, about D in length, of slightly rising pressure. This suggests that the strake has had a significant effect upon the vortical nature of the flow close to the fin and that it has reduced the relative amount of reversed flow between A_2 and A_1.

The sharp strake delays the initial pressure rise from Y= 0.0" to Y =1.75" but the pressure plateaux and valleys are of a similar level to those created by the unmodified configuration (fig. 41). For $Y \geq 3.5$" the pressure distribution for both the sharp strake and the unmodified fin are virtually identical (fig. 41 (vii) & (viii)). Note how the location of S_2 on the pressure plots for the unmodified and the modified fins has changed (fig. 41). For the unmodified model S_2 occurs in a region of falling pressure whilst S_2 for the present case is located close to the point of inflection at the bottom of the pressure valley (fig. 41 & 42). Normally, flow separates when it encounters an adverse pressure gradient and thus, when S_2 is located in a region of decreasing pressure it is indicative of the majority of the flow local to S_2 being reversed. The change in the location of S_2 implies that the strake has reduced the amount of reversed flow relative to flow in the freestream direction. This, in turn, suggests that the two vortices, V_2 and V_3, (see fig. 43 (b)) are producing similar amounts of streamwise (V_2) and reversed flow (V_3) in the vicinity of S_2.

Unfortunately for the purposes of comparison there are no data, at either sub- or supersonic speeds, available concerning strakes which have a triangular (pyramid) cross-section and a sharp, straight leading edge applied to a blunt fin. The closest strake configurations to the present one that have been investigated are those used by Kubendran et al (1988 (b)) and Devenport et al (1992) at subsonic speeds. Devenport et al's (1992) strake and Kubendran et al's (1988 (b)) 63° strake eliminated separation and prevented the formation of the horseshoe vortex.

The present results do not, in a qualitative manner, compare favourably with either of Kubendran et al's or Devenport et al's (1992) results. The reasons why this difference occurs are:

1. the fin used in the present tests was of a greater relative bluntness than those used in the subsonic tests,
2. the subsonic strakes' h/δ ratios were greater than that used at M=2.45 and,

3. the present strakes' λ_S was much greater than the λ_S values for the subsonic strakes.

Sung and Lin's (1989) computational study of five strakes applied to a NACA 0020 airfoil with the nose replaced by a 1.5:1 ellipse indicated that a strake with a sweep angle in excess of 45° would be better than one with a smaller sweep angle. Kubendran et al's strakes with sweep angles of 45° and 63° support Sung and Lin's (1989) conclusion but the present study with a 70° swept strake suggests that there is a limitation on sweep angle and h/δ after which the strake has a minimal affect.

From the results of these supersonic experiments it is believed that the key to designing a successful strake is the balancing of the favourable effects of the strake against the adverse pressure gradient produced by the fin's bluntness. Thus, the strake's sweep angle (λ_S), height (h/δ) and bluntness (D_S/δ) are the fundamental design parameters for diminishing the adverse pressure gradient generated by the unmodified configuration.

3.2.2 The Incorporation of Blunt Leading Edge Strakes

Case 6 : The Blunt Unswept Fin of $D/\delta = 0.6$

The effects of modifying leading edge diameter have been investigated by Fomison (1986). The oil flow patterns (figs. 44 (i) & 45 (i)) are similar to those obtained during Case 1 (fig. 26 (i) & (iv)) and the four vortex flow field model is deemed to be applicable to the present case (fig. 46).

The horizontal schlieren photograph (fig. 47 (a) (i)) indicates the existence of a "double bow shock" similar to all the previous cases and the schlieren images (fig. 48 (i)) of the root region illustrate the unsteadiness of the shock wave / boundary layer interaction. A high speed cine film, framed at 4 kHz, was taken of the interaction in order to assess the amplitude of the separation shock's horizontal motion and the triple point's vertical motion. Please note that the two length scales are distinct. Much discussion has already taken place (see Section 3.1.1) regarding the parameters affecting the separation shock's length scale but the data for this fin enables an analysis of the parameters affecting the length scale of the triple point. The triple point was found to posses an amplitude of about 0.27δ whilst the Case 1 fin's triple point traversed a distance of δ (see Table 4) Clearly, the change in D/δ between the Case 1 fin and the Case 6 fin has resulted in the reduction of the triple point's amplitude from δ to 0.27δ.

From the film it was found that the separation shock traversed a distance of 0.75δ (1.25D). The data for this fin is in agreement with the data obtained by Dolling and Bogdonoff (1981), by the author (1990) and for Case 1 above (see Section 3.1.1). In the film for Case 6 the separation shock does not exhibit any low frequency large scale motion as in Cases 1 & 5. The motion recorded for Case 6 is generally of a higher velocity than that experienced for Case 1. Dolling's (1993) tutorial in which unsteadiness data for blunt fin / cylinder interactions is compiled, notes that "the [separation] shock frequency decreases as D increases". Dolling's statement is based primarily upon his earlier work with Smith. Dolling and Smith (1989) plotted power spectra for four Mach 5 cylinder induced interactions and they found that an increase in diameter caused the shock frequencies to reduce. The results obtained in the present programme support Dolling's conclusions albeit the Mach numbers considered by the author and by Dolling and Smith (1989) differ by a factor of two.

Case 7 : The Blunt Unswept Fin of $D/\delta = 0.6$ with a Blunt 45^c Swept Strake of $h/\delta = 1.6$.

The plan view oil flow photograph for this model (fig. 44 (ii)) indicates that the strake influences the flow locally and that separation occurs just ahead of the root of the strake's leading edge. The separation line pattern around the strake's leading edge root (see figs. 44 (ii) & 49 (a)) implies that there are four horseshoe vortices residing around the strake as shown in fig. 49 (b). Downstream of the unswept portion of the leading edge the influence of the unswept part of the fin on the flow field is felt as a third separation and attachment line pair (S_3 & A_3) is present (figs. 44 (ii) & 49 (a)). Note how in the lower half of fig. 44 (ii) S_1 and S_3 converge and eventually run almost parallel to each other.

The side view oil flow pattern (fig. 45 (ii)) illustrates the effects of the strake on the flow on the side of the fin. The combined fin's pattern, in the vicinity of the strake / fin joint, provides evidence of the existence of a "hybrid" flow field. The strake's "jet" which passes along the strake's edge of curvature is reminiscent of the flow pattern obtained by Hussain (1985) whilst the flow pattern on the fin above the interface of the two leading edges is qualitatively similar to that for the plain fin. This second "jet" which emanates from the interface of the leading edges and climbs slowly up the fin will be termed the fin "jet". The strake "jet" follows a more varied path than the fin "jet" as it initially climbs up the strake's leading edge, until it is about 0.5" above the fin / wall joint, then it proceeds

roughly parallel to the fin / wall interface before ascending the fin again and merging with the fin "jet".

The side view schlieren images clearly illustrate that the construction of the shock structure is modified upon the introduction of the strake (fig. 48 (ii)). The strake generates its own detached bow shock, herein termed the "strake shock", which interacts with the fin's bow shock to create an Edney type IV shock / shock interaction. The unsteadiness of the upstream shock is significantly less than that obtained for the separation shock produced by the unmodified fin. The distance over which the strake shock oscillates is only 0.5D (0.32δ) compared to 1.25D for the unmodified fin and the amplitude of the triple point's motion is reduced from 0.27δ to 0.13δ. The strake shock appears to oscillate only up to a height of 1.3δ above the fin / wall interface and the section of the strake-shock between 1.3δ and the triple point is virtually motionless. Occasionally small fluctuations of the triple point occur and these are usually the result of the foot of the strake shock undergoing a larger than normal motion which does not become fully damped out before reaching the triple point.

The author has obtained data, see Table 4, regarding the length scale of the separation shock wave produced by a 45° swept wing. It was found that sweep greatly reduced the length scale of the separation shock's motion. The strake-shock has an identical length scale, when stated in terms of D, to that obtained for the 45° swept wing. This suggests that the strake-shock mirrors the behaviour of a fin with similar sweep.

The pressure distributions (figs. 50 (i) to (xvi)) for the modified fin compared to the unmodified fin demonstrate the potential that strakes possess for reducing the peak pressures experienced around an unmodified fin. Indeed, at Y = 0.25" (fig. 50 (iii) & (iv)) the peak pressure is reduced by a factor of about 2 but beyond Y = 0.75" (fig. 50 (vii) & (viii)) there is no reduction in peak pressure. In the region $0 < Y \leq 0.75$" the strake has substituted two small pressure peaks for the large peak generated by the unmodified fin. When the location of the separation and attachment lines are superimposed upon the pressure plots it is found that the two pressure peaks correspond to the pressure rises induced by the strake and the straight portion of the leading edge. Note how the pressure peak generated by the strake reduces as Y is increased.

Overall, the pressure levels experienced around the modified fin, up to just before X = -1 except for Y = 0.0", are lower than those produced by the unmodified model (fig. 50). The strake has a favourable effect upon the position of the initial pressure rise beyond Y

= 0.75". In the region $0 < Y \leq 0.75$" the strake causes the initial pressure rise to be shifted upstream of the corresponding position for the unmodified case and, as a result of this, the flow separates slightly earlier.

All the separation lines for the modified fin are located in areas of rising pressure (see fig. 50) whereas S_2 for the unmodified fin resides in a region of falling pressure. Thus, the addition of the strake into the junction has caused the amount of reversed flow relative to flow in the freestream direction about S_2 to decrease. Between A_2 and S_3 for the modified fin the pressure gradient is favourable which implies that the majority of the flow around S_3 is in the freestream direction. This, together with the oil flow picture (fig. 44 (ii)) suggests that the flow re-attaches to the wall at A_2 and separates further downstream at S_3. At S_3 the flow rolls-up to form the vortex V_5 as illustrated in the flow field model in fig. 49.

The location of the origin of the vortex V_5 cannot be ascertained from the available data. From the oil flow photographs in fig. 44 it appears that the addition of the strake causes the vortices generated by the unmodified fin to be pushed downstream. The data from Case 11 suggests that for large h/δ vorticity is generated at the strake / fin leading edge interface and that vortices trail downstream against the surface of the fin (see Case 11 and fig. 59 (iv)). Unfortunately, none of the data in this thesis conclusively indicates that the origin of the vortex V_5 is located at the strake / fin leading edge interface as is indicated in fig. 49 (b) but we do have information on the two extremes (i.e. the unmodified fin in Case 6 and the vortices on the fin's surface in Case 11). Thus, it is believed that the vorticity produced by the strake / fin interface is responsible for the creation of the vortex V_5.

The distance between the separation line, S_1 and S_3, appears to be dependent upon Y (fig. 44 (ii)). The separation line S_2 appears to merge with S_3 close to the fin, leaving only S_1 and S_3 (figs. 44 (ii) & 49). This implies that V_3 and V_4 (fig. 49 (b)) either dissipate or merge with the other vortices. The vortex pair V_1 and V_2 is weaker than V_5 (see fig. 49 then compare fig. 50 (vi) & (viii)) and therefore, the latter dominates in the far field region.

Kleifges (1993) recently tested a similar configuration with a D/δ ratio of 1.27 and h/δ =1.4 (h represents the height of the strake) at Mach 4.95 (δ=0.59", $Re_\delta = 0.7 \times 10^6$). He conducted a number of tests on this configuration including oil flow, and measurements of the centre line mean and unsteady pressure levels. His oil flow results (fig. 51) were

very similar to those generated by the modified fin tested here. The strake was found to reduce the mean and the RMS pressure levels by 75% and 45% respectively relative to his unmodified fin (fig. 52). Kleifges (1993) also tested a 45° fin of the same D/δ ratio as the strake in order to assess the effects of the strake upon the flow field. He found that the mean and the RMS pressure distributions in the vicinity of the strake correlated exactly with those which he had measured on the swept fin (fig. 52). Kleifges' (1993) data therefore, indicates that there is a region of flow in which the strake affects the flow field in a manner similar to that caused by a fin possessing the same sweep and D/δ as the strake. Kleifges' (1993) data implies that V_1 to V_4 in figure 44 (ii) are generated by the strake and whose properties are dependent upon the design parameters of the strake itself. Thus, like in Case 5 above (see Section 3.2.1) the strake generates a region of flow which is strake dominated and the rest of the interaction flow field is dominated by the properties of the fin.

The flow fields generated by the sharp strake (see Case 5 above), Kleifges' (1993) strake and the present strake can be used to give an insight into the effects of variations in λ_s and the strake's bluntness. The parameter "L" (positive in the downstream direction - see fig. 44 (ii)) can be used to denote the distance from the unswept portion of the leading edge to the most upstream point of the fin's influence on the flow field. The L/δ values for the sharp fin and the present model are -1.9 and 1.3 respectively (Table 5). The difference in the L/δ must be connected to the parameters that have been altered between the two models. Hence, L/δ must be a function of the parameter set $\left\{\frac{D}{\delta}, \lambda_s, \frac{D_s}{\delta}\right\}$.

Kleifges (1993) has shown that the pressure gradients generated by the strake are equivalent to those generated by a fin of the same properties. Any change in the parameters $\frac{D_s}{\delta}$ and λ_s will alter the magnitude of the pressure gradients generated by the strake. The experimental results obtained through the present programme do support the belief that L/δ is strongly dependent upon D_s/δ, and λ_s for a given D/δ. The present data and Kleifges' (1993) data imply that one may be able to increase the quantity of strake dominated flow by altering any of the design parameters of the strake. Thus, for a set diameter fin, any increase in the strake's bluntness, height or length is likely to increase the relative amount of strake dominated flow. Further discussion on the independent parameters affecting L/δ is postponed until Case 11 (see Section 3.3).

Finally, it can be stated that the blunt strake has had a net positive effect on the flow field with respect to the programme's aims and that the blunt strake is an excellent way to obtain the benefits of leading edge sweep without sacrificing the surface area of a control surface.

3.3 Investigations into the Importance of the Height of a Blunt Strake

Case 8 : The Independent Blunt 45° Swept Strake of h/δ=1.6.

The strake used in this experiment (fig. 25 (i)) had identical h/δ and λ_s to the model used in Case 7 (fig. 21 (c) (ii)). The D/δ value for this model was slightly greater than that used for the Case 7 model which was tested in the 9" x 9" wind tunnel. This value of D/δ was chosen because earlier work by the author had indicated that a smaller diameter fin would encounter severe mounting problems and that a small increase in the diameter of the fin above $D/\delta = 0.682$ would cause the tunnel to choke. Additionally, it was expected that if any correlations to a straight unmodified fin, at the same freestream properties, were required then the data contained in Blank (1991) could be used. However, the increase in D/δ was relatively small as the current model's D/δ value was 0.682 whilst that for the Case 7 fin was 0.6. The plan view oil flow photograph (fig. 53 (i)) indicates the presence of three distinct separation lines. The first two of which, S_1 and S_2, are located in a horseshoe manner around the leading edge of the fin whilst the third separation line leaves the shoulder of the model at a slight angle until it is deflected outwardly. This outward movement of S_3 appears to be caused by the mounting arrangement used to hold the model in place because a comparison of the streamline patterns for the series of 45° hemi-cylindrically blunted fins tested by Hussain (1985) and the Case 3 model (fig. 34 (i)) do not indicate the existence of any similar effects on S_3.

The side view oil flow photograph (fig. 54 (i)) indicates the existence of a "jet" like flow towards the leading edge of the fin. Similar "jet" like flows have also been reported in Hussain (1985) and noted in Case 3. The streamline pattern obtained from the oil flow photographs (figs. 53 (i) & 54 (i)) imply that the flow field is similar to that sketched in fig. 35 (b).

Analysis of the side view schlieren images (fig. 55 (i)) indicates that the separation shock wave is contained within a distance of about 0.5 D from the leading edge root. This

figure is in good agreement with the results of the Case 3 and the Case 7 fin (see Table 4).

Case 9 : The Blunt Unswept Fin of $D/\delta = 0.682$ with a Blunt 45^c Swept Strake of $h/\delta = 1.6$.

The plan view oil flow photograph for this model, fig. 53 (ii), suggests that the flow field for this model (fig. 56) is similar to that generated by the Case 7 fin (fig. 49) as was expected. The location of the primary separation line, S_1, until it approaches S_4 is identical to the position of the primary separation line generated by the model used in Case 8. This implies that there is a region of flow within the modified fin's flow field which assumes the characteristics of the flow field generated by the strake.

The qualitative character of the oil flow patterns on the wall do not appear to have been affected by the 27% change in Re_δ or the 20% variation in H nor the 12% alteration in D/δ between the Case 7 and Case 9 models (see Table 5). Indeed the L/δ value for this fin is 1.3 which is identical to the value for Case 7. This suggests that the parameter L/δ is independent of small changes in D/δ when $D_s/\delta = D/\delta$ and moderate variations in Re_δ and the boundary layer shape parameter, H (δ^*/θ). As both D_s/δ and D/δ were altered simultaneously the beneficial effects of an increase in D_s/δ were probably negated by the increase in D/δ. Hence we can conclude that the increase in Re_δ from 41.6×10^3 to 57.3×10^3 and the increase in H from 3.75 to 4.66 did not affect L/δ in any perceivable manner.

A comparison of the qualitative character of the flow field produced by the present fin (fig. 53 (ii)) to Kleifges' (1993) oil flow data (fig. 51) reveals that the separation and attachment line patterns are similar. Furthermore, Kleifges' (1993) data indicates that L/δ can remain positive at values of h/δ lower than those used in the present study (i.e. part of the flow field remains strake dominated) albeit at a higher Mach number (Table 5). Kleifges (1993) used a much lower h/δ than those examined in the present study and the Mach number, Re_δ and H values for his flow were also much higher than those used in the present study. The present study shows that the L/δ value for a wing is independent of moderate changes in Re_δ and H. Thus, one may conclude that either Mach number effects or the use of a lower h/δ value are responsible for the lower value of L/δ obtained by Kleifges (1993). A further examination of the parameters influencing L/δ is in Case 11 (see Section 3.3).

A photograph of the side view oil flow pattern is in fig. 54 (ii) and the major features of the side view oil flow pattern are sketched in fig. 57 (b). The flow on the side of the fin has characteristics similar to both the unmodified fin and the independent strake as two "jet" like flows are located on the side of the fin. The lower one, the "strake jet", follows an identical path to the "jet" generated by the independent strake until the "strake jet" is in the proximity of the interface between the strake and the outer portion of the fin. Although the "strake jet" appears to split into two streams in fig. 54 (ii), the lower stream can be disregarded because it was formed during tunnel shut down.

The strake "jet" paths for Cases 8 & 9 are compared in fig. 57 (a) & (b). They are identical until the strake's leading edge joins with the outer portion of the wing. This indicates that the path taken by the strake "jet" in the present case is, at least initially, independent of the presence of the outer portion of the wing. Thus, the path taken by the strake "jet" downstream of the straight portion of the leading edge is dependent upon the flow field created by the strake / fin combination.

A comparison of the flow patterns on the side of the Case 7 fin and the present fin indicates that the two patterns are very similar but not identical (figs. 58). In Case 7 (fig. 58 (a) (i)) the strake and the fin "jet" coalesce 2.5D (4δ) downstream of the unswept leading edge whilst the two "jets" for the present fin do not coalesce at all. Table 5 shows that the only parameters that have been changed between Case 7 and the present case are D/δ, Re_δ and H. Due to the scarcity of data, it is extremely hard to pinpoint the variable responsible for this change in the side view oil flow patterns. In both cases, approximately two thirds of the strake is immersed within the oncoming boundary layer and therefore, any change in the properties of the boundary layer can easily affect the oil pattern. However, as the Reynolds number was increased by only about 16×10^3 this parameter is not believed to be responsible for the alteration in the oil flow patterns. Thus, the change in D/δ between the Case 7 and 9 model and / or the variation in H between the two facilities is / are believed to be responsible for the alteration in the oil flow patterns.

The streamline pattern produced by this model is sketched in fig. 56 (a) and the corresponding vortex skeleton representation is in fig. 56 (b). There are a number of vortices, (at least four as represented by V_1-V_4) generated by the interaction of the strake on the flow field and the unswept fin's influence on the flow field creates a fifth vortex, V_5, which emanates from the side of the fin in a manner reminiscent of the vortices generated by the unmodified configuration. The vortices V_3 and V_4 either

dissipate or merge with V_5 because their foot print on the wall gradually disappears as they approach V_5. This hypothesis is identical to the explanation put forward for the equivalent vortices generated by the Case 7 fin as the two flow fields are almost identical.

An evaluation of the side view schlieren photographs (fig. 55 (ii)) indicates that the strake shock's foot is contained within a distance of 0.5D upstream of the strake's leading edge root. The addition of the straight portion of the model has caused two lambda feet to be created. One of the feet is located at the base of the strake shock close to the boundary layer whilst the other lambda foot, the inviscid one, is located at the top of the strake. It is interesting to note that the rear shock of the inviscid lambda foot appears to encounter the strake slightly below the fin / strake interface and that the shear layer strikes the fin just above the fin / strake joint (fig. 55 (ii)). A comparison of figs. 48 (ii) & 55 (ii) indicates that small changes in Mach number and D/δ (D_S/δ), and moderate alterations in Re_δ do not affect the construction of the shock system as was expected.

This modified model, the Case 7 model and Kleifges' (1993) data all illustrate that the majority of the flow field's qualitative features remain similar over the range of Mach and Reynolds numbers over which experiments have been conducted to date. The only exception to this is the path of the strake "jet" which, in this case, does not coalesce with the fin "jet".

Case 10 : The Independent Blunt 45° Swept Strake of h/δ=3.2.

Two separation lines, S_1 & S_2, are identifiable in the plan view oil flow photograph for this model, (fig. 59 (i)) but their accompanying attachment lines, A_1 & A_2, are not as easily identifiable. The separation and attachment line pattern produced by this model suggests that the flow rolls-up to form a number of horseshoe vortices around the leading edge of the wing in a manner similar to that for Case 8 above. The location of S_1 for the present model and the model used in Case 8 are identical. This implies that the increase in strake height between Cases 8 & 10 has not affected the location of the primary separation line. No change in the location of the separation line was expected because the majority of the shock wave for the $h/\delta = 1.6$ model is located where the inviscid shock wave would be located. Thus, any increase in the model's height above $h/\delta = 1.6$ will not affect what happens at the root of the fin.

The oil flow pattern produced on the side of the fin is shown in fig. 59 (b) (iii). The path of the "jet" has been plotted in fig. 57 (c) and fig. 58 (b) to enable a comparison with other fins. A comparison of the strake "jets" paths in fig. 58 (b) (i) and (ii) reveals that the location of the "jet" paths are identical until they are above a height of 0.15" from the fin / wall interface. There is a small difference in the paths beyond this point and this may be due to end-effects occurring on the h/δ=1.6 model. When one compares both of the models to Hussain's (1985) sketch (fig. 58 (b) (iii)) one can notice that the path of the "jet" in fig. 58 (b) (i) is different to the "jets" in the other two pictures, particularly towards the top of the fin. It is believed that the parameter h/δ is responsible for this difference in the "jet" paths. The h/δ value for fig. 58 (b) (i) is 1.6 and this is probably insufficient to enable the path of the jet to be entirely isolated from end-effects.

The side view schlieren images (fig. 60 (i)) are very similar to those obtained for Cases 3 & 8, and by Hussain (1985). Analysis of a series of schlieren photographs reveals that the separation shock is contained within a distance of 0.5D upstream of the strake's root. The triple point is located just outside of the boundary layer, at about 1.06δ, and it does not appear to be susceptible to any significant unsteadiness.

In summary, the flow field created by this model is very similar to the flow fields created by Cases 3 & 8 (fig. 35 (b)) and the effects of extending the height of the model from h/δ = 1.6 have been found to be limited to minor changes in the path of the strake "jet".

Case 11: The Blunt Unswept Fin of D/δ=0.682 with a Blunt 45^c Swept Strake of h/δ =3.2.

The oil flow pattern produced by this wing on the wall is shown in fig. 59 (ii). The location of the primary separation line, S_1, coincides with the location of the primary separation line, S_1, generated by the independent strake in Case 10 (fig. 59 (i)) until slightly upstream of the combined fin's trailing edge.

The change in h/δ between the Case 9 and the Case 11 fin has caused the region of strake dominated flow to increase dramatically. Unlike in Cases 7 & 9 (see Sections 3.2.2 & 3.3), the secondary separation line deviates from the position of the secondary separation line produced by the independent strake prior to any deviation in the path of the primary separation line occurring. This has occurred, most probably, because the strake dominates a far greater quantity of the flow than for the two previous blunt strake examples and the corresponding Y position for the primary separation line, relative to the

other models, is too far outboard of the fin to enable the primary separation line to be influenced first. Note that there is no separation line that corresponds to S_3 in Cases 7 & 9 and that the fin's influence on the flow field is merely the deviation of the separation lines S_1 & S_2. The parameter "L" has been used to denote the distance between the unswept leading edge and the most upstream point at which the oil flow patterns are influenced by the presence of the outer portion of the wing. Thus, the non-dimensional parameter L/δ is 4.2 for this wing. Table 5 indicates that the only independent parameter that has been changed between Case 9 and Case 11 is h/δ. Furthermore, Table 5 shows that a 100% change in h/δ caused a change in L/δ in excess of 300% when all the other parameters remained constant. It can be stated therefore, that L/δ is not dependent upon h/δ through a first order relationship such as $\left(\frac{L}{\delta}\right)=A\ \left(\frac{h}{\delta}\right)$, where A = a constant.

The availability of the L/δ value for this model enables a more detailed discussion of the independent parameters affecting L/δ than previously possible. During the part of the present experimental programme concerned with investigating the effects of blunt strakes, the following parameters were altered : D/δ, h/δ, M, and Re_δ. Hence, we can state that L/δ is some function of the parameter set $\left\{\frac{D}{\delta},\ M,\ Re_\delta,\ \frac{h}{\delta}\right\}$ when $D/\delta = D_s/\delta$ and λ_s remains constant.

Table 5 indicates that a large number of parameters have been altered between Kleifges' (1993) experiment and the experiments performed during the present programme. This does not aid the identification of the prime independent variables controlling L/δ. The work of previous researchers (notably, Fomison (1986) & Saida and Hattori (1984)) indicates that the position of the primary separation line generated by a hemi-cylindrically blunted fin in a turbulent boundary layer remains similar regardless of the values for Re_δ and M used by the researchers (fig. 61). It must be noted that the bands over which data was obtained are limited and different effects are expected over larger ranges of Mach number (see below). The researchers did indicate that the location of the primary separation was dependent upon D/δ (fig. 61). Therefore, if D is increased and all the other parameters remain the same, one can expect that the location of the most upstream point of the fin's influence on the flow field will move upstream. A downstream movement can be expected when D_s is increased and all the other parameters remain constant.

The stand-off distance of the bow shock wave around a circular cylinder decreases as Mach number is increased (Liepmann and Roshko (1957)). The adverse pressure gradient across the bow shock wave causes the separation of the boundary layer and the characteristic lambda foot is formed. Thus, as the Mach number of the incoming flow increases one would suspect that the most upstream point of the fin's influence on the flow field would move downstream in a similar manner to that for the location of the bow shock wave. This would result in an increase in the propagation angle, ε (see the diagram with Table 6).

The parameter h/δ is believed to be a dominant parameter for these types of interactions. If h is small such that the majority of the strake is immersed in the boundary layer the effects of the strake are expected to be muted. Such a strake is unlikely to influence the flow field to any significant extent. When h is large such that all of the fin is effectively part of the strake, then the flow field generated by the model will be identical to those of a swept fin. The angles at which the fin's influence on the flow field has propagated from the fin / strake interface are tabulated in Table 6. The values for ε for Cases 7 & 9 are identical, as one would expect, but the ε value for Kleifges (1993) is also the same albeit Kleifges (1993) used a much higher Mach number. All of the propagation angles are greater than their corresponding Mach angles and this implies that the disturbance is dependent upon the subsonic flow's properties. The data in Table 6 indicates that as h/δ is increased the propagation angle of the fin's influence on the flow field decreases such that the area of strake dominated flow increases. This suggests that for a given location of the fin's influence on the flow field one particular value of h/δ will satisfy the given condition. Although the value for ε obtained from Kleifges (1993) data is the same as ε for Cases 7 & 9 it is expected that the change in Mach number between the author's and Kleifges' (1993) tests may account for the similarity between the data. As Mach number increases the stand-off distance of the bow shock wave around a cylinder decreases. Thus, one would expect that the position of the upstream influence of the fin on the flow field will move downstream, decreasing ε. Hence, the ε value for a strake of $h/\delta = 1.4$ at Mach 2.43 is expected to be greater than 51°.

The sweep of the strake is also very important, even though it has not been altered during the present experimental investigation into the effects of blunt strakes. Strakes with little or no sweep are unlikely to affect the flow field as their pressure fields will almost match the unmodified fin's. Fins with high sweep angles (fig. 33) do not cause significant effects upon the flow field when they are inserted into flow field independently. Thus, the sweep of the strake has to be moderate and hence, between the

two extremes. Based upon the results for swept fins produced by Hussain (1985) (fig. 33) it is believed that the strake should have at least 30° of sweep and no more than 60° if significant mitigation effects in vortex strength are desired.

On the side view oil flow photograph of the Case 11 fin (fig. 59 (iv)), one can see that the oil flow patterns are by far more complex than those obtained for the models used in Cases 7 & 9. In Cases 7 & 9 (figs. 45 (ii) & 54 (ii)) two jet like flows are discernible however, for the present model three pairs of separation and attachment lines (S_4-S_6 and A_4-A_6) reside in the gap between the upper (the fin "jet") and the lower (the strake "jet") "jet" (see fig. 59 (iv) and then fig. 57 (d)).

The fin "jet's" position and character is reminiscent of the fin "jets" found in Cases 7 & 9 but it the height above the wall at which it resides is greater than the corresponding value for the Case 9 fin. Therefore, we have evidence to conclude that the height at which the fin "jet" resides is a function of h/δ and this evidence supports intuition.

Slightly beneath the fin "jet", a feature unique to this model is located. This feature consists of three pairs of separation and attachment lines (S_4-S_6 and A_4-A_6). The presence of these separation and attachment lines upon the side of the fin indicate that a number of vortices reside outboard of the fin's side (fig. 62 (b)).

When the sharp leading edge strake (Case 5) was incorporated into the junction, it was found that the flow field was dominated by the characteristics of the unmodified fin (compare fig. 63 (i) & (ii)). The unmodified fin generated a number of horseshoe vortices located around its leading edge. The oil flow photograph (fig. 63 (ii)) for the sharp strake suggests that the horseshoe vortices originate from on top of the strake (fig. 63 (ii)). The term "fin vortices" was used to denote these vortices as they were generated through the influence of the unmodified portion of the wing on the flow.

The influence of the unswept portion of the leading edge on the flow field can be seen in the oil flow photographs for Cases 7 & 9 (fig. 63 (iii) & (iv)). It is believed, that the downstream separation and attachment lines denote the presence of a vortex generated due to the presence of the unswept portion of the leading edge (fig. 63 (iii) & (iv)). The horseshoe vortices generated by the strake, in Cases 7 & 9, were located around the base of the strake's leading edge whilst the vortices created through the interaction of the unmodified portion of the fin on the flow field resided downstream of the unswept portion of the leading edge. In both Cases 7 & 9 (fig. 63 (iii) & (iv)) a separation line

denoted by S_3 exists in a manner reminiscent of the pattern produced by S_1 for the unmodified fins but moved downstream (Cases 6 & 8 - see figs. 44 (i) & 53 (i)). In Case 7 the location of this separation line and its accompanying attachment line (S_3 & A_3) were found to correspond to the second hump in the pressure plots and they were found to be dominant in the far field pressure plots where the pressure distributions produced by the modified model reverted to the distribution produced by the unmodified model.

A comparison of the oil flow photographs for Cases 8 & 9 (fig. 53) and Cases 10 & 11 (fig. 59) indicates that the vortices generated upstream of the strake's leading edge are similar to those caused by a wing with identical design parameters to those of the strake. However, in Case 11 there is no separation line that can be deemed to be the direct equivalent of S_3 in Cases 7 & 9 but there are a number of separation lines on the side of the fin which appear to originate from around the junction of the strake and the unswept portion of the model. Such separation lines are not present in the oil flow patterns for any of the other fins and so it appears that as h/δ is increased the "fin vortices" no longer interact with the wall but they lift off the wall to relocate themselves on the side of the fin (fig. 62 (b)).

Towards the base of the model the path taken by the strake "jet" is evident (fig. 59 (iv)). The strake "jet" has created an oil flow pattern which is identical to that for a wing of identical D/δ and λ (see fig. 59 (iii)) until 0.1" (0.65D) downstream of the leading edge of the unswept fin (fig. 57 (c)). After this point which is also equivalent to the local height maxima of the strake "jet", the influence of the outboard portion of the wing on the strake "jet" is clearly identifiable as the strake "jet" descends and creates a plateau which extends to the model's trailing edge (fig. 57 (d)). Clearly, the value of h/δ affects the relative location of the fin "jet" and the strake "jet", and the presence of any separation or attachment lines between the two "jets".

Analysis of the schlieren images (fig. 60 (ii)) of the flow in the root region indicates that the separation shock is contained within 0.5D upstream of the strake's leading edge root. This length scale is in good agreement with the results for the swept fins (Cases 3, 8 & 10) and those for the blunt strakes (Cases 7 & 9) (see Table 4). The majority of the separation shock's unsteadiness occurs within the boundary layer and the portion of the strake shock outside of the boundary layer can be considered reasonably stable.

4. Conclusions

An experimental investigation into the effects of strakes and fillets on the glancing shock wave / turbulent boundary layer interaction produced by hemi-cylindrically blunted fins was conducted. The investigation was at a Mach number of about 2.45 and at Reynolds numbers ($R_{e\delta}$) of 4.1×10^4 and 5.8×10^4. A number of fins with a variety of diameters and sweep angles were utilised during the course of the research. A number of modifications were investigated including ramp-type fillets, sharp leading edge strakes and blunt leading edge strakes. The study involved mean static pressures measured on the side wall, surface oil flow pictures taken over the side wall and the fin, and schlieren pictures taken in two planes normal to each other. In addition, laser light sheet flow visualisation and high speed ciné films were taken of the shock systems produced by some of the models.

A. The Effects of Filleting the Junction

1. Fins with Zero Sweep

The fillet tested :

- did not eradicated separation nor did it improve the flow field properties.
- produced a more highly complex flow field,
- induced an upstream movement of the primary separation line and increased the disturbed flow area.

2. Fins with Sweep

The fillet attached to the swept fin produced similar results to the fillet attached to the straight wing except for its effects upon the shock system's unsteadiness. Upon the addition of the fillet to the swept wing the root of the shock system no longer consisted of a lambda foot but two invisicd shock waves. The two inviscid shock waves both exhibited local unsteadiness at their roots (i.e. the fillet / wall and the fillet / fin interfaces) whereas the unmodified swept fin's shock system displayed unsteadiness from the triple point and below.

B. The Effects of Incorporating Strakes into the Junction

1. Sharp Leading Edge Strakes

The incorporation of a sharp leading edge strake into the wing / fuselage junction resulted in :

- the creation of two regions of flow ("strake" and "fin" dominated) in which the two different components of the wing dominated the flow field structure,

- the length scale of the triple point's motion being attenuated and the separation shock wave became more stable,

2. Blunt Leading Edge Strakes

When a blunt leading edge strake was incorporated into the junction it affected the flow field such that :

- there are regions of both "strake" and "fin" dominated flow and the flow in each of these regions mirrors the flow field generated by the components of the wing when used independently, and,

- fitting a blunt strake to the leading edge of the wing reduced the unsteadiness of the flow field.

The data from all of the strake models indicate that the key to improving the flow field's characteristics via the employment of strakes, is the appropriate choice of the strake sweep angle, bluntness and height. To achieve worthwhile improvements in the flow field's properties the strake must have a height of at least 1.5δ, between 30 and 60 degrees of sweep and a diameter equivalent to the fin's diameter.

Recommendations for Future Work

There are two paths which further investigations can follow. Firstly, the understanding of the flow field can be improved and secondly, the benefits of applying strakes to aircraft should be investigated.

Issues that may be investigated under the former category are :

1. The off centre-line characteristics of the flow field could be visualised in order to give greater understanding of the vortex paths. Laser flow visualisation systems could prove to be an invaluable tool during these investigations. Additionally, water tunnels may be able to yield some qualitative data which may aid the interpretation of supersonic data.

2. The origin of the vortex V_5 in Case 7 needs to be clarified. Further discussion on this issue can be found in Case 7.

3. The pulsation effect noted in the cine films for Cases 1 & 5 needs to be further examined. It is unknown whether this is caused by wind tunnel effects (when loaded with essentially the Case 1 model) or whether the pulsation effect is induced by some flow field property.

It is suggested that research assessing the benefits of using strakes on aircraft considers the following points :

1. Data indicating that strakes can weaken the vortex field around a blunt fin has been presented. However, the effects of strakes on the drag, lift and pitching moment of an aircraft is unknown. The influence of strakes on these parameters needs to be investigated.

2. Aeroplanes operating at supersonic speeds usually have swept wings. Thus, the influence of sweep upon the strake's design parameters needs to be investigated.

References

Alvi, F. S., and Settles, G. S., "A Physical Model of the Swept Shock / Boundary Layer Interaction Flow Field", AIAA 91-1768, 1991.

Baker, A. J., "The CMC:3DPNS Computer Program for Prediction of Three Dimensional Subsonic Turbulent Aerodynamic Juncture Region Flow" NASA CR 3645, November 1982.

Baker, C. J., "The Laminar Horseshoe Vortex" J. Fluid Mech., Vol. 95, No. 2, 1979.

Beckwith, I. E., "Experimental Investigation of Heat Transfer and Pressures on a Swept Cylinder in the Vicinity of its Intersection with a Wedge and Flat Plate at Mach Number 4.15 and High Reynolds Numbers" NASA TN D-2020, 1964.

Bhargava, R. K. and Rishi, S. R., "An Experimental Study of Near Wall Flow Parameters in the Blade End-Wall Corner Region" NASA CR 4211, 1989.

Blank, S. C., "Glancing Interaction", MSc Thesis, College of Aeronautics, Cranfield Institute of Technology, 1991.

Boatwright, D. W., "An Experimental Investigation of Fillet Design For Application to Airship Fins" Research Note 12, Aerophysics Department, Mississippi State University, November 1960.

Bradshaw, P., "Compressible Turbulent Shear Layers", Ann. Rev. Fluid Mechanics, Vol. 9, p. 33-54, 1977.

Burke, R. W, "Numerical Calculation of Appendage Flat Plate Junction Flow" DTNSRDC Report 87/002, September 1987.

Bushnell, D. M., "Interference Heating on a Swept Cylinder in the Region of its Intersection with a Wedge in Hypersonic Flow" NASA TN D-3094, 1965.

Bushnell, D. M., "Effects of Shock Impingement and Other Factors on Leading Edge Heat Transfer" NASA TN D-4544, April 1968.

Bushnell, D. M., The 32nd Lanchester Lecture "Longitudinal Vortex Control - Techniques and Applications", Aeronautical Journal, Oct. 1992.

Chen, C. L. and Hung, C. M., "Numerical Study of Juncture Flows" AIAA 91-1660, 1991.

Creel, T. R., and Hunt, J. L., "Photographing Flow Fields and Heat Transfer Patterns Simultaneously" Astronautics & Aeronautics, pp. 54-55, April 1972.

Devenport, W., Agarwal, N., Dewitz, M., Simpson, R. and Poddar, K., "Effects of Fillet on the Flow Past a Wing Body Junction" AIAA J. December 1990 Vol. 28, No. 12, pp. 2017-2024 and AIAA 89-0986, 1989.

Devenport, W. J., Simpson, B. L., Dewitz, M. B. and Agarwal, N. K., "Effects of Strake on the Flow Past a Wing Body Juncture" AIAA Paper 91-0252 and AIAA Jnl. 30, No. 9., September 1992

Dickman, C. C., "Glancing Interaction with a Turbulent Boundary Layer" College of Aeronautics Memo 7706, Cranfield Institute of Technology, AFOSR-76-3006, 1977.

Dolling, D. S., "Unsteadiness of Supersonic and Hypersonic Shock Induced Turbulent Boundary Layer Separation", AGARD Report 764 - Special Course on Three-Dimensional Supersonic / Hypersonic Flows Including Separation. FDP/VKI/CPP, 1989.

Dolling, D. S., "Fluctuating Loads in Shock Wave / Turbulent Boundary Layer Interaction : Tutorial and Update", AIAA 93-0284, 1993.

Dolling, D. S., and Bogdonoff, S. M., "An Experimental Investigation of the Unsteady Behaviour of Blunt Fin Induced Shock Wave Turbulent Boundary Layer Interactions" AIAA 81-1287, 1981.

Dolling, D. S., and Bogdonoff, S. M., "Blunt Fin Induced Shock Wave Turbulent Boundary Layer Interaction", AIAA J. Vol. 20, pp. 1674-1680, December 1982.

Dolling, D. S., and Narlo, J. C., "Driving Mechanism of Unsteady Separation Shock Motion in Hypersonic Interactive Flow", AGARD CP 428, Paper 7, 1987.

Dolling, D. S., and Rodi, P. E., "Upstream Influence and Separation Scales in Fin-Induced Shock Turbulent Boundary Layer Interaction", J. of Spacecraft and Rockets, Vol. 25, No. 2, March-April 1988.

Dolling, D. S., and Smith, D. R., "Separation Shock Dynamics in Mach 5 Turbulent Interactions Induced by Cylinders", AIAA Jnl. Vol. 27, No. 12, pp. 1698-1706, Dec. 1989.

East, L. F., and Hoxley, R. P., "Boundary Layer Effects in an Idealised Wing Body Junction at Low Speeds", RAE TR. 68161, 1968.

Edney, B. E., "Anomalous Heat Transfer and Pressure Distributions on Blunt Bodies at Hypersonic Speeds in the Presence of an Impinging Shock" FFA Report 115, The Aeronautical Research Institute of Sweden, Stockholm, Sweden, February 1968.

Erengil, M. E., and Dolling, D. S., "Effects of Sweepback on Unsteady Separation in Mach 5 Compression Ramp Interactions", AIAA 92-0430, 1992.

Fomison, N. R., "The Effects of Bluntness and Sweep on Glancing Shock Wave Turbulent Boundary Layer Interaction", PhD Thesis, College of Aeronautics, Cranfield Institute of Technology, 1986. See also Fomison, N. R. and Stollery, J. L., "The Effects of Sweep and Bluntness on a Glancing Shock Wave Turbulent Boundary Interaction", AGARD CP 423, 1987.

Fulker, J. L., Ashill, P. R., and Shires, A., "A Theoretical and Experimental Investigation of the Flow Over Supersonic Leading Edge Wing / Body Configurations", The 1993 European Forum on Recent Developments and Applications in Aeronautical CFD, Bristol 1993.

Gonsalez, J. C., and Dolling, D. S, "Correlation of Interaction Sweepback Effects on the Dynamics of Shock-Induced Turbulent Separation", AIAA 93-0776, 1993.

Gramann, R. A., and Dolling, D. S., "Unsteady Separation in Shock Wave Turbulent Boundary Layer Interaction", AIAA 86-1033, 1986.

Green, J. E., "Interactions Between Shock Waves and Turbulent Boundary Layers", Prog. in Aero. Sci., Vol. 11, Ed. D. Kuchemann, 1970.

Gulbran, C. E., Redeker, E., Miller, D. S. and Strack, S. L., "Heating in Regions of Interfering Flow Fields, Part II : Leading Edge Shock Impingement" AFFDLM TR. 65-49, January 1967.

Guta, A. K., "Hydrodynamic Modification of the Horseshoe Vortex at a Vertical Pier Junction with Ground" Phys. Fluids, Vol. 30, No. 4, April 1987.

Haines, A. B., "Aerodynamic Interference - A General Overview" AGARD Report 712, 1983.

Hains, F. D., and Keyes, J. W., "Shock Interference Heating in Hypersonic Flows" AIAA J. Vol. 10, No. 11, pp. 1441-1447, November 1972.

Haq, Z. U., "Hypersonic Vehicle Interference Heating", PhD Thesis, Department of Aeronautics and Astronautics, University of Southampton, August 1993.

Hiers, R. S. and Loubsky, W. J., "Effects of Shock Wave Impingement on the Heat Transfer on a Cylindrical Leading Edge" NASA TN D-3859, February 1967.

Hoerner, S. F., "Fluid Dynamic Drag", published by the author 1965.

Hubbart, J., McMahon, H. and Oguz, E., "Exploratory Tests of Flow in Wing Root Junctures" Lockheed-Georgia, Order No. CK27034P, March 1976.

Hung, C. M., and Buning, P. G., "Simulation of Blunt Fin Induced Shock Wave and Turbulent Boundary Layer Interaction", J. Fluid Mech. Vol. 154, pp. 163-185 and AIAA 84-0457, 1984.

Hussain, S., "A Study of the Interaction Between a Glancing Shock Wave and a Turbulent Boundary Layer - The Effects of Leading Edge Bluntness and Sweep", PhD Thesis, College of Aeronautics, Cranfield Institute of Technology, November 1985.

Jacobs, E., N., and Ward, K. E., "Interference of Wing and Fuselage From Tests of 209 Combinations in the NACA Variable Density Tunnel", NACA Report No. 540, 1935.

Jupp, J. A., "Interference Aspects of the A 310 High Speed Wing Configuration" AGARD CP 285 Subsonic / Transonic Configuration Aerodynamics, 1980.

Keyes, J. W., and Hains, F. D., "Analytical and Experimental Studies of Shock Interference Heating in Hypersonic Flows", NASA TN D-7139, May 1973.

Kleifges, K., "An Experimental Investigation of the Effects of Leading Edge Geometry on the Dynamics of Blunt Fin-Induced Shock Wave Turbulent Boundary Layer Interaction", MSE Thesis, The University of Texas at Austin, May 1993.

Koide, S, and Stollery, J. L., "Effects of Junction Modifications on Sharp Fin Induced Shock Wave / Boundary Layer Interaction", AIAA 93-2935, 1993.

Korkegi, R. H., "Survey of Viscous Interactions Associated with High Mach Number Flight", AIAA J. Vol. 9, No. 5, May 1971, pp. 771-784, May 1971.

Krenz, G., "Transonic Configuration Design", AGARD Report 712, 1983.

Kubendran, L. R., "Study of Turbulent Flow in a Wing Fuselage Type Junction" PhD Dissertation, Georgia Institute of Technology, 1983.

Kubendran, L. R., McMahon, H. M. and Hubbartt, J. E, "Turbulent Flow Around a Wing Fuselage Type Junction" AIAA 85-0400, 1985.

Kubendran, L. R., Bar-Sever, A. and Harvey, W. D., "Flow Control in a Wing Fuselage Type Juncture", AIAA Paper 88-0614, 1988.

Kubendran, L. R., Sung, C. H. and Yang, C. I., "Experiments and Code Validation for Juncture Flows" Paper P11-1, AGARD CP-437, 1988.

Kubota, H., "A Flow Field Model of the Glancing Shock Turbulent Boundary Layer Interaction", AFOSR-76-300613,CIT-COA-M-7907, 1979.

Kubota, H., "Investigation of Three Dimensional Shock Wave Boundary Layer Interactions", PhD Thesis, College of Aeronautics, Cranfield Institute of Technology, 1980.

Lakshmanan, B., Tiwari, S. N. and Hussaini, M. Y., "Control of Supersonic Intersection Flow Fields Through Filleting and Sweep" AIAA 88-3534, July 1988. See also Lakshmanan, B., Tiwari, S. N. and Hussaini, M. Y., 1988, "Control of Supersonic Interaction Flow Fields Through Filleting and Sweep", AIAA/ASME/SIAM/APS First National Fluid Dynamics Congress, July 1988.

Levy, R., "Analysis of the Submarine Appendage Flow Field" SRA Report R88920028-F (AD-A212344), 1988.

Liepmann, H. W., and Roshko, A, "Elements of Gas Dynamics", John Wiley & Sons Inc., 1957.

McConnell, J. M., "New Soviet Methods for Anti-Submarine Warfare", Naval War College Review, pp 16-27, July-August, 1985.

McMaster, D. L. and Shang, J. S., "A Numerical Study of Three Dimensional Separated Flows Around a Sweptback Blunt Fin" AIAA 88-0125, 1988.

Mehta, R. D., "Effect of Wing Nose Shape on the Flow in a Wing/Body Junction" Aeronaut. J. Vol. 88, December 1984.

Newlander, R. A., "Effect of Shock Impingement on the Distribution of Heat Transfer Coefficients on a Right Circular Cylinder at Mach Numbers of 2.65, 3.51 and 4.44" NASA TN D-642, January 1961.

Niedoroda, A. W. and Dalton, C., "A Review of the Fluid Mechanics of Ocean Scour" Ocean Eng., Vol. 9 No. 2, 1982.

Nielson, J. N., "Non-Linearities in Missile Aerodynamics", AIAA Paper 78-20, 1978.

Ohring, S., "Appendage Flow Computations Using the INS3D Computer Code" DTRC Report 89/028, October 1989 (AD-A215689).

Partala, A., "Possibilities of Radar Detection of Submarines From Space", Morskoy Sbornik, 1985.

Peake, D. J., and Tobak, M., "Three Dimensional Interactions and Vortical Flows with Emphasis on High Speeds" AGARDograph No. 252, 1980.

Poisson-Quinton, P., "Energy Conservation Aircraft Design and Operational Procedures", AGARD LS 96, Aircraft Engine Future Fuels and Energy Conservation, 1978.

Price, A. E., and Stallings, R. L., "Investigation of Turbulent Separated Flows in the Vicinity of Fin Type Protuberances at Supersonic Mach Numbers", NASA TN-D-3804, 1967.

Rao, D. M., and Campbell, J. F., "Vortical Flow Management Techniques" Prog. Aero. Sci., Vol. 24, pp. 173-224, 1987.

Saida, N., and Hattori, H., "Shock Wave-Turbulent Boundary Layer Interactions Induced by a Blunt Fin", Transactions of the Japan Society for Aeronautical and Space Sciences, Vol. 27, No. 76, 1984.

Schmisseur, J. D., and Dolling, D. S., "Unsteady Separation in Sharp Fin-Induced Shock Wave / Turbulent Boundary Layer Interaction at Mach 5", AIAA 92-0748, 1992.

Sedney, R., and Kitchens, C. W., "The Structure of Three-Dimensional Separated Flows in Obstacle, Boundary Layer Interactions", AGARD CP 168, No. 37, May 1975.

Sedney, R., and Kitchens, C. W., "Separation Ahead of Blunt Protuberances in Supersonic Turbulent Boundary Layers", AIAA J., Vol. 15, No. 4, 1977.

Skow, A. M. and Erickson, G. E., "Modern Fighter Aircraft Design for High Angle of Attack Manoeuvring" Paper 4, AGARD LS 121, 1982.

Stollery, J. L., "Glancing Shock - Boundary Layer Interactions", AGARD Report No. 764 - Special Course on Three-Dimensional Supersonic / Hypersonic Flows Including Separation. FDP/VKI/CPP, 1989.

Stollery, J. L., Fomison, N. R., and Hussain, S., "The Effects of Sweep and Bluntness on Glancing Interaction at Supersonic Speeds", ICAS 86-1.2.1, 1986.

Stone Jr, R. W. and Polhamus, E. C., "Some Effects of Shed Vortices on the Flow Fields Around Stabilising Tail Surfaces", AGARD Report 108, 1957.

Sung, C. H., and Lin, C. W., "Numerical Investigation on the Effect of Fairing on the Vortex Flows Around Airfoil / Flat-Plate Junctions", AIAA 88-0615, 1988.

Sung, C. H., Griffin, M. J., and Coleman, R. M., "Numerical Evolution of Vortex Flow Control Devices" AIAA 91-1825, 1991.

Sung, C. H., Yang, C. I. and Kubendran, L. R., "Control of Horseshoe Juncture Flow Using Fillet" Proceedings from Symposium on Hydrodynamic Performance Enhancement for Marine Applications, Newport, RI, October 31-November 1 1988.

Sutton, E. P., In "Incompressible Aerodynamics", B. Thwaites, Oxford at the Clarendon Press, 1987.

van Driest, E. R., "Turbulent Boundary Layer in Compressible Fluids", J. Aero. Sci., Vol. 18, p. 145-160, 1957.

Visbal, M. R., "Numerical Investigation of Laminar Juncture Flows" AIAA 89-1873, 1989.

Wettern, D., "Soviet SSNs Close the Acoustic Gap", Jane's Defence Weekly, 5 September, 1987.

Woo, H. G. C., Paterka, J. A. and Cermak, J. E., "Wind Tunnel Measurements in the Wakes of Structures" NASA CR 2806, 1977.

Young, F. L., Kaufmann, L. G., and Koregi, R. H., "Experimental Investigation of Interactions Between Blunt Fin Shock Waves and Adjacent Boundary Layers at Mach Numbers 3 and 5", ARL 68-0214, 1968.

Appendix A : The YNU Ray Tracing Method

YNU ray tracing is a simple yet quite accurate method for tracing the path of paraxial light rays through an optical system. It was developed at and is used extensively by the Institute of Optics at the University of Rochester. Before describing this technique, a set of conventions must be defined:

1. A right hand co-ordinate system applies with the z axis defining the optical axis, positive y direction upward on the page from z, and positive x into the plane of the page.

2. Light initially enters the system from the left.

3. Surface curvatures are positive if the centre of curvature lies to the right of the surface, negative if it lies to the left. This convention applies to both lens and mirror surfaces.

4. Surfaces are numbered in the sequence they are encountered by an entering light ray.

5. Thicknesses or separations are positive if a high numbered surface lies to the right of a low numbered surface, negative to the left.

6. Primes (') are used to differentiate variables pertaining to the physical conditions (index of refraction, ray angles, etc.) beyond a surface, from the conditions before.

7. Refractive indices are positive if the ray travels through a space from left to right, negative when travelling right to left.

8. Angles inclining relative to the optical axis are positive; declining negative.

It can be shown that a paraxial ray of height y with an angle of inclination to the optical axis of u strikes a spherical surface of radius r_c with an angle of incidence (fig. A1)

$$\theta = y / r_c + u$$

Substituting this into the paraxial form of Snell's Law this yields the "refraction equation":

$$n'u' = nu - y\phi$$

where we have defined the "surface power" ϕ:

$$\phi = \frac{n' - n}{r_c}$$

If after refracting the ray travels a distance t within the optical material it will encounter the next surface at a height predicted by the "translation formula":

$$y_2 = y_1 + tu$$

whereupon it will again refract. Sequentially applying these formulae at and between each surface of a given optical system for a specified entering ray yields an accurate prediction of the path that the ray will follow.

To further simplify this procedure, a YNU Ray Trace Worksheet has been developed by the University of Rochester (fig. A2). Use of this chart involves:

1. Entering the lens or lens system data in the top part of the chart (Part A).

2. Calculating the quantities in the middle part of the chart (Part B). If the effect of a thin lens is to be traced, it is necessary only to insert $\phi = 1/f$ directly in Part B to completely account for its effect.

3. Initialising a ray height (y_0) and angle (u_0) at any point within the lens in Part C.

The ray can then be translated or refracted as required by :

4. Multiplying it by the number directly above it in Part B.

5. Adding to the product obtained the value above or below it and one-half space to the left in Part C; and,

6. Recording this (the desired) value one-half space to the right in Part C.

This process is repeated sequentially until the entire system has been traversed. By the principle of reversibility of light, it may also be carried out in reverse to work backward through a lens system.

The design conditions for the laser light flow visualisation system used were :

1. The diameter of the laser beam was assumed to be 2 mm, hence y_0 was set to be 1 mm.
2. The laser beam's axis was parallel to the optical axis and therefore u_0 was equivalent to 0.
3. The physical geometry of the experimental rig set a minimum value for t_{78} to be 10 inches (see fig. 24 (c)).
4. For the spherical lenses the distance between the intersection points of the laser beam and the lens surface was assumed to be equivalent to the lens' thickness. Hence, t_{01} and t_{23} were the same as the lens' thickness. However, for cylindrical lenses there is a significant variation between the thickness of the lens and the distance between the intersection points. As a rough first approximation the lens thickness was used but

the values of t_{45} and t_{67} were modified during the iteration process necessary to select the component lenses.

5. The minimum value that y_8 could attain was determined as 40 mm. This parameter determined the semi-height of the scattered laser beam inside the working section of the tunnel.

The YNU Ray Trace Worksheet

Part A	Surface radius, r_c	r_0	r_1	r_2	r_3
	Thickness or separation, t		t_1	t_2	t_3	t_4
	Refractive index, n		n_1	n_2	n_3	n_4
Part B	$-\phi_2 = \frac{n - n'}{r_c}$			$-\phi_2 = \frac{n_2 - n_3}{r_2}$	
	$\frac{t}{n}$	+	$\frac{t_1}{n_1}$	+	×
Part C	y		y_0 ×	y_1 =	y_2
	nu		n_1u_1	n_2u_2 =	n_3u_3

Fig. A1. Worksheet for carrying out the YNU Method of Paraxial Ray Tracing.

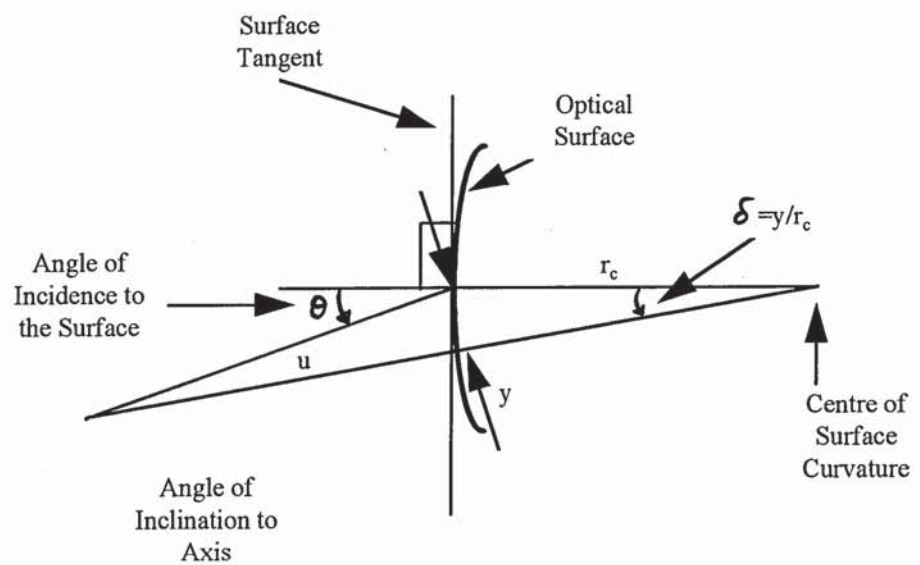


Fig. A2. Illustration of the Angle of Incidence of an Optical Surface made by a Paraxial Ray.

Tables and Figures

Table 1. Applications of Longitudinal Vortex Control

Applications Control	Vortex Source	Issue Requiring Vortex Control
1. Transport aircraft	Wing tip Flap (salient) edges Intersection regions	Wake vortex hazard Drag due to lift enhancement Vortex interactions with engine exhausts. Drag reduction, incl. pressure drag, drag due to lift, friction drag.
2. Agricultural aircraft	Wing tip Flap (salient) edges	Chemical disposition
3. Submersibles	Body Intersection regions Tips	Acoustic & non-acoustic stealth, drag, cavitation, vibration, observables.
4. Turbomachinery	Blade tips Intersection regions	Drag / performance Heat transfer
5. Missiles	Intersection regions	Controllability, drag.
6. Fighter aircraft	Intersection regions LEX	Vortex bursting, tail / buffet fatigue, controllability. Inlet / engine vortex ingestion / distortion.
7. Hypersonic lifting bodies	Nose Body Intersection regions	Lee surface induced interference Heat transfer

Table 2. Wind Tunnel Tests

(a) Tests conducted in the 9" x 9" Continuous Supersonic Wind Tunnel

Case No.	Description	Oil Flow	Horizontal Schlieren	Vertical Schlieren	Mean Static Pressure	High Speed Photography (4 kHz Cine film)	Laser Flow Visualisation
1	Unswept, D/δ= 1.6	*Y*	*Y*	*Y*	*Y*	*Y*	*Y*
2	Case 1 + Fillet	*Y*	*Y*	*Y*	*Y*	N	N
3	Swept, D/δ= 1.6	*Y*	*Y*	*Y*	*Y*	N	N
4	Case 3 + Fillet	*Y*	*Y*	*Y*	*Y*	N	N
5	Case 1 + Sharp Strake	*Y*	*Y*	*Y*	*Y*	*Y*	*Y*
6	Unswept, D/δ =0.6	*Y*	*Y*	*Y*	*Y*	*Y*	N
7	Case 6 + Blunt Strake	*Y*	*Y*	*Y*	*Y*	*Y*	N

(b) Tests conducted in the 2.5" x 2.5" Intermittent Supersonic Wind Tunnel

Case No.	Description	Oil Flow	Vertical Schlieren
8	Independent Strake of h/δ=1.6	*Y*	*Y*
9	Strake of h/δ=1.6 + Wing	*Y*	*Y*
10	Independent Strake of h/δ=3.2	*Y*	*Y*
11	Strake of h/δ=3.2 + Wing	*Y*	*Y*

Table 3. YNU Ray Tracing Method Results for the LFV System used in the 9"x9" Wind Tunnel.

Lens	Manufacturer	Catalogue No.	r_1	r_2	t	n
S_1	Newport	KBX022	11.86	11.86	6.68	1.523
S_2	Newport	KBX055	64.22	64.22	5.54	1.523
C_1	Newport	CKX019	∞	9.82	5.33	1.517
C_2	Ealing Electro-optics	23-7416	∞	52.03	8.00	1.523

Notation

n Refractive index of the lens material
r Surface radius of the lens. Subscript 1 denotes the side facing the laser beam.
t Thickness of the lens.

Note

This chart for the lenses was developed from the *YNU Ray Tracing Method* developed by the Institute of Optics at the University of Rochester.

Table 4. The Interactions' Length Scales

(a) The Present Series of Tests

Case Number	Wind Tunnel	Fin Description	Separation Shock's Length Scale	Triple Point's Vertical Motion Length Scale
1	9"x9"	D=1", Unswept	D	δ
2	9"x9"	Case 1 + Fillet	D	0.9 - 1.3δ #
3	9"x9"	D=1", 45° Sweep	0.5D	-
4	9"x9"	Case 3 + Fillet	-	-
5	9"x9"	Case 1 + Sharp Strake	2D	0.8δ
6	9"x9"	D=0.375", Unswept	1.25D	0.27δ
7	9"x9"	Case 6 + Blunt Strake	0.5D	0.13δ
8	2.5"x2.5"	D=0.157", h/δ=1.6, 45 ° Sweep, Strake Only	0.5D	-
9	2.5"x2.5"	Case 8 + Unswept Fin	0.5D	-
10	2.5"x2.5"	D=0.157", h/δ=3.2, 45 ° Sweep, Strake Only	0.5D	-
11	2.5"x2.5"	Case 10 + Unswept Fin	0.5D	-

(b) Comparison to Other Researcher's Data for the Straight (Unmodified) Fins

Model	Length Scales		M	Re /m x10^7	D mm	D/δ	δ mm	δ* mm	θ mm
	Separation Shock	Triple Point							
Dolling and Bogdonoff (1981)	D	-	2.95	6.3	12.7, 25.4	0.12 to 1.26	3, 4.2, 5.2, 16	-	-
Blank (1991)	D	0.2δ	2.3	1.0	4.08	0.68	6	1.78	.38
Case 1	D	δ	2.45	0.26	25.4	1.6	15.8	3.8	1.01
Case 6	1.25D	0.27δ	2.45	0.26	9.5	0.6	15.8	3.8	1.01

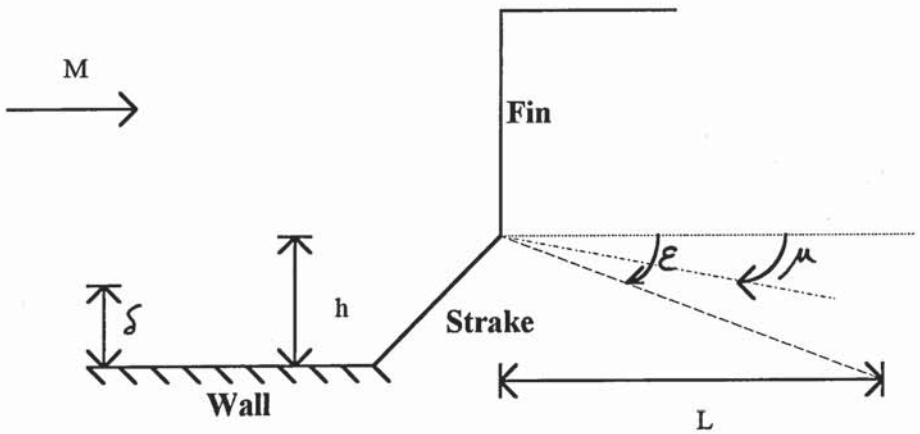
Table 5. Data Table for the Strake / Fin Combinations

Model	D/δ	h/δ	L/δ	M	Re_δ x 10^3	δ in inches	δ^* in inches	θ in inches	H
Case 5	1.6	1.6	-1.9	2.45	41.6	0.625	0.15	0.040	3.75
Case 7	0.6	1.6	1.3	2.45	41.6	0.625	0.15	0.040	3.75
Case 9	0.682	1.6	1.3	2.43	57.3	0.23	0.07	0.015	4.667
Case 11	0.682	3.2	4.2	2.43	57.3	0.23	0.07	0.015	4.667
Kleifges (1993)	1.27	1.4	1.14	4.95	717	0.59	0.26	0.026	10

Dependent upon the choice of measuring criteria (compression waves or distinct shock waves).

Table 6. Disturbance Propagation Angles for the Strake / Fin Combinations

Model	D/δ	h/δ	L/δ	M	tan ε	ε degrees	μ degrees
Case 7	0.6	1.6	1.3	2.45	1.23	51	22
Case 9	0.682	1.6	1.3	2.43	1.23	51	22
Case 11	0.682	3.2	4.2	2.43	0.76	37	22
Kleifges (1993)	1.27	1.4	1.14	4.95	1.28	51	11



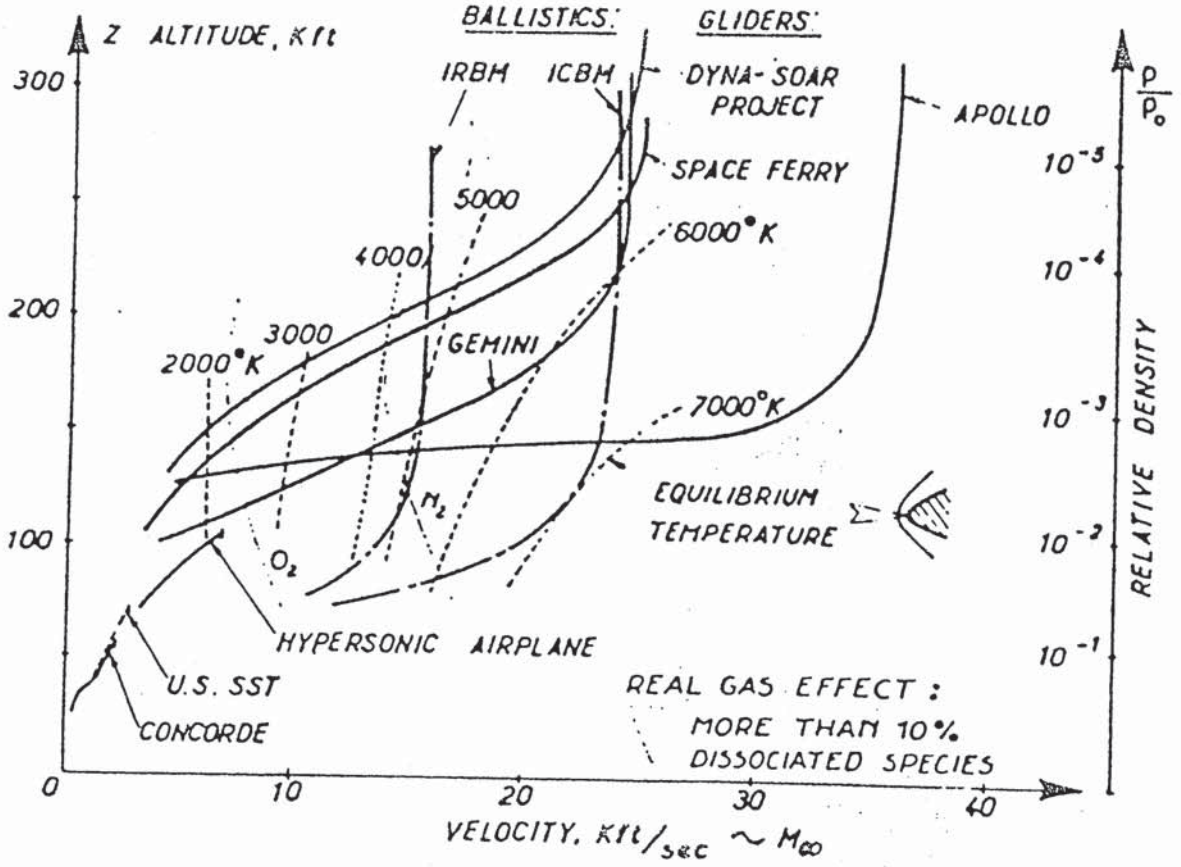


Fig. 1. Flight corridors for typical high speed vehicles with indications of the equilibrium stagnation temperature and the onset of air dissociation encountered at high speed (from Poisson-Quinton (1978)).

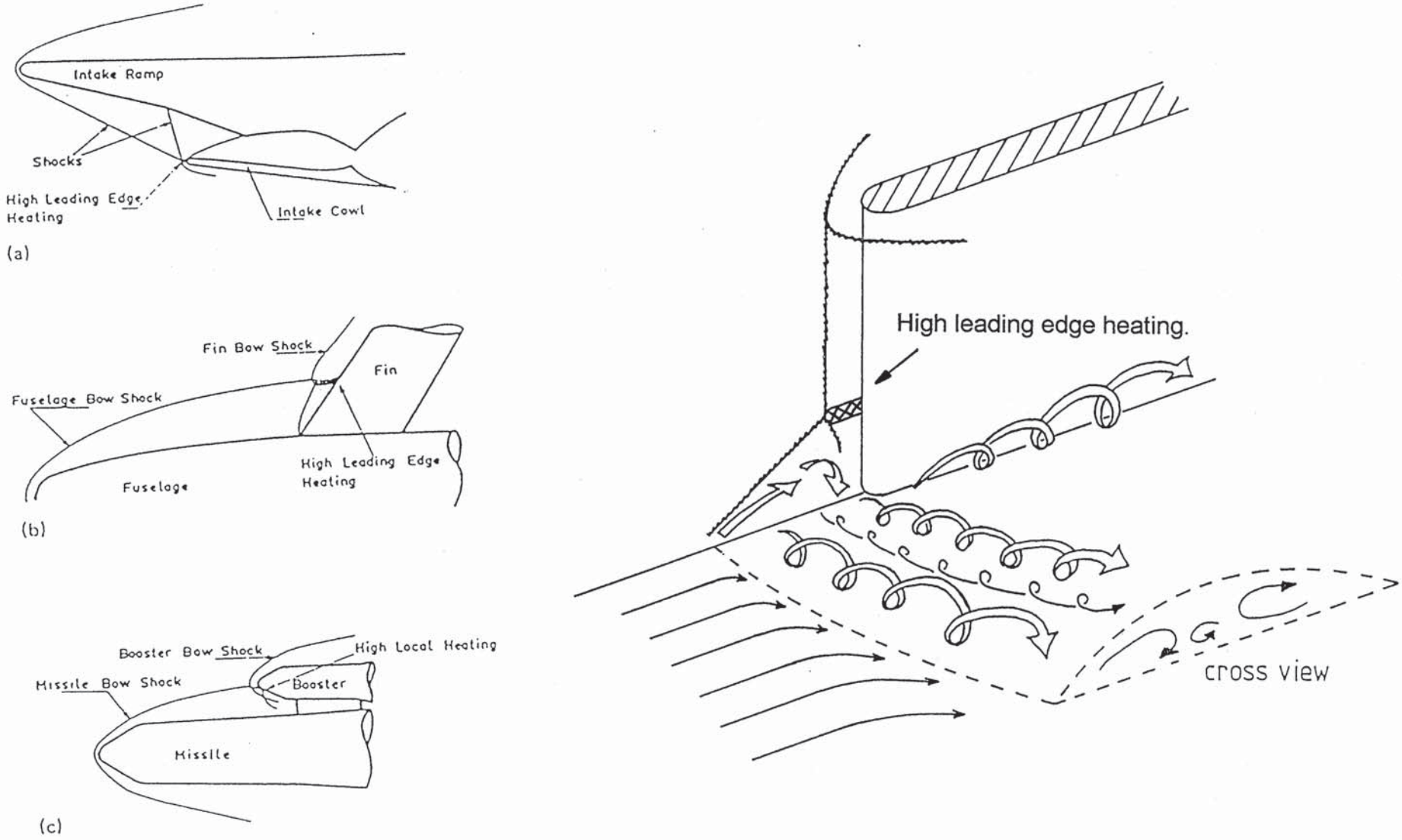


Fig. 2. Practical examples of shock-impingement heating
(from Edney (1968) (left) and Kaufman et al
(AIAA J. Vol. 11, p. 1363-64 (1974)) (right)).

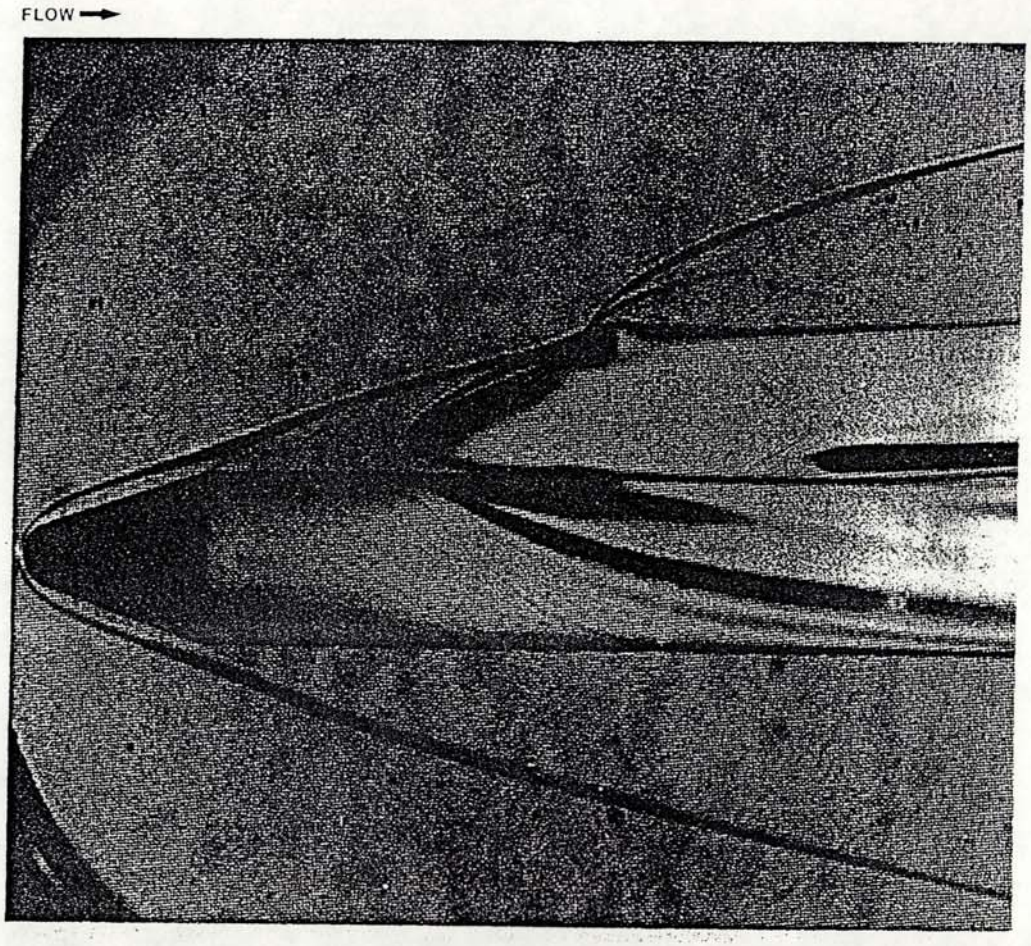
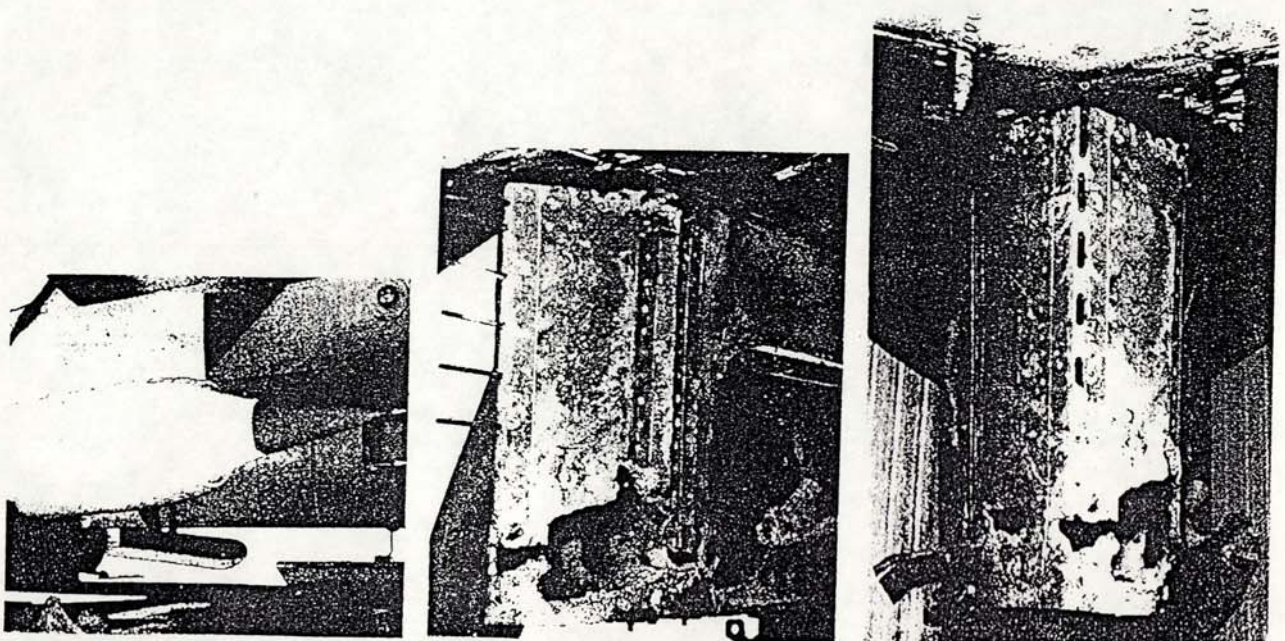


Fig. 3. Combined schlieren and phase-change coating techniques revealing shock-on-shock interactions and aerodynamic interference heating (from Peake and Tobak (1980)).

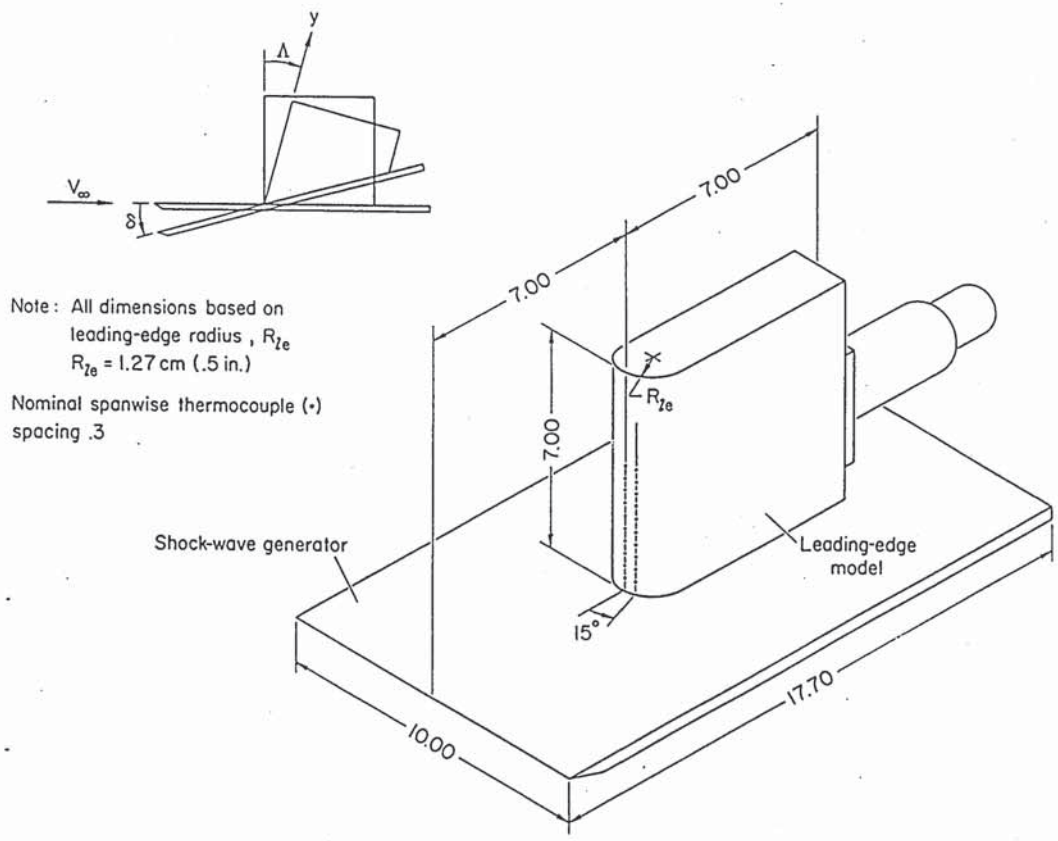


(a) RAM JET MODEL MOUNTED ON VENTRAL FIN OF X-15A-2 AIRCRAFT PRIOR TO TEST FLIGHT. (PHOTO COURTESY OF NASA)

(b) SIDE VIEW OF VENTRAL FIN SHOWING DAMAGE DUE TO SHOCK IMPINGEMENT. (PHOTO COURTESY OF NASA)

(c) FRONT VIEW OF VENTRAL FIN SHOWING DAMAGE DUE TO SHOCK IMPINGEMENT. (PHOTO COURTESY OF NASA)

Fig. 4. Damage to ventral fin on NASA X-15A-2 aircraft from shock impingement (from Peake and Tobak (1980)).



(a) The shock generator used by Hiers and Loubsky (1967).

Fig. 5. Effect of shock impingement on fin leading edge heat transfer at $M_\infty = 14$ (from Hiers and Loubsky (1967)).

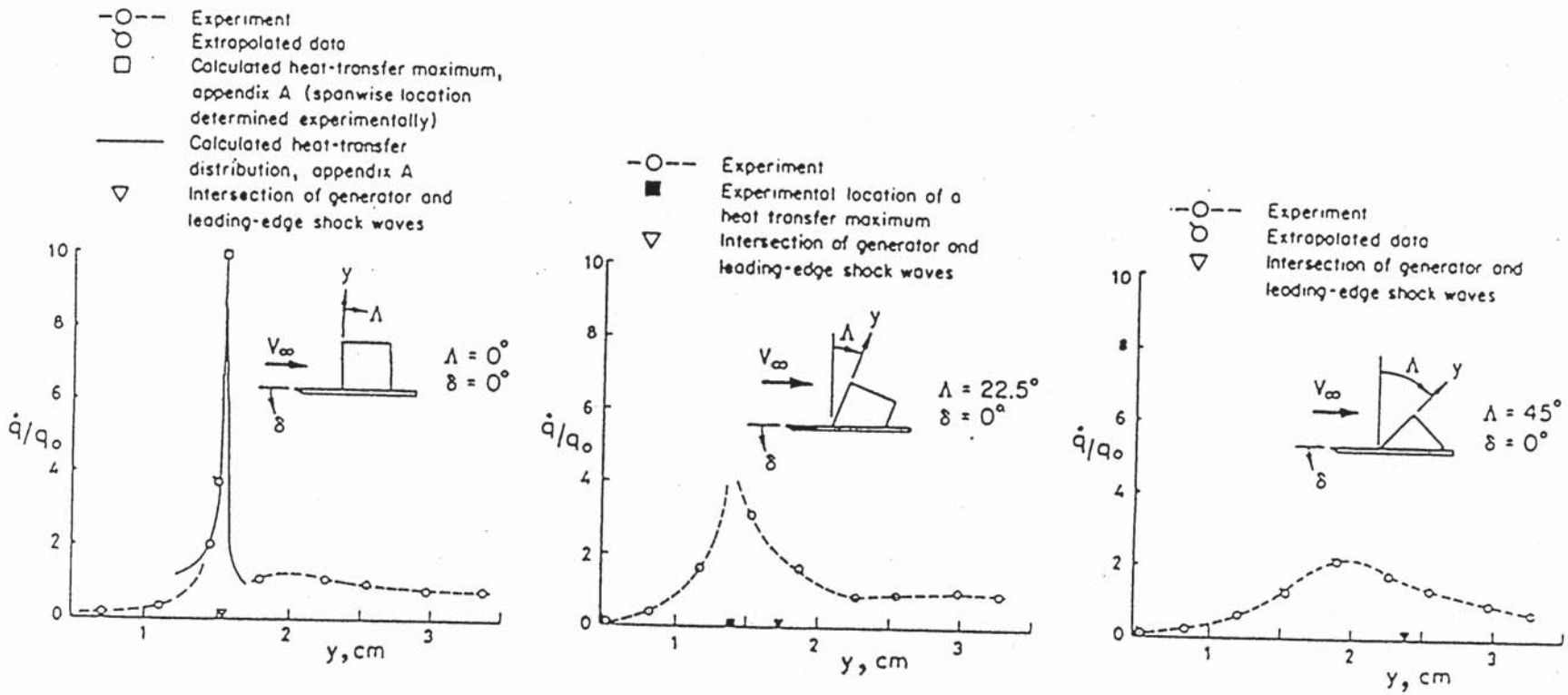


Fig. 5 (b). Heat transfer results along the leading edge.

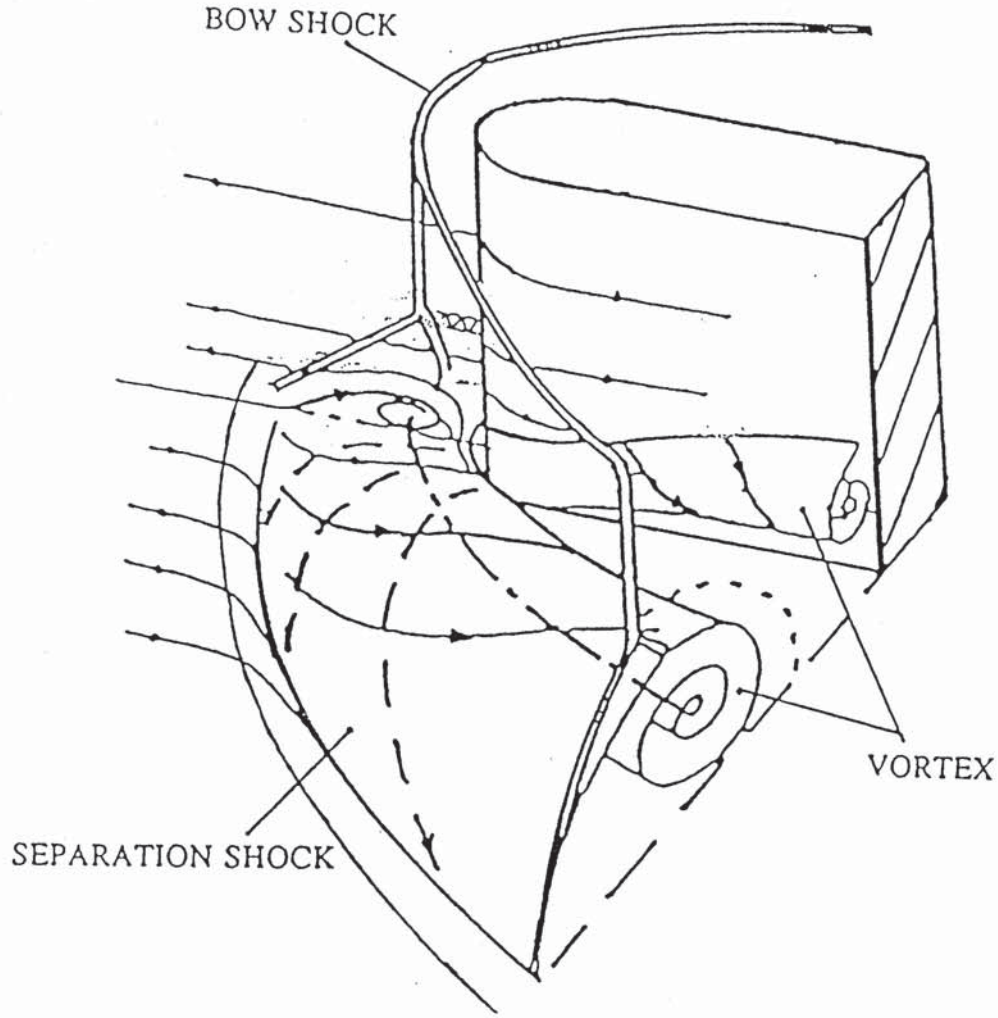
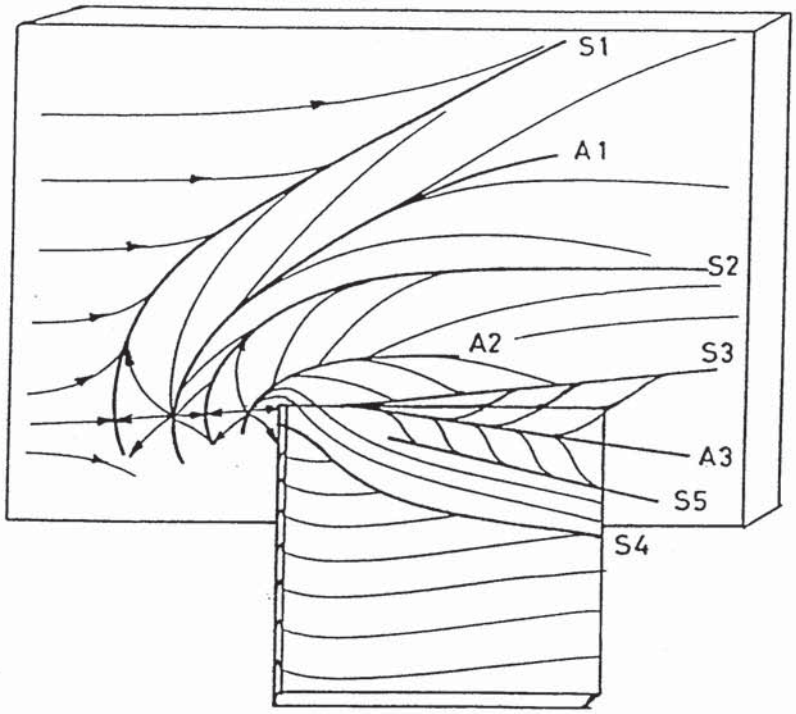
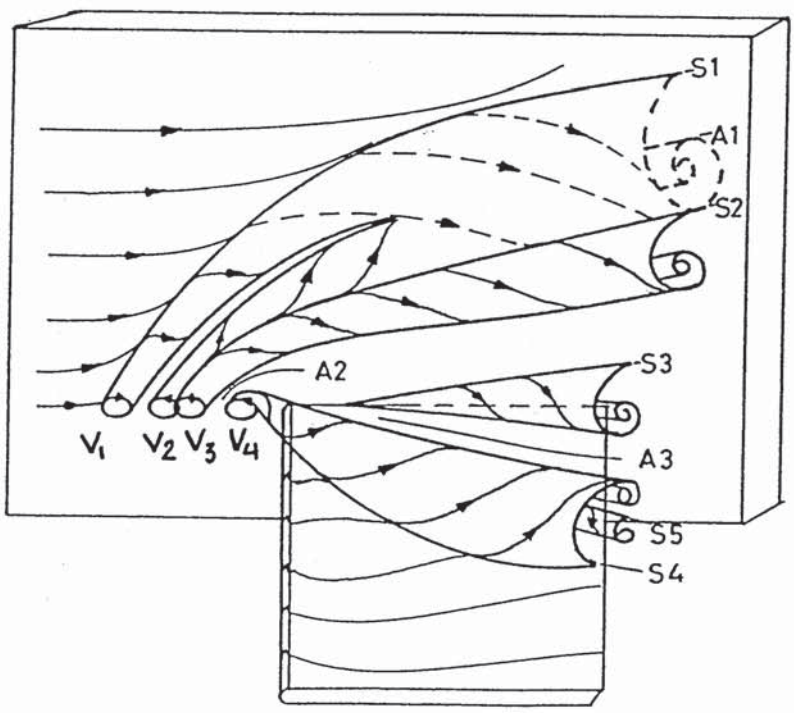


Fig. 6. General characteristics of blunt fin induced shock wave turbulent boundary layer interaction.



Surface Streak Pattern



Vortex Skeleton Representation

(a) Hussain's (1985) flow field model .

Fig. 7. Flow field models for straight blunt fins.

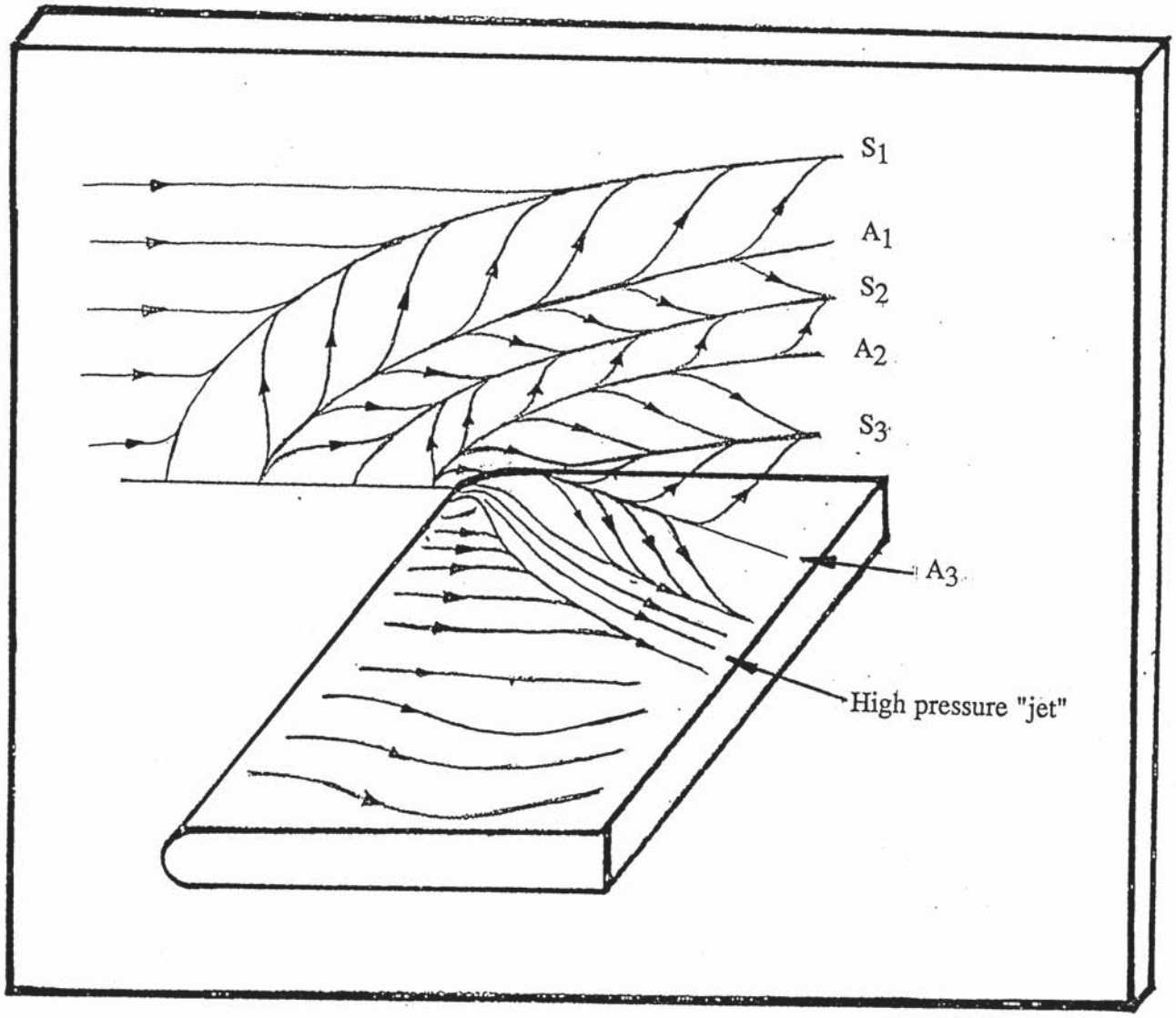


Fig. 7 (b). Streak line pattern given by Fomison (1986) for straight blunt fins.

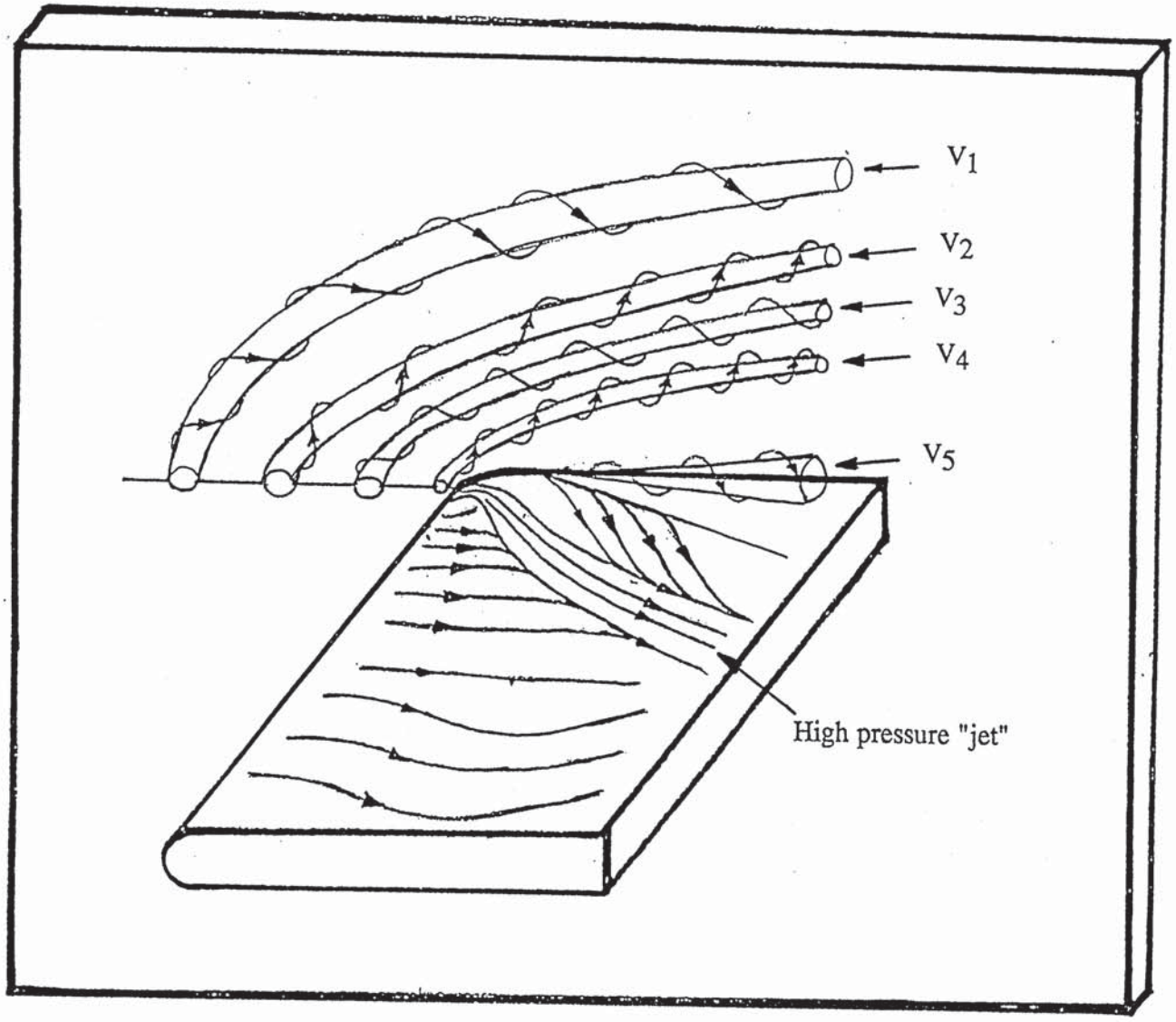


Fig. 7 (c) Vortex skeleton representation for straight blunt fins.

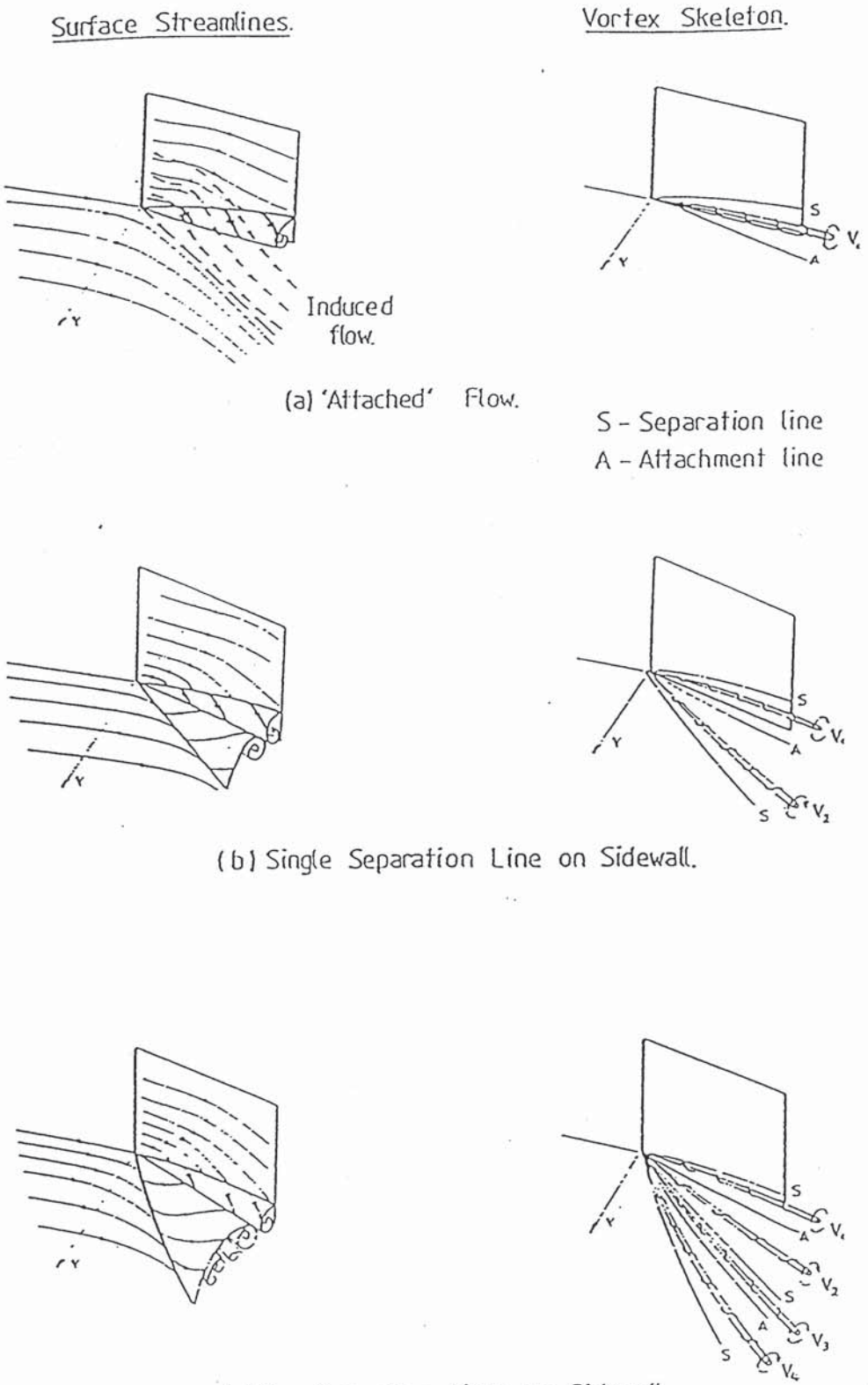
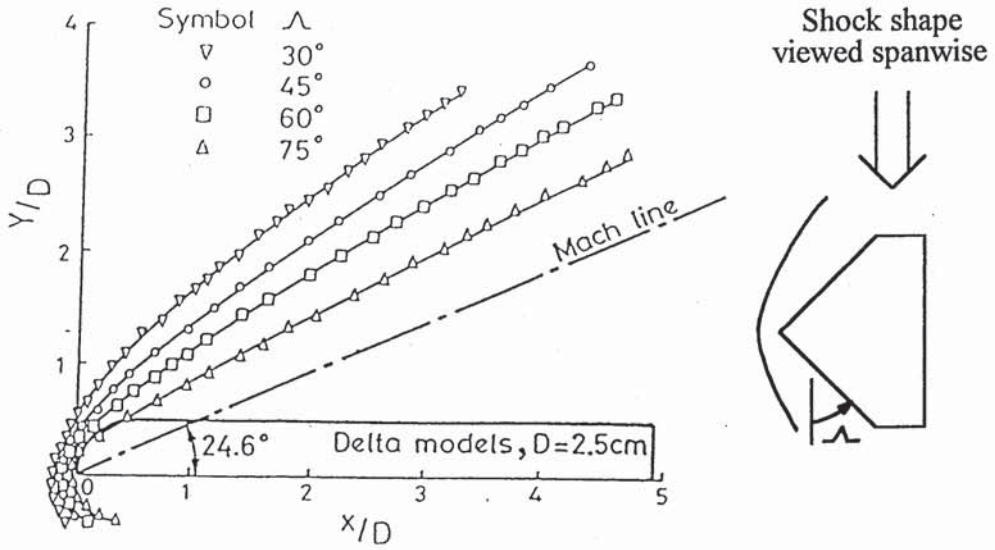
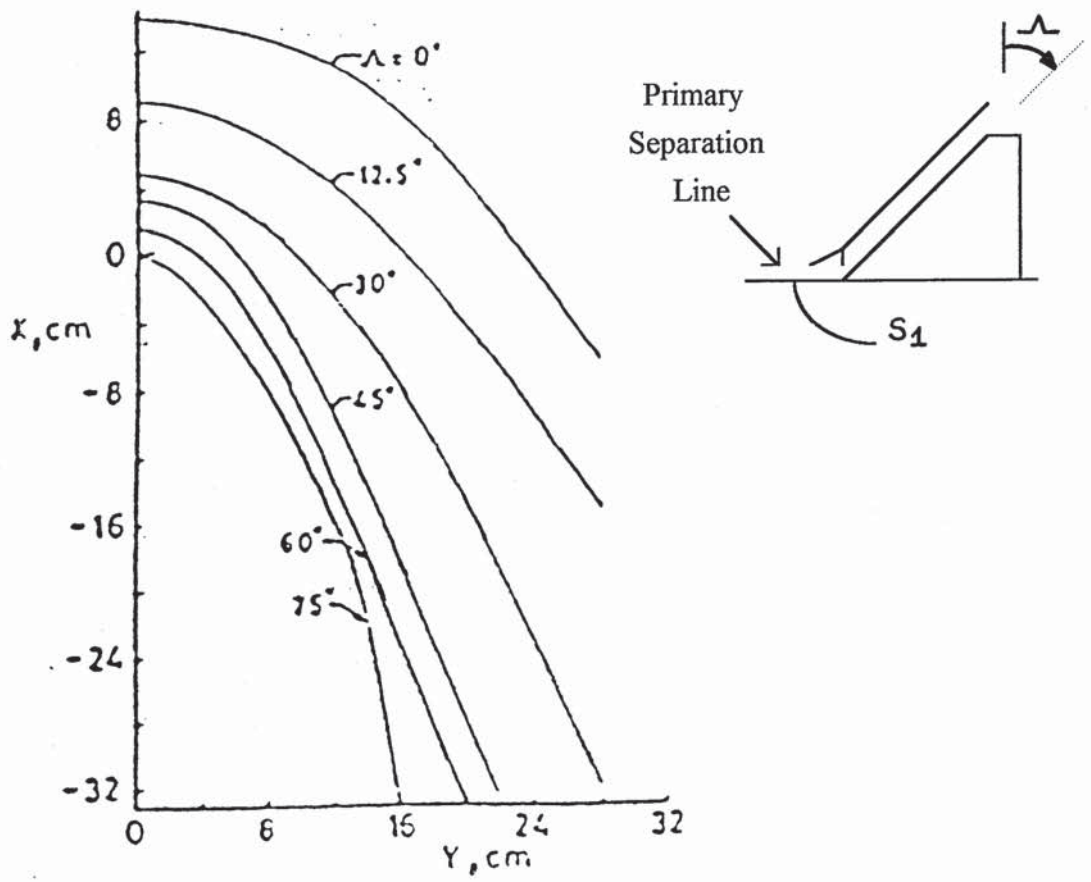


Fig. 8. Sharp generator flow field models (from Kubota (1980)).

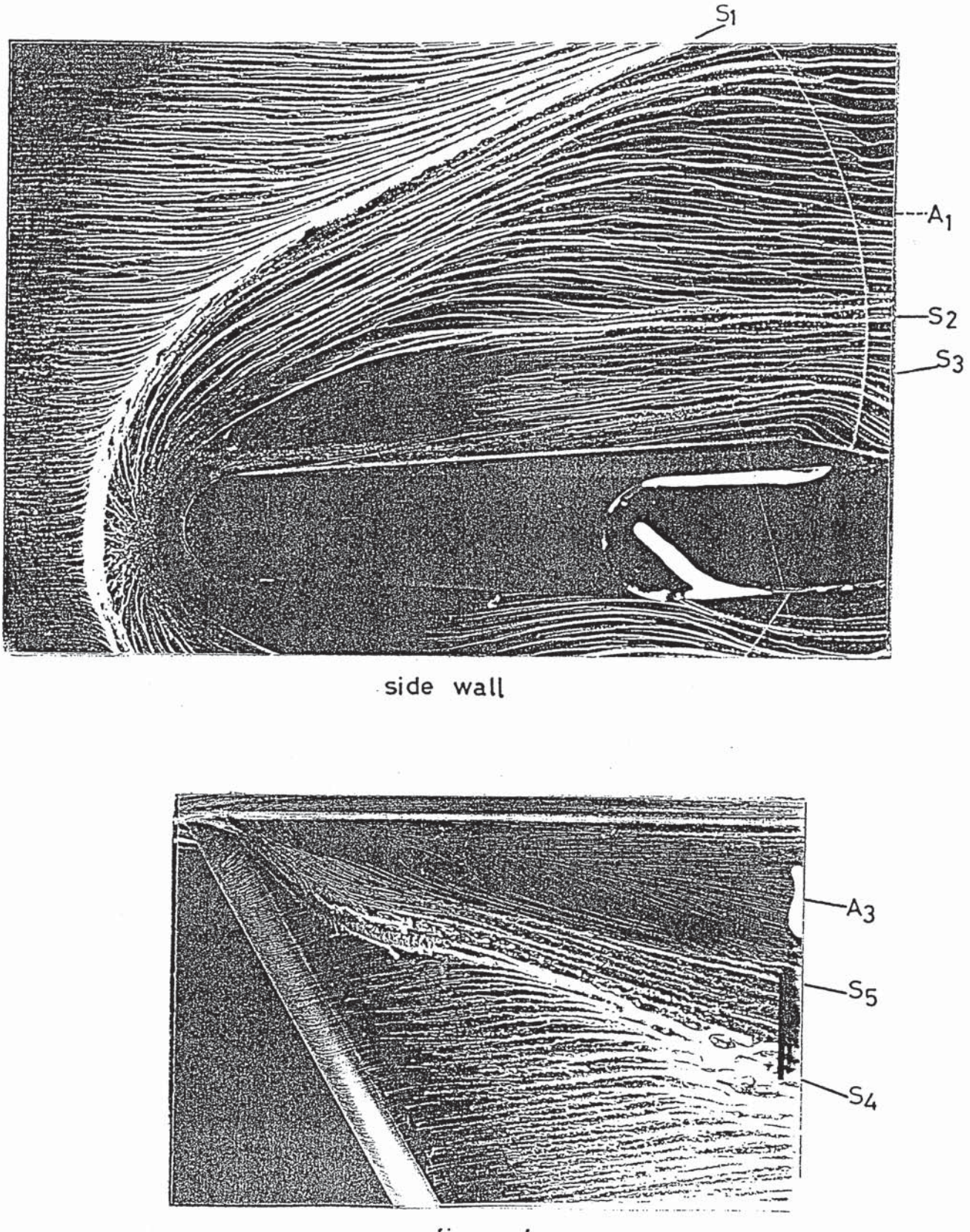


(a) Effect of sweep angle on the shock profile, $\alpha = 0\ °$, D = 2.5 cm (from Stollery et al (1986)).



(b) The effects of sweep on the primary separation line (Price and Stallings (1967)).

Fig. 9. Effect of leading edge sweep.



(a). 30° sweep.

Fig. 10. Side view oil flow pattern for a swept fin of $D/\delta=1.6$ (from Hussain (1985)).

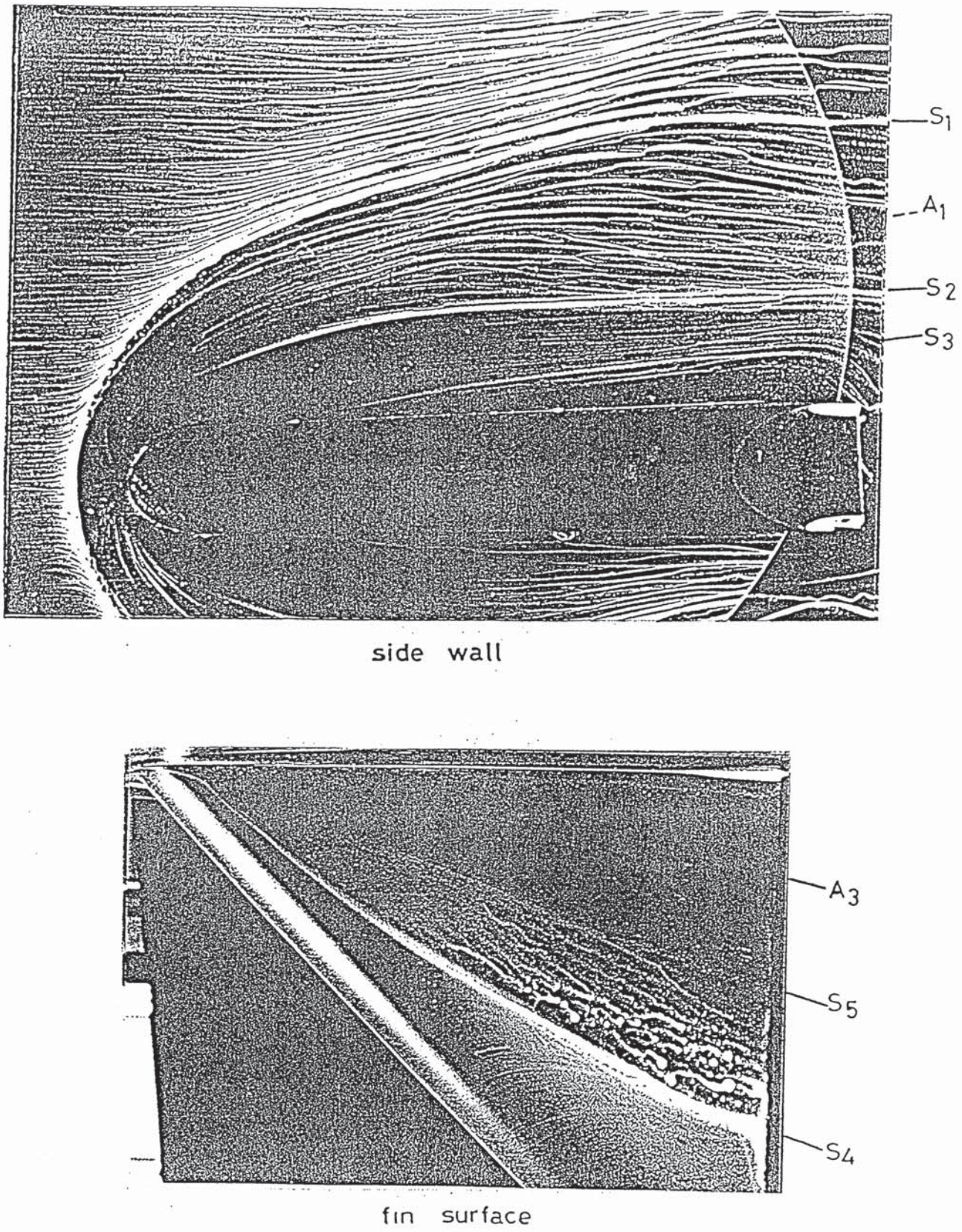
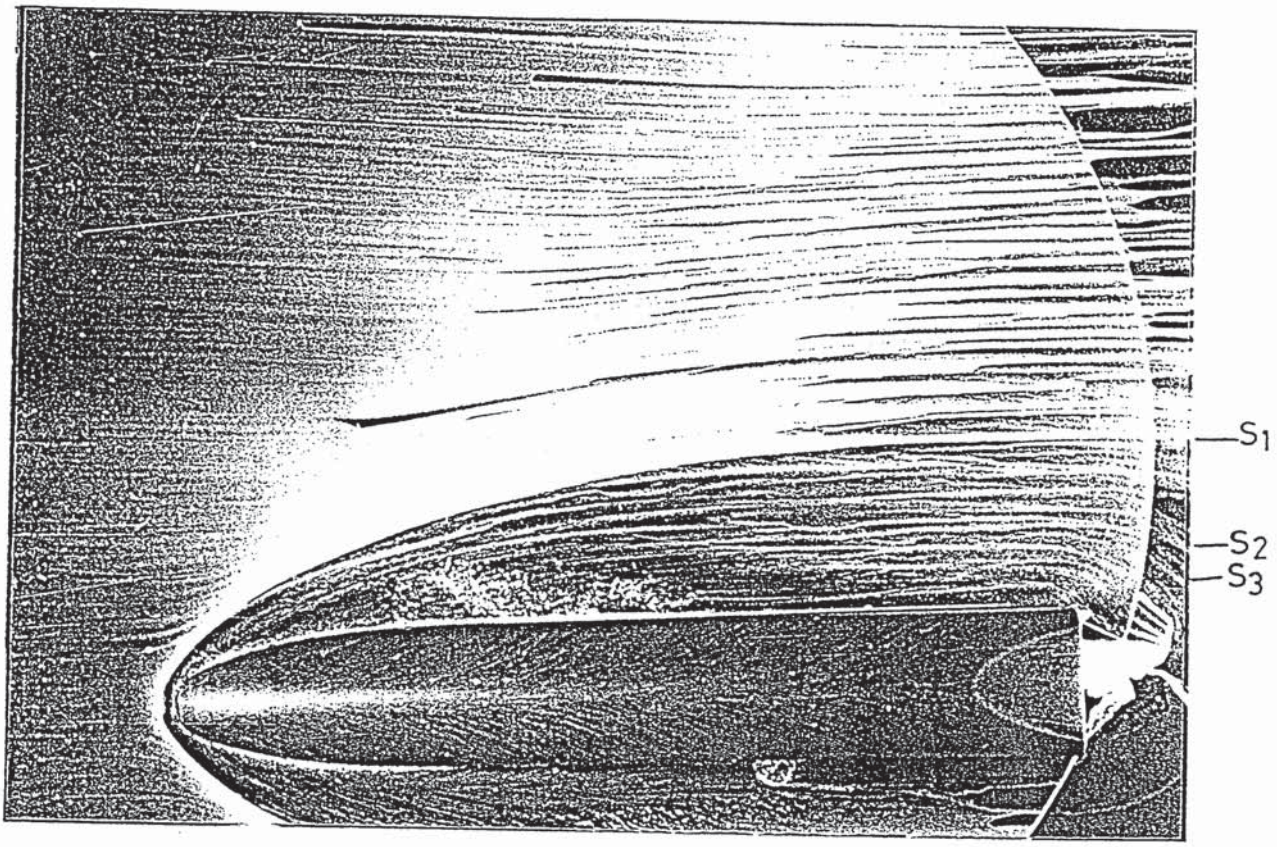


Fig. 10 (b). 45° sweep.



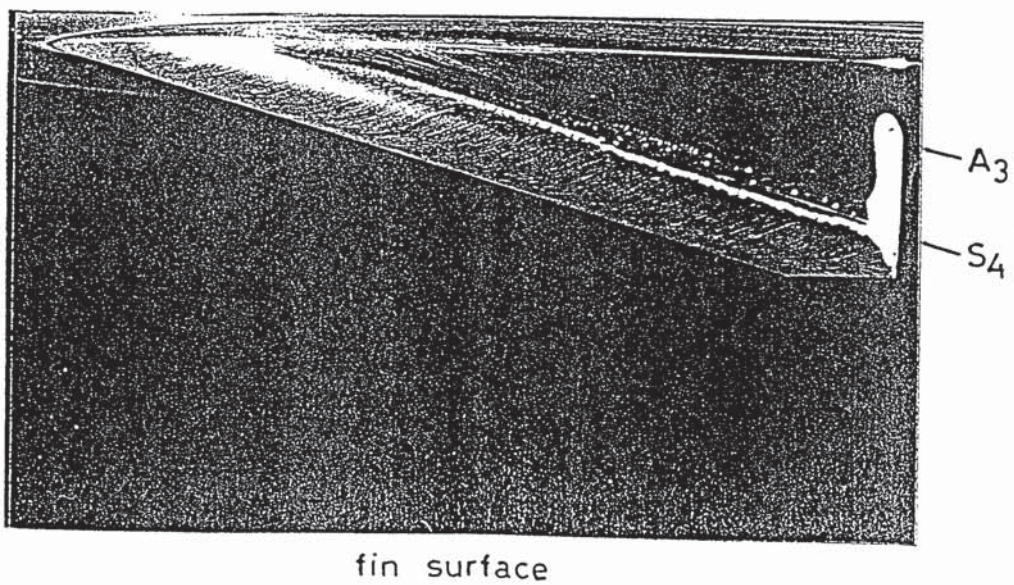
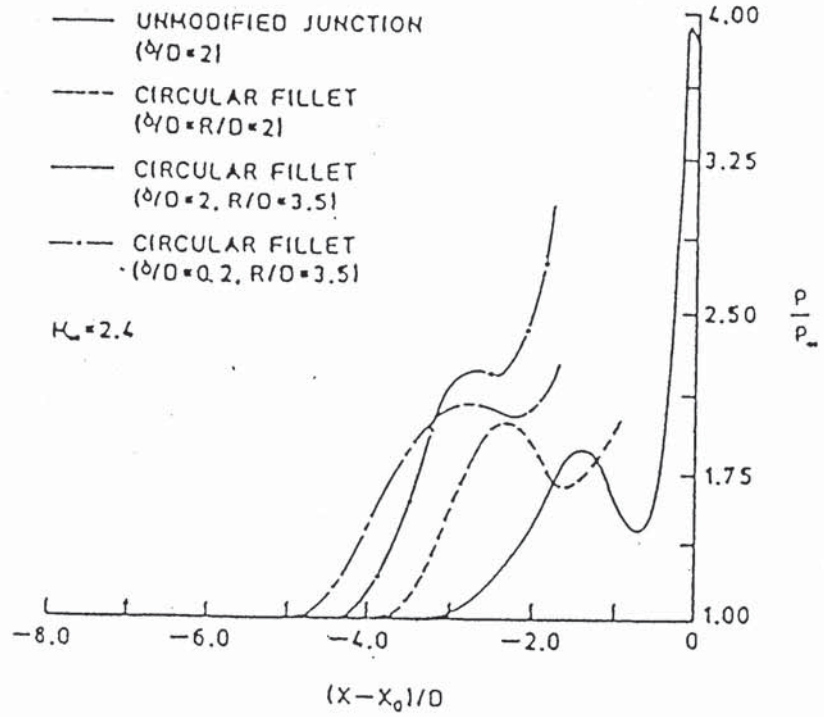


Fig. 10 (c). 70° sweep.



(a) Centre line pressure distributions on a flat plate for various junctions (from Lakshmanan et al (1988))

Fig. 11. The effects of circular cross sectional fillets around blunt fins.

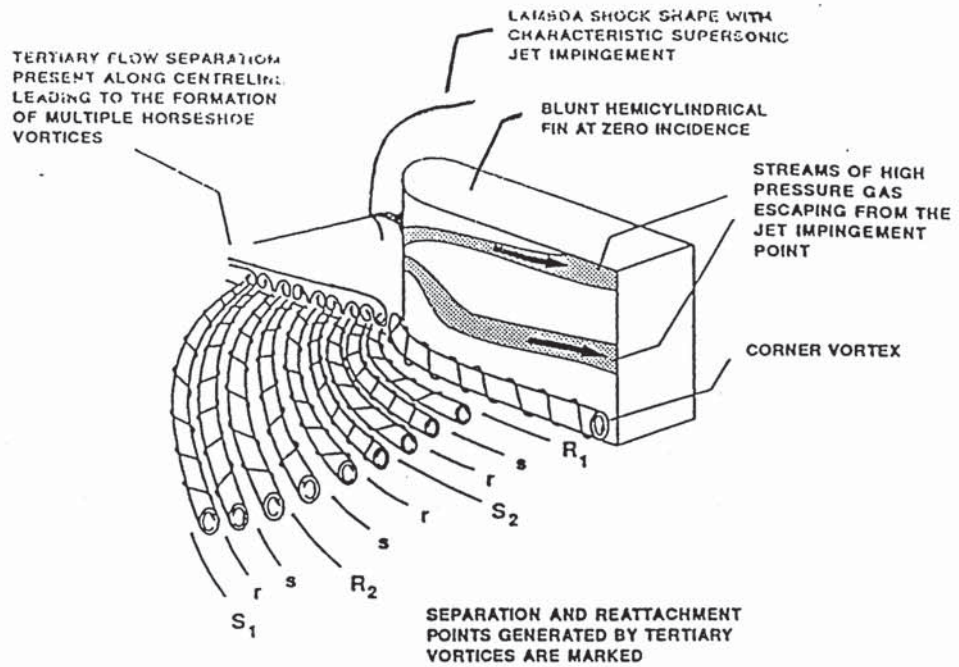


Fig. 11 (b). Proposed flow structure for a blunt fin at zero incidence (from Haq (1993)).

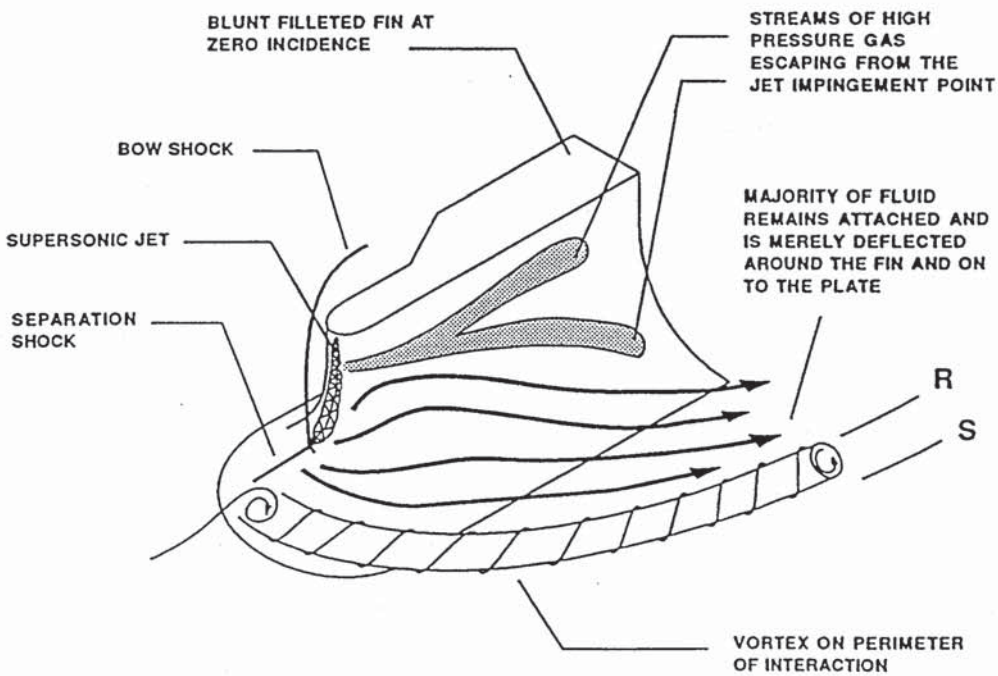


Fig. 11 (c) Proposed flow structure for a filleted fin (from Haq (1993)). Note that only one vortex exists and the flow mainly remains attached.

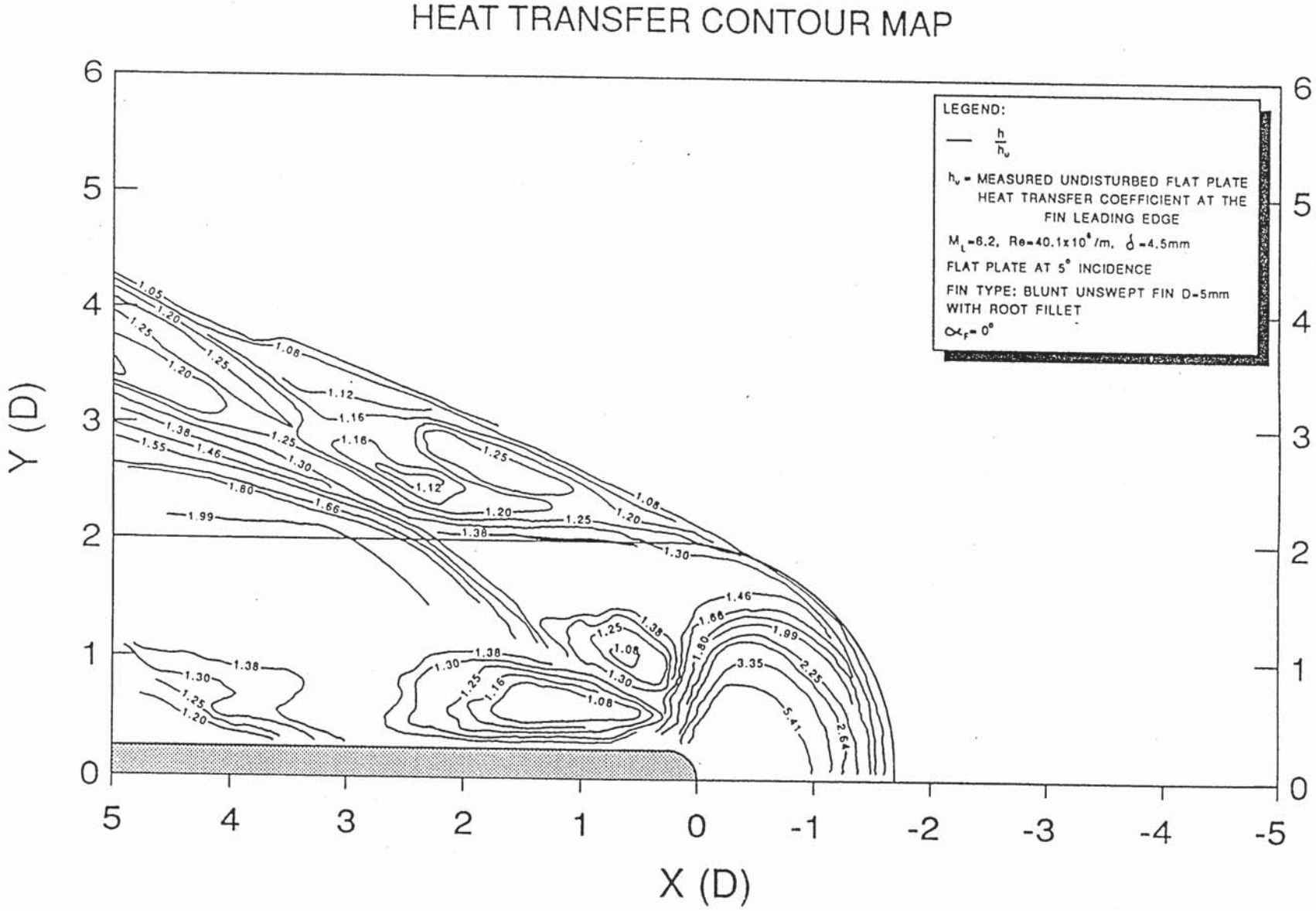


Fig. 11 (d). Heat transfer plot for a blunt fin with a circular cross sectional fillet of 3.5D radius (from Haq (1993)).

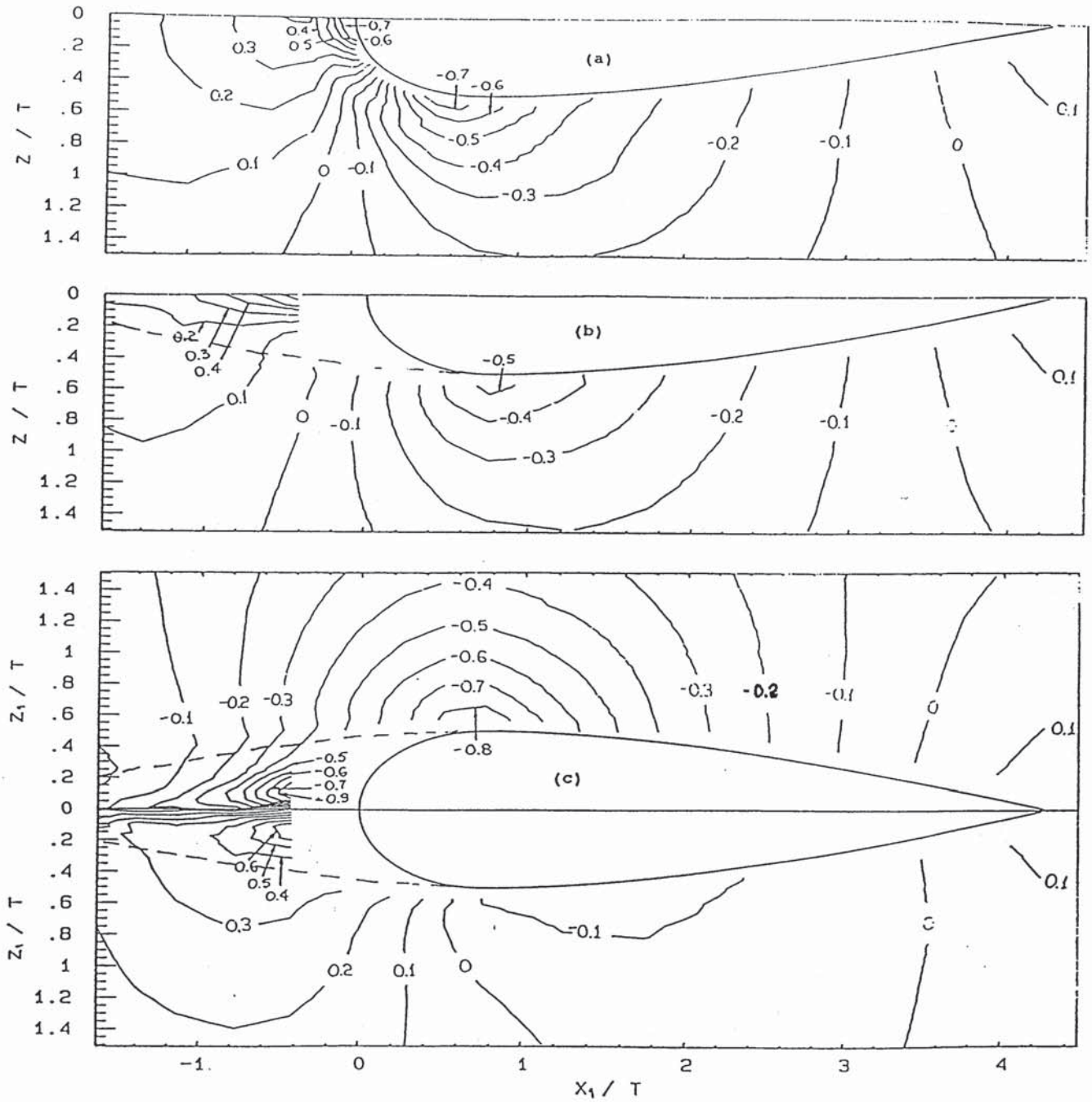


Fig. 12. Contours of mean surface pressure coefficient C_P on the test wall with the thin approach boundary layer. (a) Baseline wing, 0° angle of attack (top), (b) Wing with strake, 0° angle of attack (centre), (c) Wing with strake, 12° angle of attack (bottom). From Devenport et al (1991).

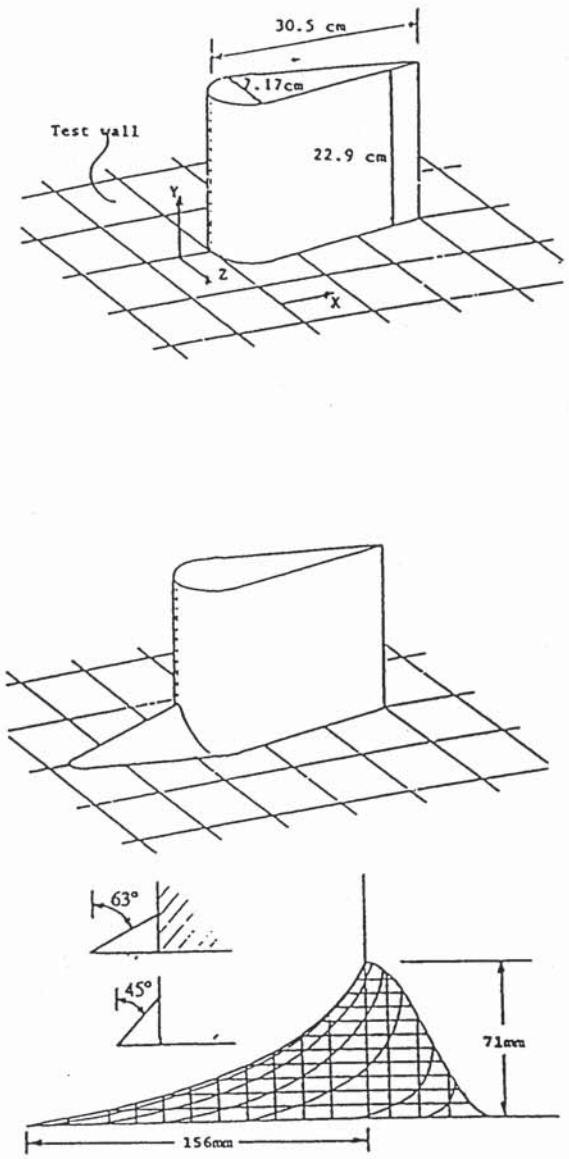


Fig. 12 (d) the baseline model used by Devenport et al (1991) (top), (e) notional sketch of the configuration used by Kubendran et al (1988) (centre) and (f) the strake used by Devenport et al (1991) (bottom). The insert in (f) shows the strake angles used by Kubendran et al (1988).

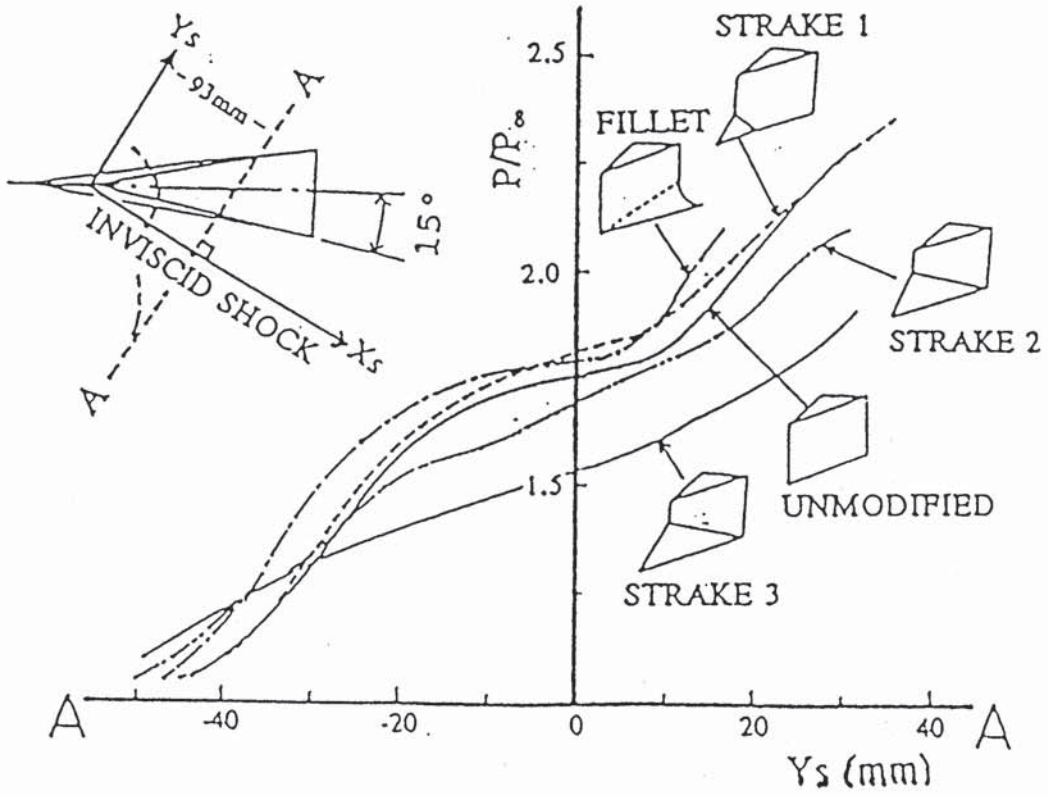


Fig. 13. Wall pressure distributions for a modified sharp leading edge fin (from Koide and Stollery (1993)).

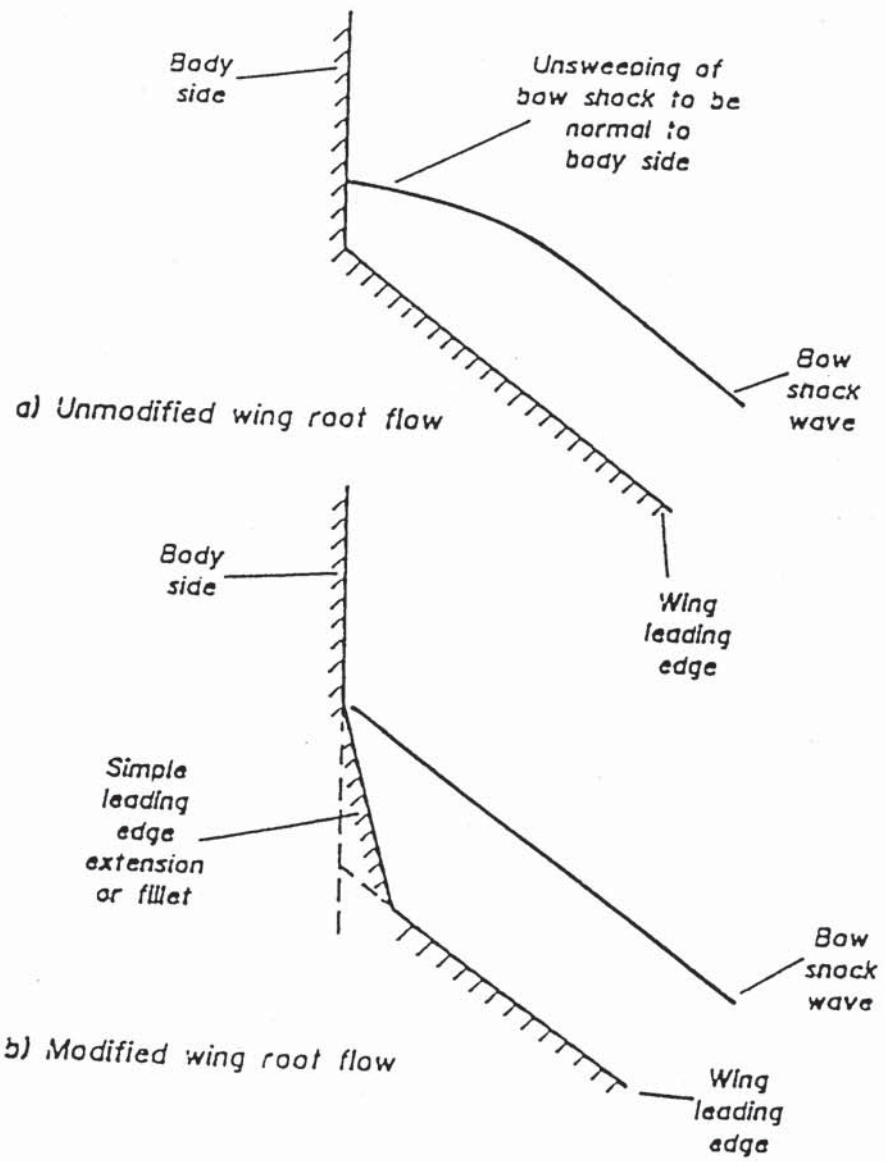


Fig. 14. The effects of including a cone like extension at the wing leading edge root (Fulker et al (1993)).

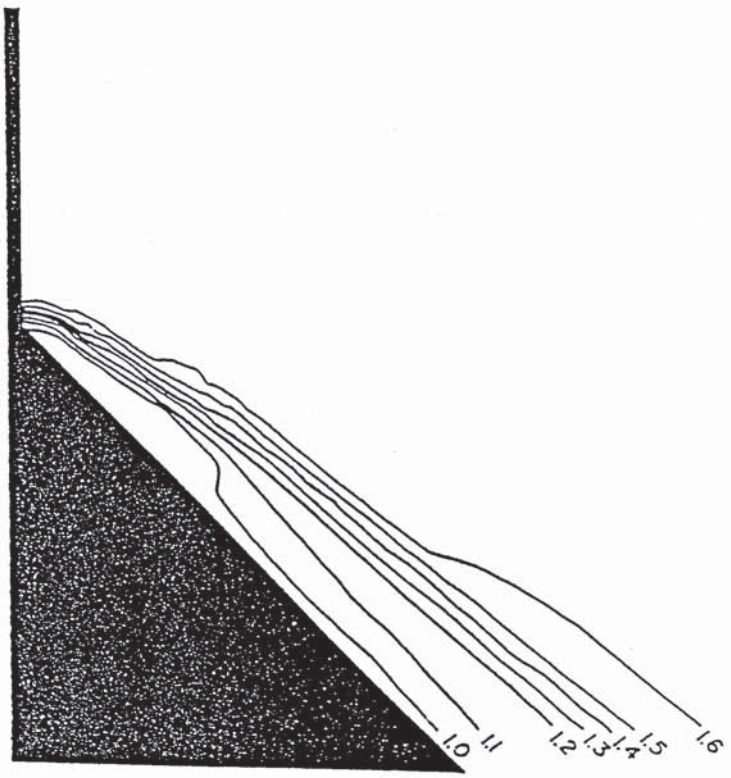


Fig. 14 (c). Theoretical Iso-Mach contours in the region of the "novel" wing root.

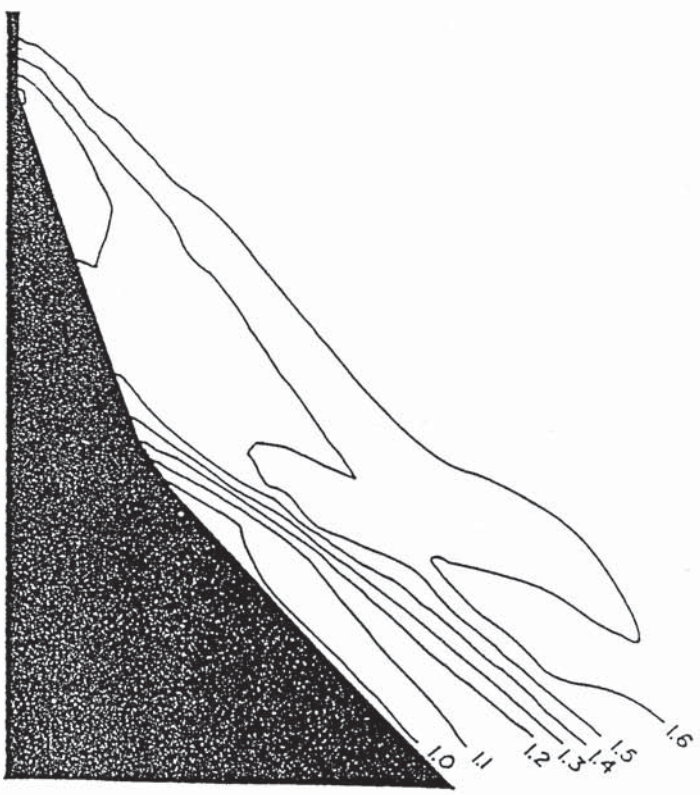


Fig. 14 (d). Theoretical Iso-Mach contours in the region of the "novel" wing root with a cone like extension.

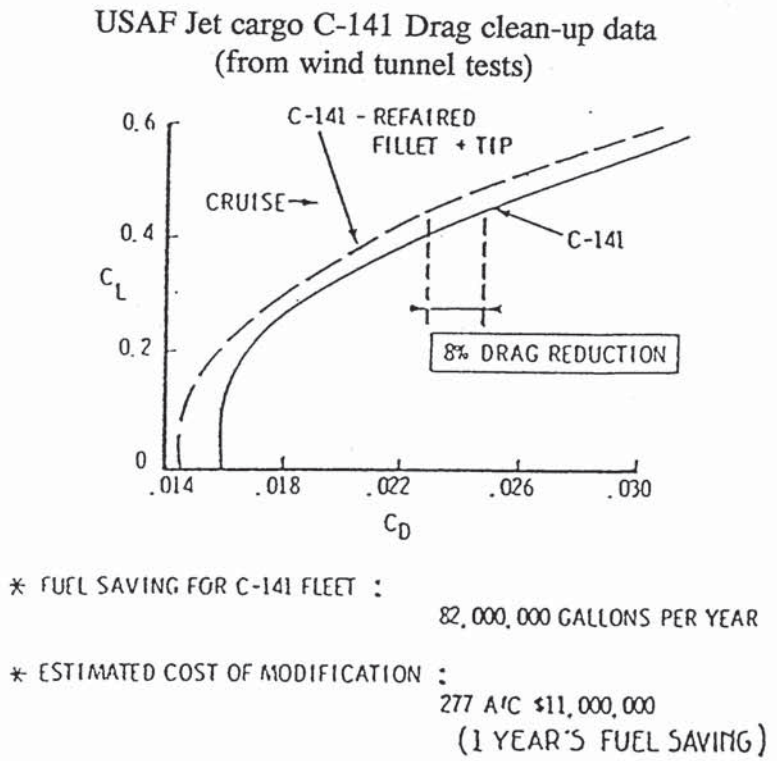
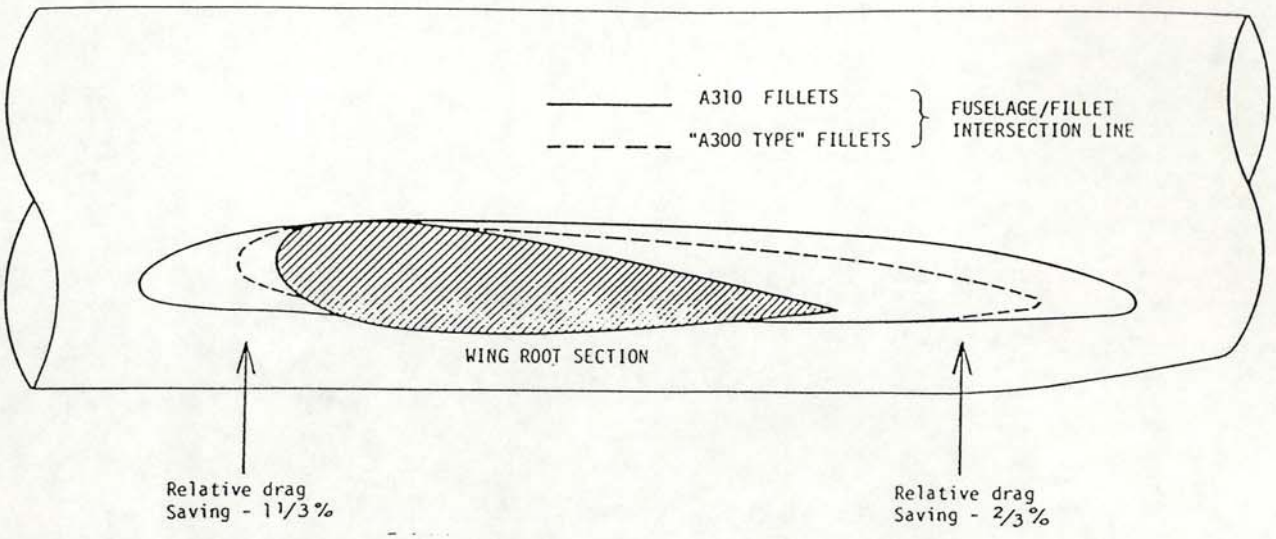
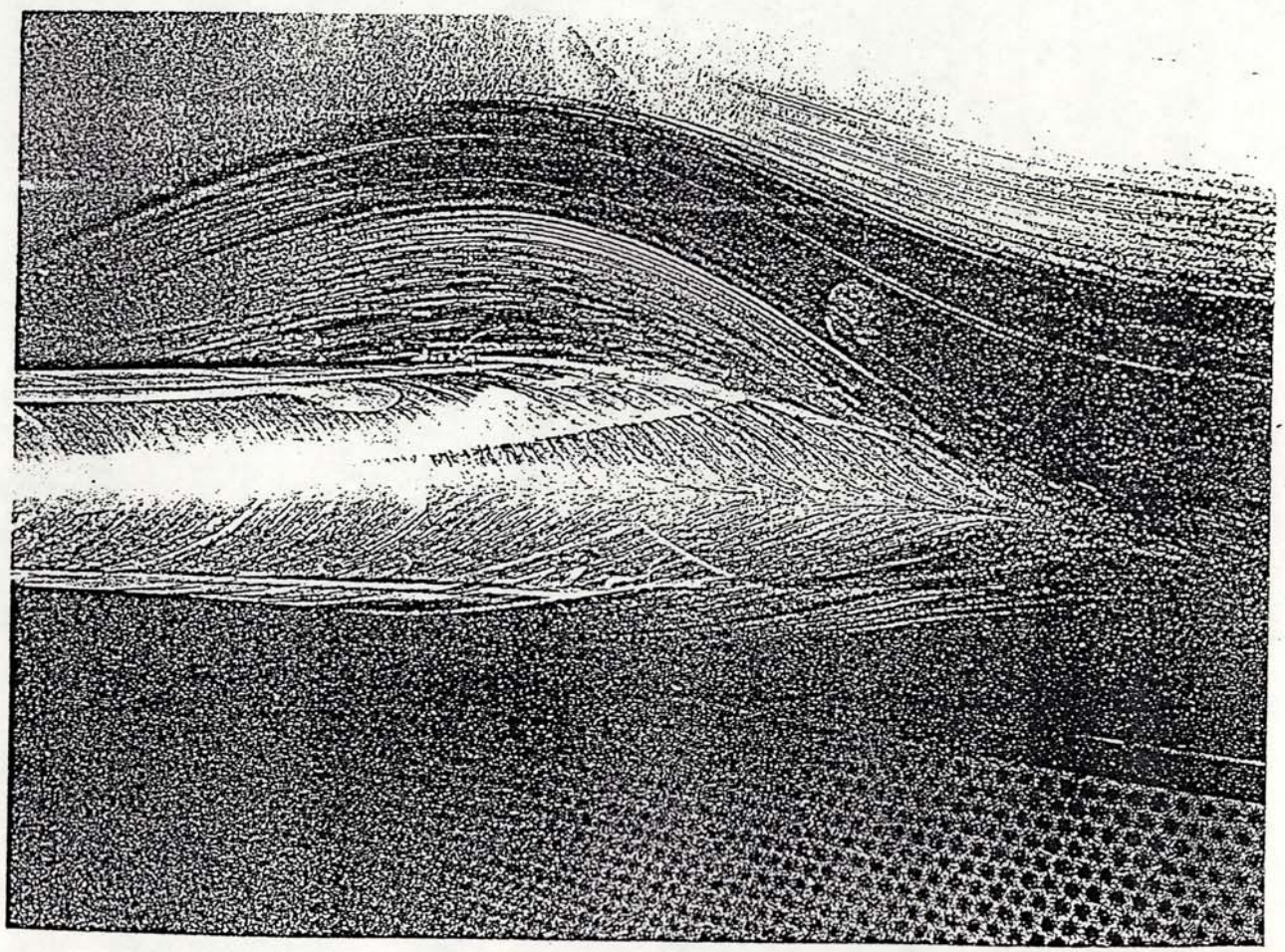


Fig. 15. Reduction of parasitic drag (Poisson-Quinton (1980)).



(a) Optimisation of A 310 wing root fillets - drag improvements relative to "A 300" type.



(b) Surface flow streamlines over the A 310 wing root leading edge fillet.

Fig. 16. Wing root fillets as used on the A 310 (from Jupp (1980)).

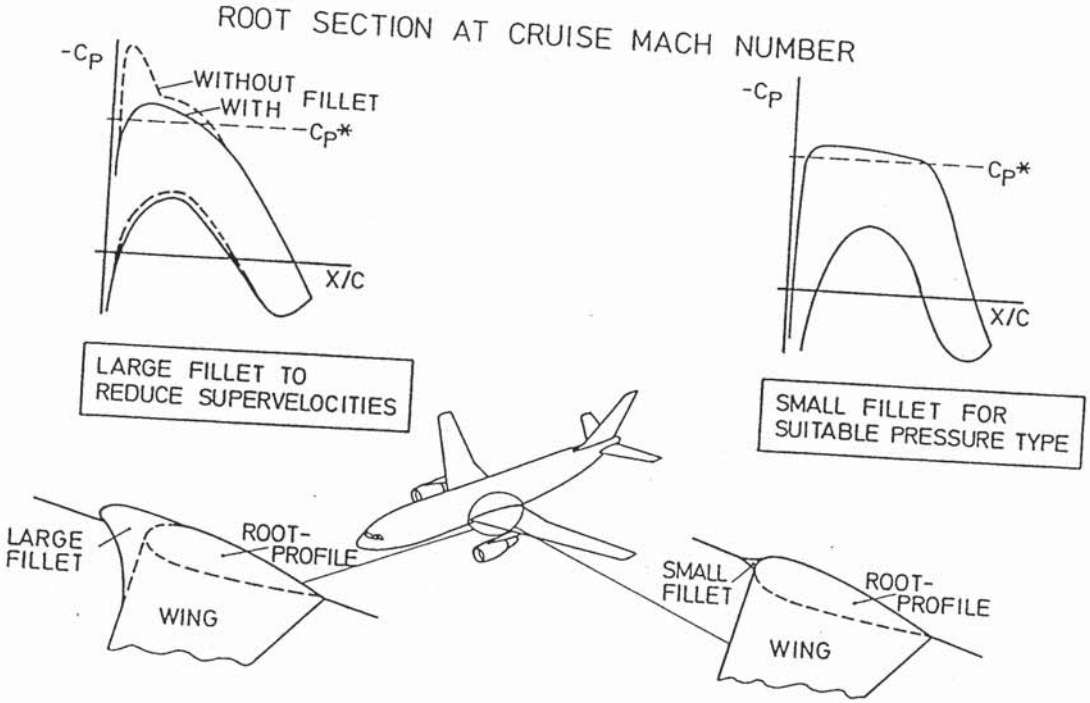


Fig. 17. Correlation of fillet size and pressure distribution (Krenz (1983)).

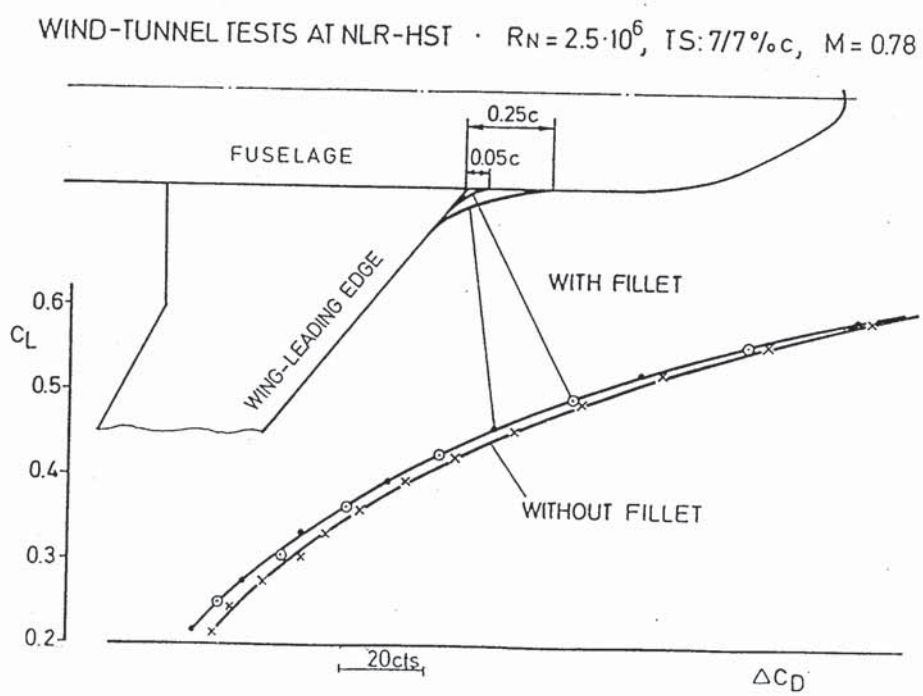
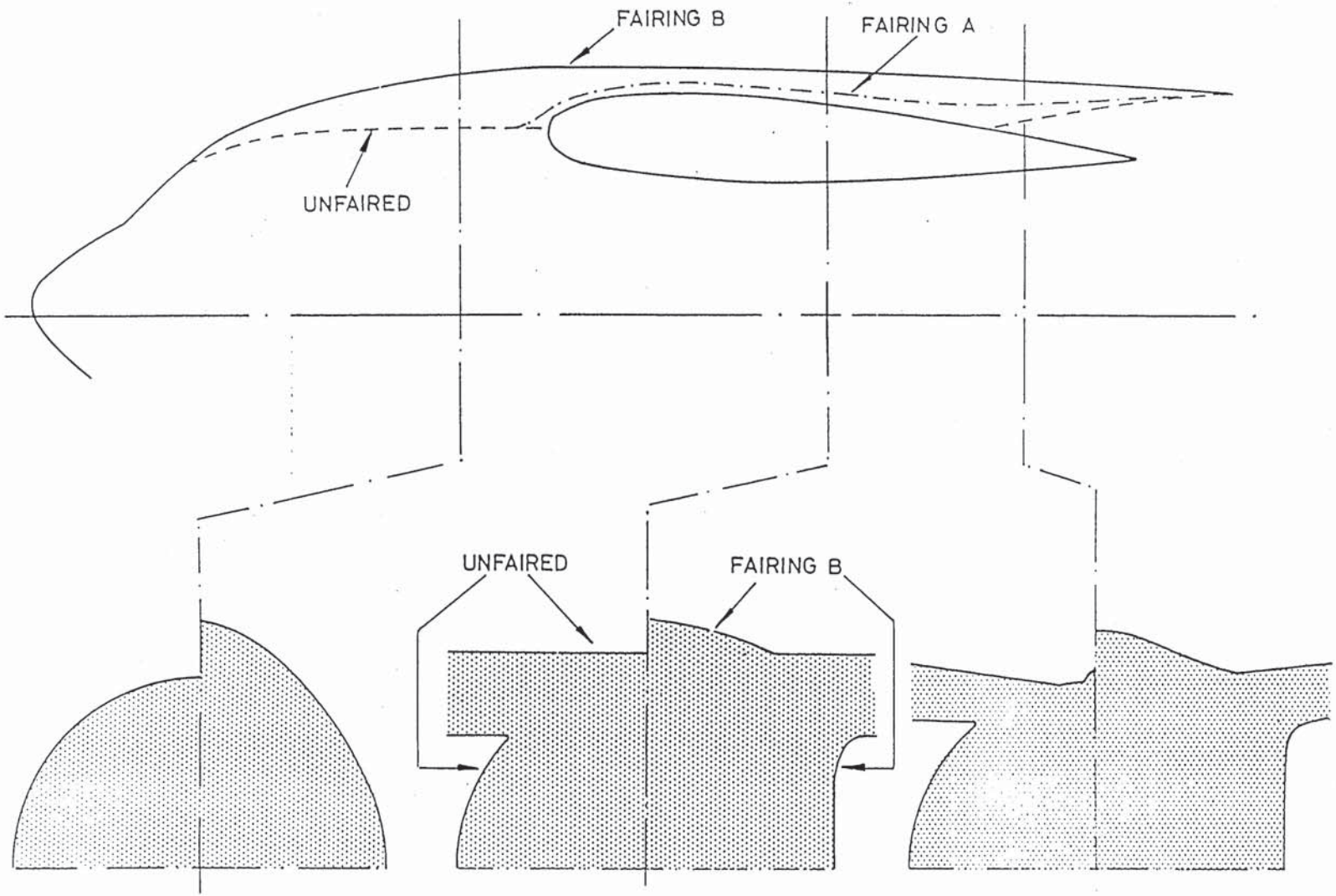
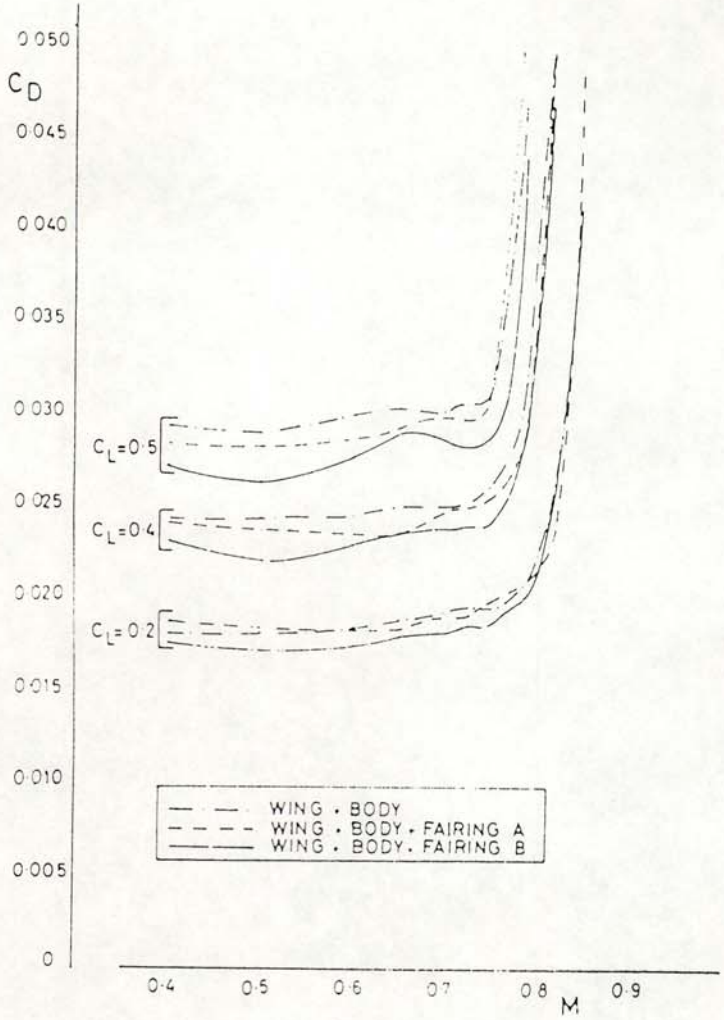


Fig. 18. Effect of wing fuselage fillet on drag for a research wing of Airbus-type (Krenz (1983)).

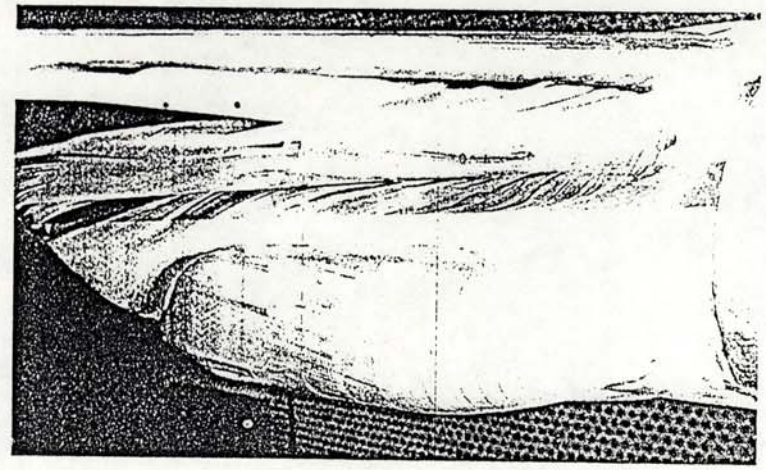


(a) Geometry of fairings

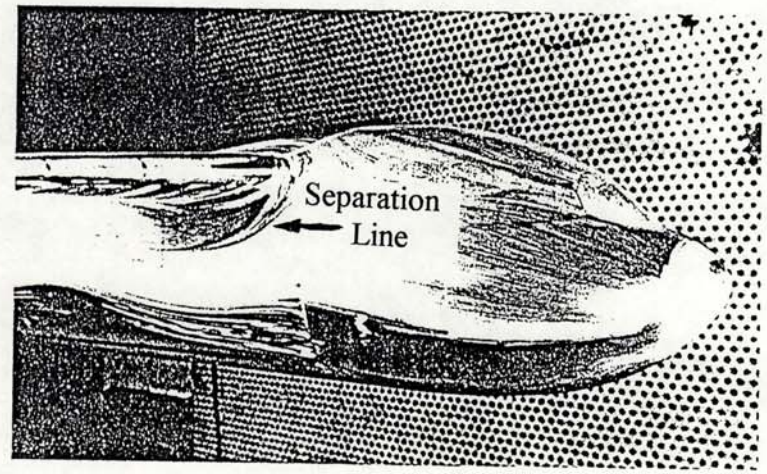
Fig. 19. Wing-body fairing research : High wing subsonic transport (Haines (1983)).



(b) Comparative drag data



FAIRING A



FAIRING B

(c) Oil flow at design condition, M=0·71, C_L=0·5.

Fig. 19. (Contd.).

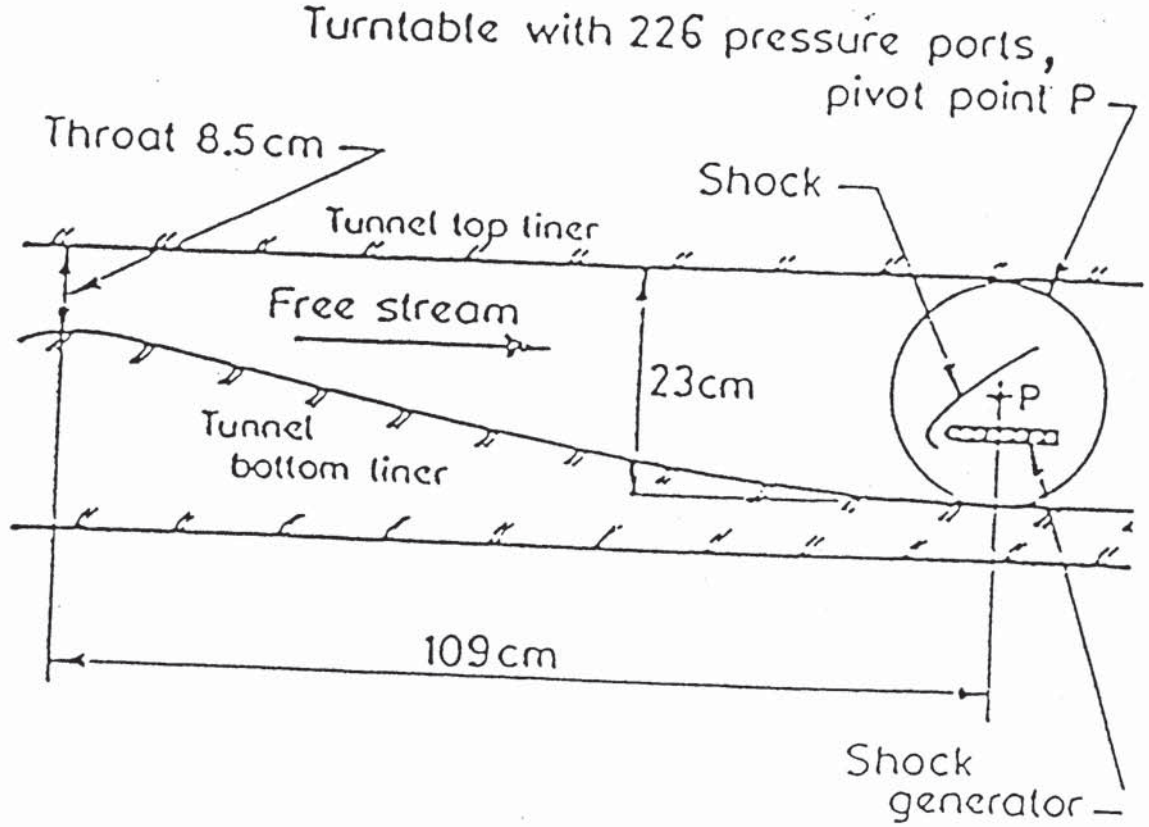
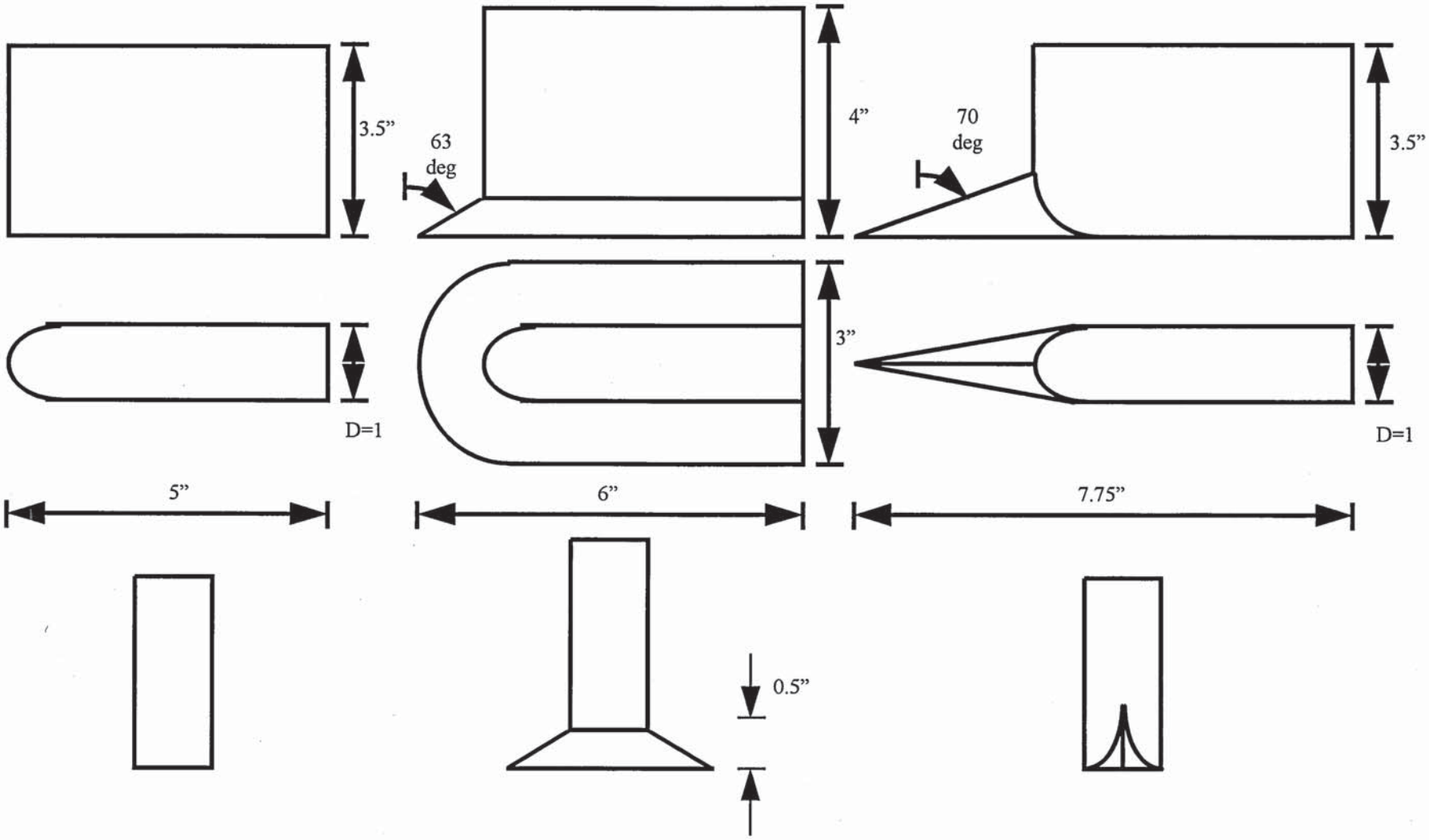
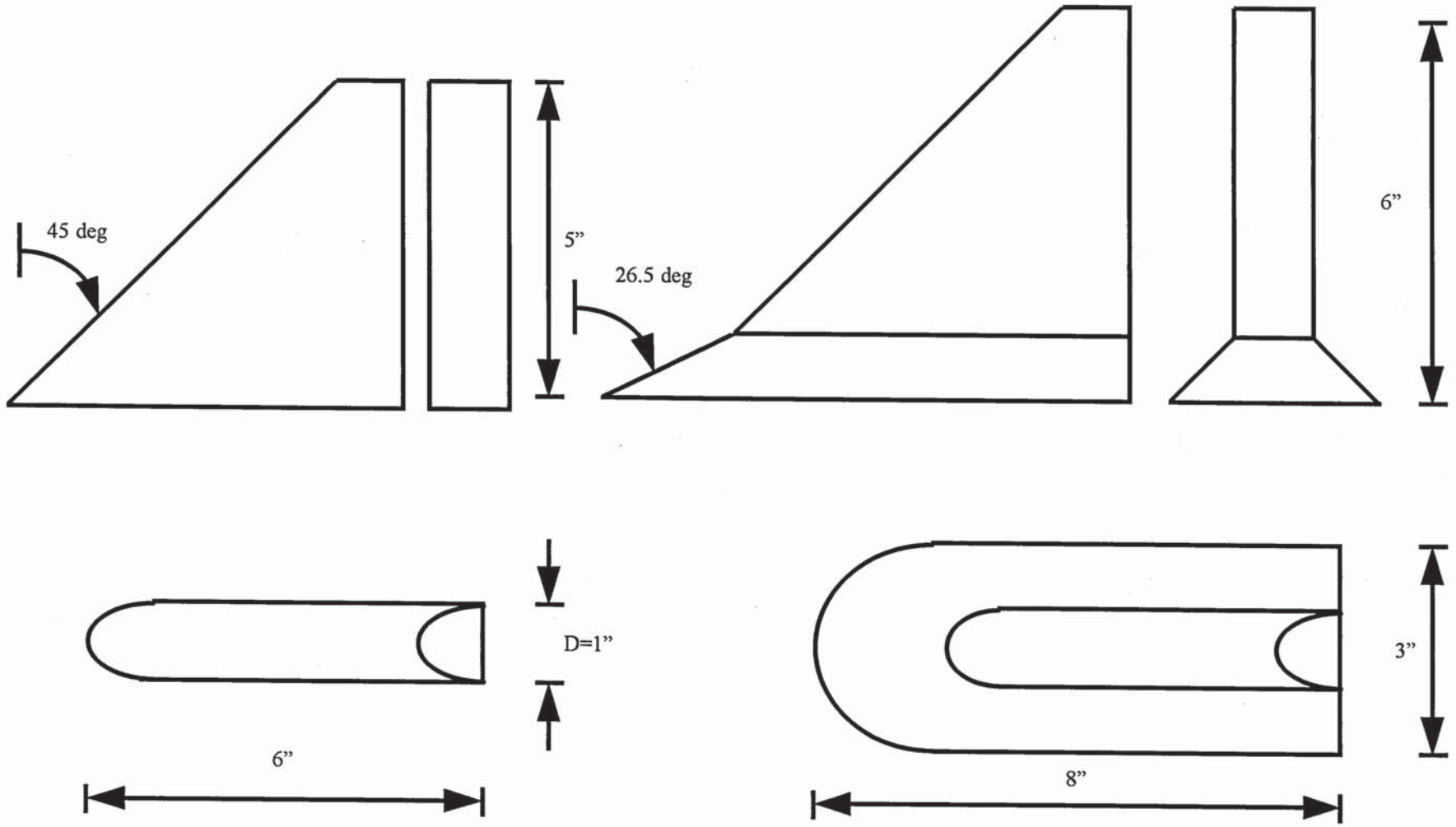


Fig. 20. Experimental arrangement in the 9" x 9" (23 cm x 23 cm) wind tunnel.



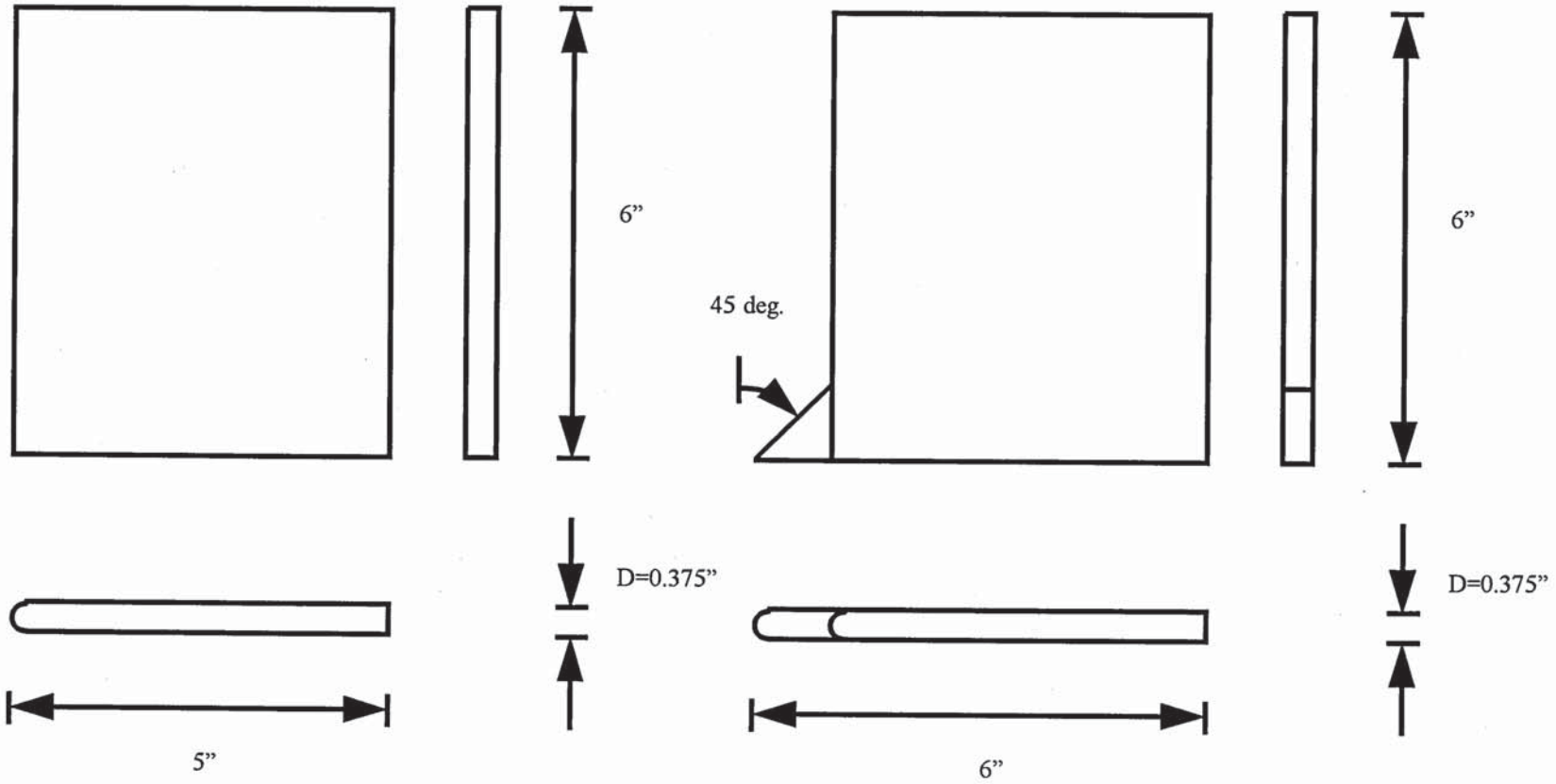
a. The Unswept Models of D/delta = 1.6

Fig. 21. Models used in the 9" x 9" wind tunnel.



b. The Swept Models of D/delta = 1.6

Fig. 21. (Contd.1).



i) Unmodified Model

ii) With Blunt Leading Edge Strake

c. The Models of D/delta = 0.6

Fig. 21. (Contd. 2).

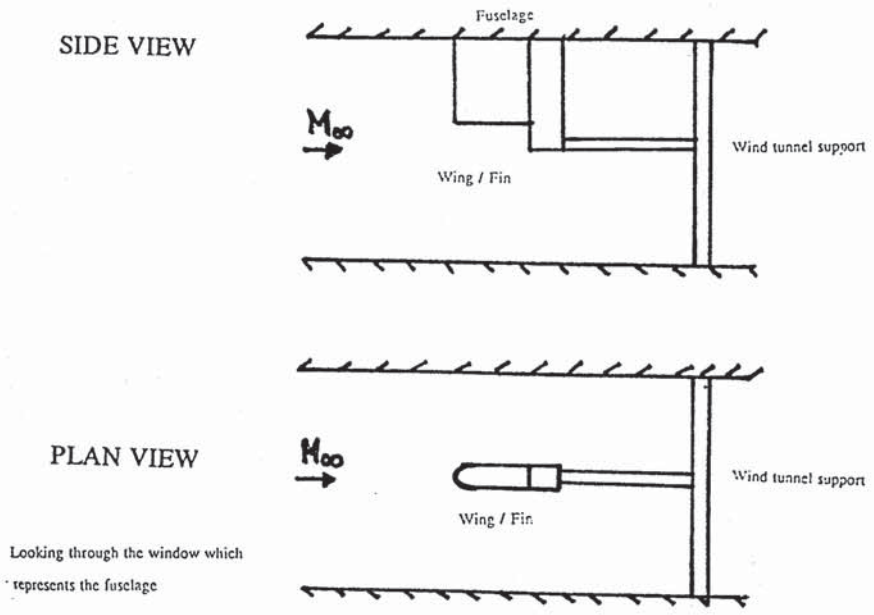


Fig. 22. The mounting methods used in the 9" x 9" wind tunnel for the schlieren tests.

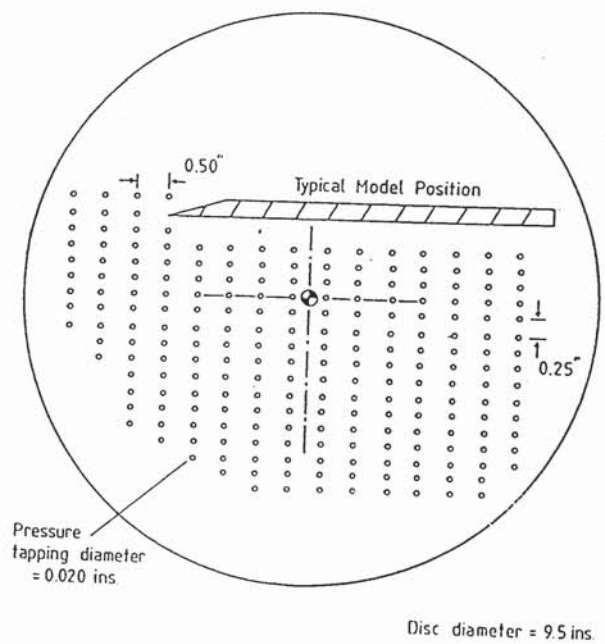
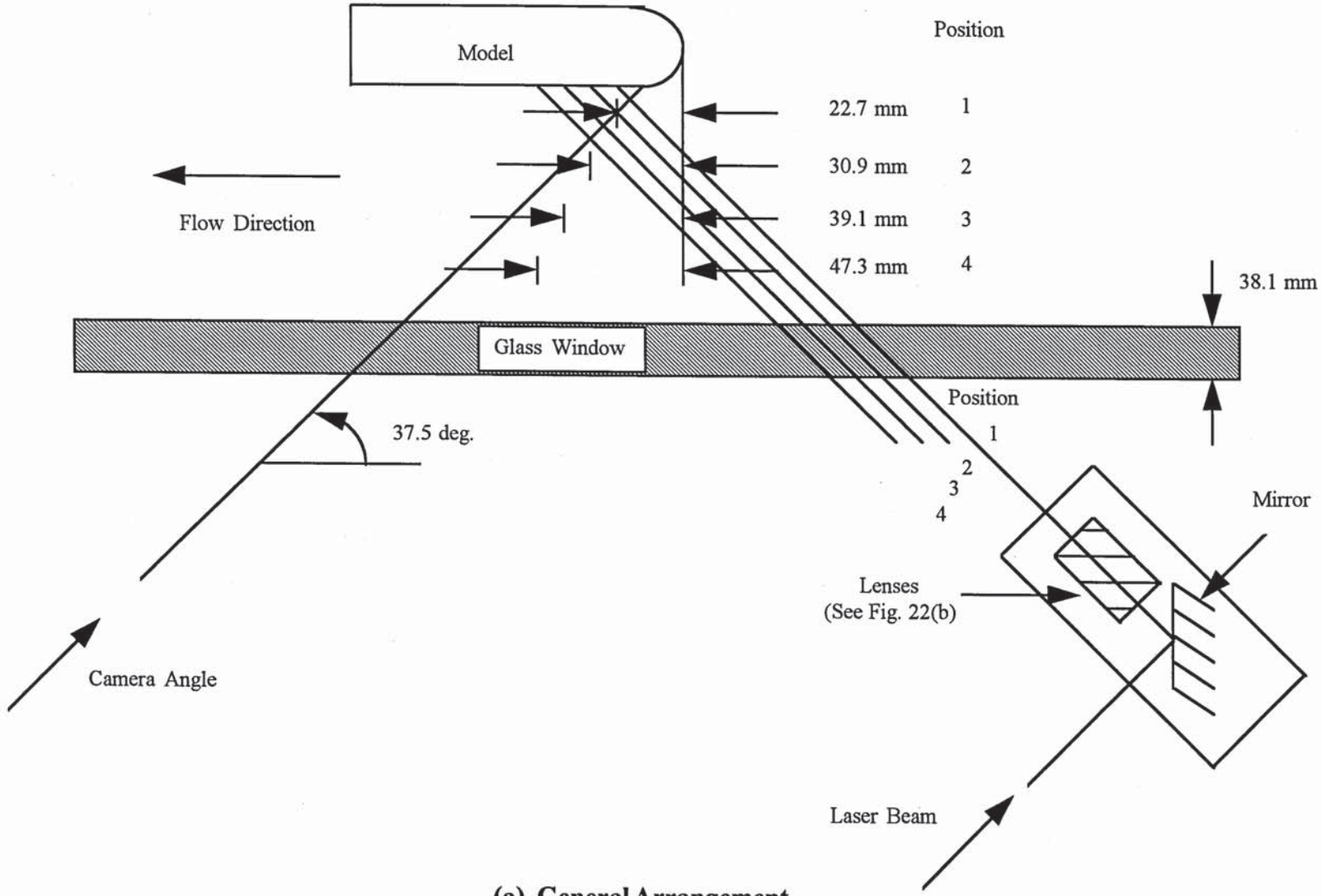
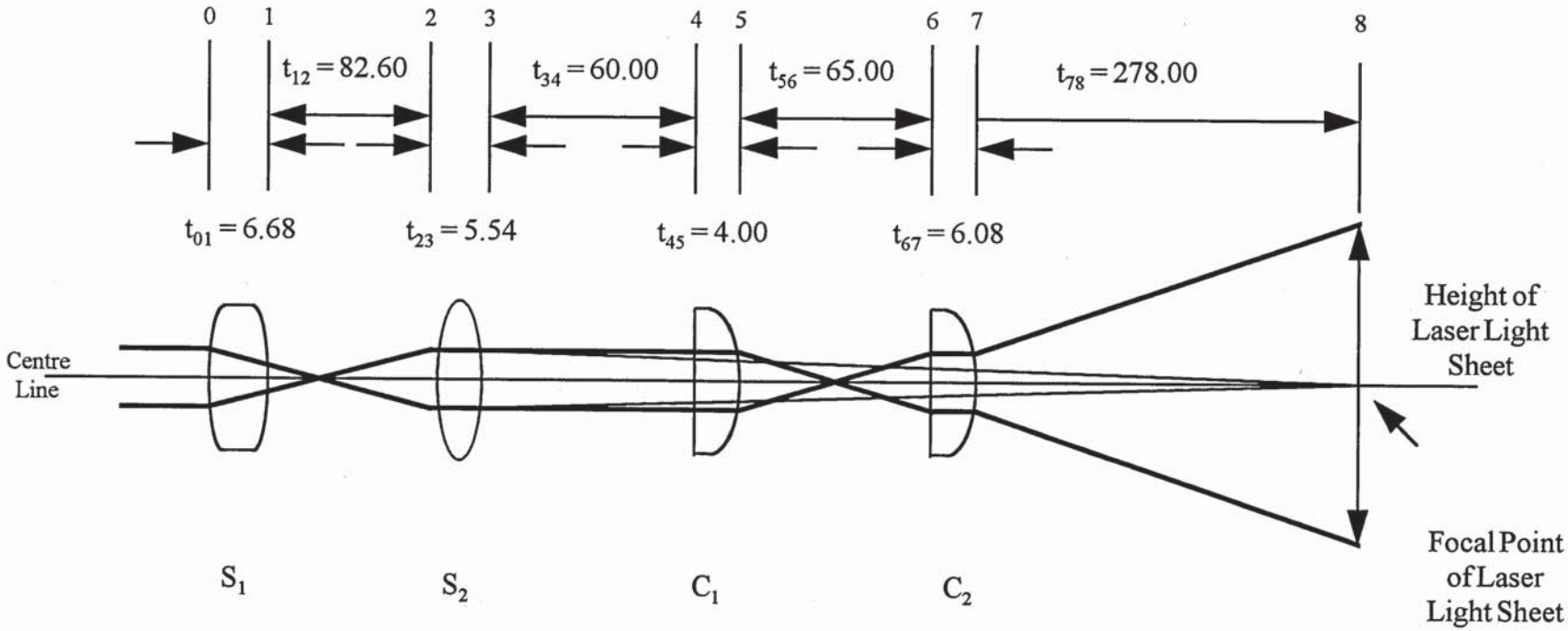


Fig. 23. The pressure tapped disc used to gather the pressure measurements.



(a). General Arrangement

Fig. 24. The Arrangement of the LFV System



The output of S_1 & S_2 is focused at the tunnel's centreline (thin line).
Then, C_1 & C_2 are added to obtain the light sheet (thick line).

See also Table 3

Fig. 24 (b). The Arrangement of the Lenses in the LFV System

All dimensions are in mm

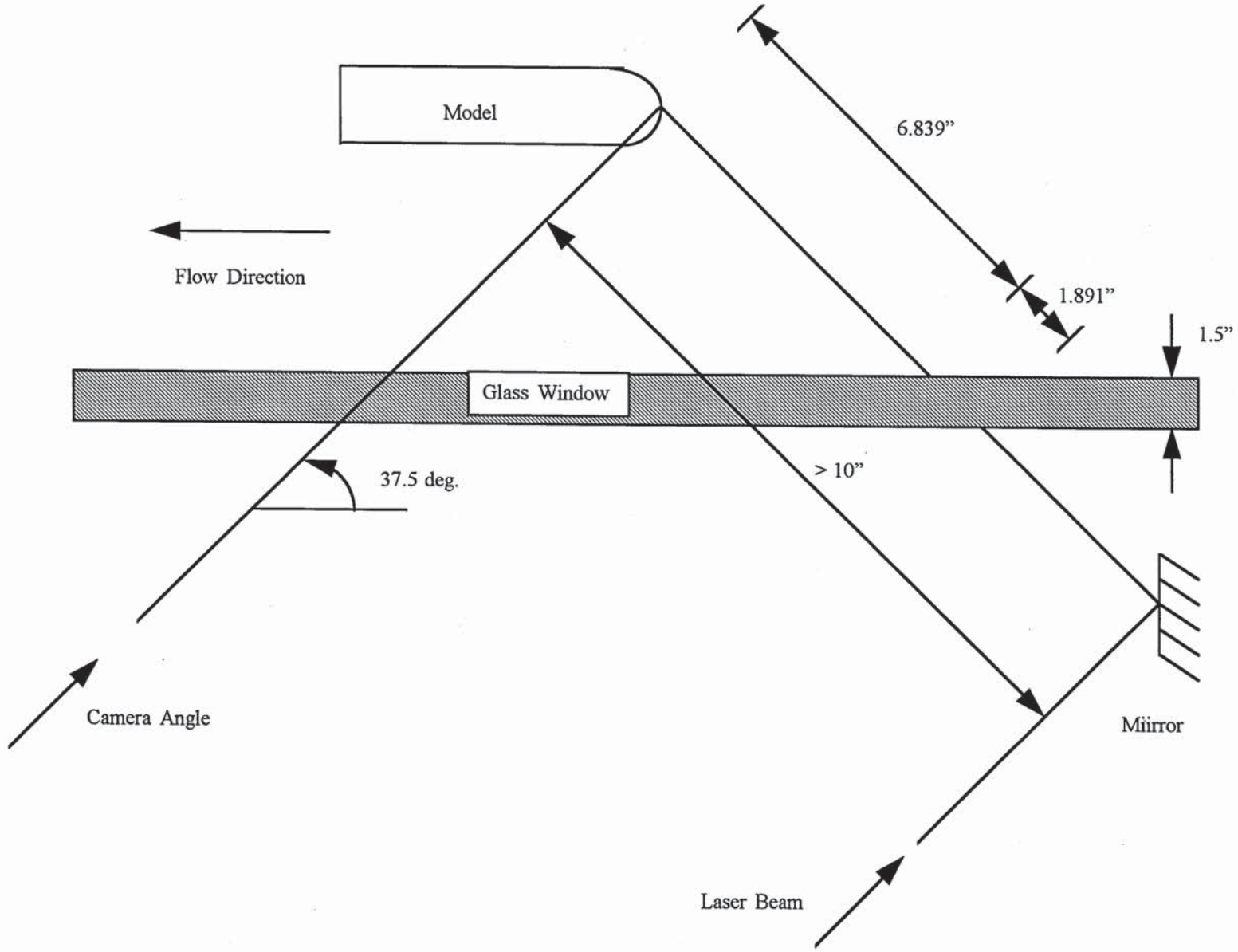


Fig. 24 (c). Limitations on the LFV Equipment

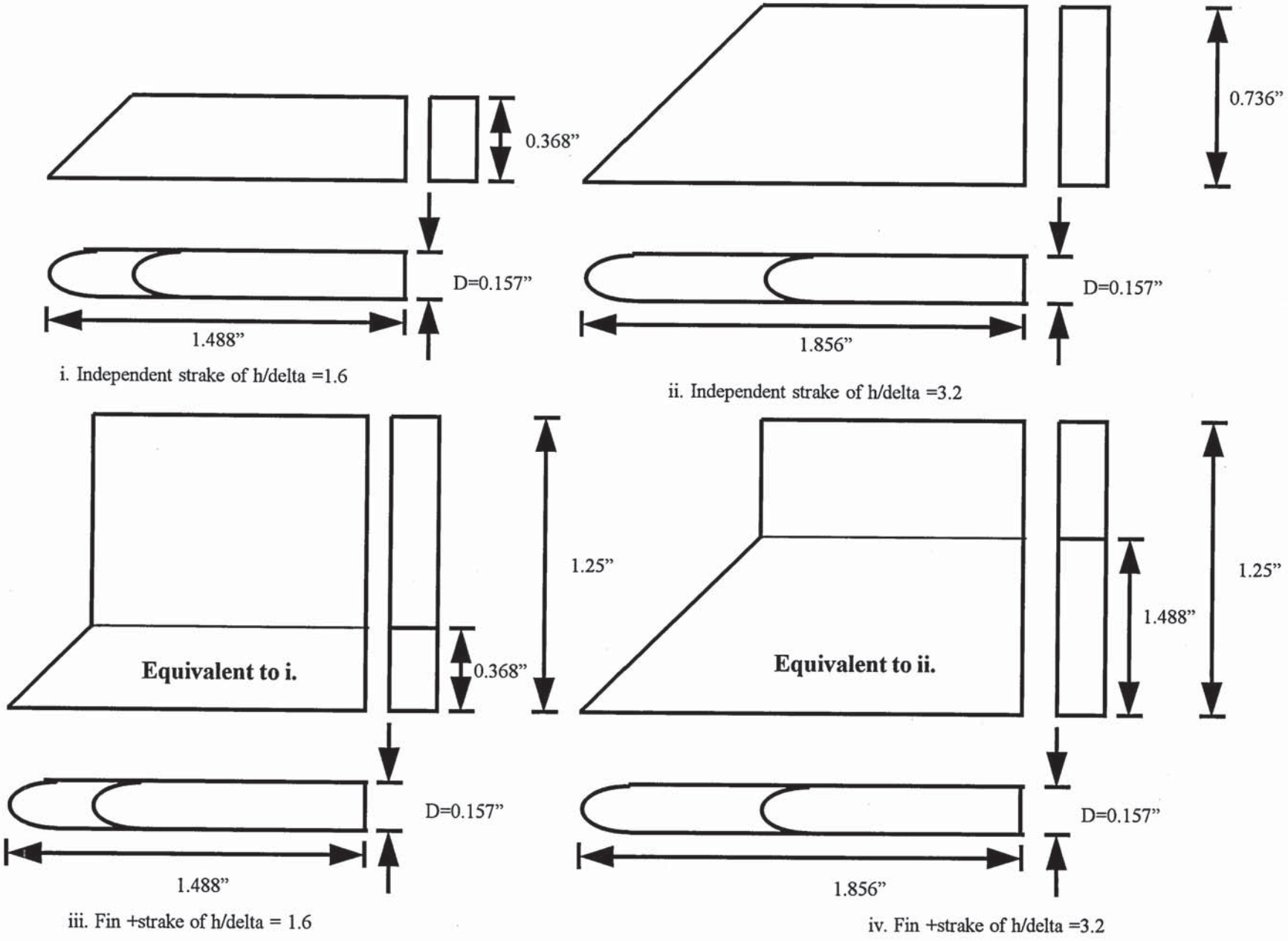
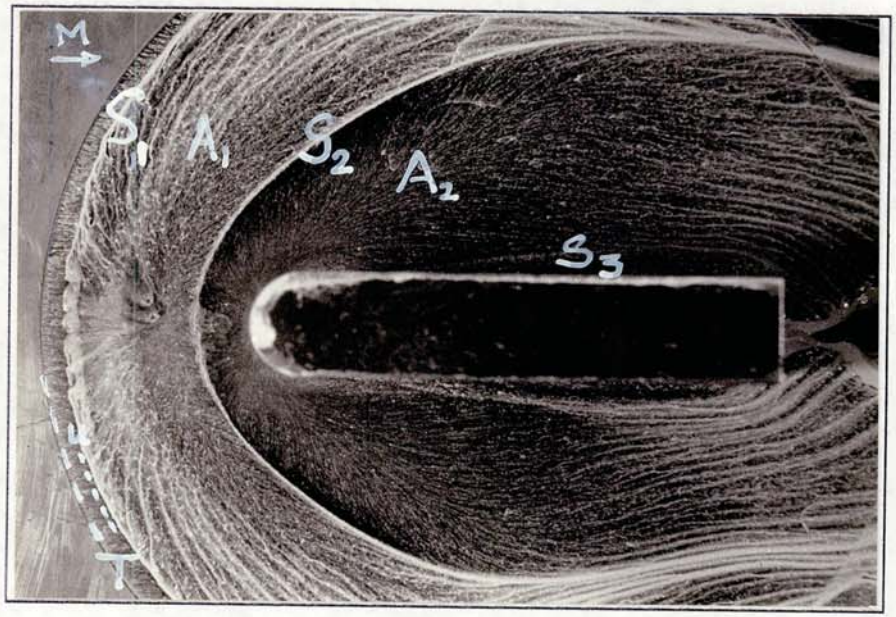


Fig. 25. The models used in the 2.5" x 2.5" wind tunnel (D/δ=0.682).



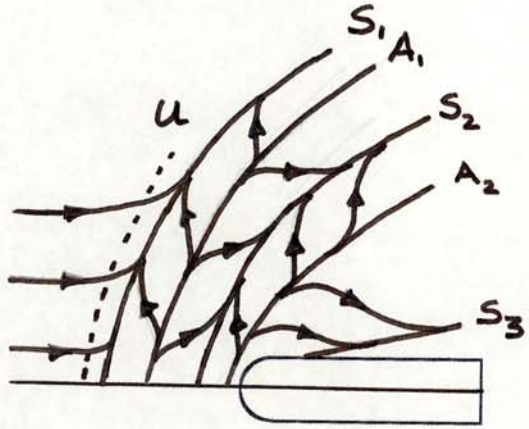
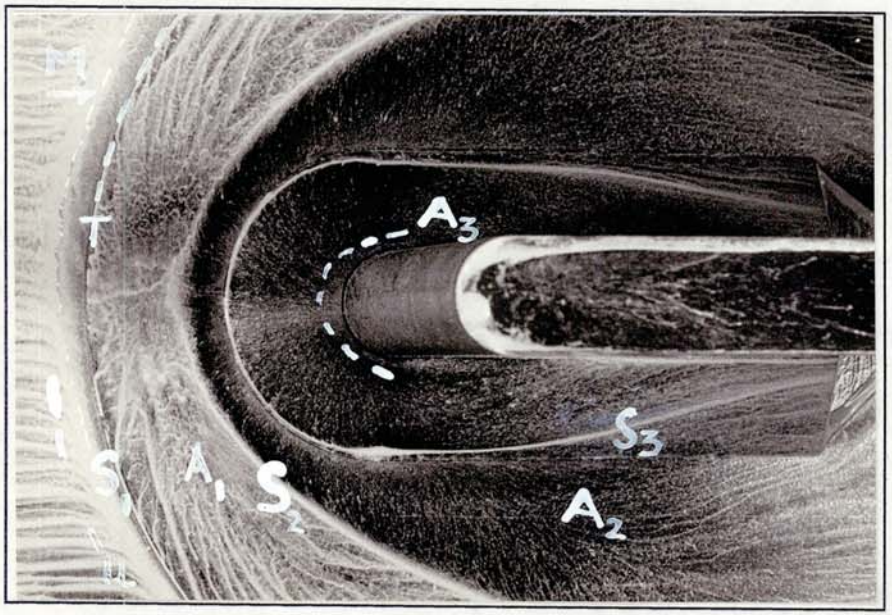


Fig. 26. Oil flow photographs for the straight model of $D/\delta = 1.6$ and its derivatives.
(i) Unmodified fin



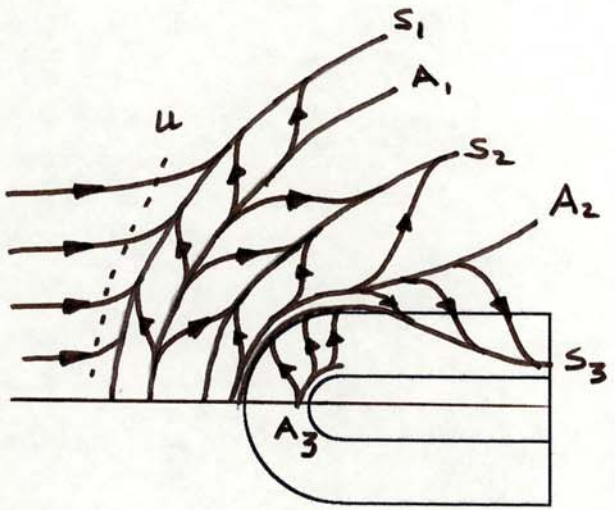
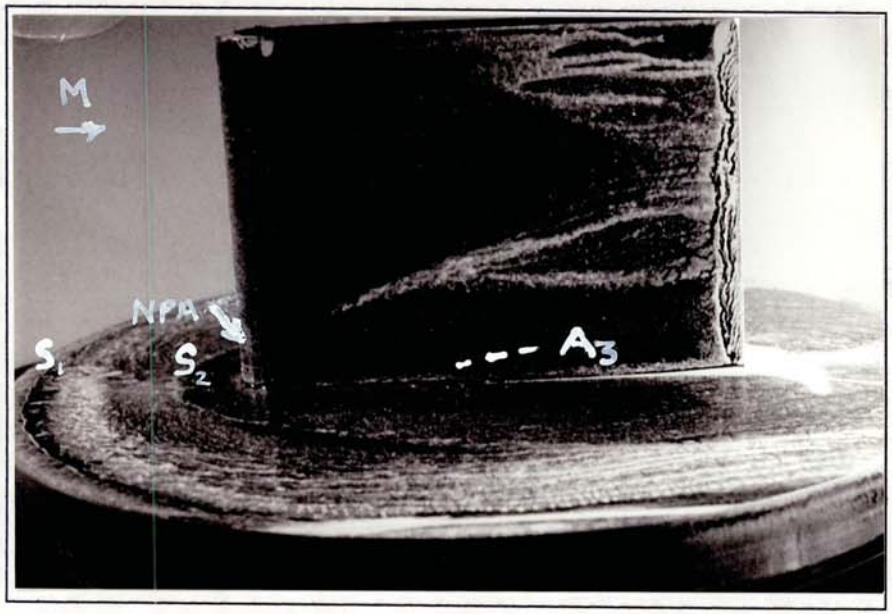


Fig. 26. Contd. 2.
(ii) Fin with Fillet.



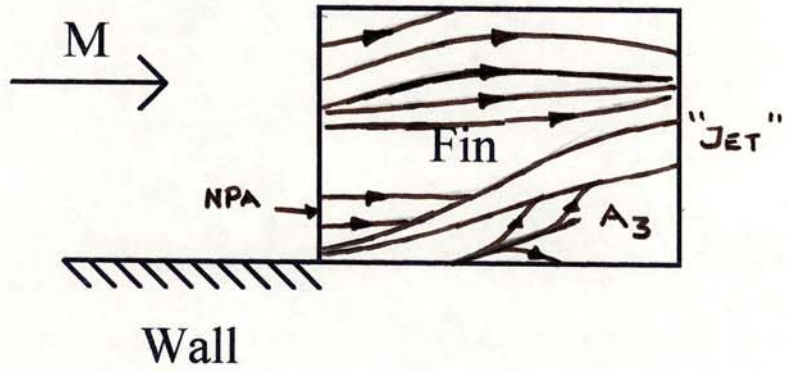
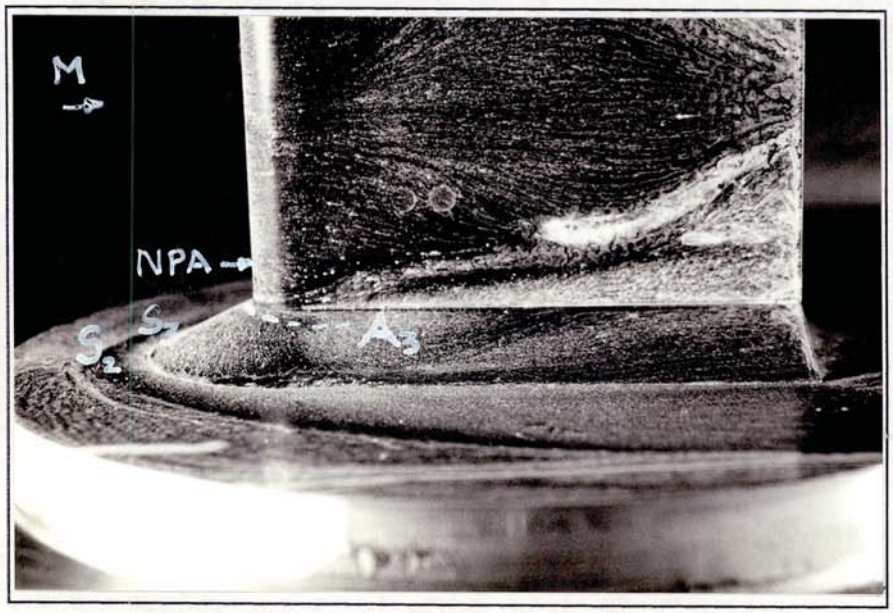


Fig. 26. Contd 4
(iv) Unmodified fin.



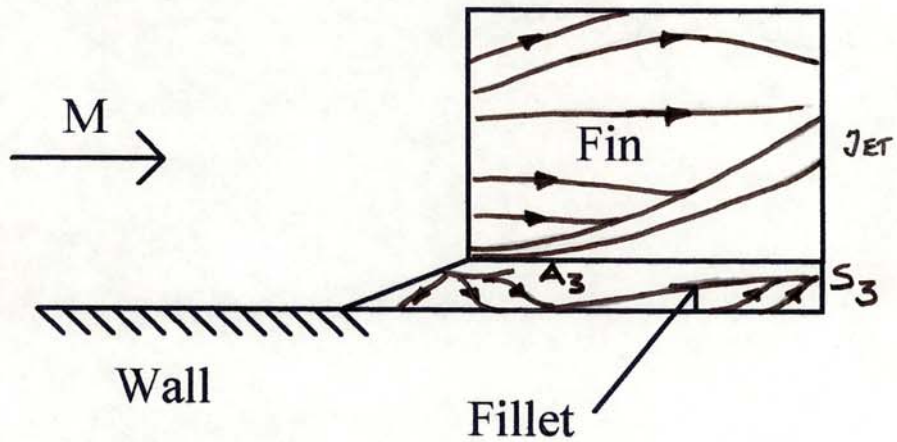
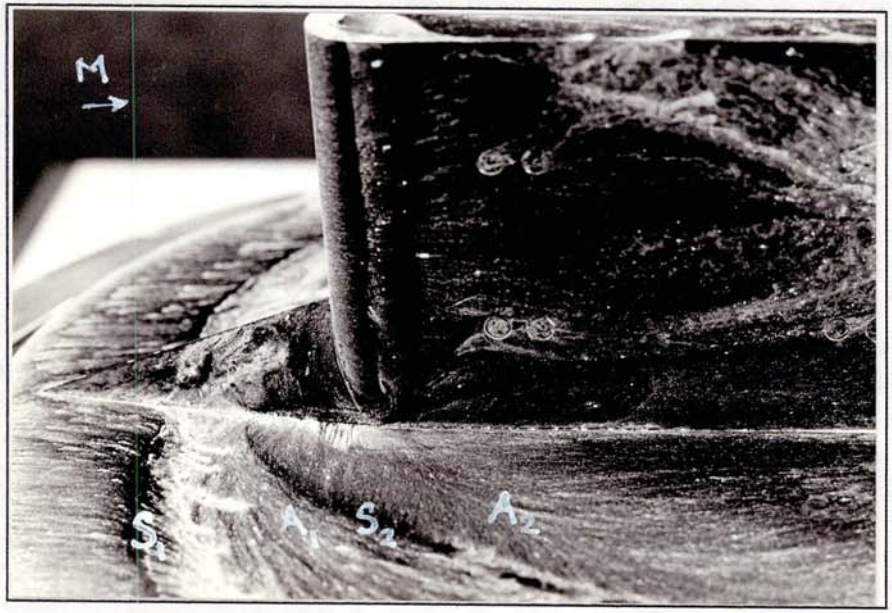


Fig. 26. Contd. 5.
(v) Fin with Fillet.



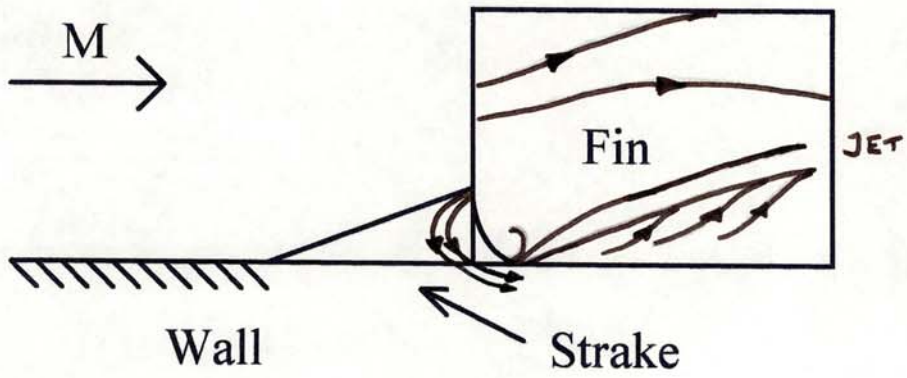


Fig. 26. Contd. 6.
(vi) Fin with sharp strake.

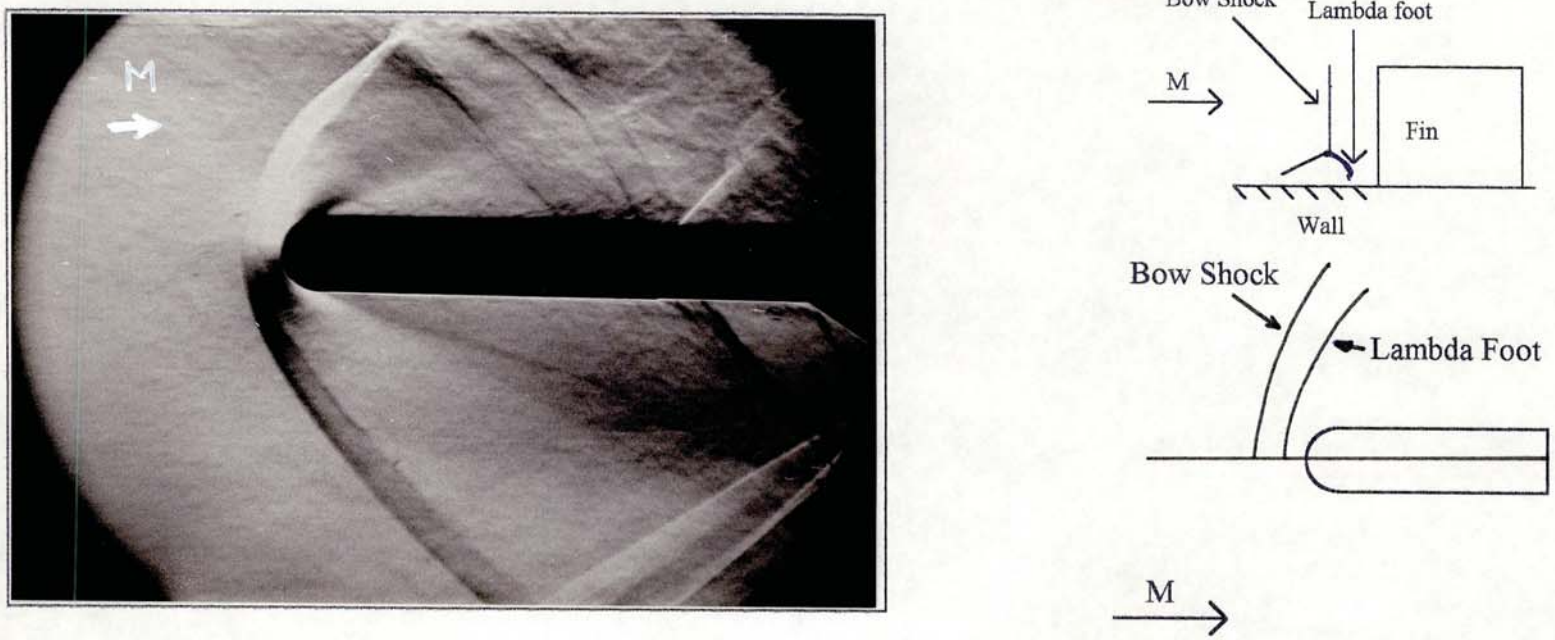
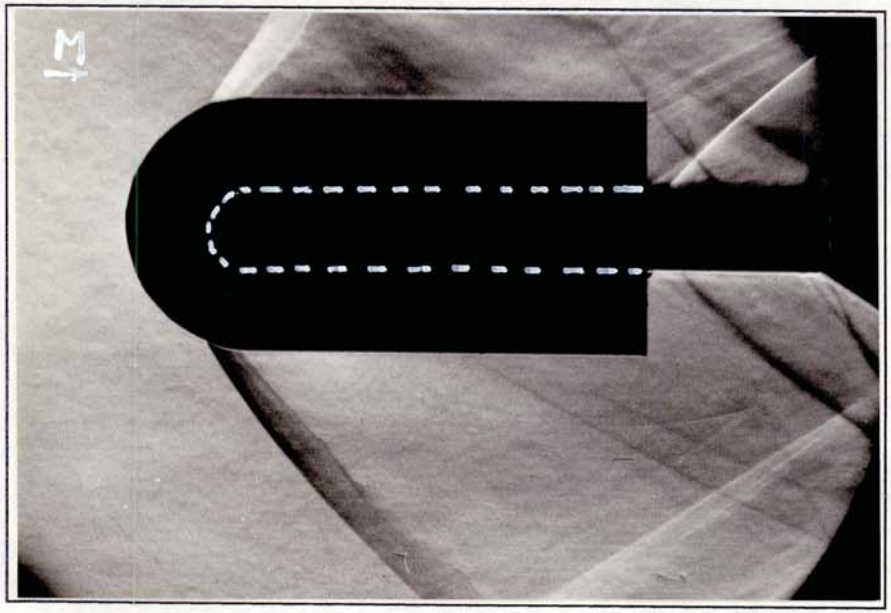


Fig. 27. The location of the shock waves for the straight fin of $D/\delta = 1.6$ and its derivatives.
(a) Photographs of the shocks.
(i) Unmodified fin.



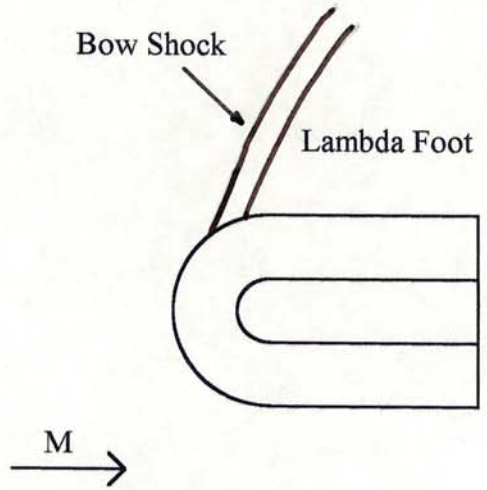
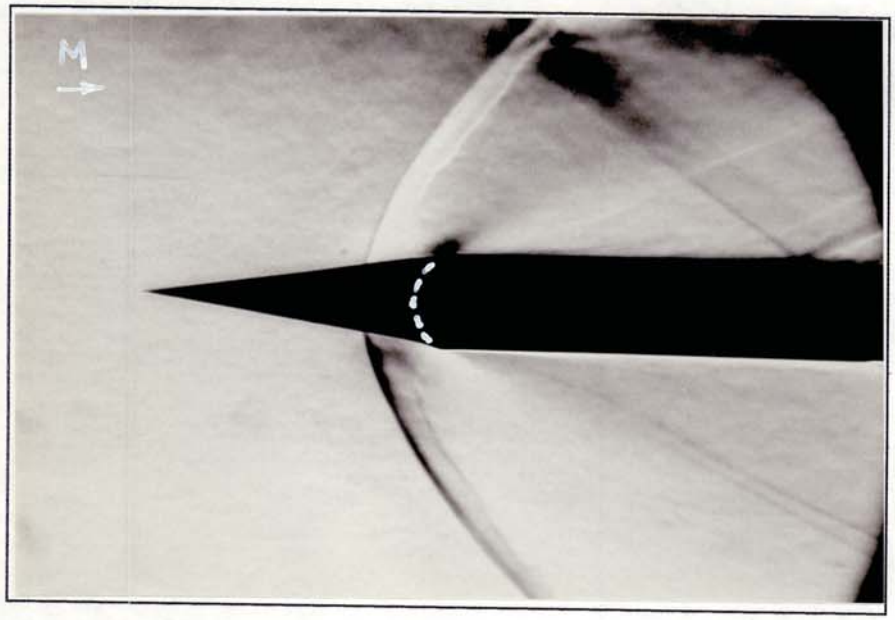


Fig. 27 (a). Contd. 1.
(ii) Fin with Fillet.



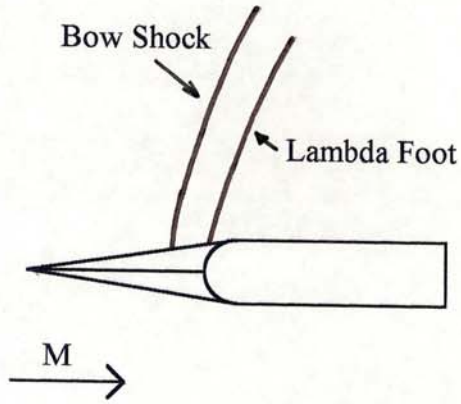


Fig. 27 (a). Contd. 2.
(iii) Fin with Sharp Strake.

Fig. 27 (b). The location of the bow shock waves for the straight fin of $D/\delta = 1.6$ with and without a fillet.

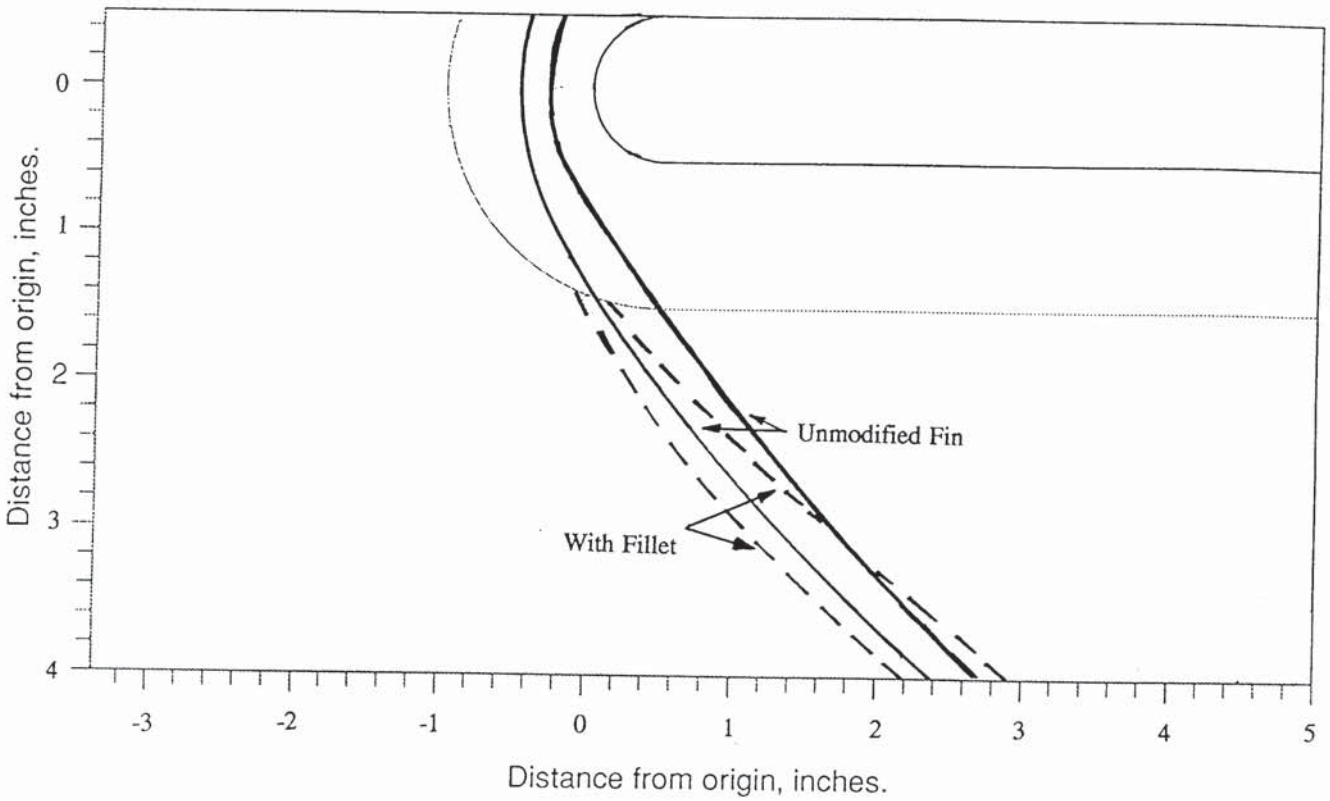
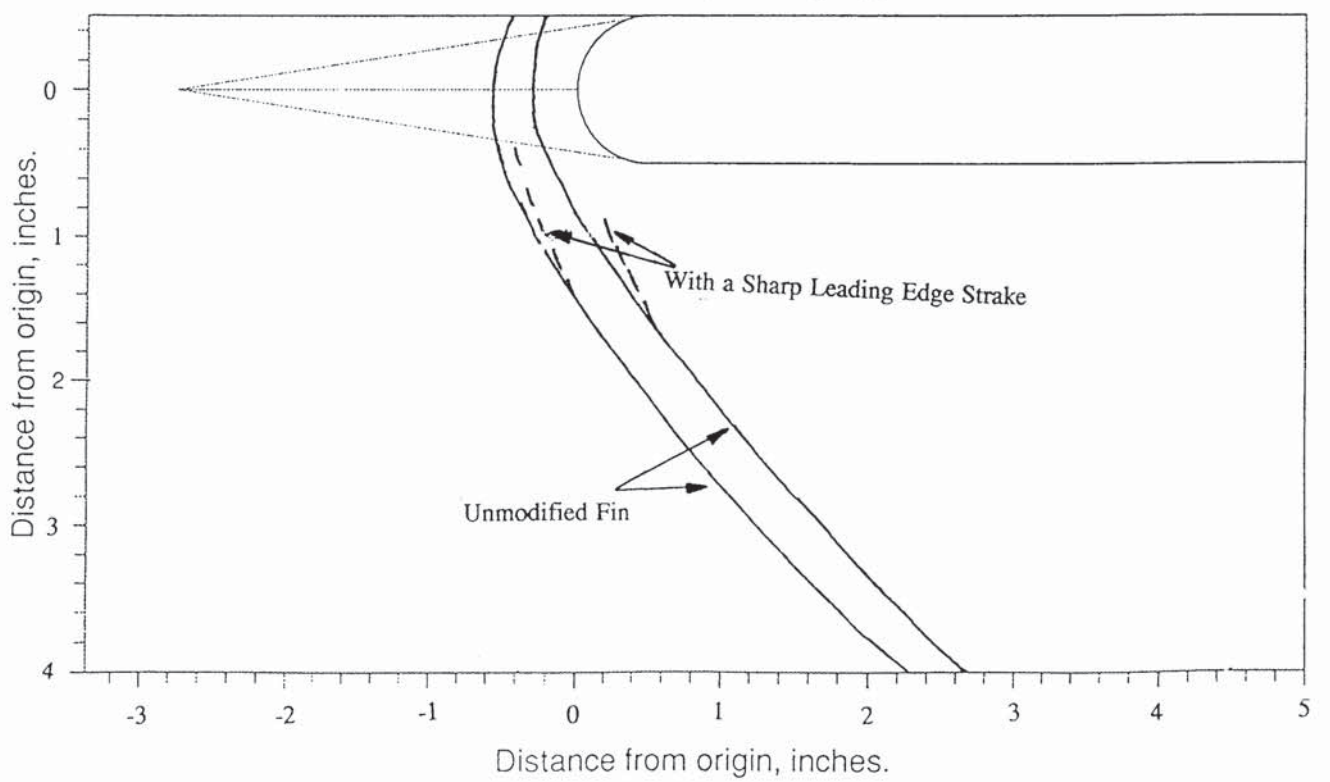
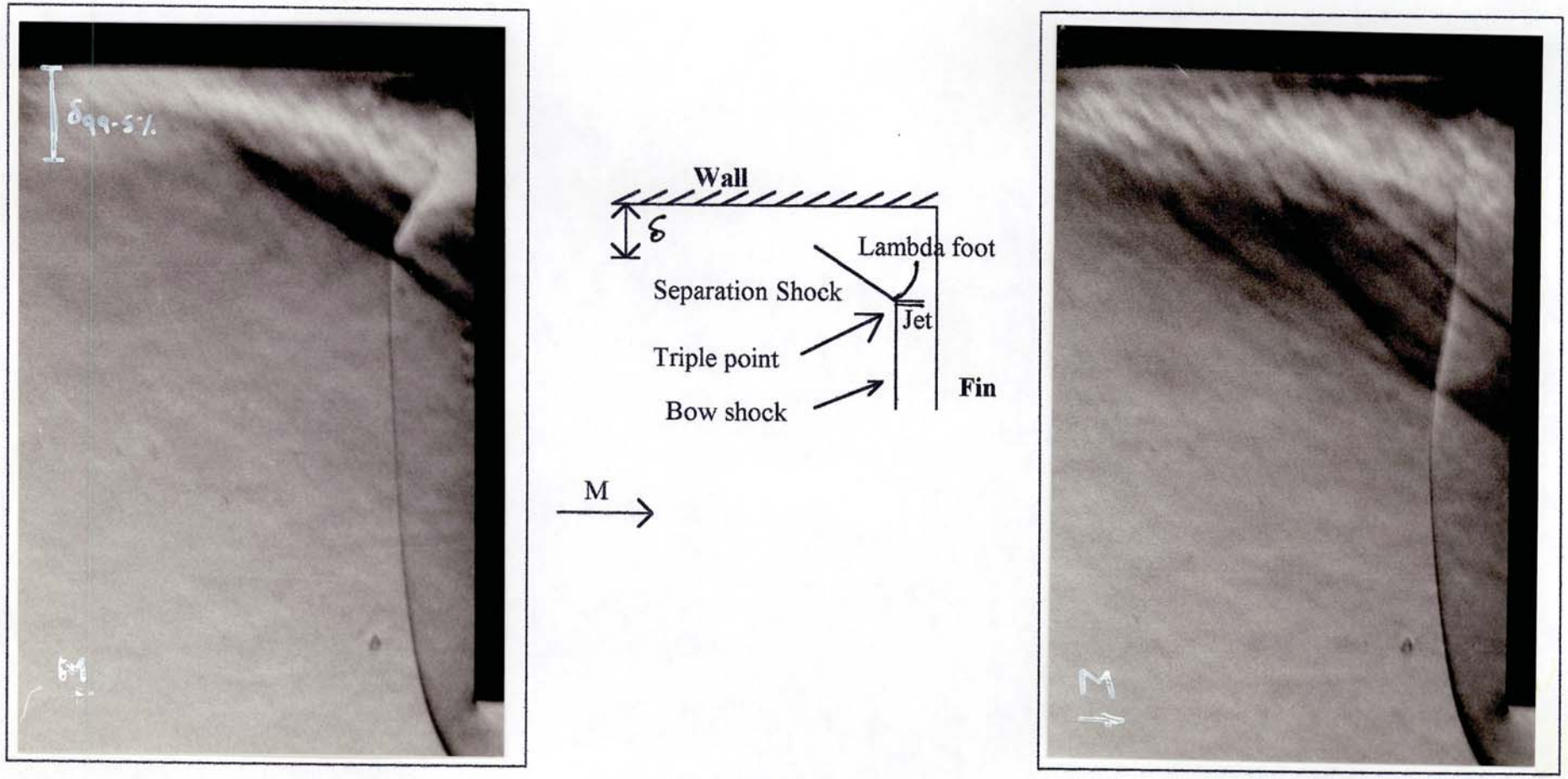


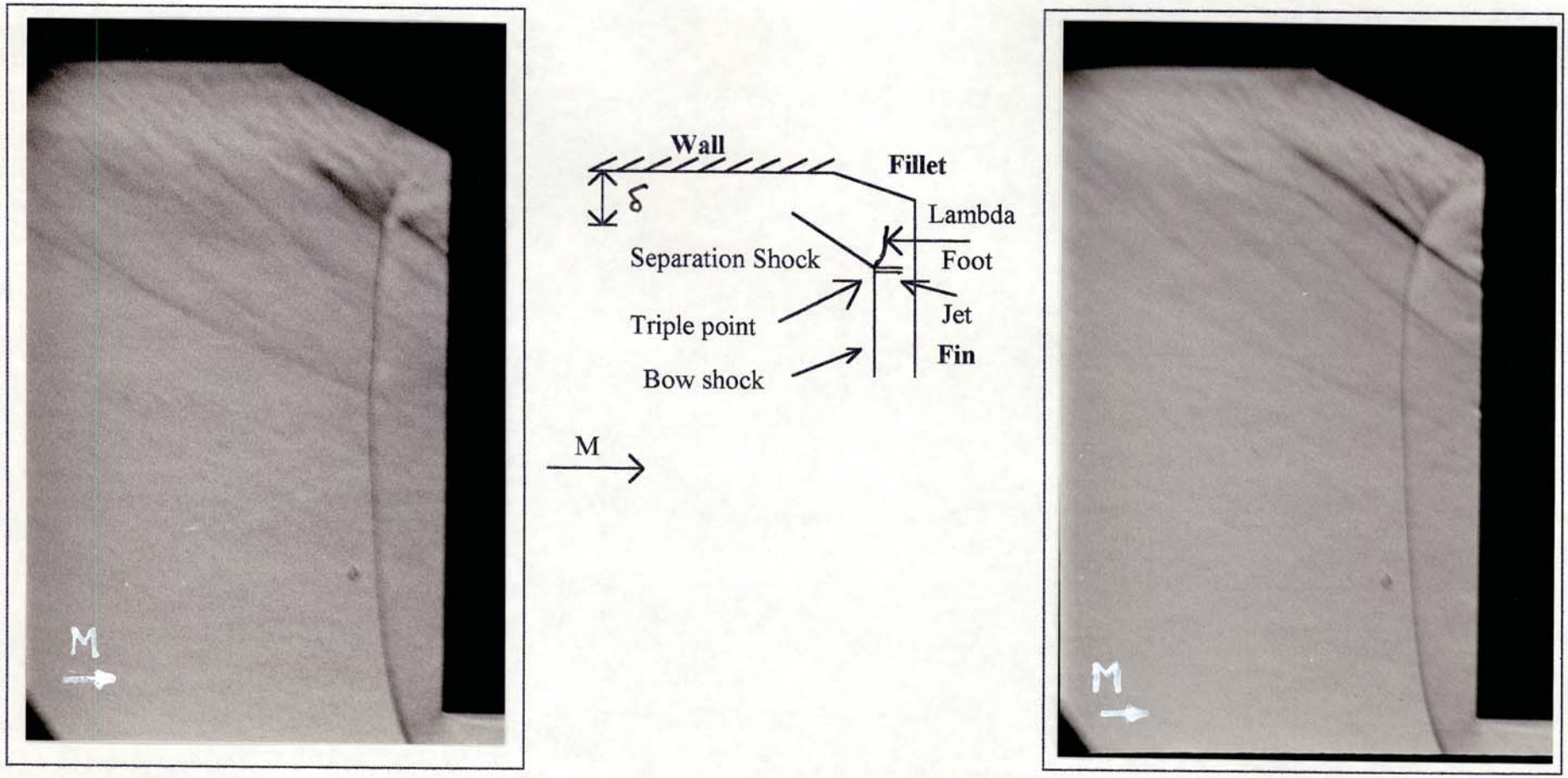
Fig. 27 (c). The location of the bow shock waves for the straight fin of $D/\delta = 1.6$ with and without a sharp leading edge strake.





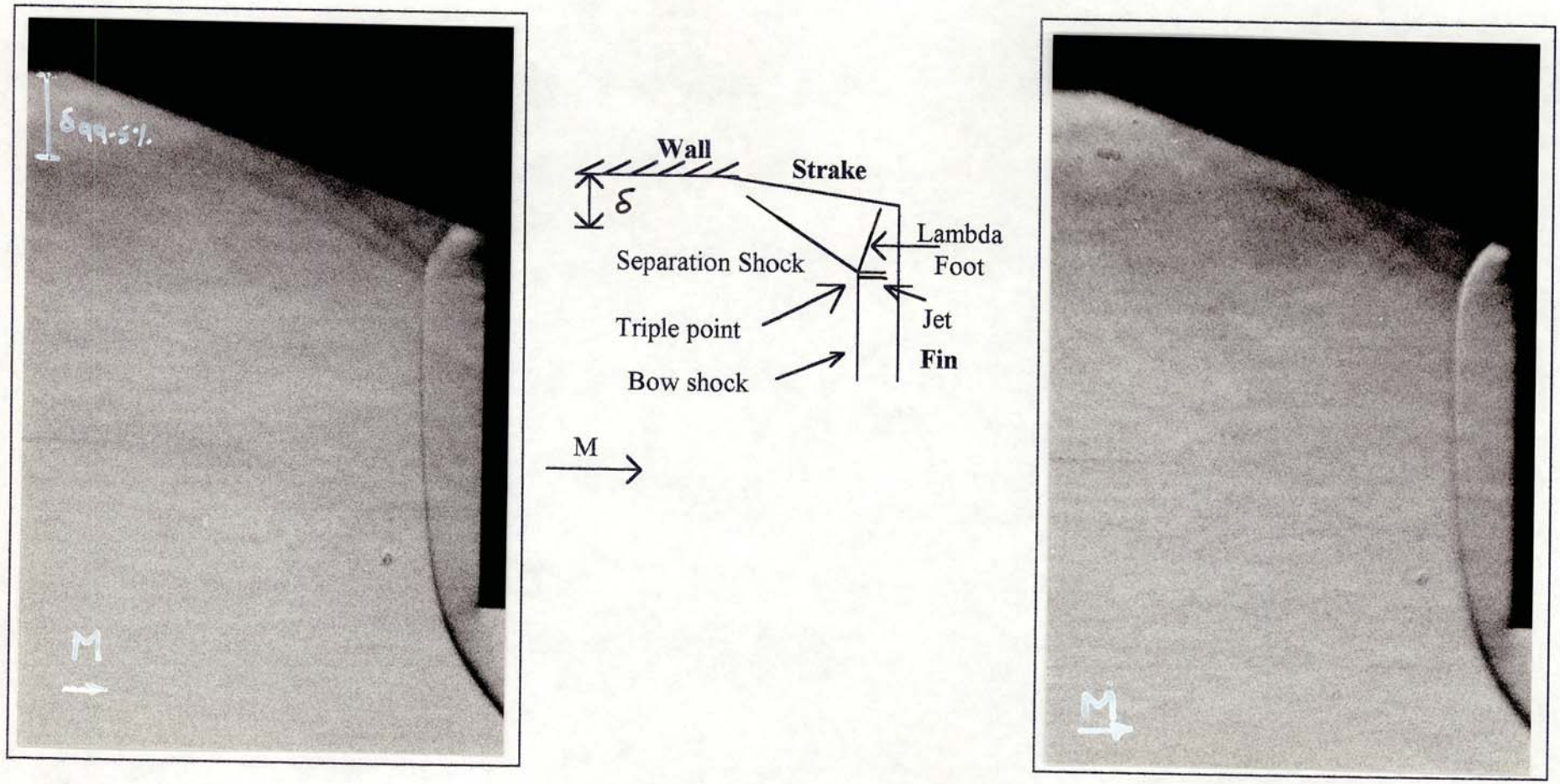
(i) Unmodified Fin

Fig. 28. Individually exposed side view schlieren photographs for the straight fin of $D/\delta = 1.6$ and its derivatives.



(ii) Filleted Fin

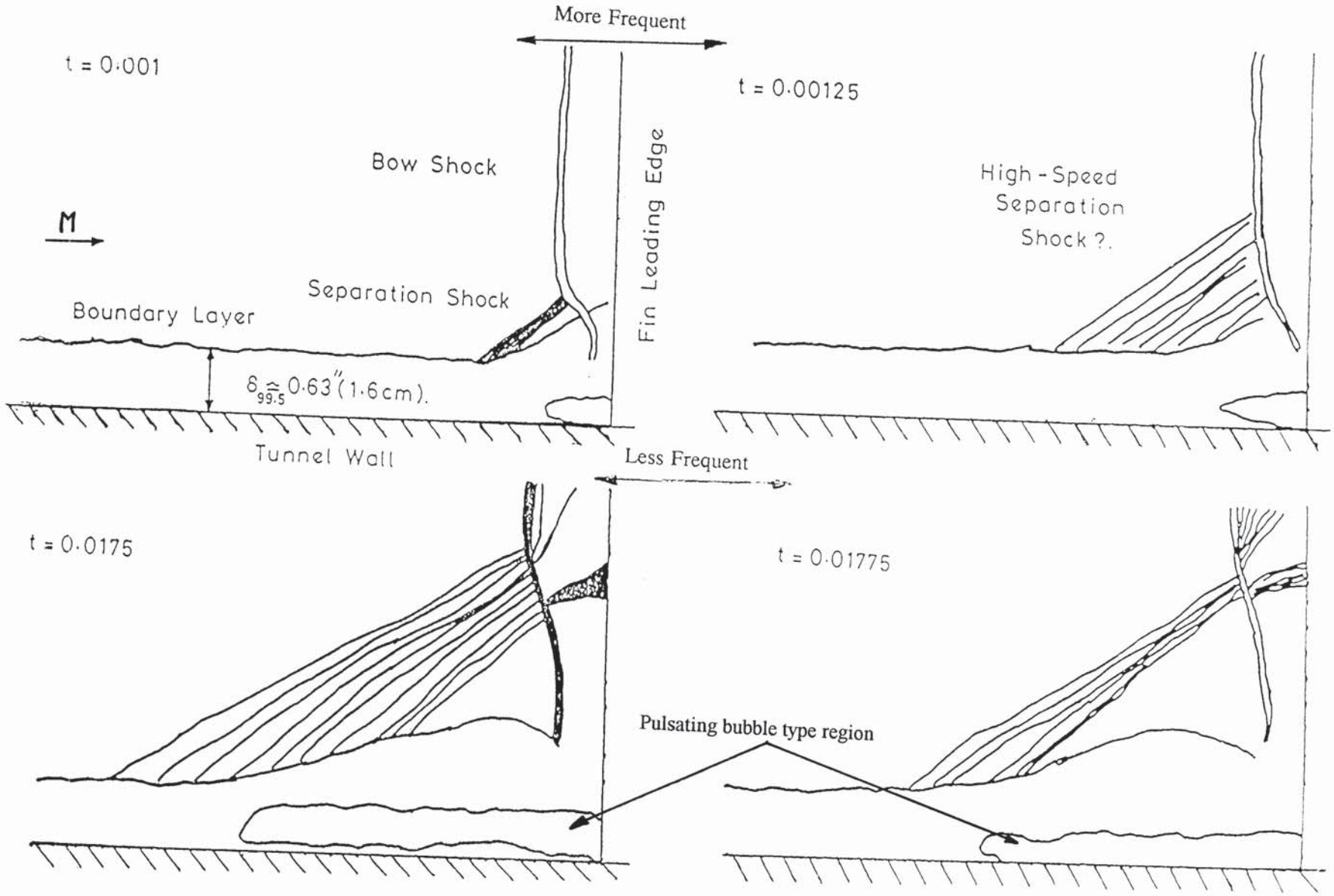
Fig. 28. (Contd. 1).

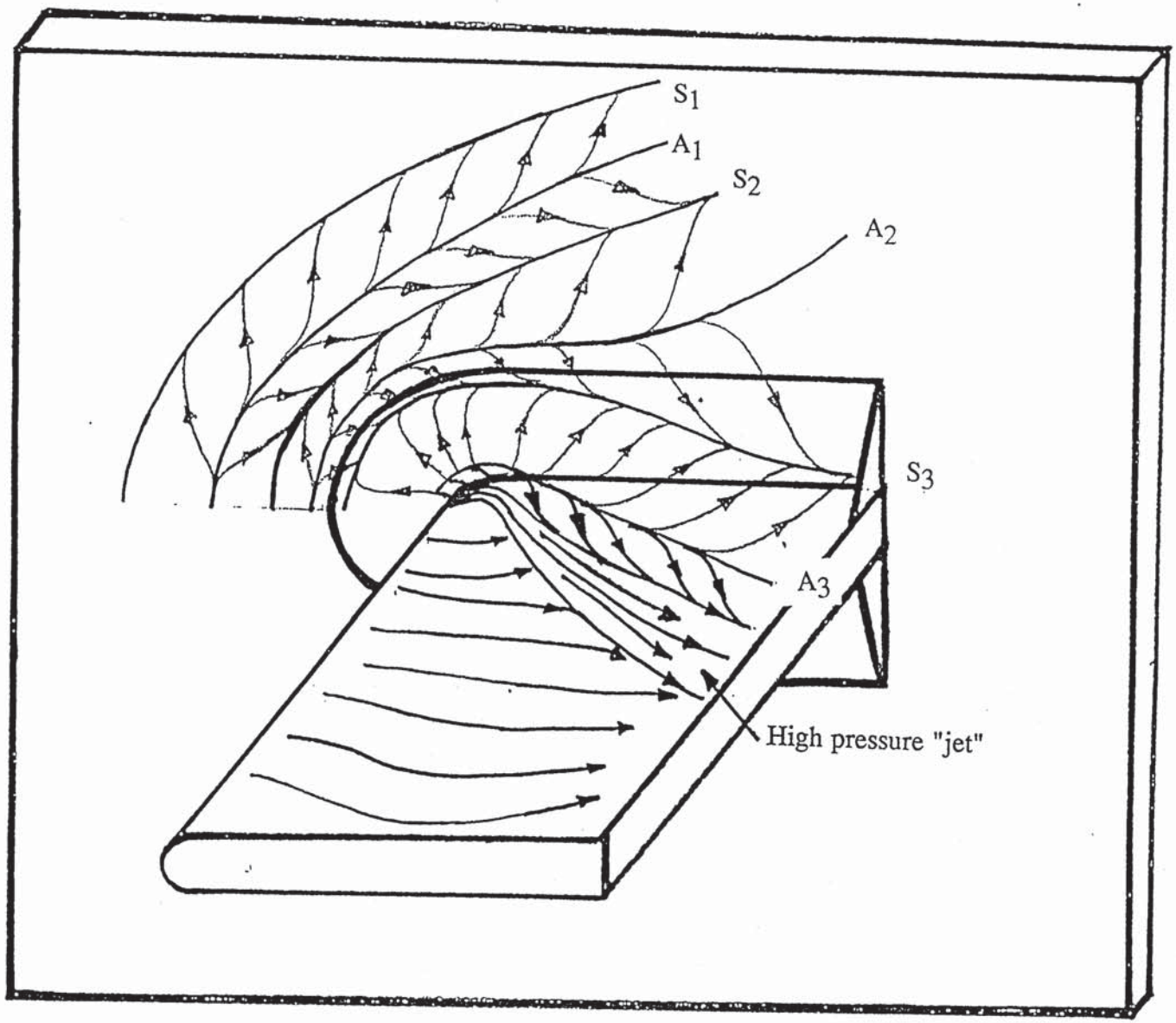


(iii) Fin with Sharp Strake

Fig. 28. (Contd. 2)

Fig. 29. Selected frames from a high speed cine film taken at 4 kHz of a straight blunt fin, leading edge diameter = 1".





(a) Streak line pattern

Fig. 30. Flow field model for the straight fin of $D/\delta = 1.6$ with a fillet.

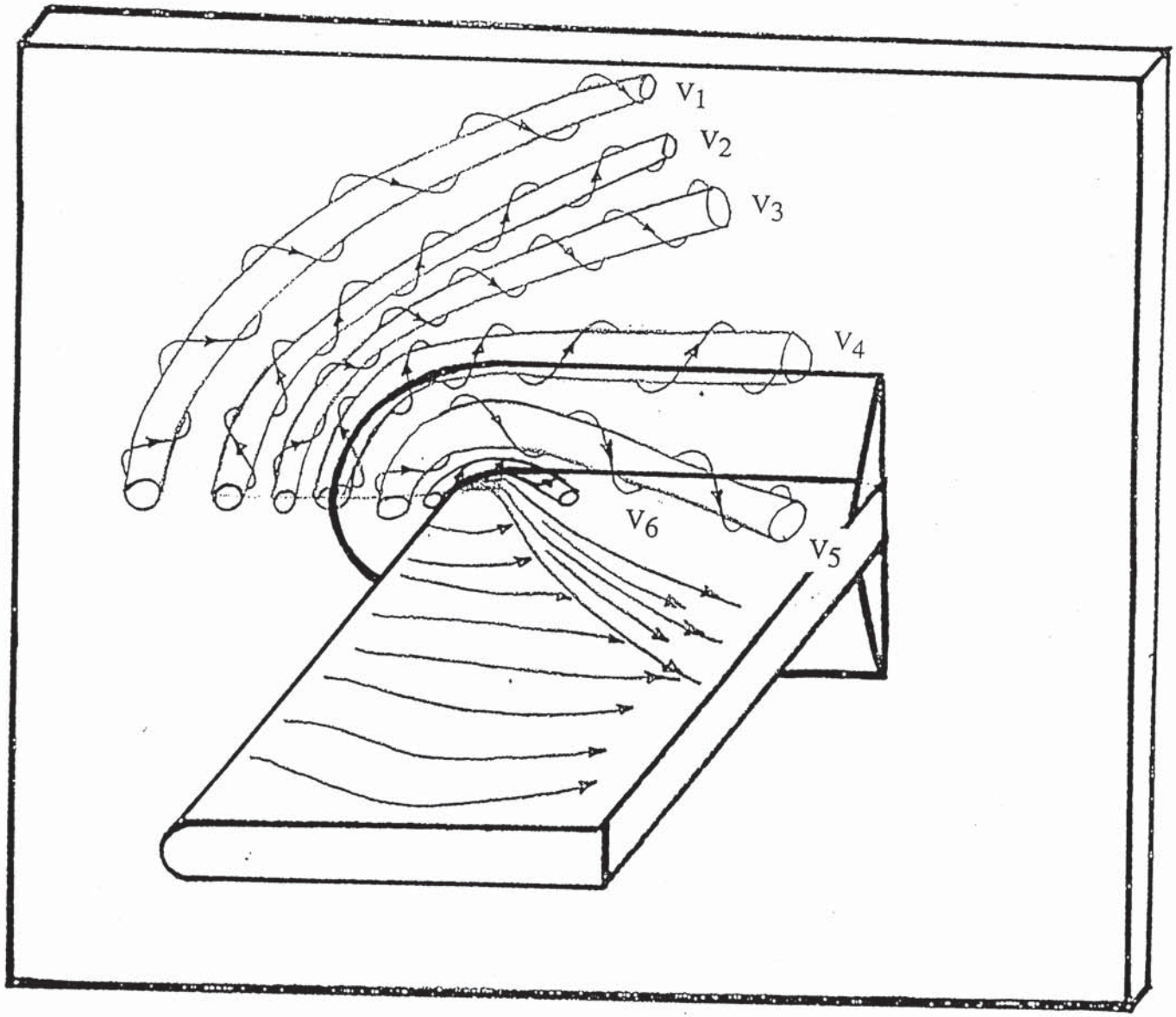


Fig. 30 (b). Vortex skeleton representation

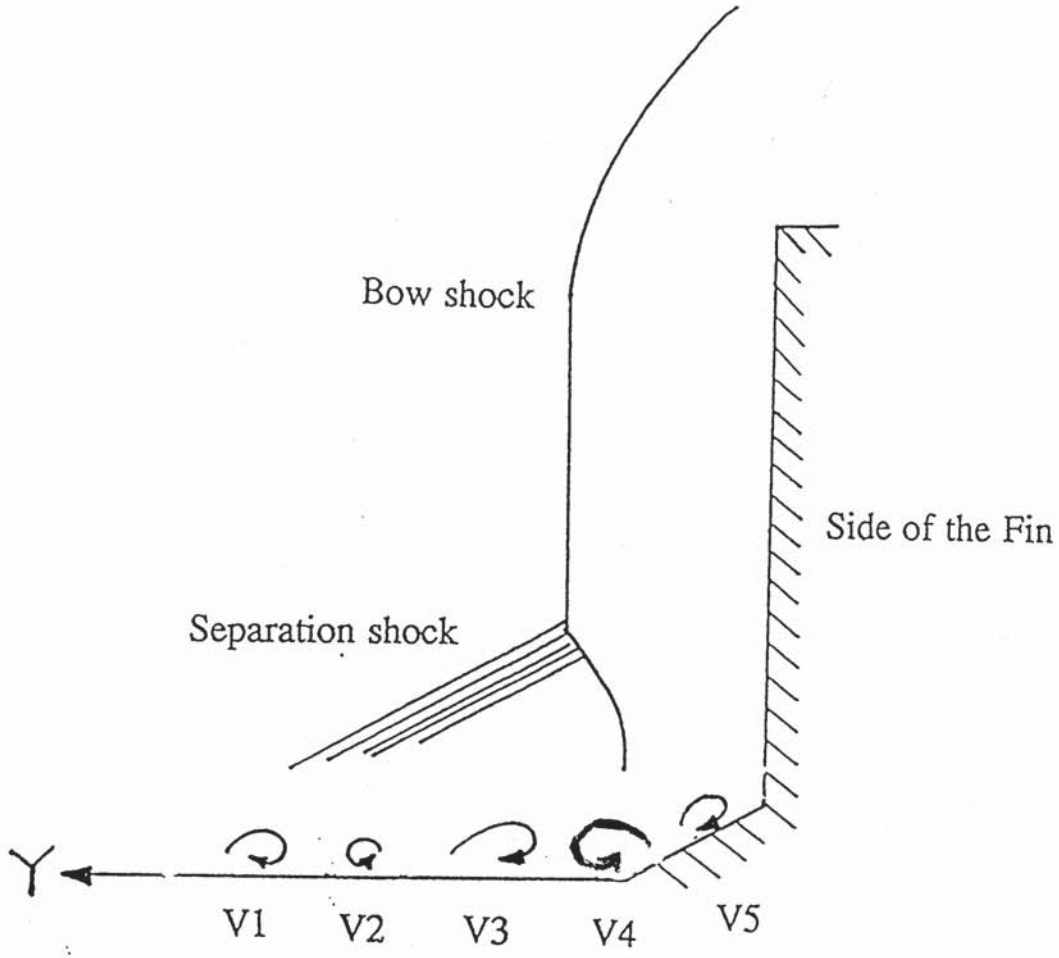
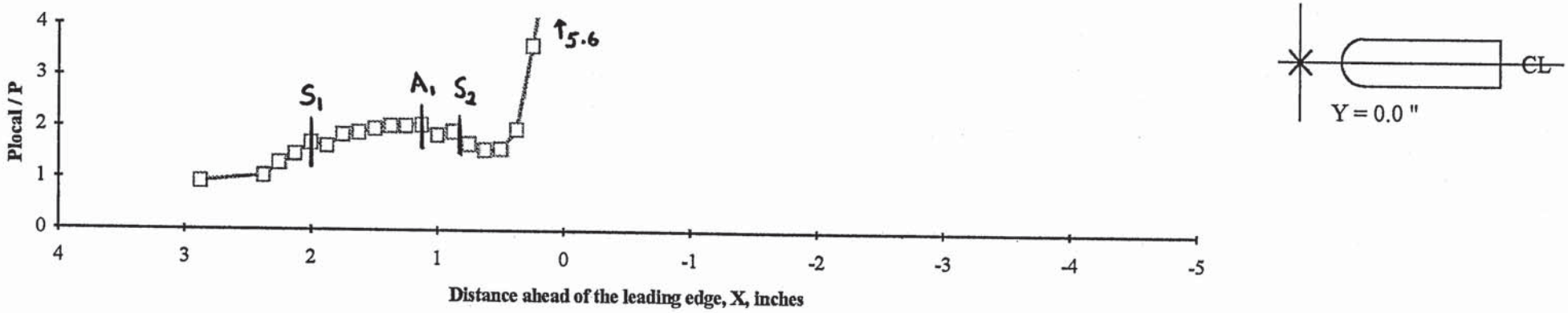


Fig. 30 (c). Slice throught the flow field generated by the unswept fin of $D/\delta = 1.6$ with a fillet at $x = 2.5"$.

The Straight Fin with and without a Fillet, Y = 0.0"

i. The Straight Fin



ii. With Fillet

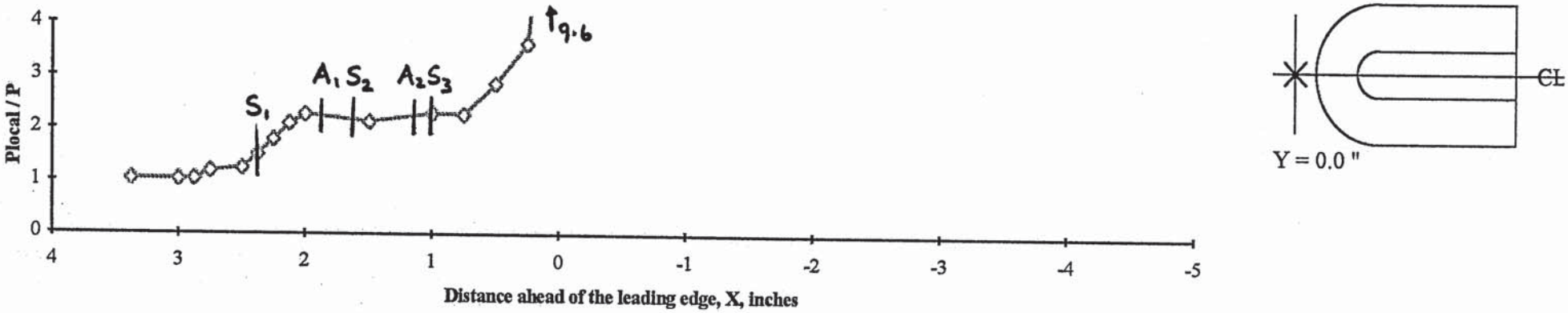
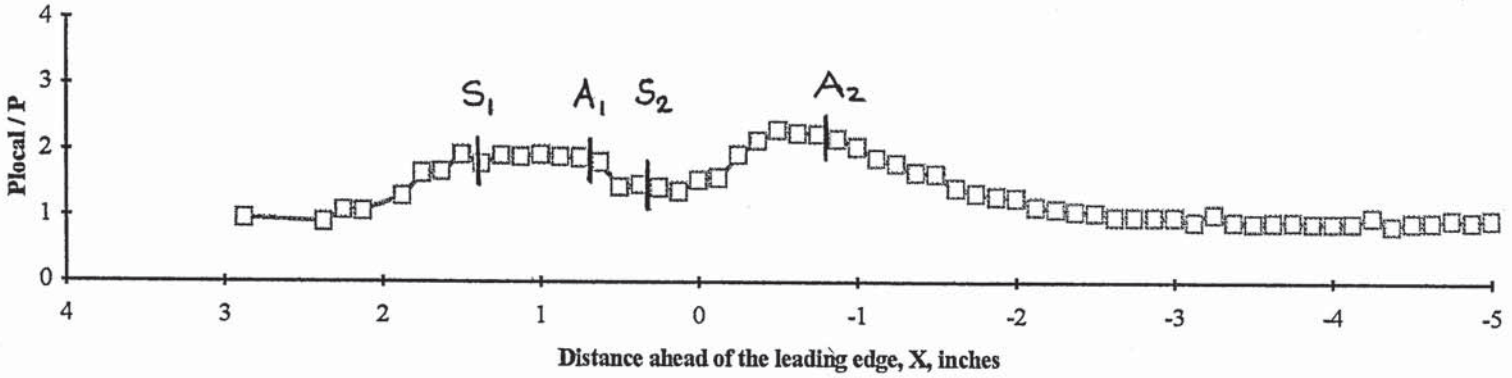
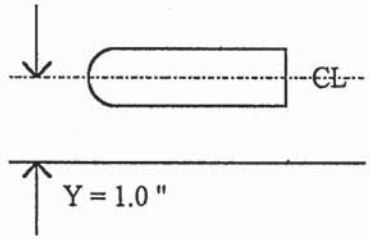


Fig. 31. Pressure Plots for the Straight Fin of D/δ = 1.6 with and without a Fillet

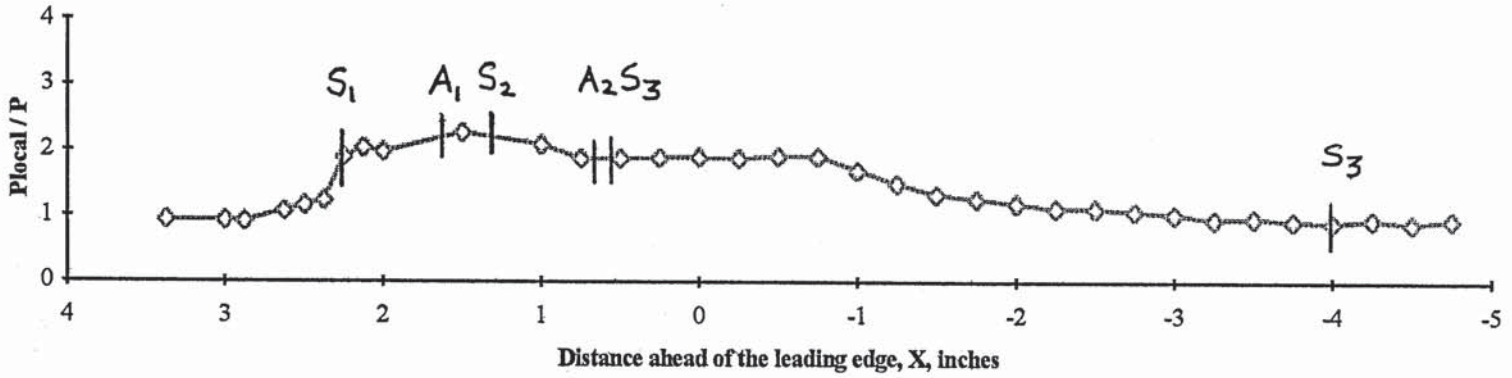
The Straight Fin with and without a Fillet, Y = 1.0"

iii. The Straight Fin





iv. With Fillet



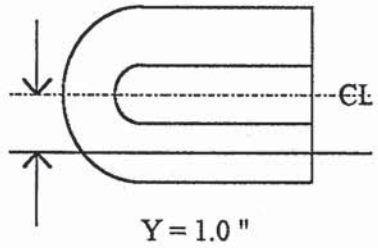
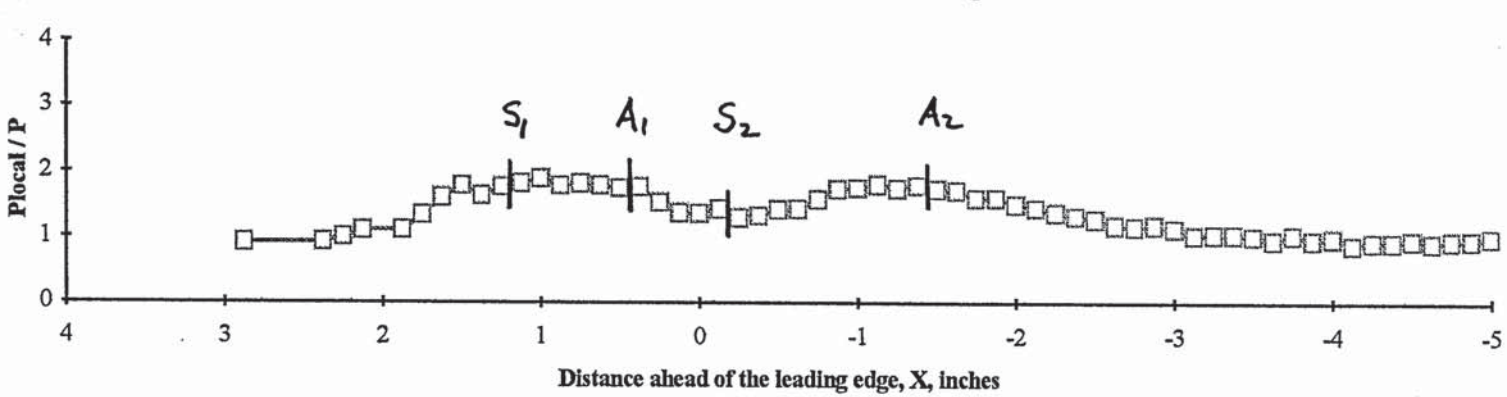
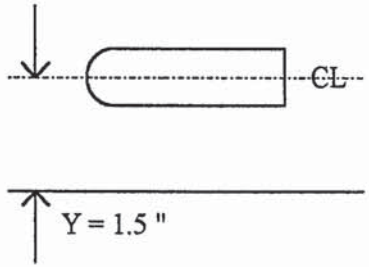


Fig. 31 (Contd. 1).

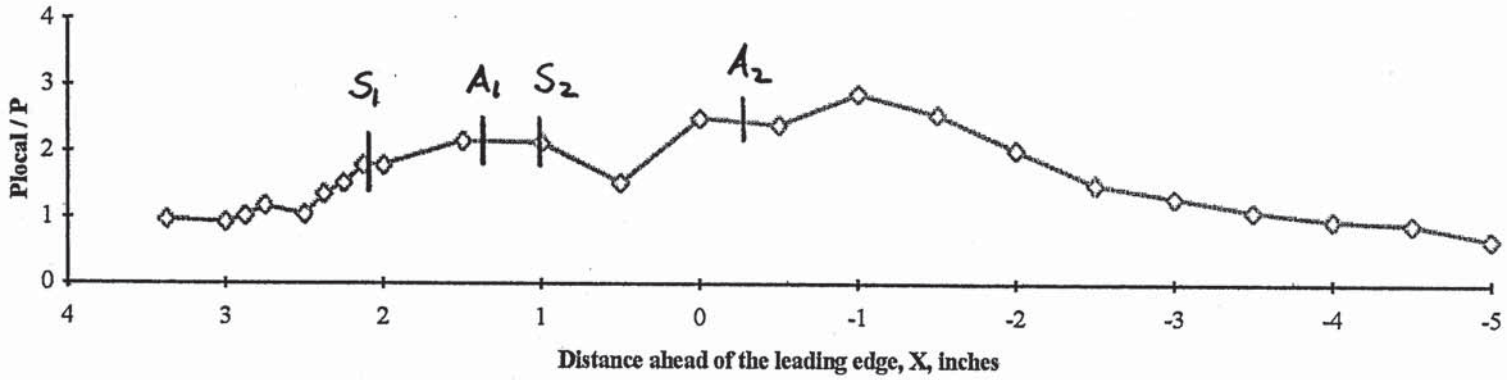
The Straight Fin with and without a Fillet, Y = 1.5"

v. The Straight Fin





vi. With Fillet



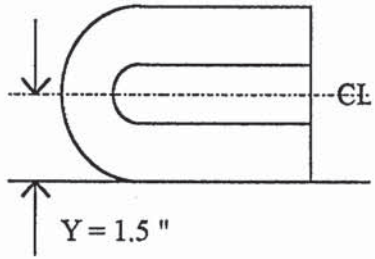
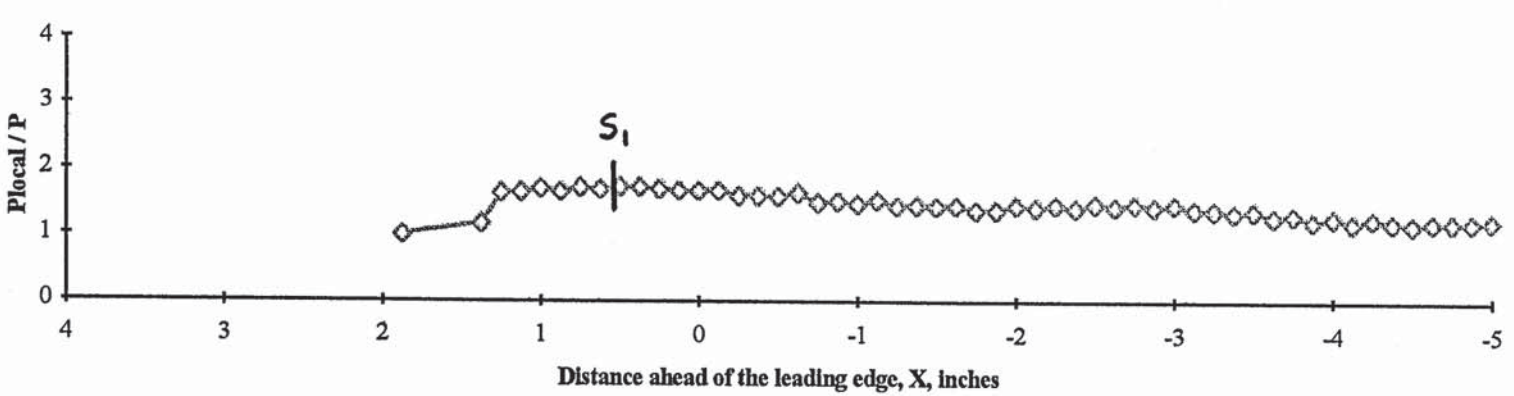
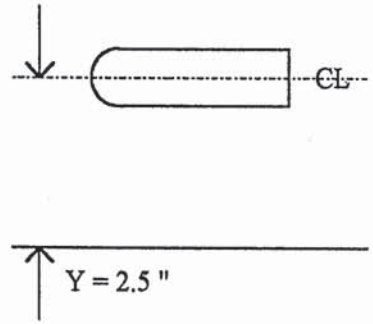


Fig. 31 (Contd. 2).

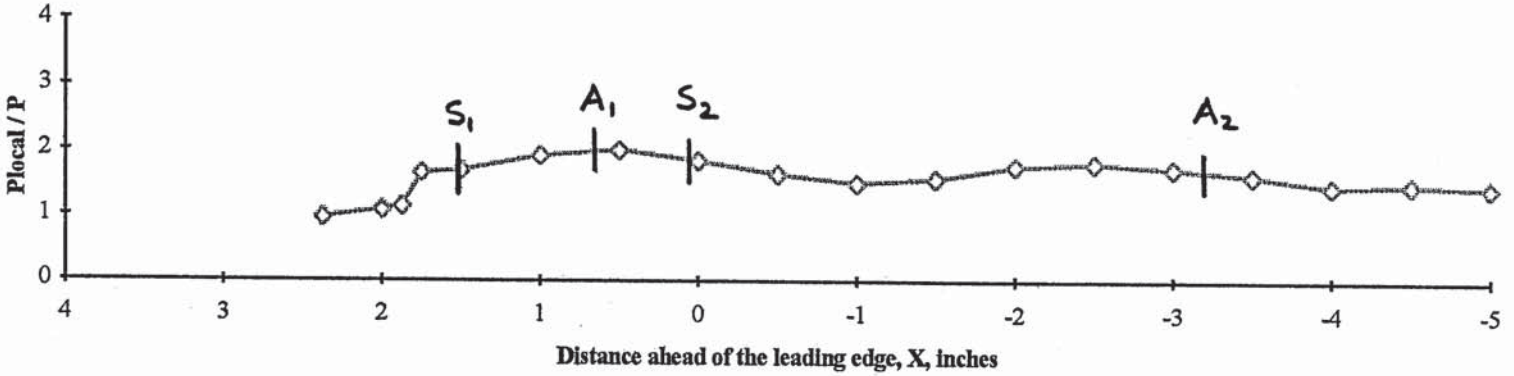
The Straight Fin with and without a Fillet, Y = 2.5"

vii. The Straight Fin





viii. With Fillet



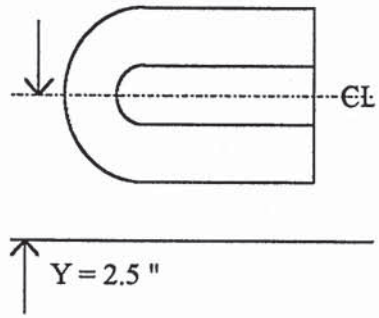
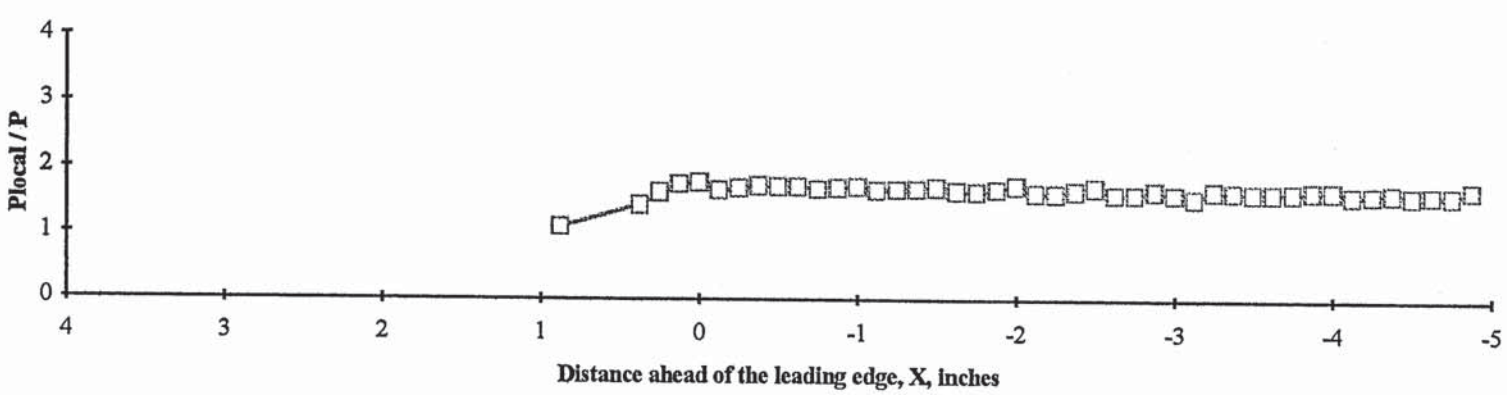
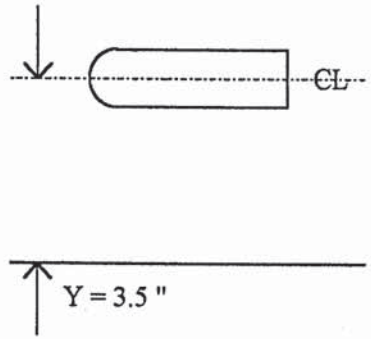


Fig. 31 (Contd. 3).

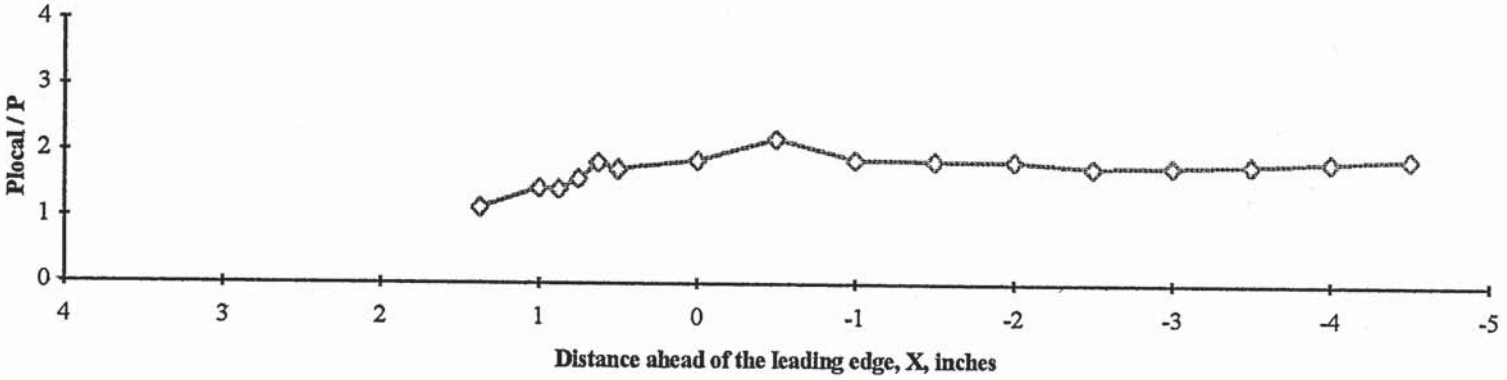
The Straight Fin with and without a Fillet, Y = 3.5"

ix. The Straight Fin





x. With Fillet



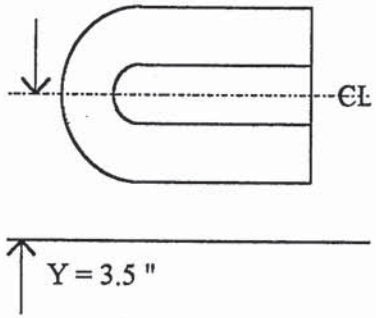
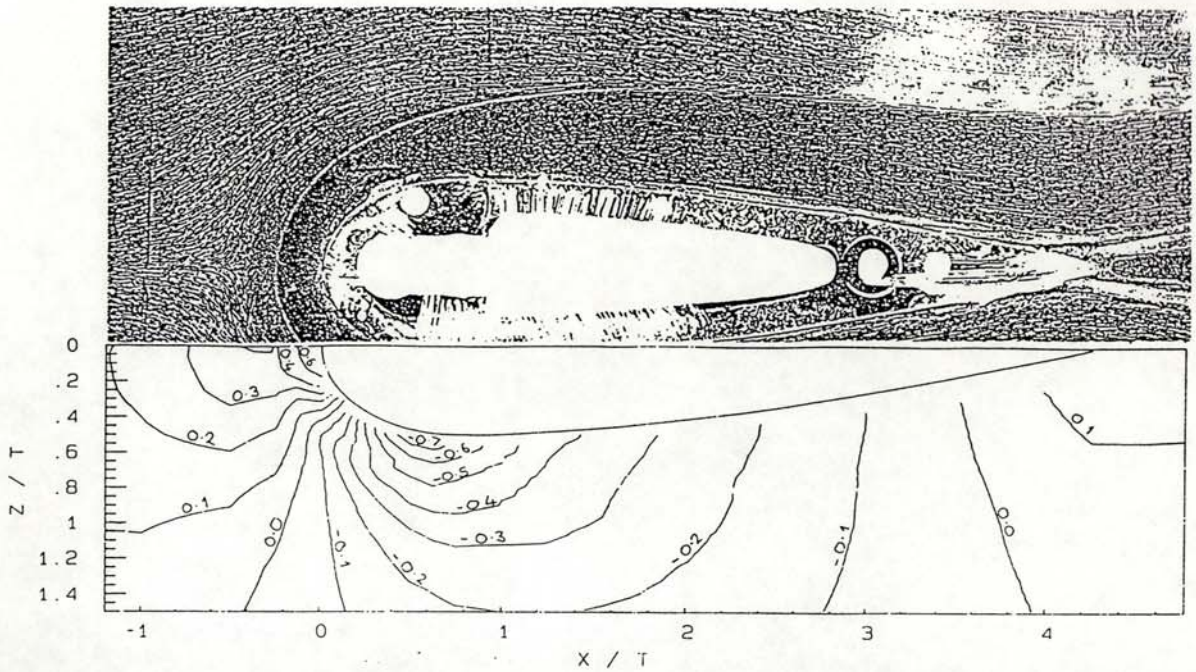
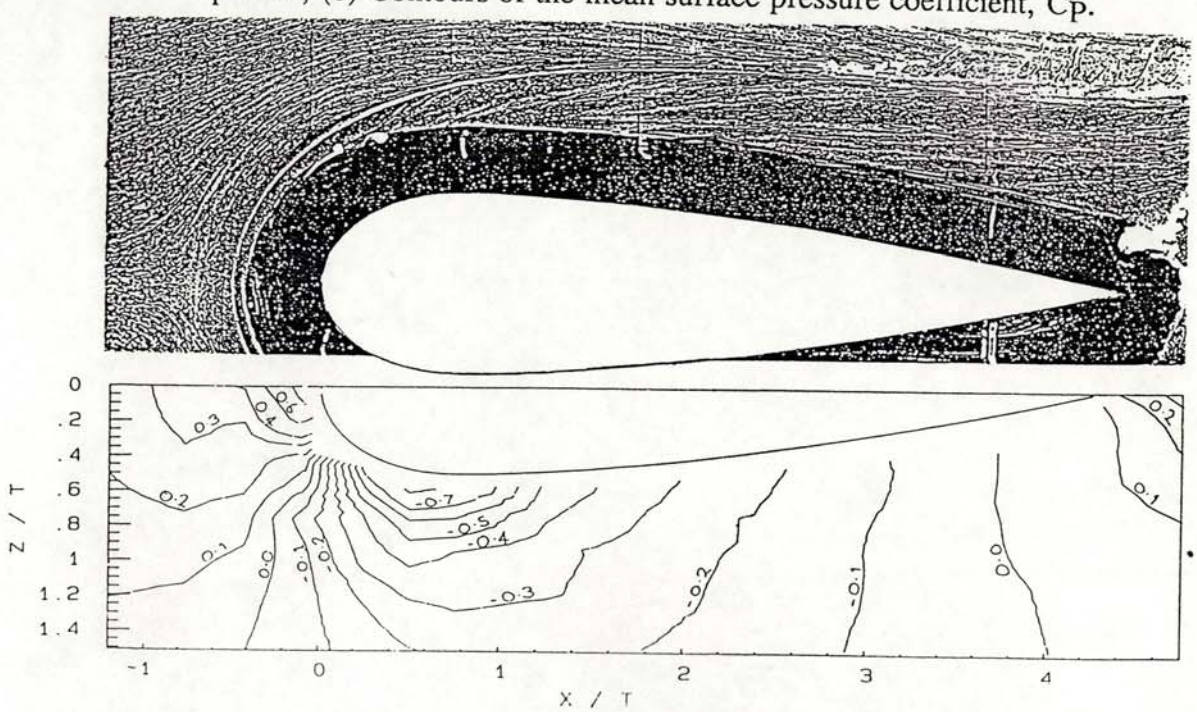


Fig. 31 (Contd. 4).

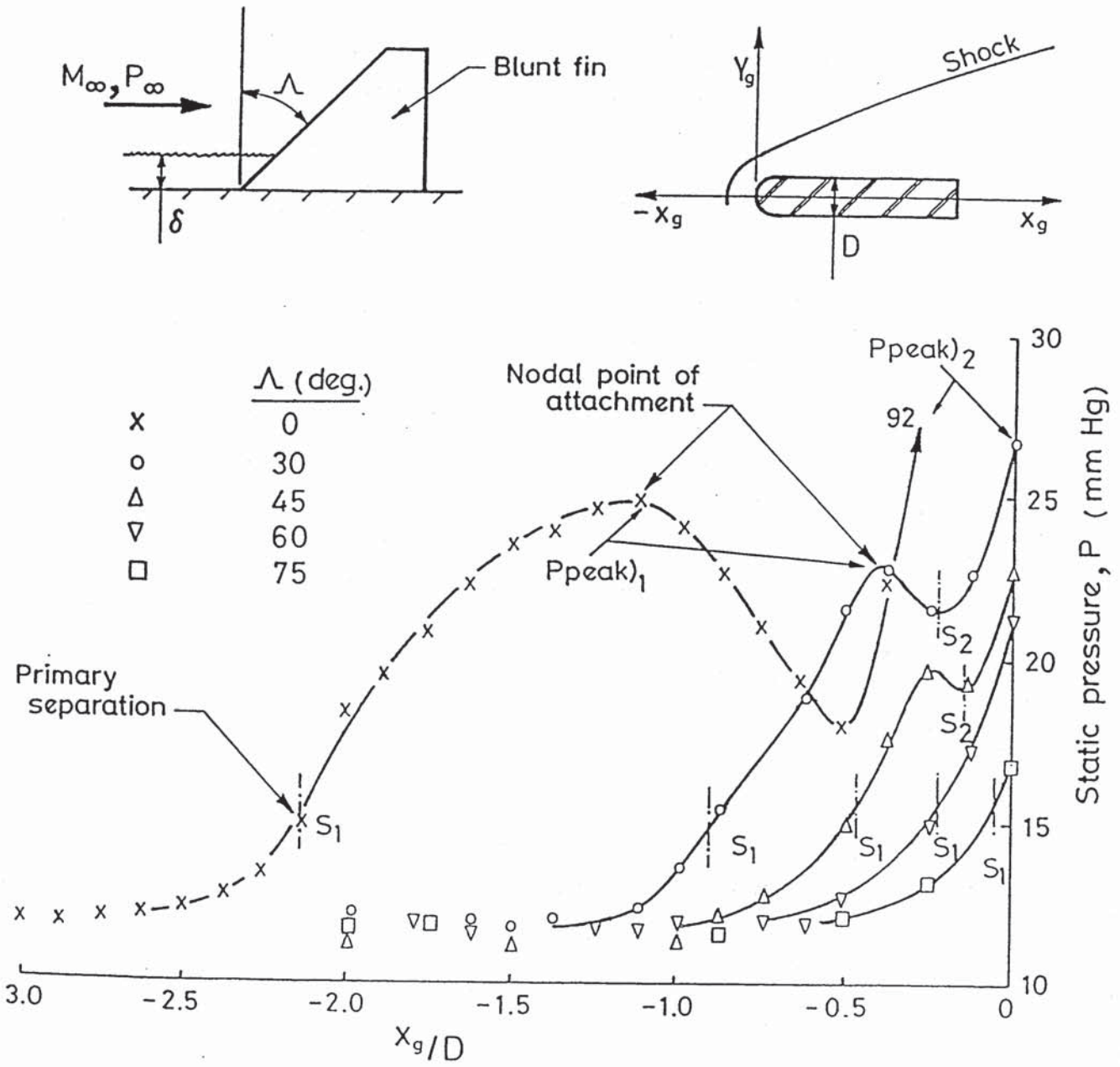


Results from the unmodified wing at zero degress angle of attack. (a) Oil flow pattern, (b) Contours of the mean surface pressure coefficient, C_P.



Results from the wing with fillet at zero degress angle of attack. (a) Oil flow pattern, (b) Contours of the mean surface pressure coefficient, C_P.

Fig. 32. The effects of filleting at subsonic speeds (Devenport et al (1989)).



(a). Centre line pressure distribution D = 1", $\alpha = 0°$, $Y_g/D = 0$.

Fig. 33. The effects of sweep on the wall pressure distributions generated by a blunt fin (Hussain (1985)).

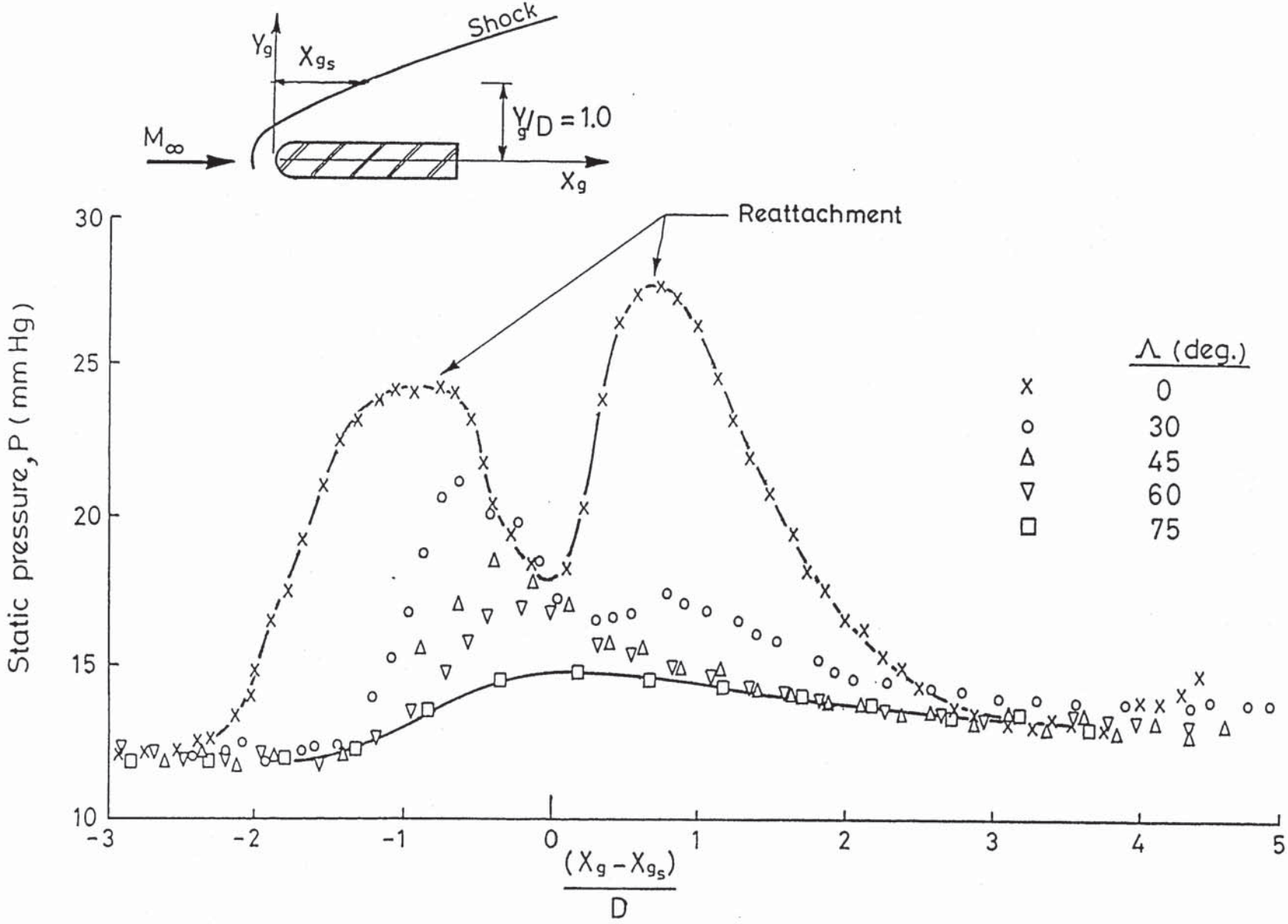


Fig. 33 (b). D = 1", $\alpha = 0°$, $Y_g/D = 1$.

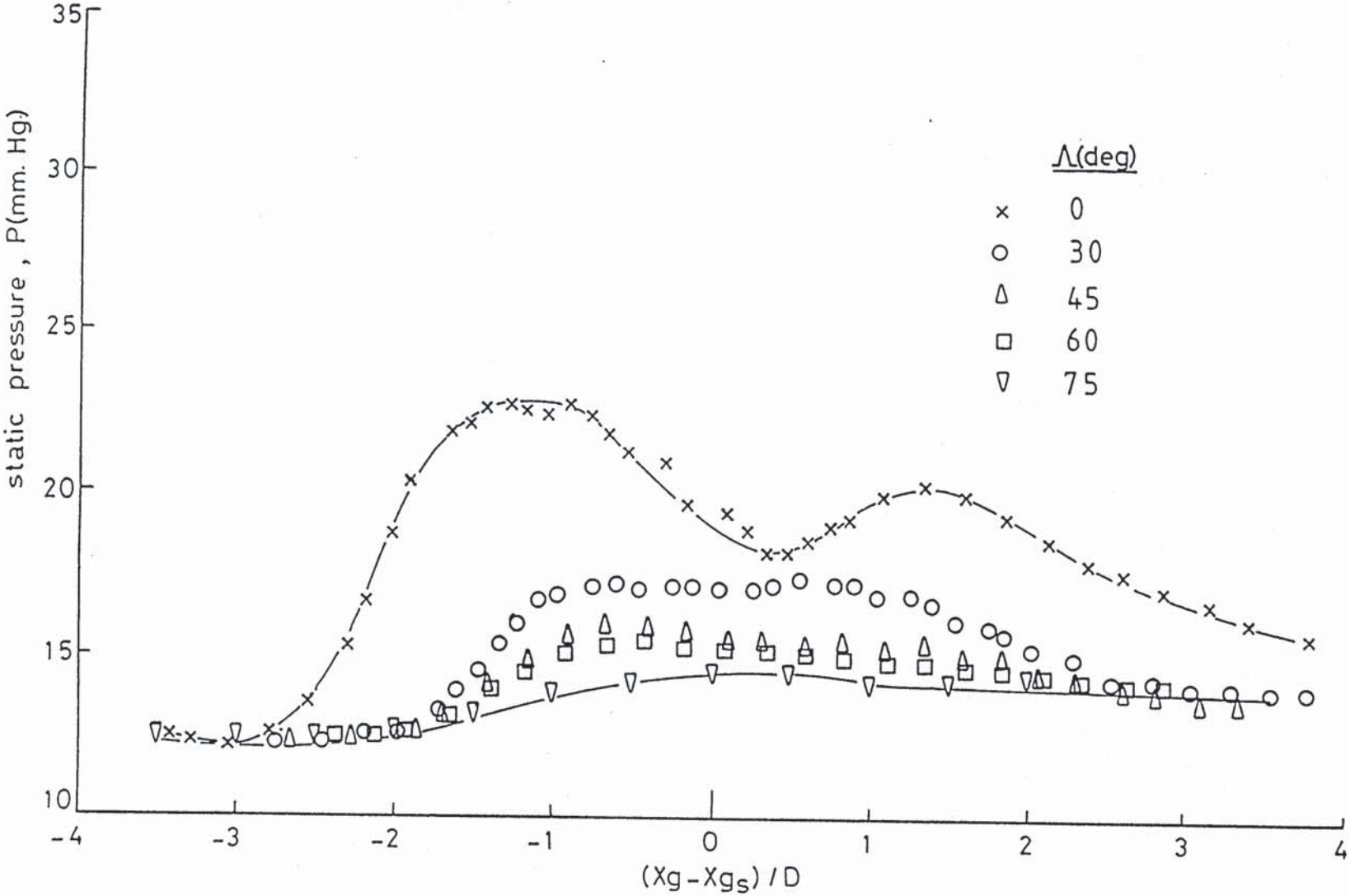


Fig. 33 (c). D = 1", $\alpha = 0°$, $Y_g/D = 2$.

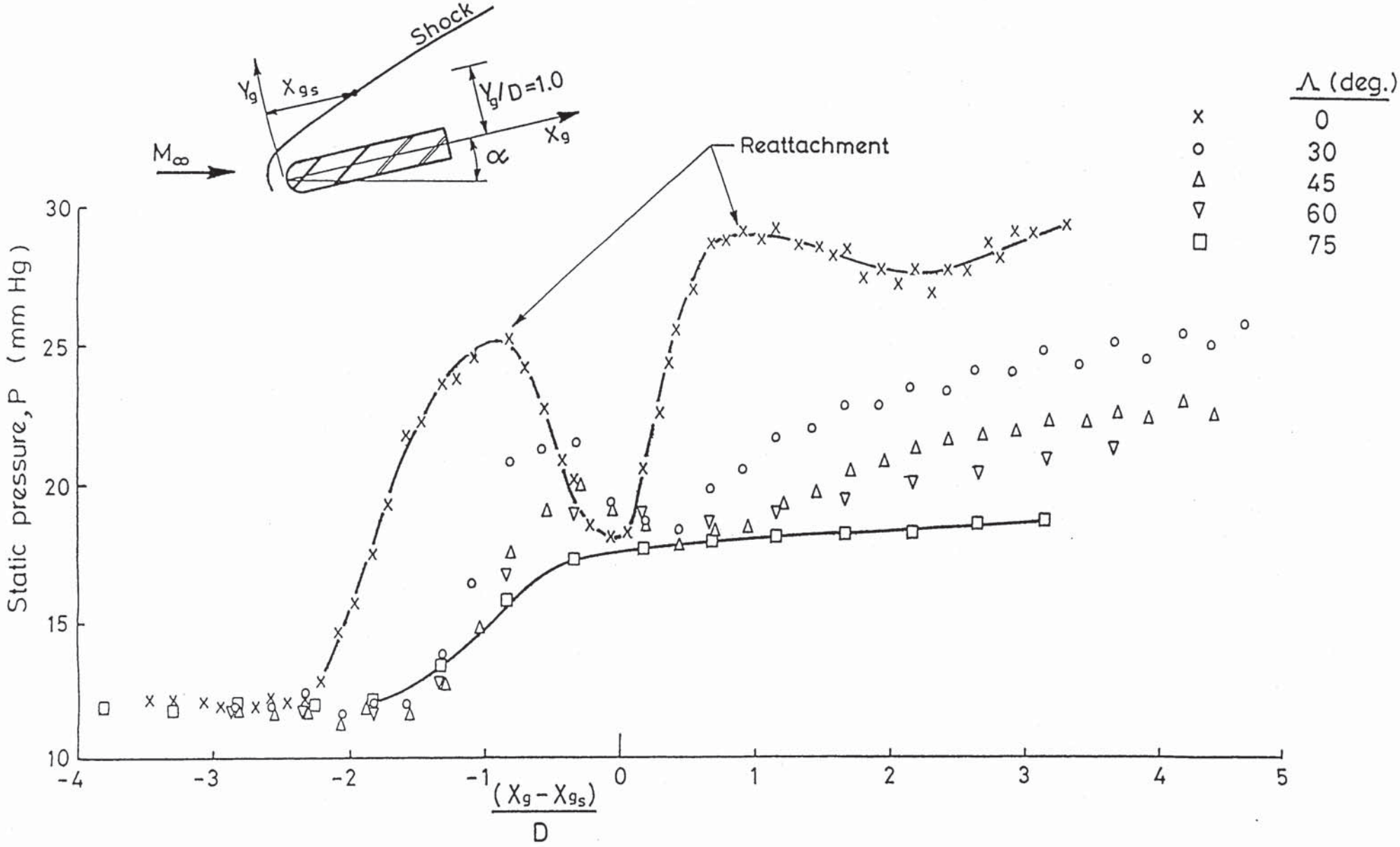
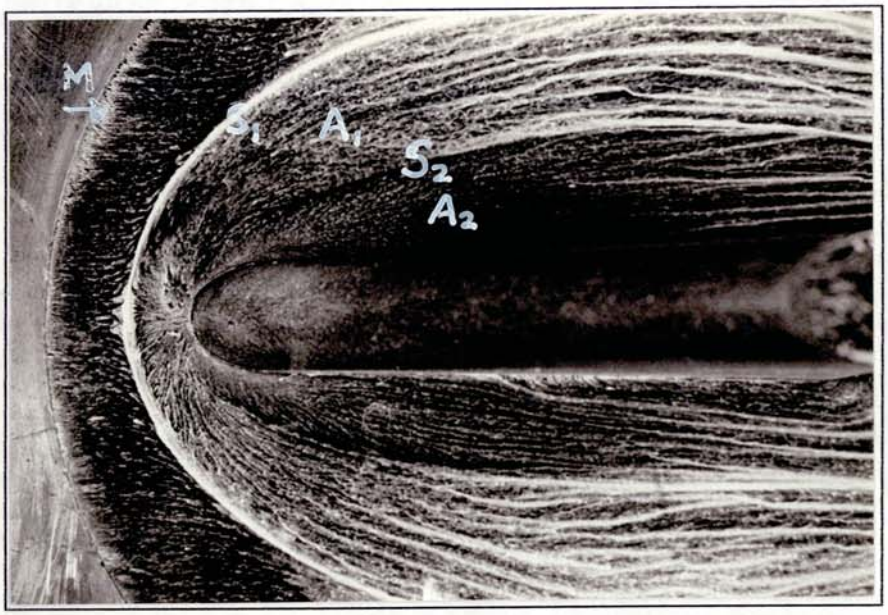
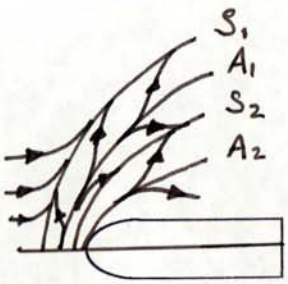
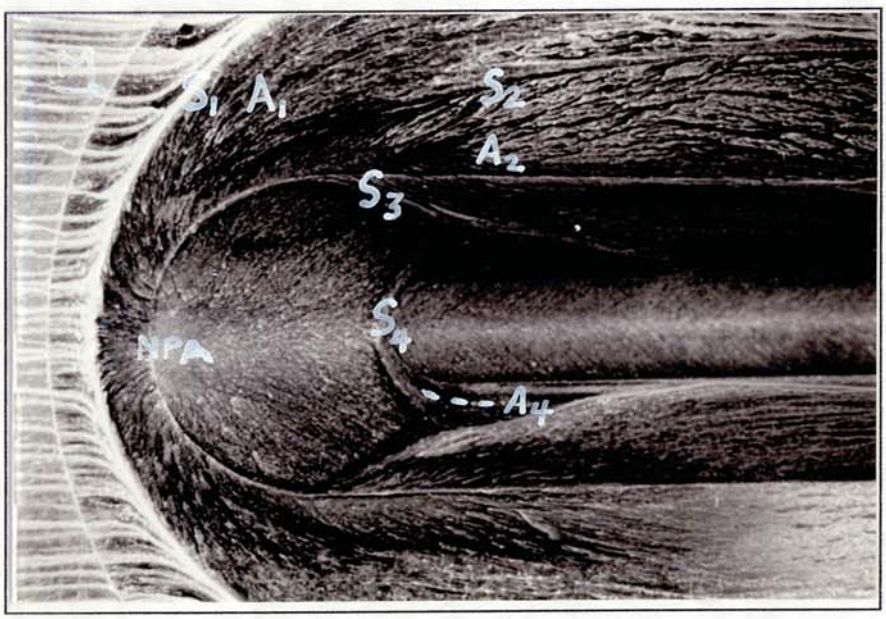


Fig. 33 (d). D = 1", $\alpha = 13°$, $Y_g/D = 1$.







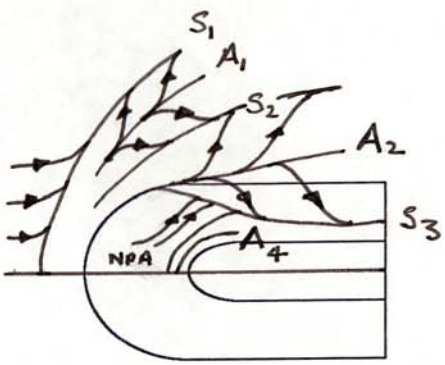
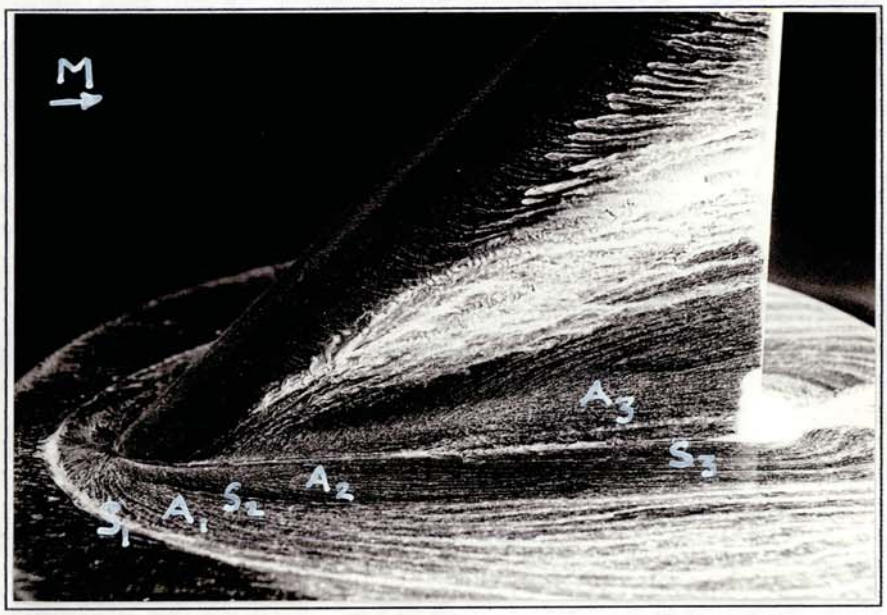
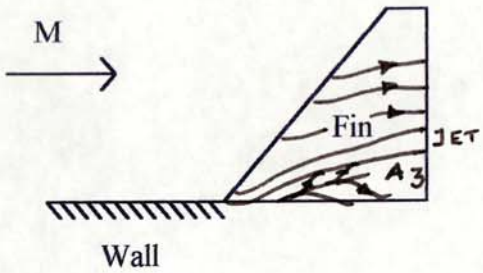
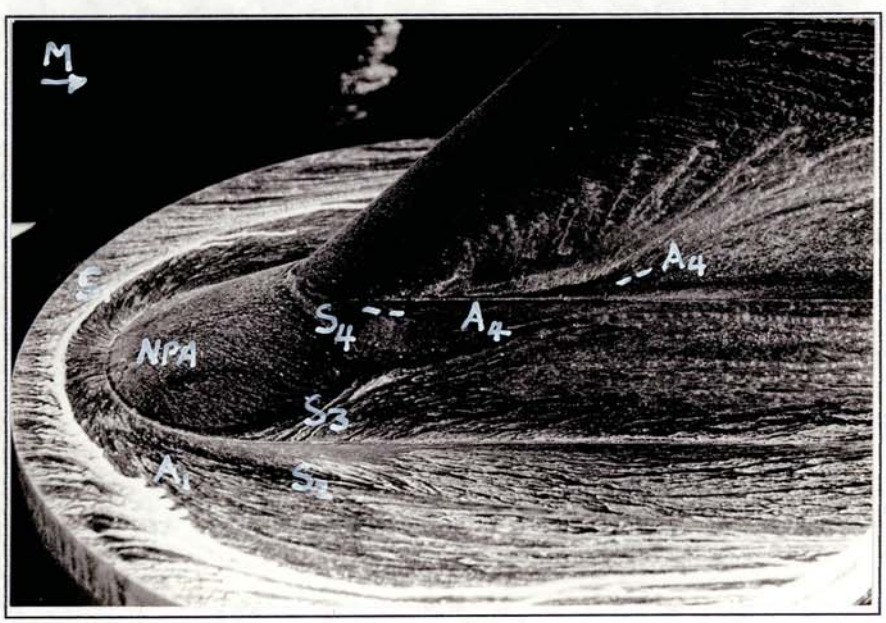


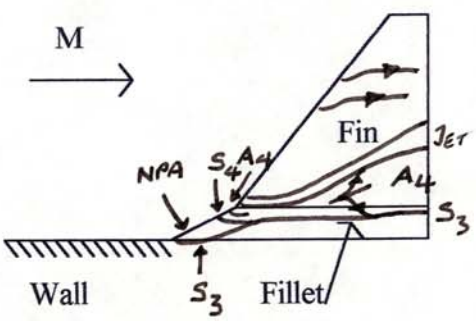
Fig. 34. Oil flow photographs for the swept model of $D/\delta = 1.6$ and its derivative. (i) Unmodified model (top) and (ii) Filleted model (bottom)





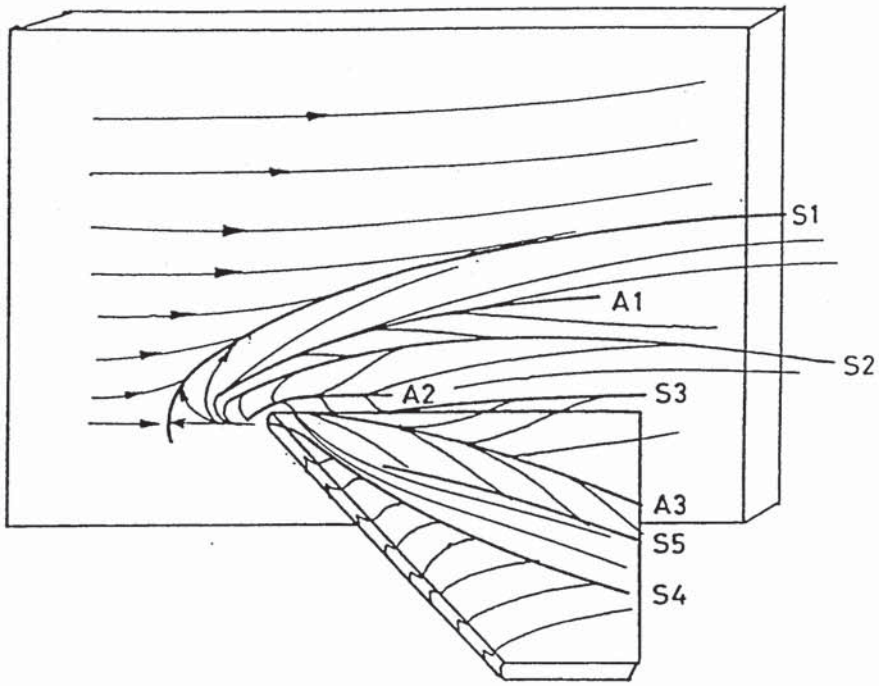
(iii) Unmodified fin



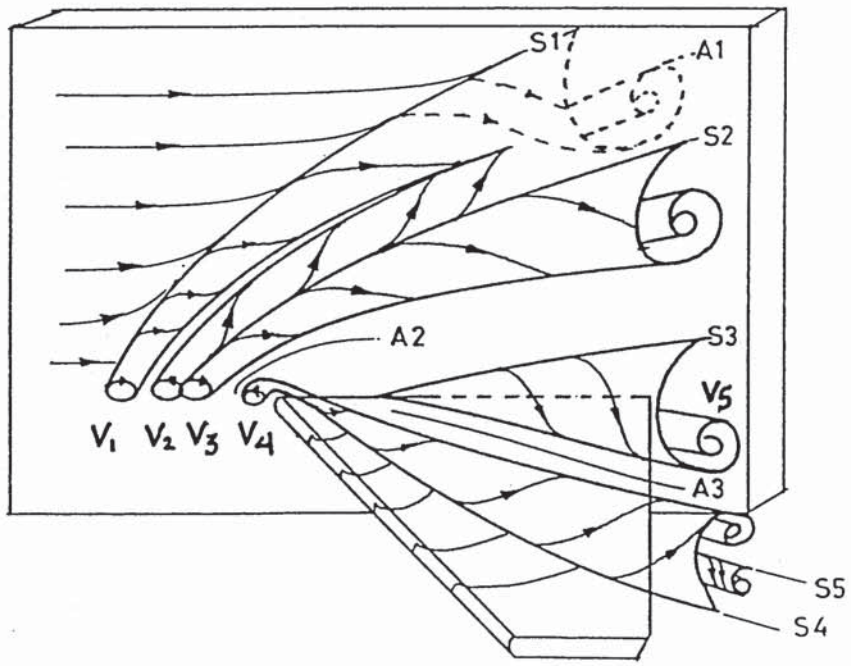


(iv) Filleted fin

Fig. 34. (Contd 1).



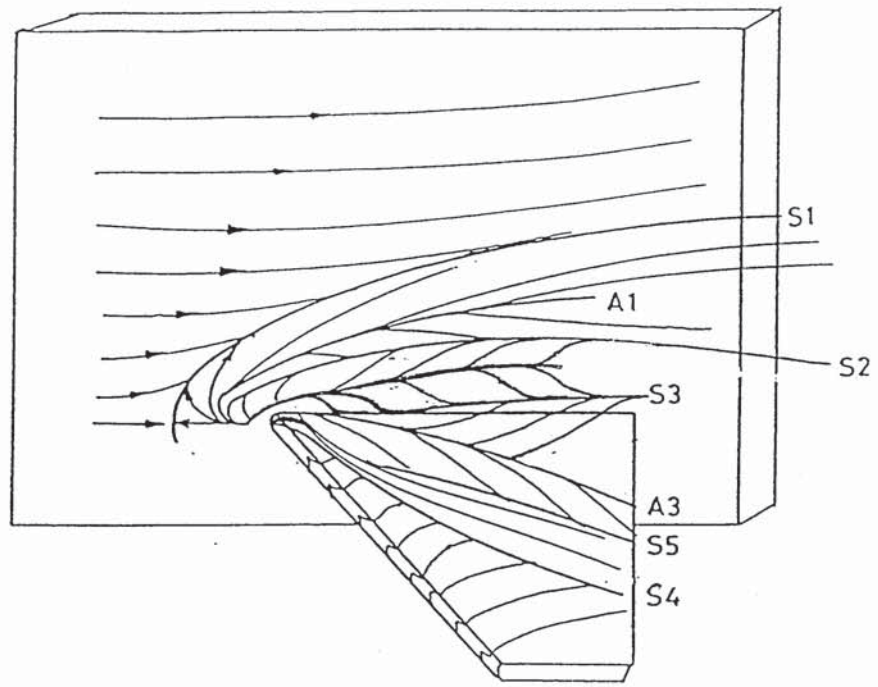
Surface Streak Pattern



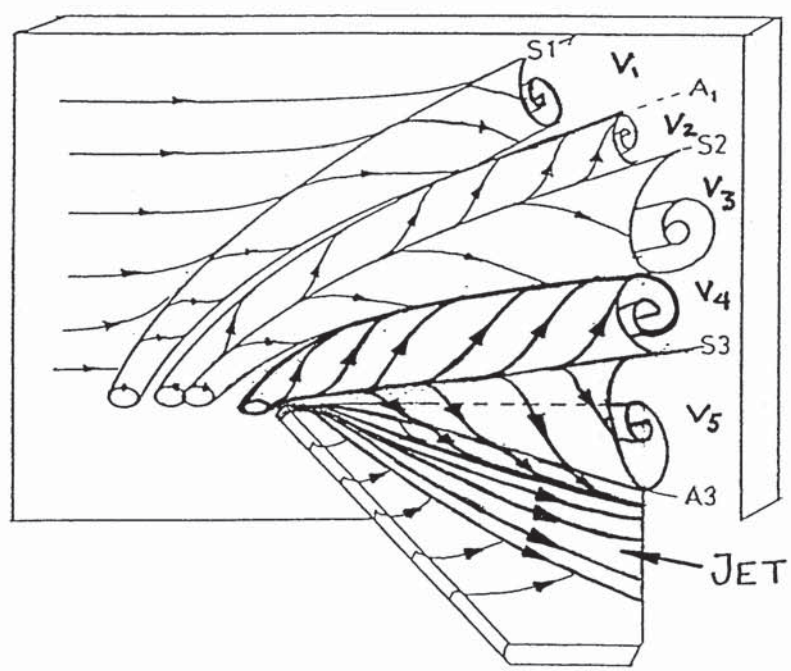
Vortex Skeleton Representation

(a) Hussain's flow field model (Hussain (1985)).

Fig. 35. Flow field models for a blunt swept fin of 45° sweep and $D/\delta=1.6$.

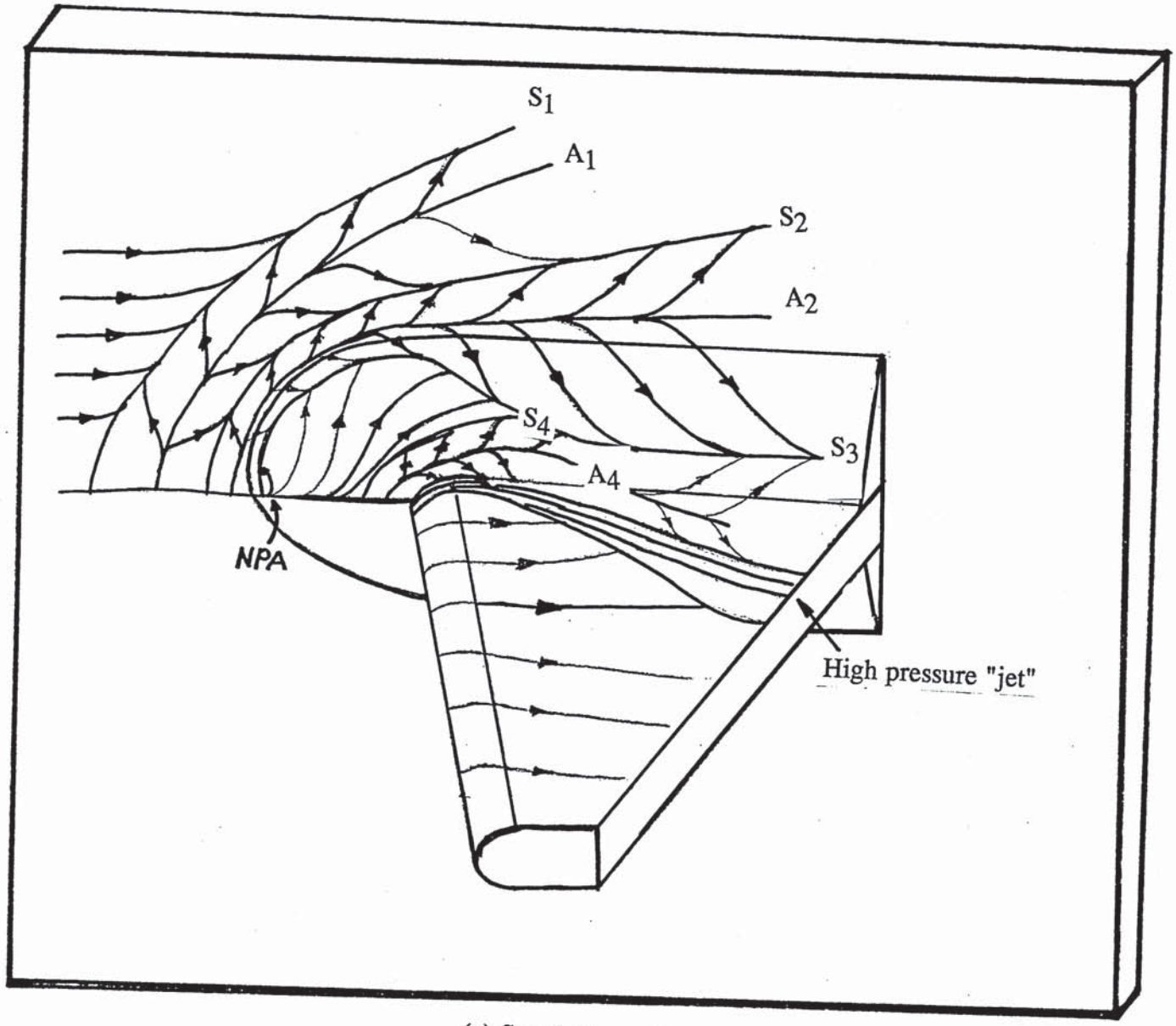


Surface Streak Pattern



Vortex Skeleton Representation

Fig. 35 (b). Proposed flow field model.



(a) Streak line pattern

Fig. 36. Flow field model for the swept fin of $D/\delta=1.6$ with a fillet.

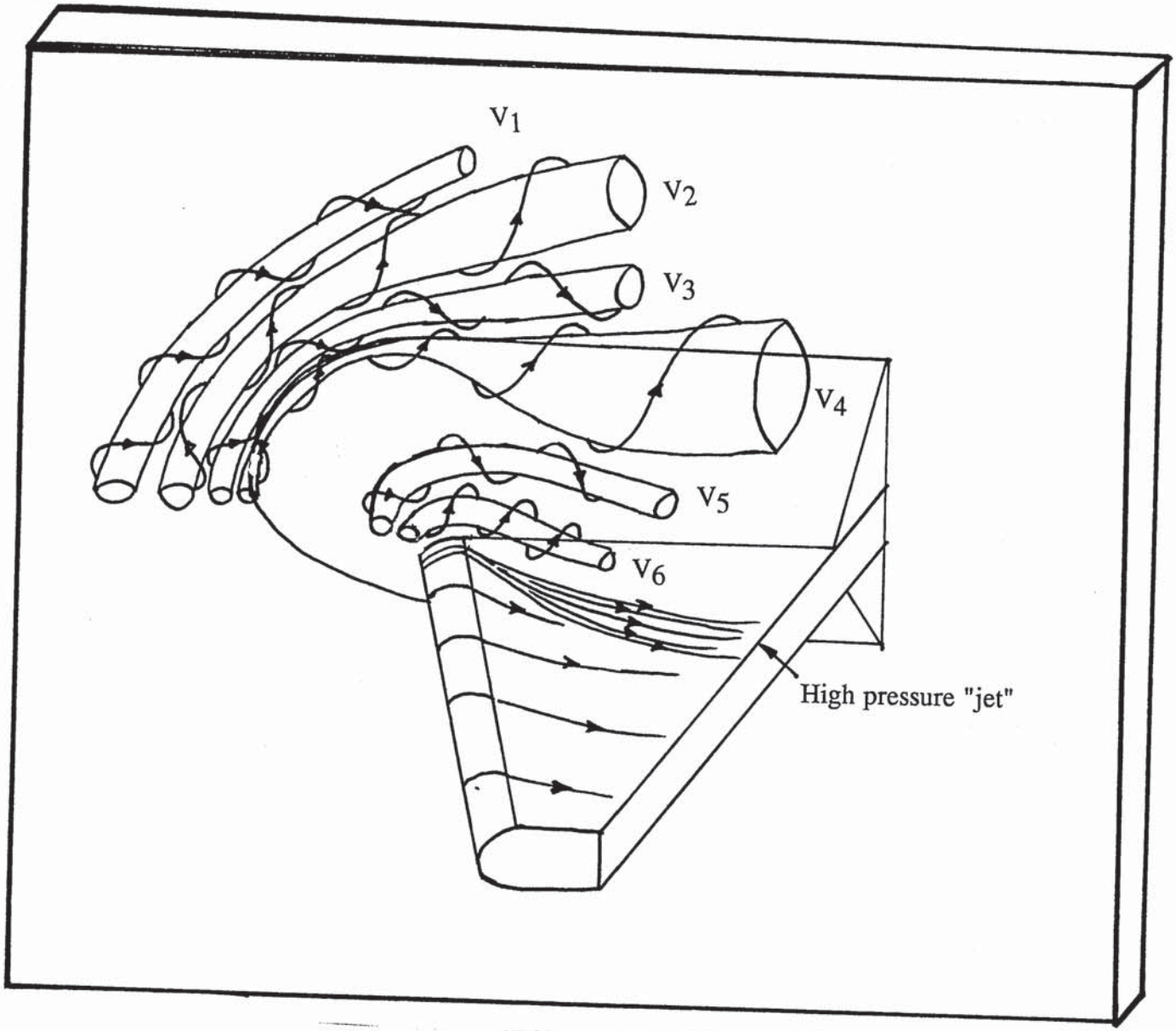
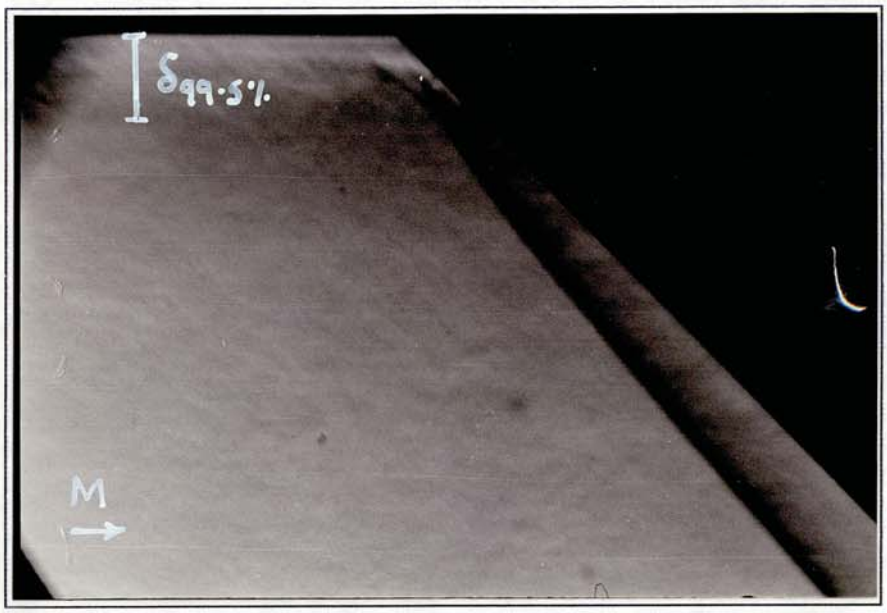
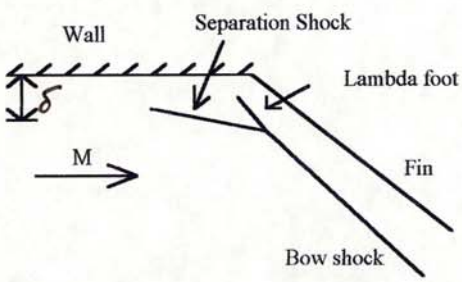
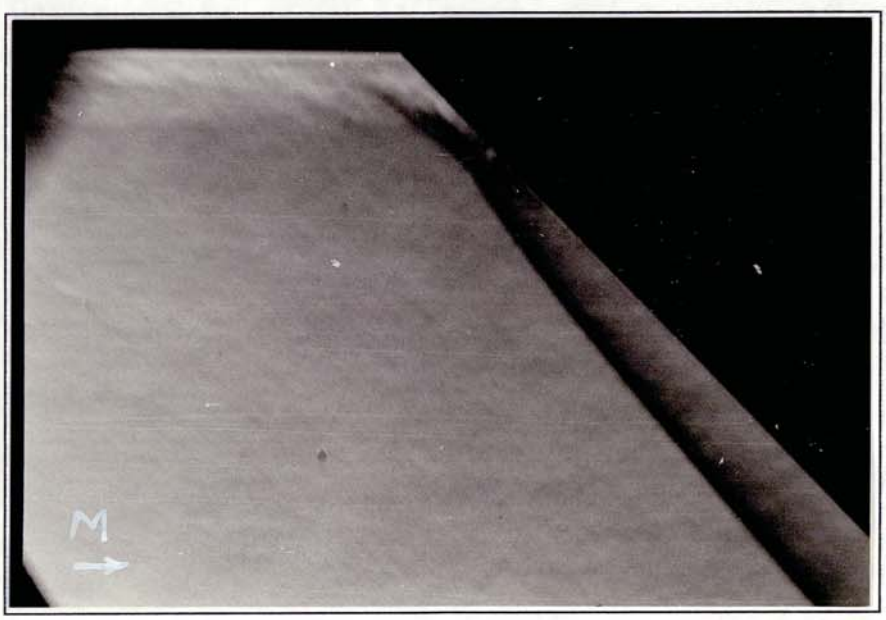


Fig. 36 (b). Vortex skeleton representation

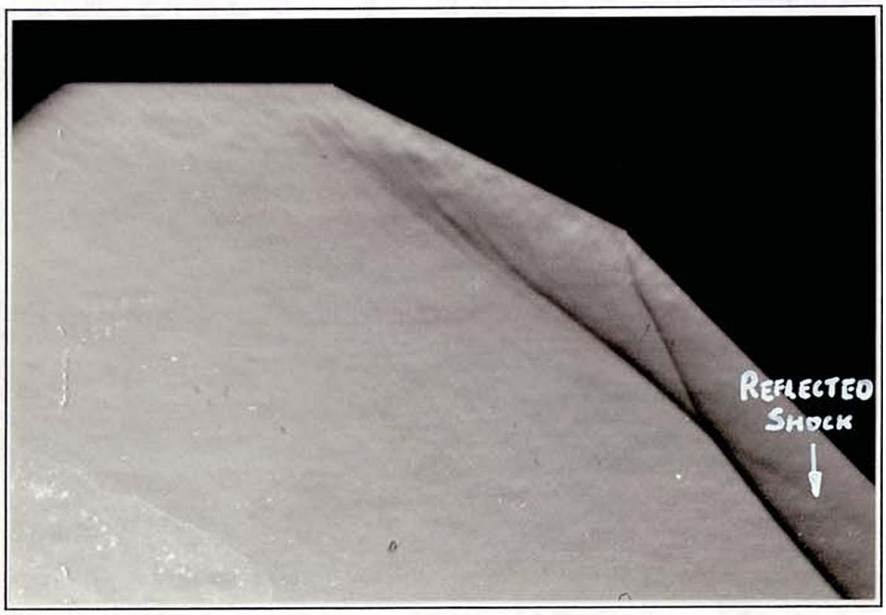


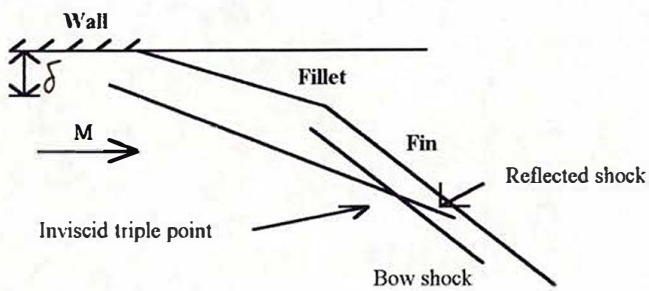


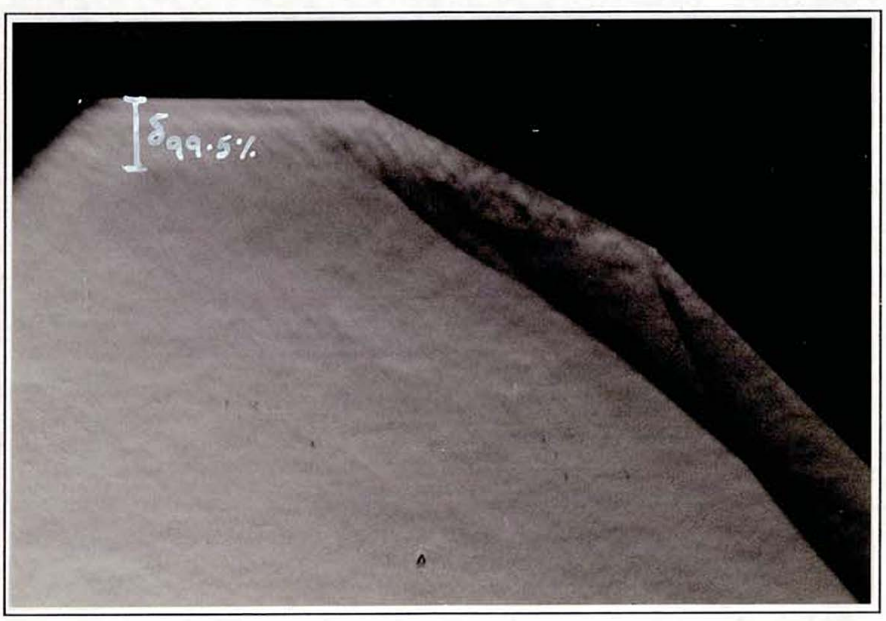


(i) Unmodified fin

Fig. 37. Side view schlieren images for the swept fin of $D/\delta = 1.6$ and its derivative.
(a) Photographs.







(ii) Filleted fin

Fig. 37 (a). (Contd 1).

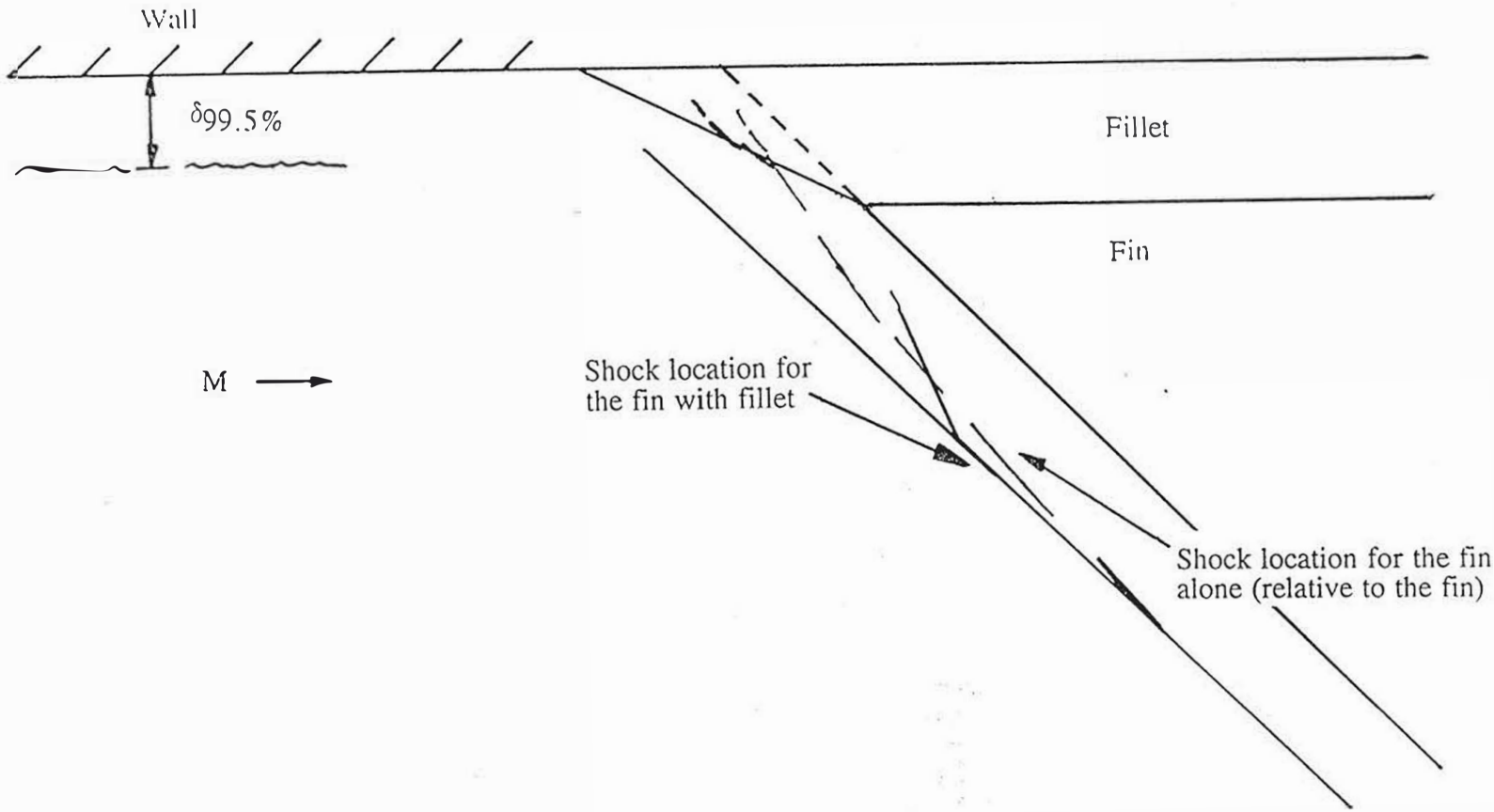
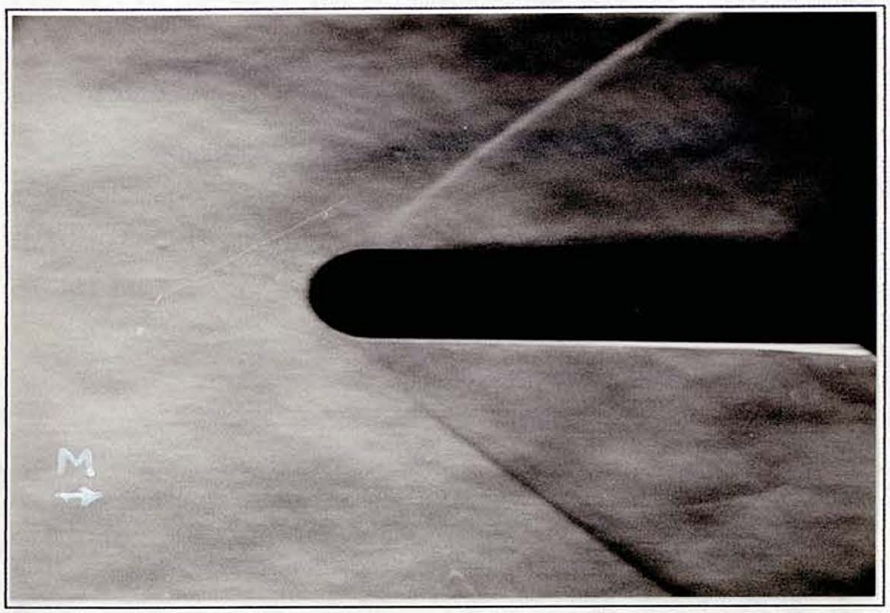
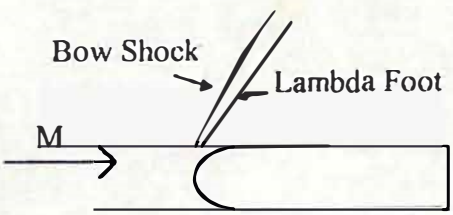
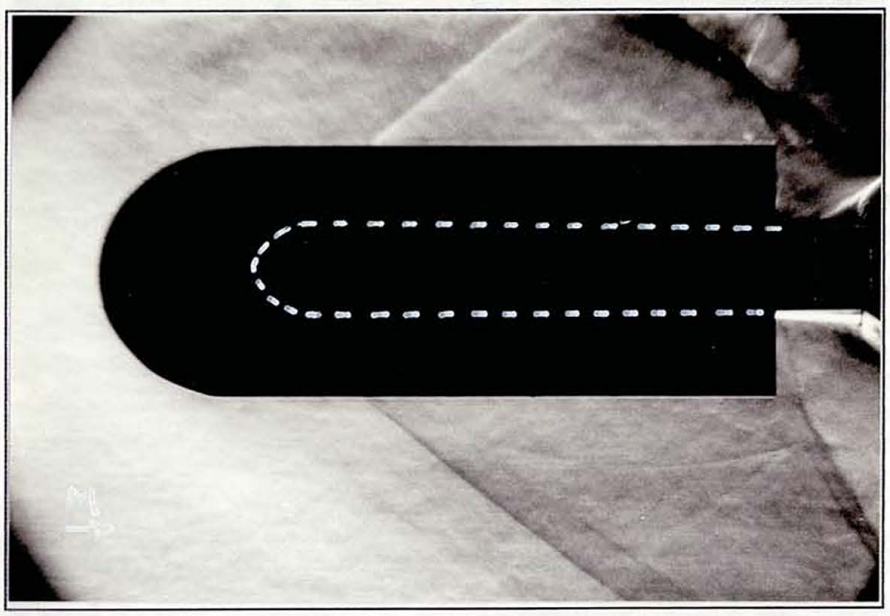
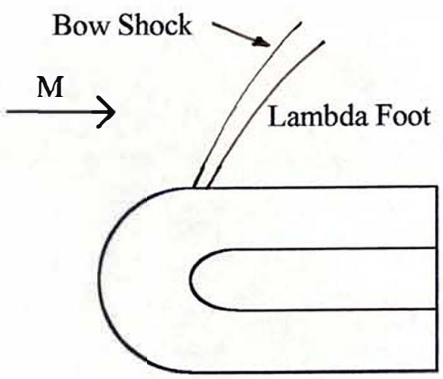


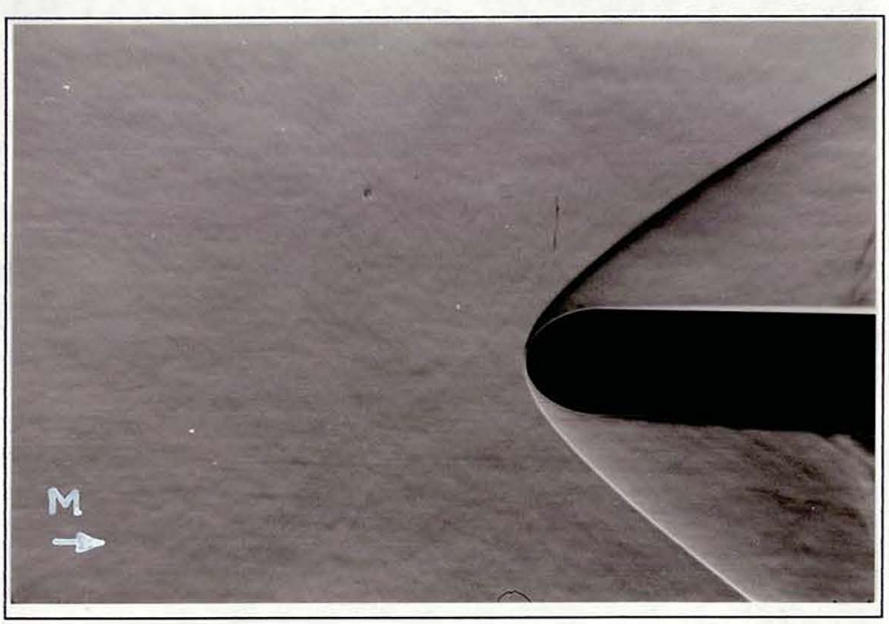
Fig. 37 (b). Comparison of the location of the shock waves produced by a 45° swept fin with and without a fillet.











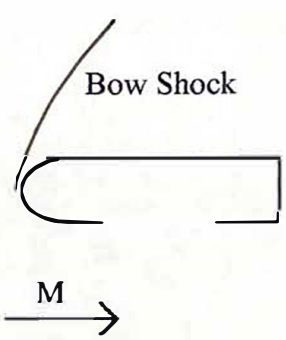


Fig. 38. The plan view schlieren images of the (i) unmodified swept fin (top), (ii) the filleted fin (centre) and (iii) a 45° delta wing (bottom).

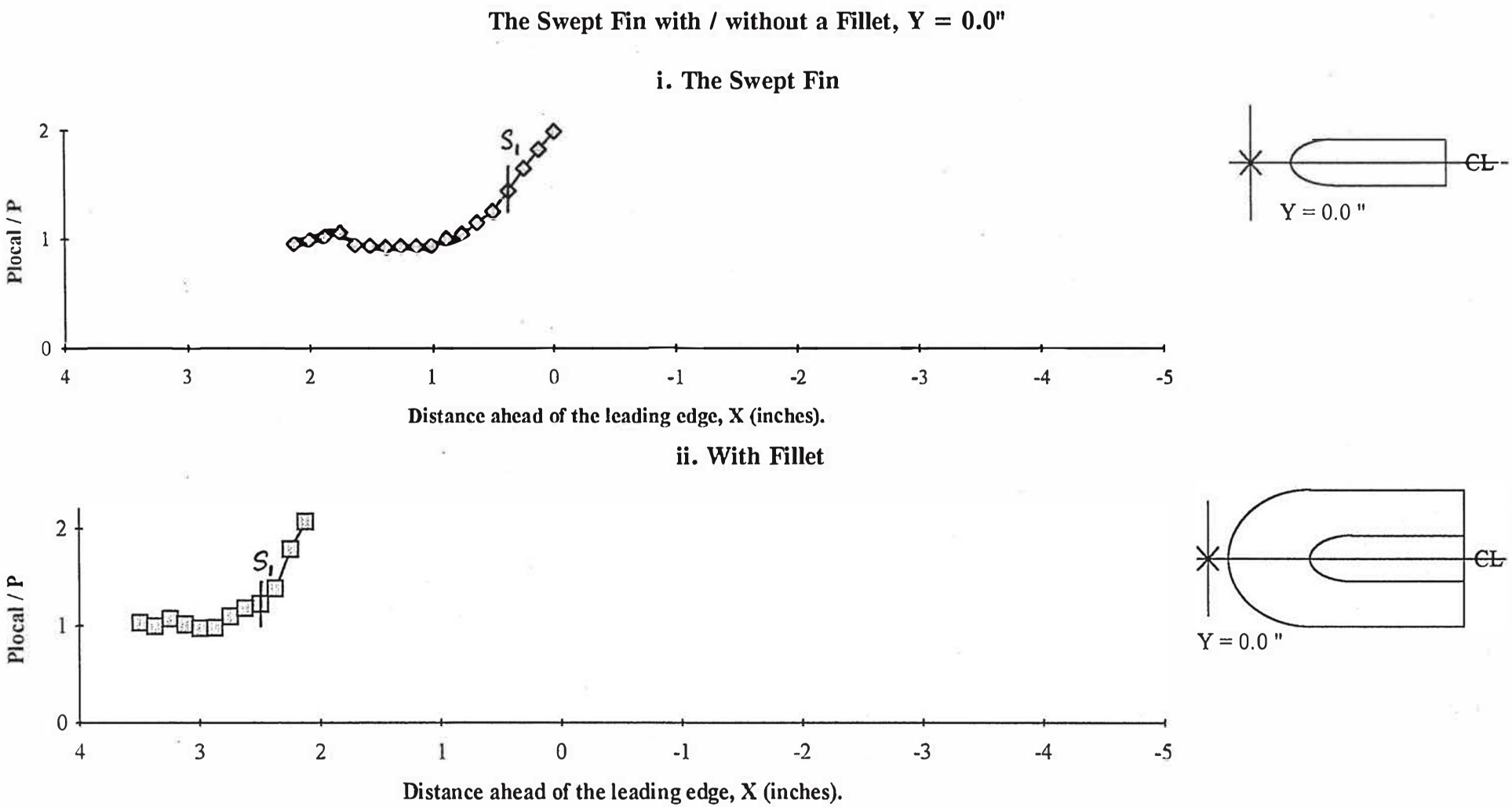
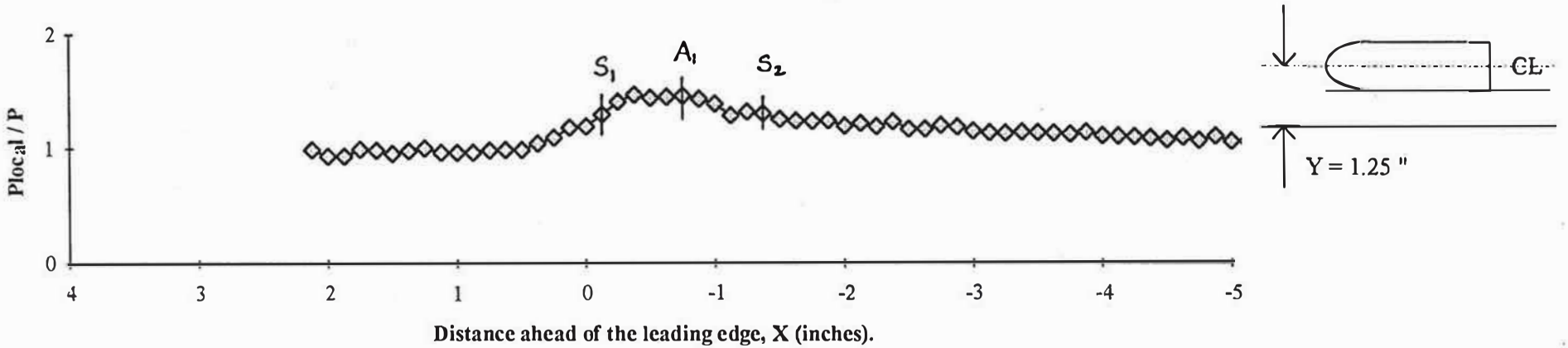


Fig. 39. Pressure Plots for the 45° Swept Fin of D/δ = 1.6 With and Without a Fillet.

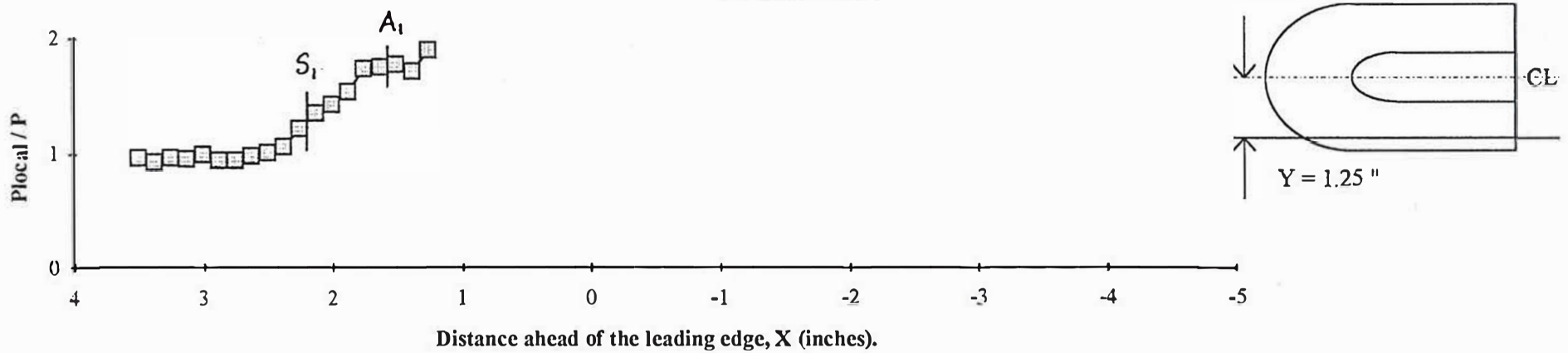
The Swept Fin with / without a Fillet, Y = 1.25"

iii. The Swept Fin



Distance ahead of the leading edge, X (inches).

iv. With Fillet

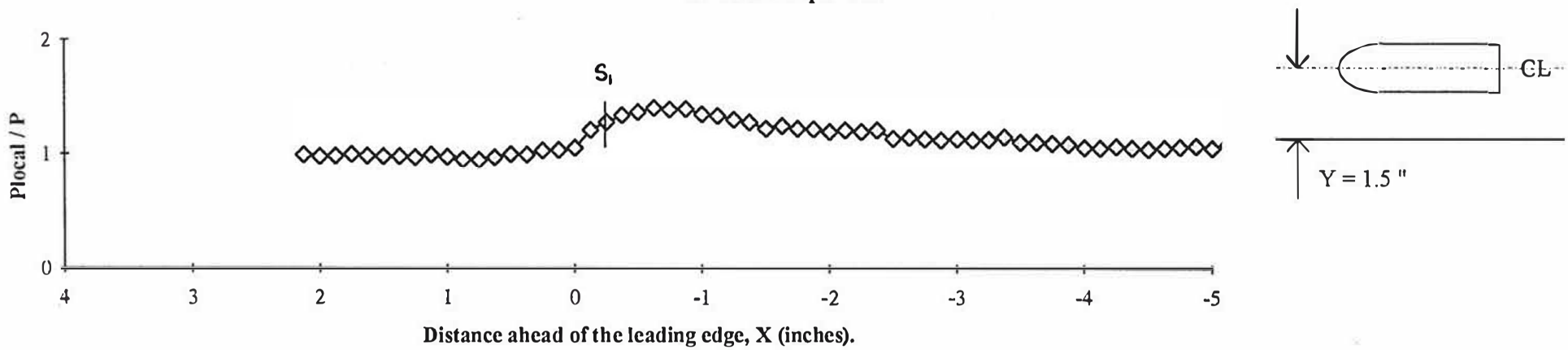


Distance ahead of the leading edge, X (inches).

Fig. 39 (Contd. 1).

The Swept Fin with / without a Fillet, Y = 1.5"

v. The Swept Fin



vi. With Fillet

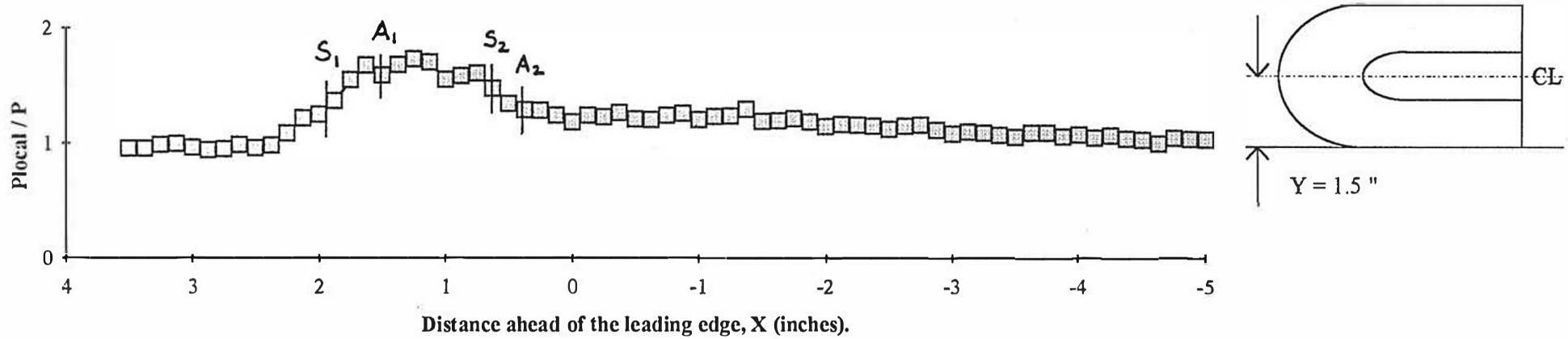
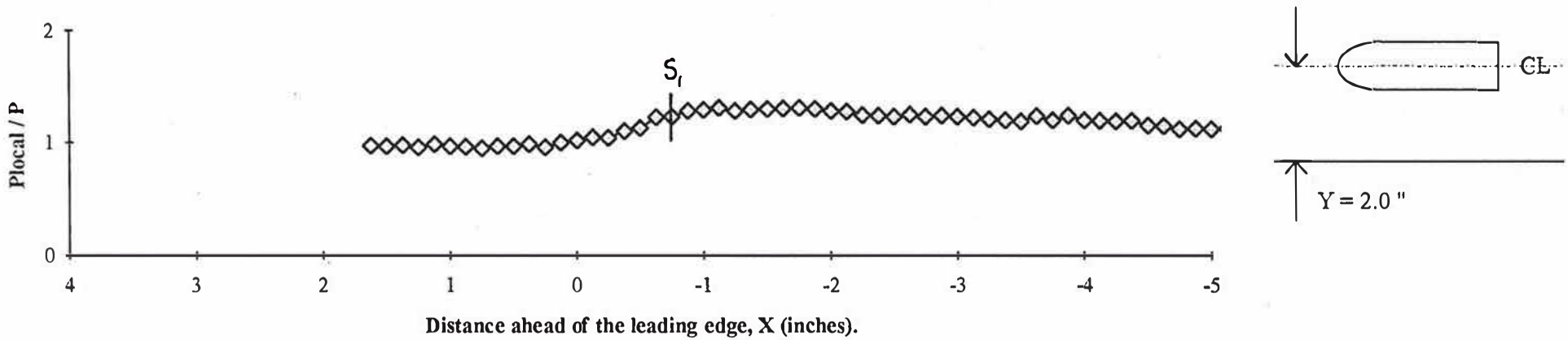


Fig. 39. (Contd. 2).

The Swept Fin with / without a Fillet, Y = 2.0"

vii. The Swept Fin



viii. With Fillet

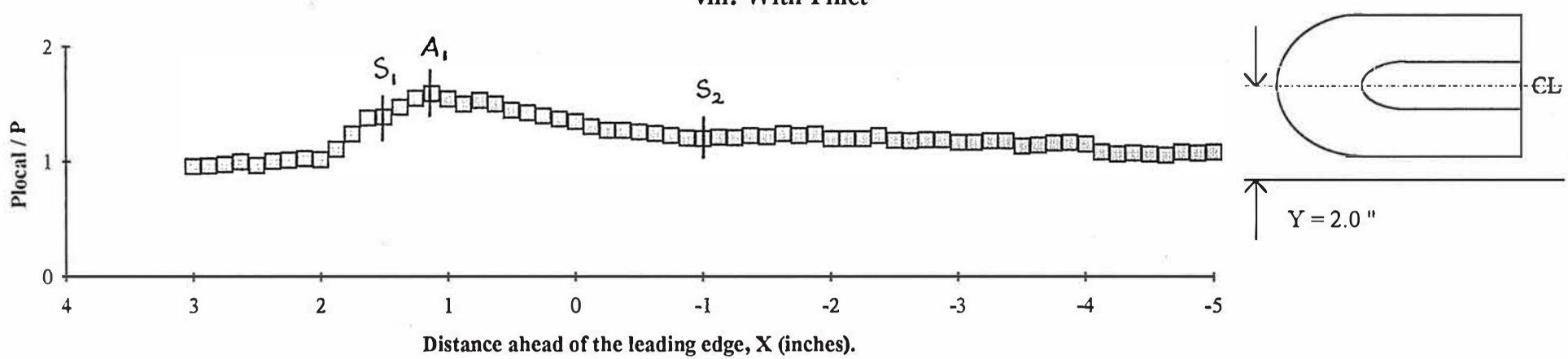
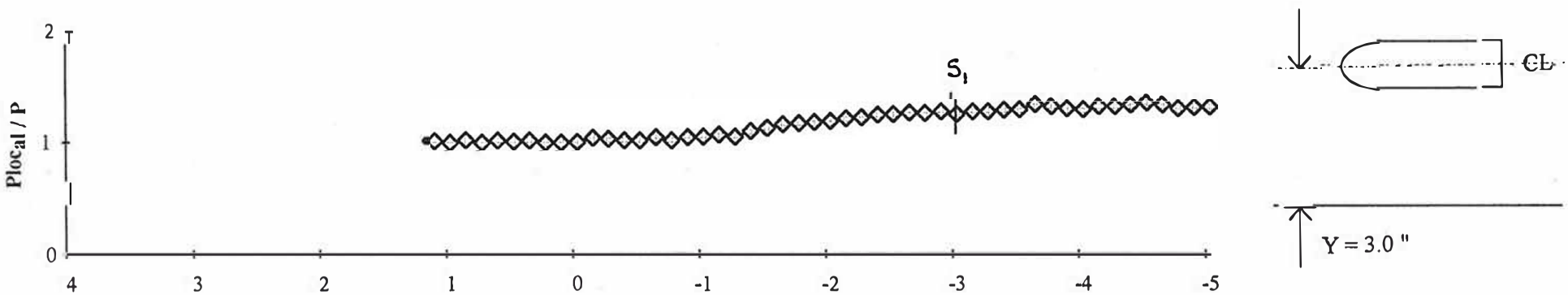


Fig. 39 (Contd. 3).

The Swept Fin with / without a Fillet, Y = 3.0"

ix. The Swept Fin



x. With Fillet

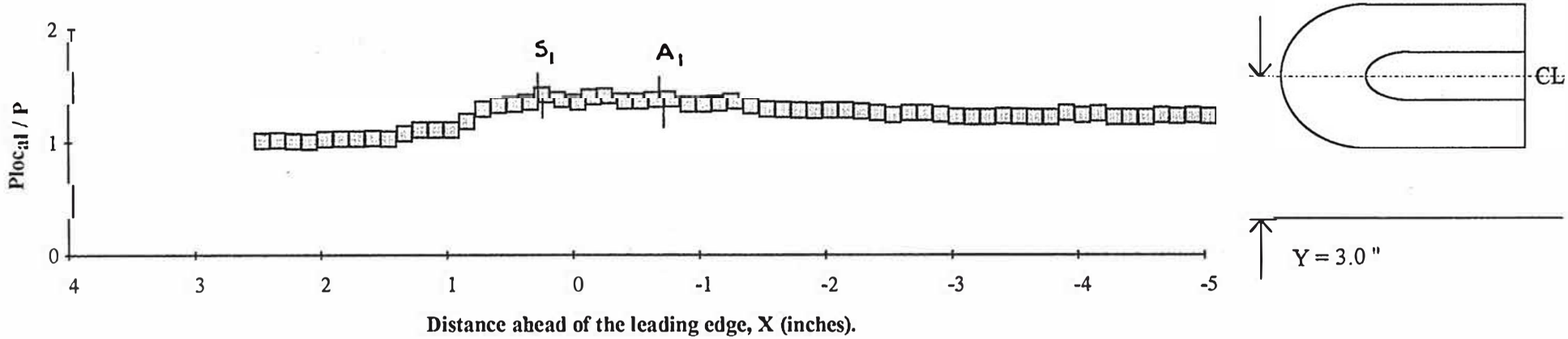
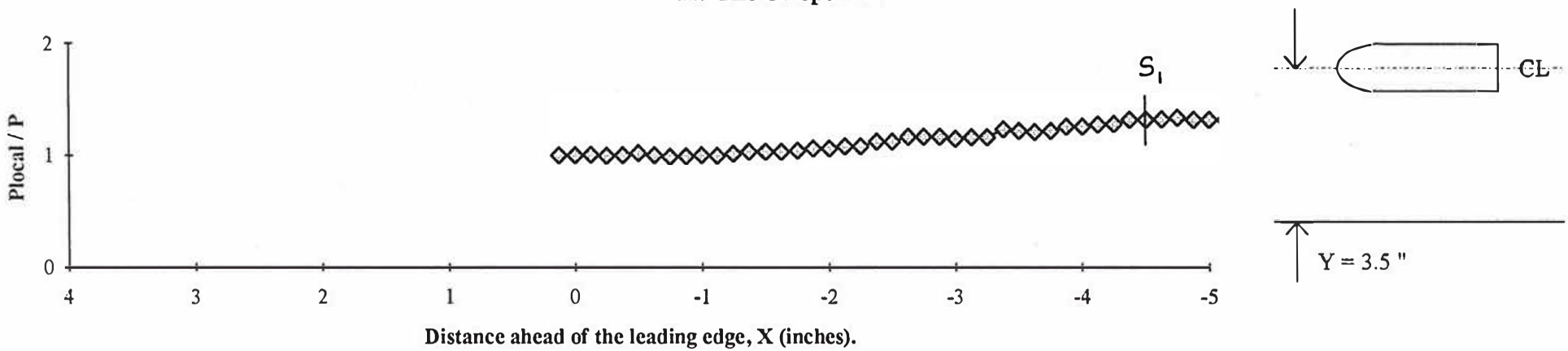


Fig. 39 (Contd. 4).

The Swept Fin with / without a Fillet, Y = 3.5"

xi. The Swept Fin



xii. With Fillet

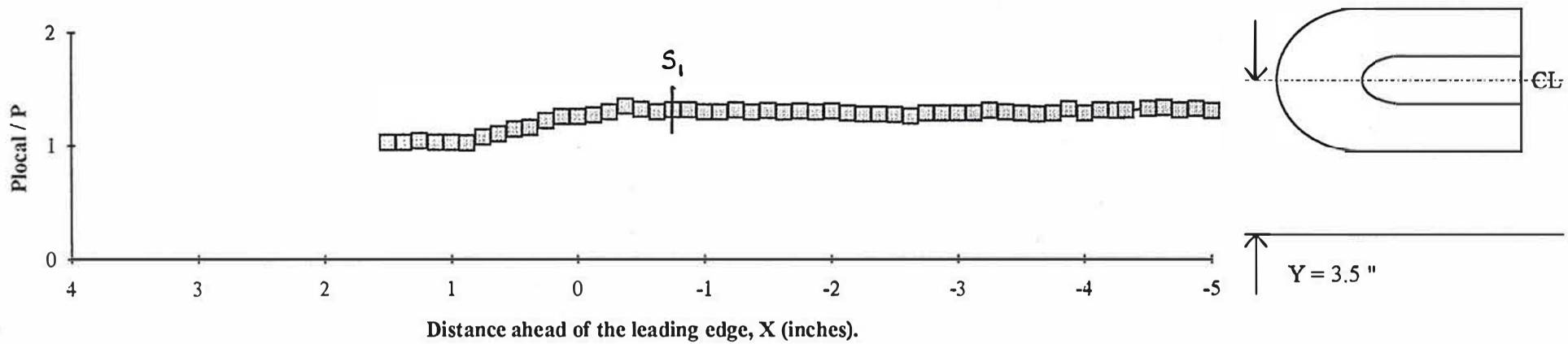


Fig. 39 (Contd. 5).

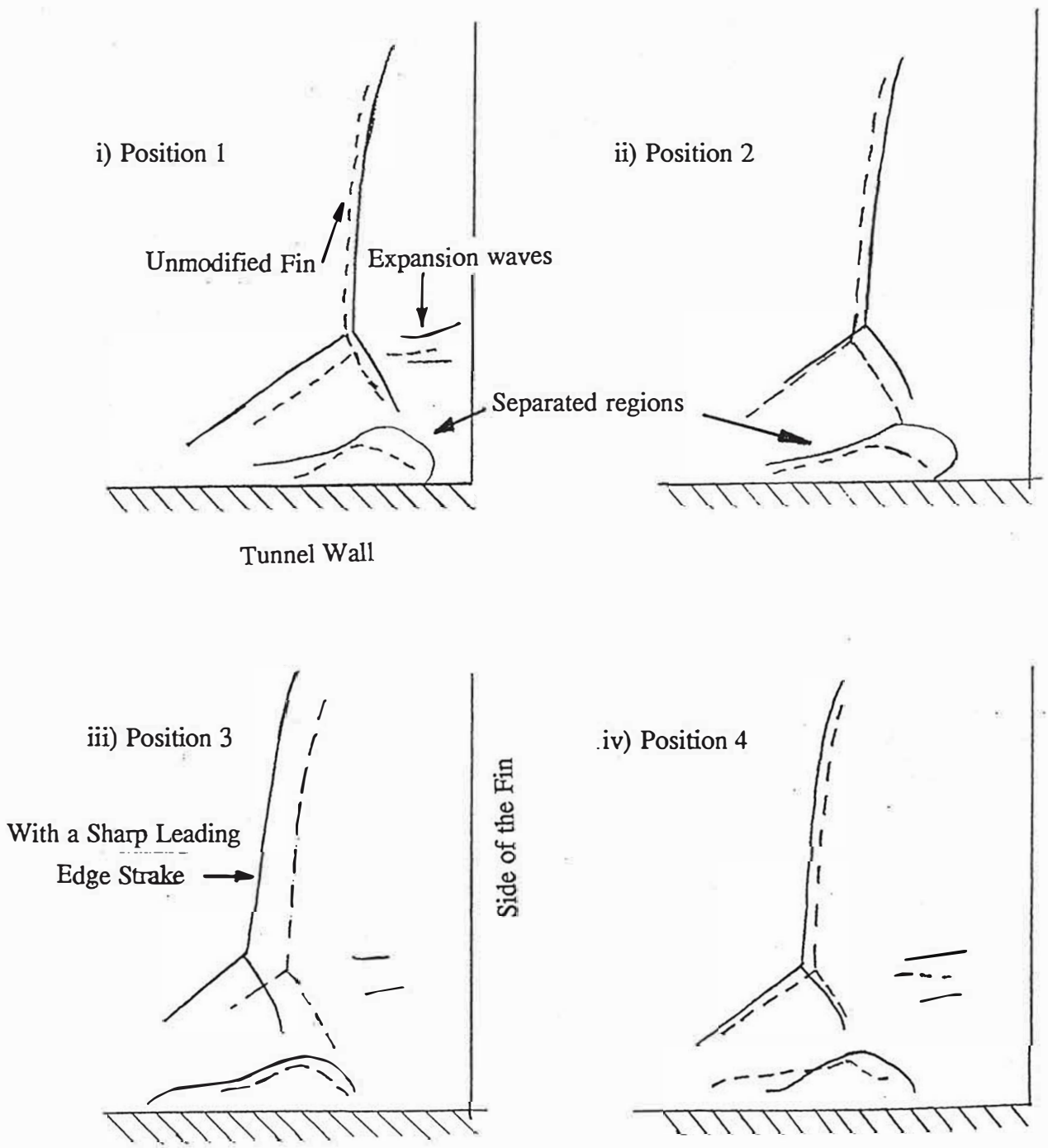


Fig. 40. Laser Flow Visualisation images of the flow fields for the unswept fin of $D/\delta=1.6$ with and without a sharp leading edge strake (see fig. 24 for the location of positions).

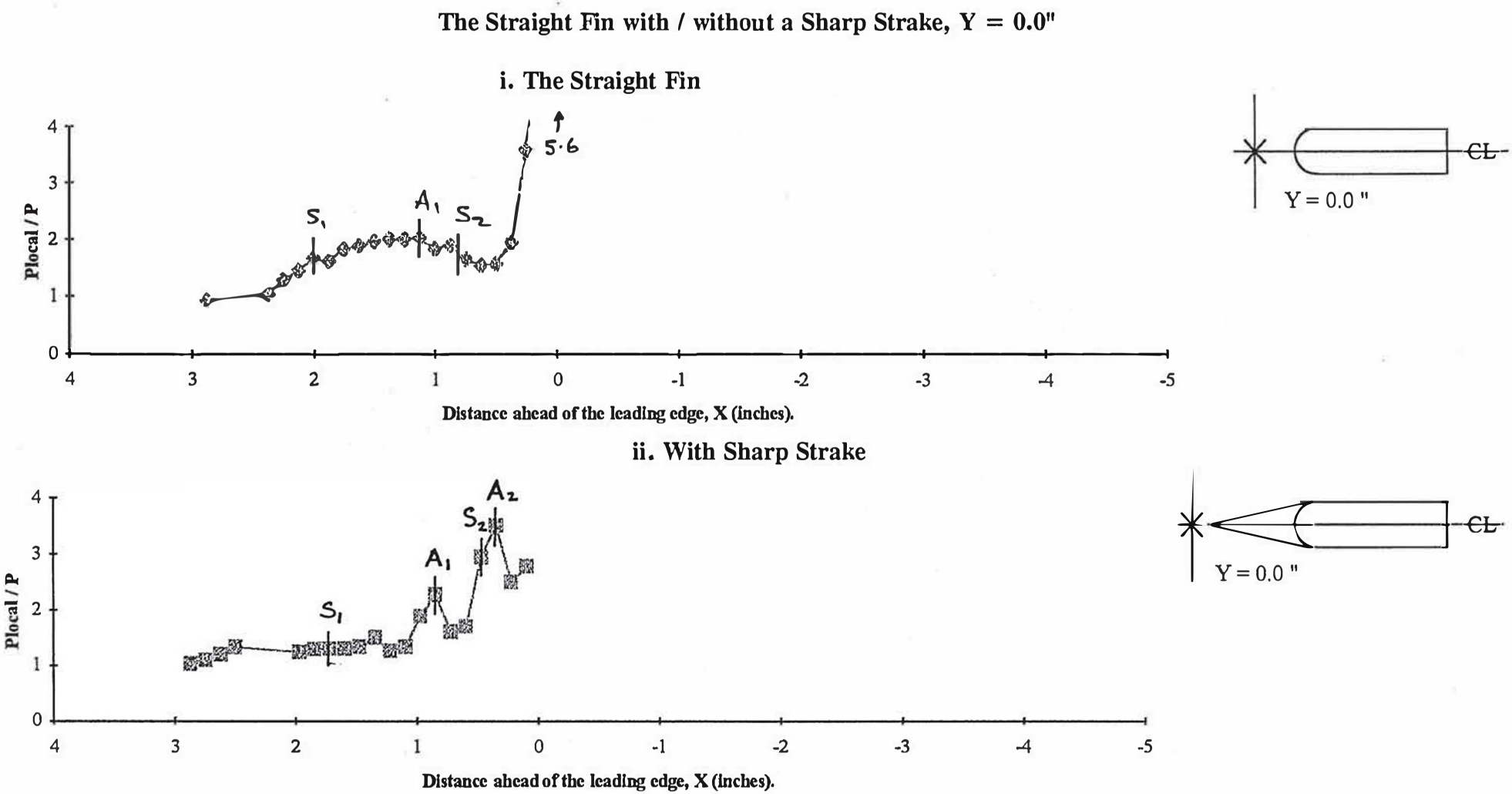
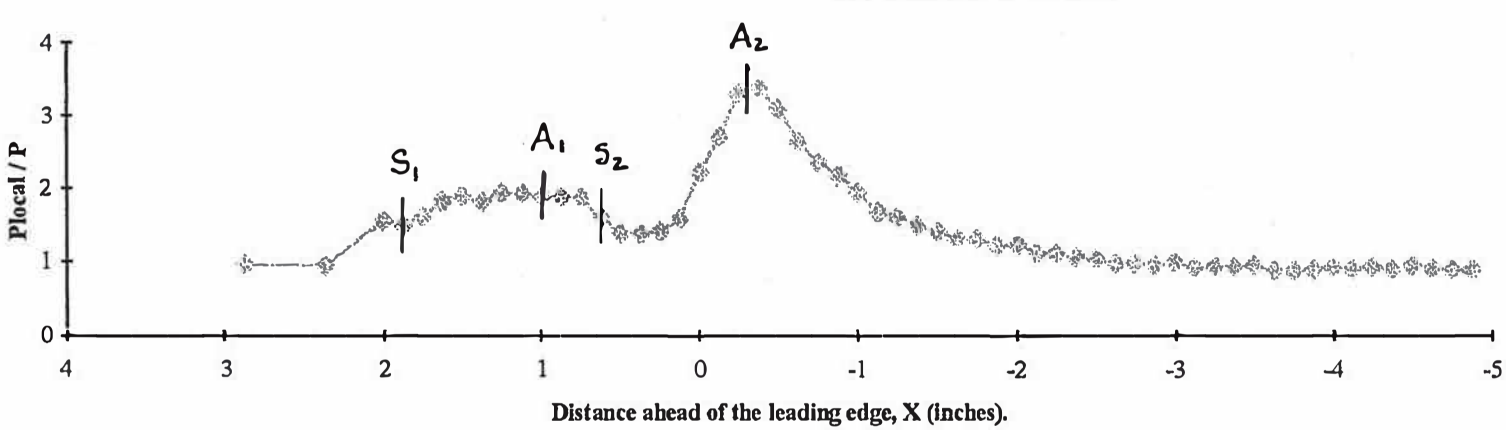
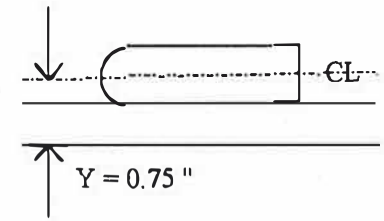


Fig. 41. Pressure plots for the fin of $D/\delta = 1.6$ with and without a sharp leading edge strake.

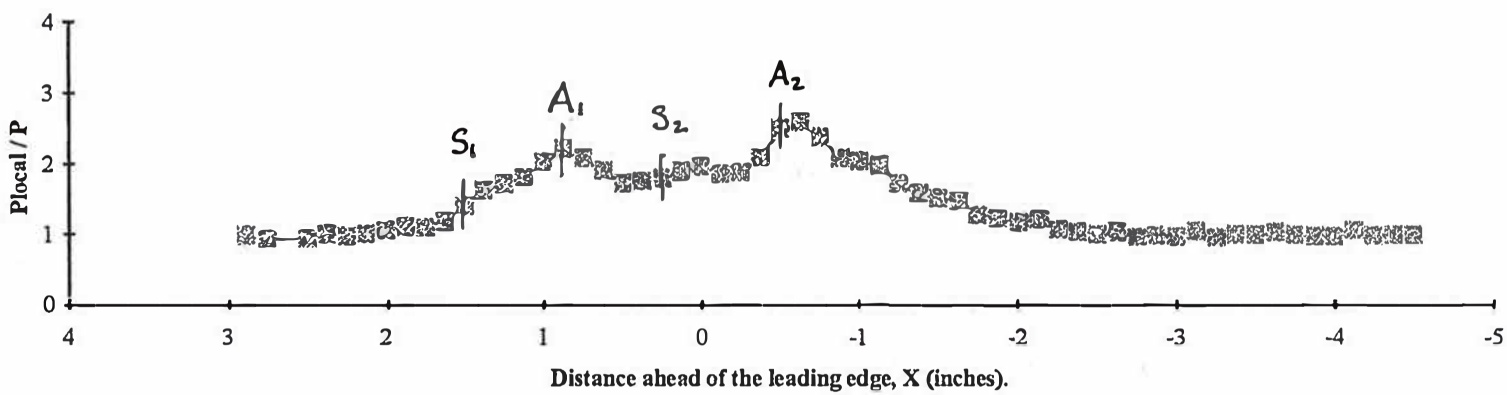
The Straight Fin with / without a Sharp Strake, Y = 0.75"

iii. The Straight Fin





iv. With Sharp Strake



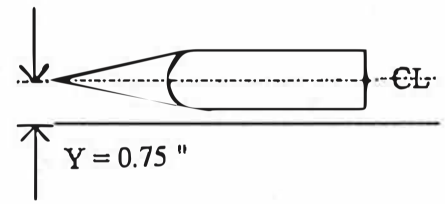
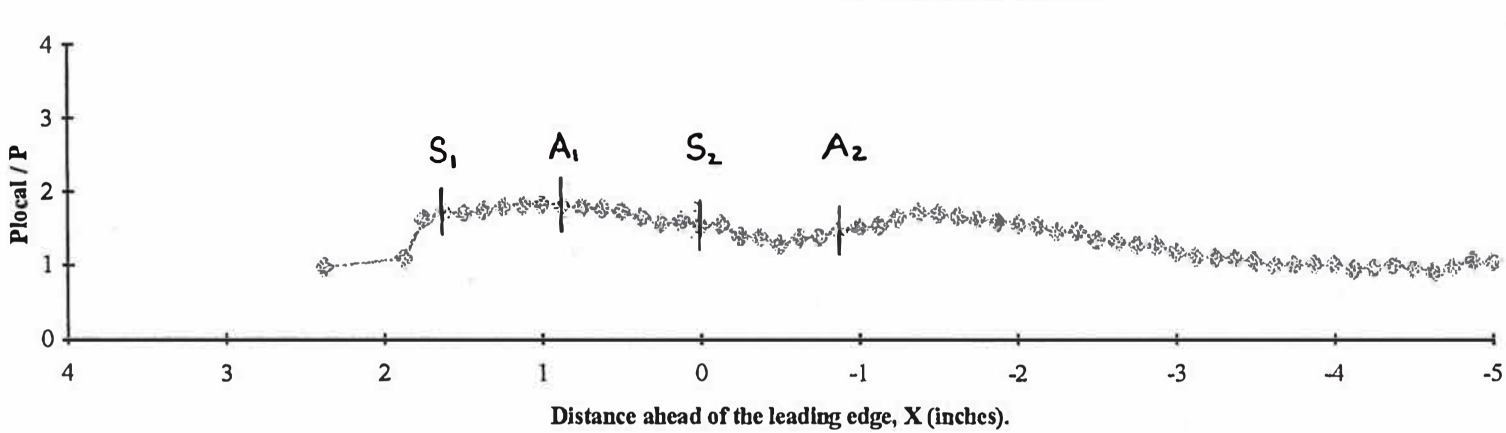
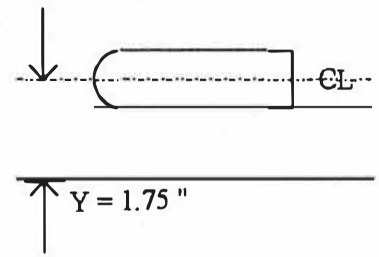


Fig. 41 (Contd. 1)

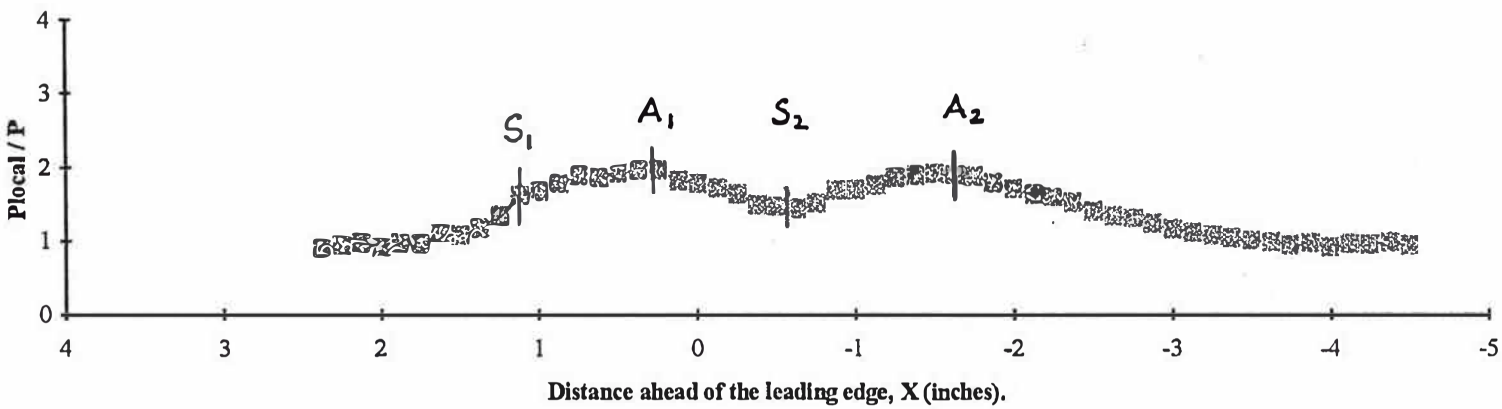
The Straight Fin with / without a Sharp Strake, Y = 1.75"

v. The Straight Fin





vi. With Sharp Strake



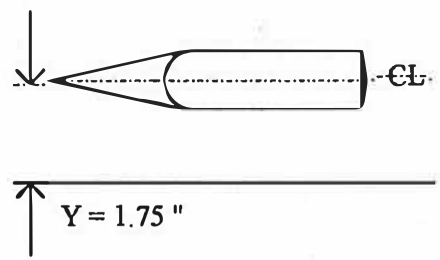
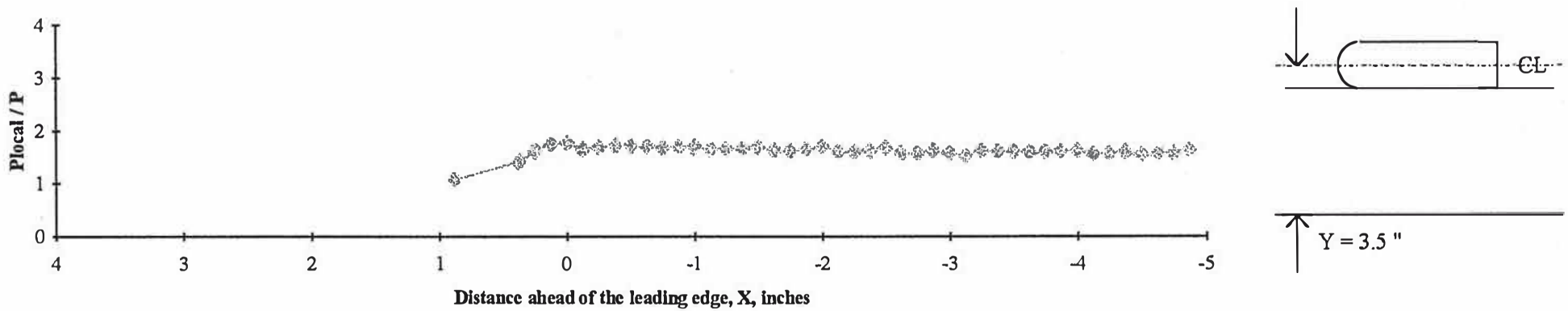


Fig. 41 (Contd. 2)

The Straight Fin with / without a Sharp Strake, Y = 3.5"

vii. The Straight Fin



viii. With Sharp Strake

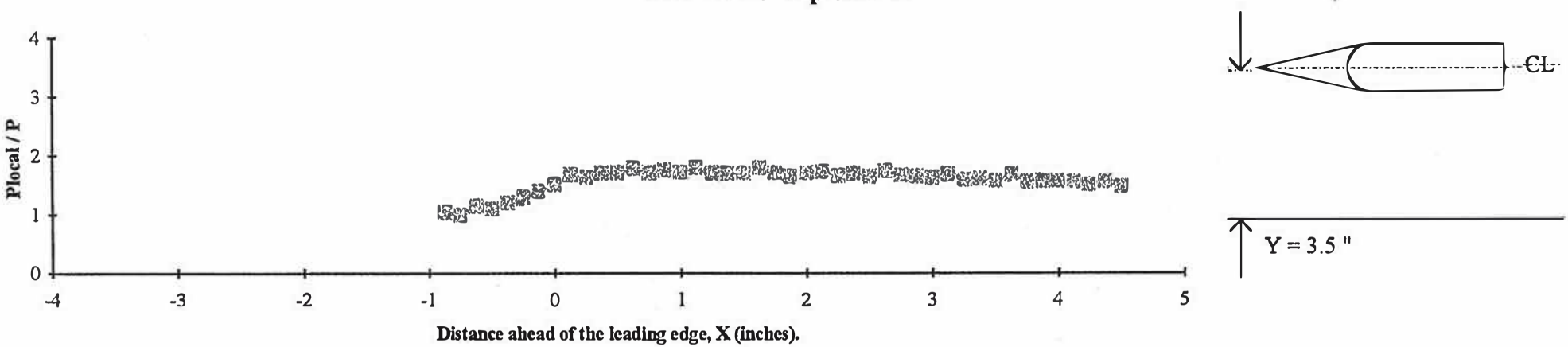
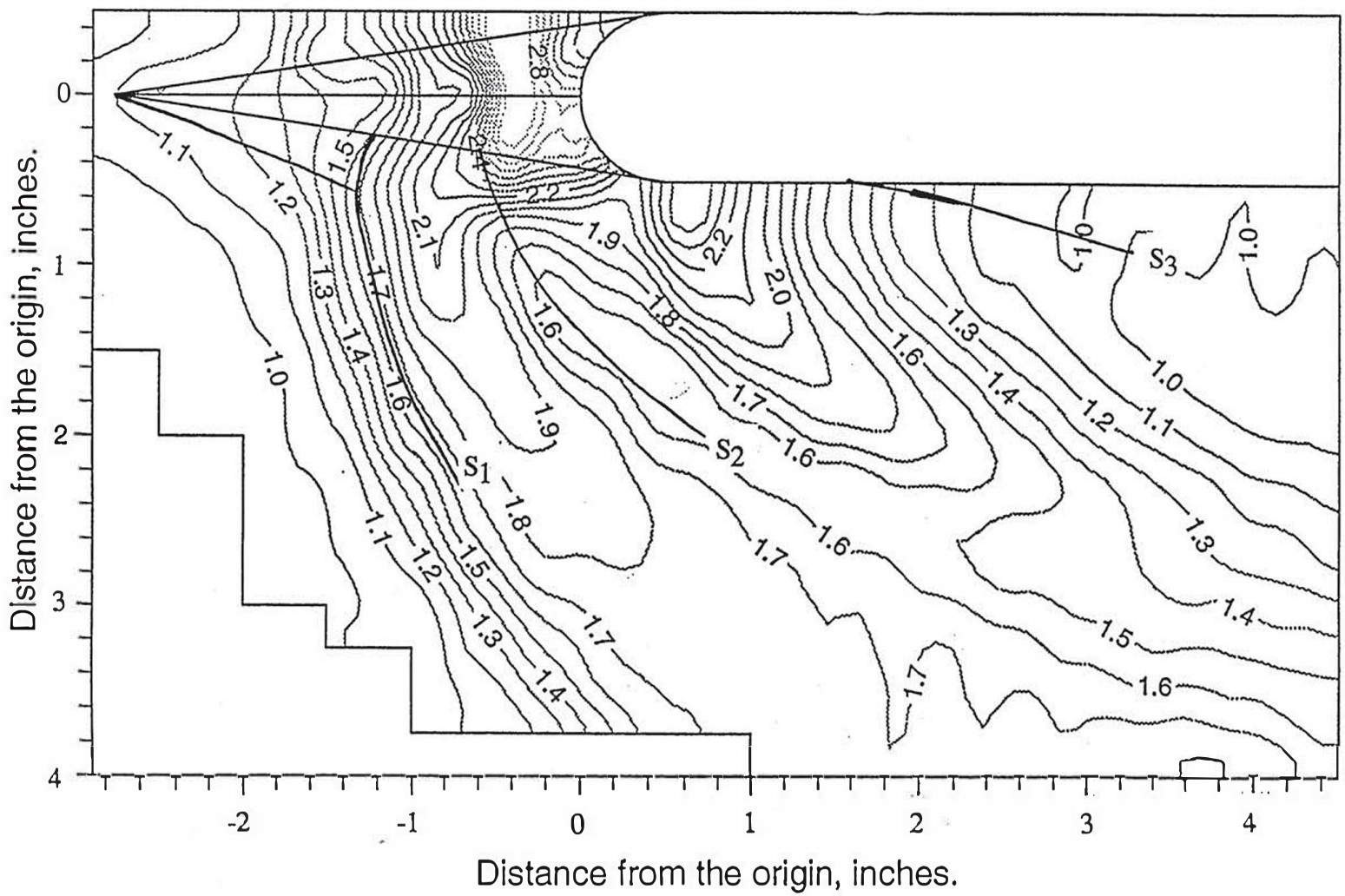
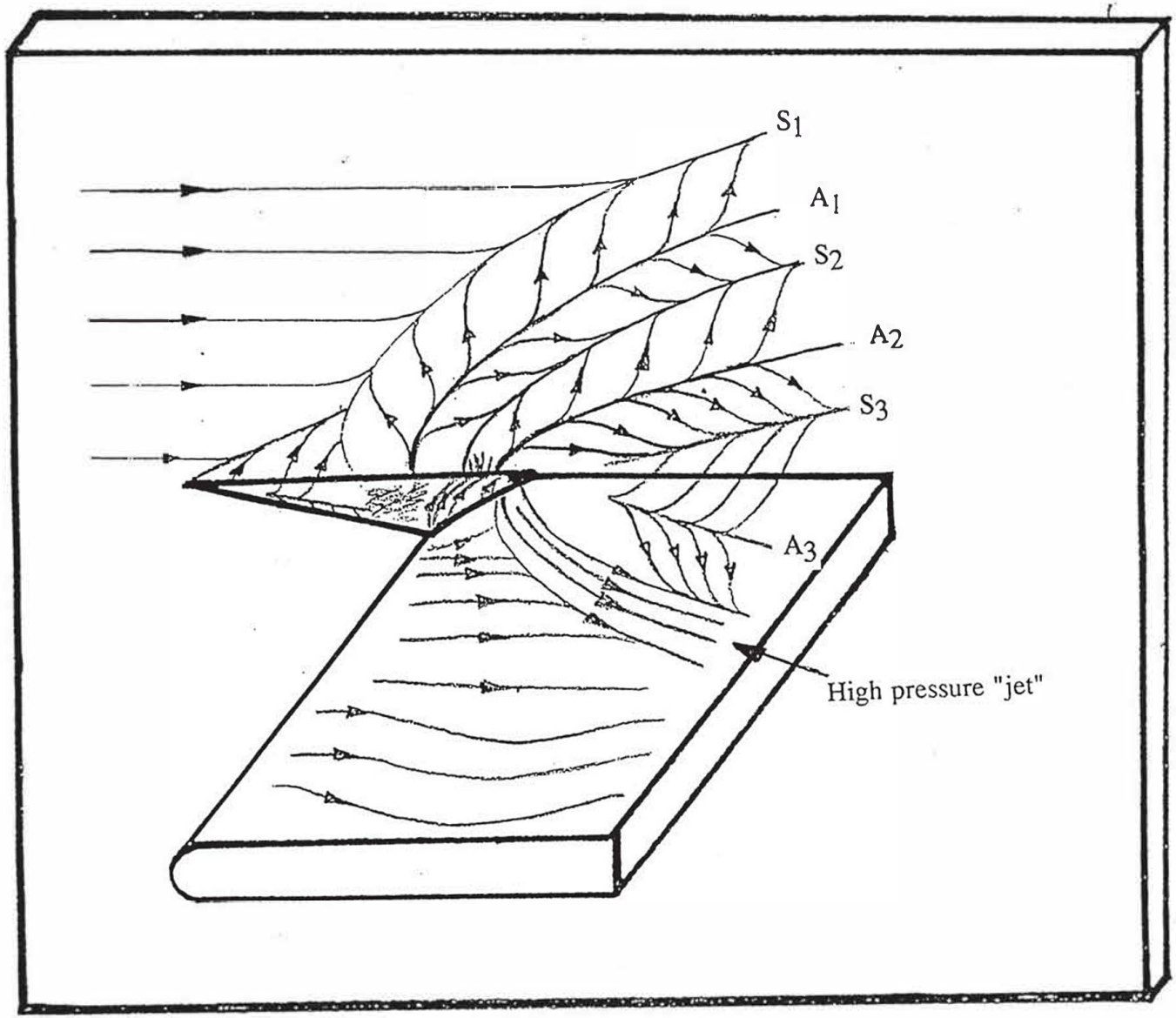


Fig. 41 (Contd. 3)

Fig. 42. Pressure contour plot with the separation lines for the $D/\delta = 1.6$ fin with a sharp leading edge strake.





(a) Streak line pattern.

Fig. 43. Flow field model for the unswept fin of $D/\delta=1.6$ with a sharp leading edge strake.

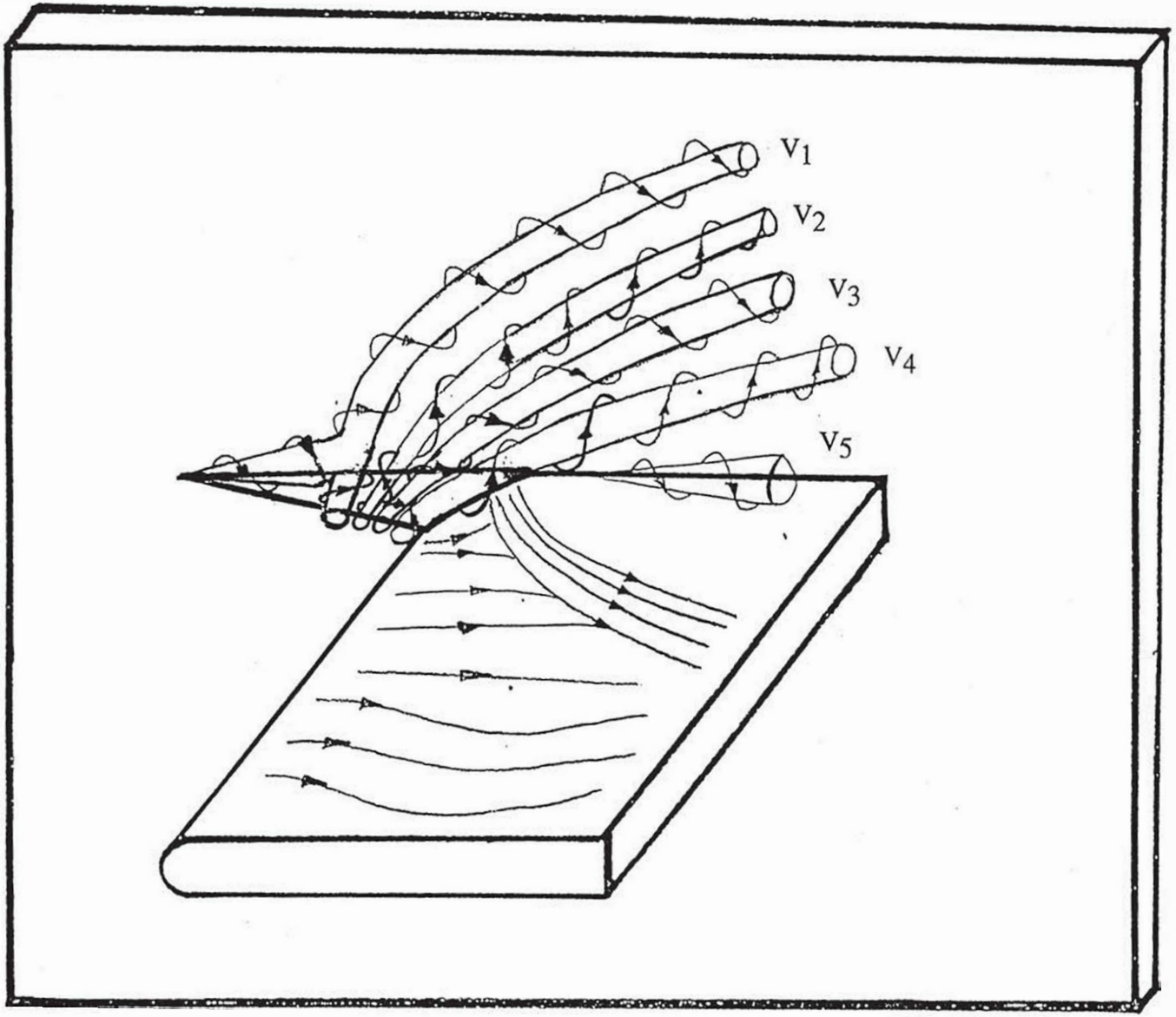


Fig. 43 (b). Vortex skeleton representation.

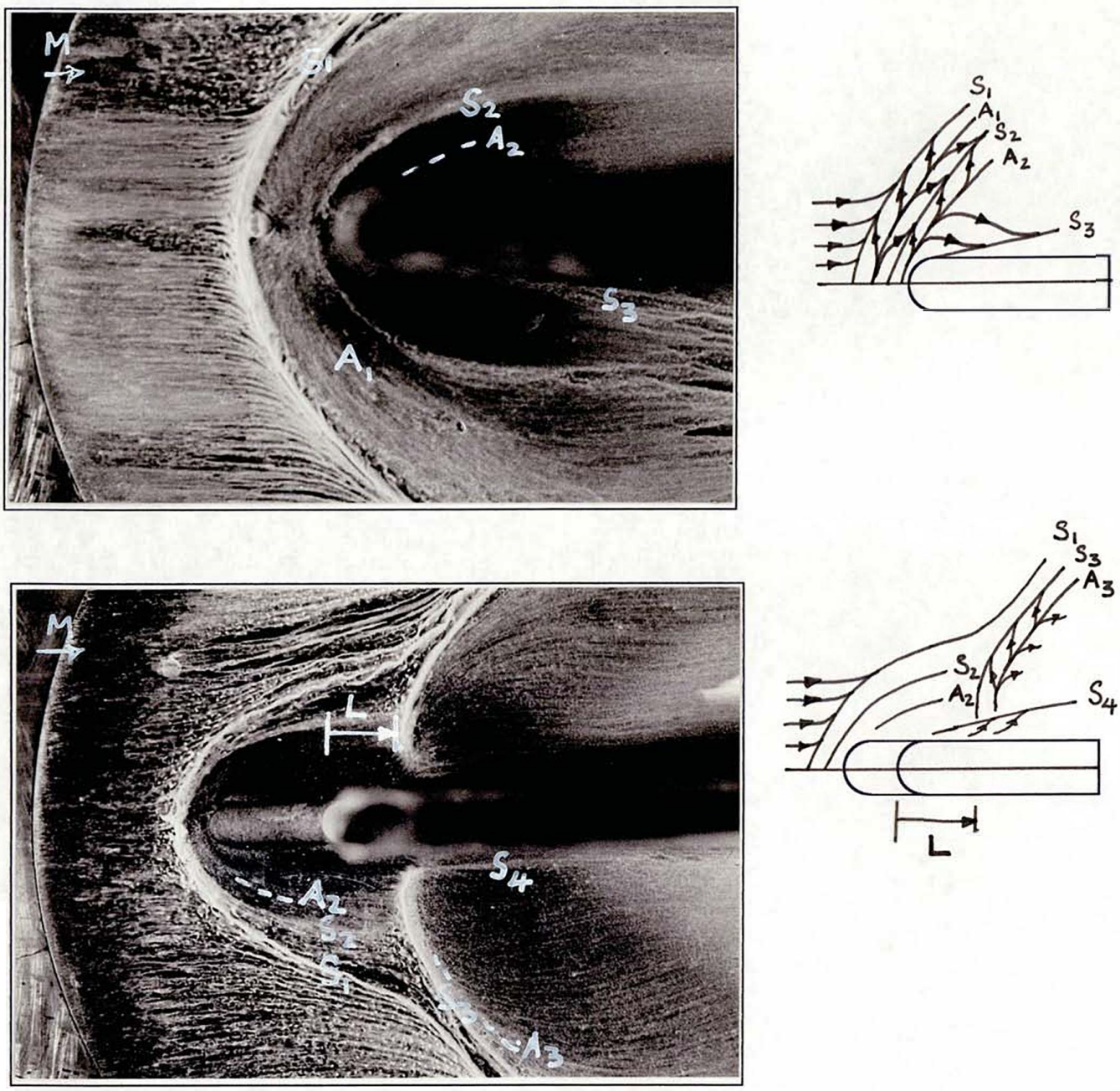
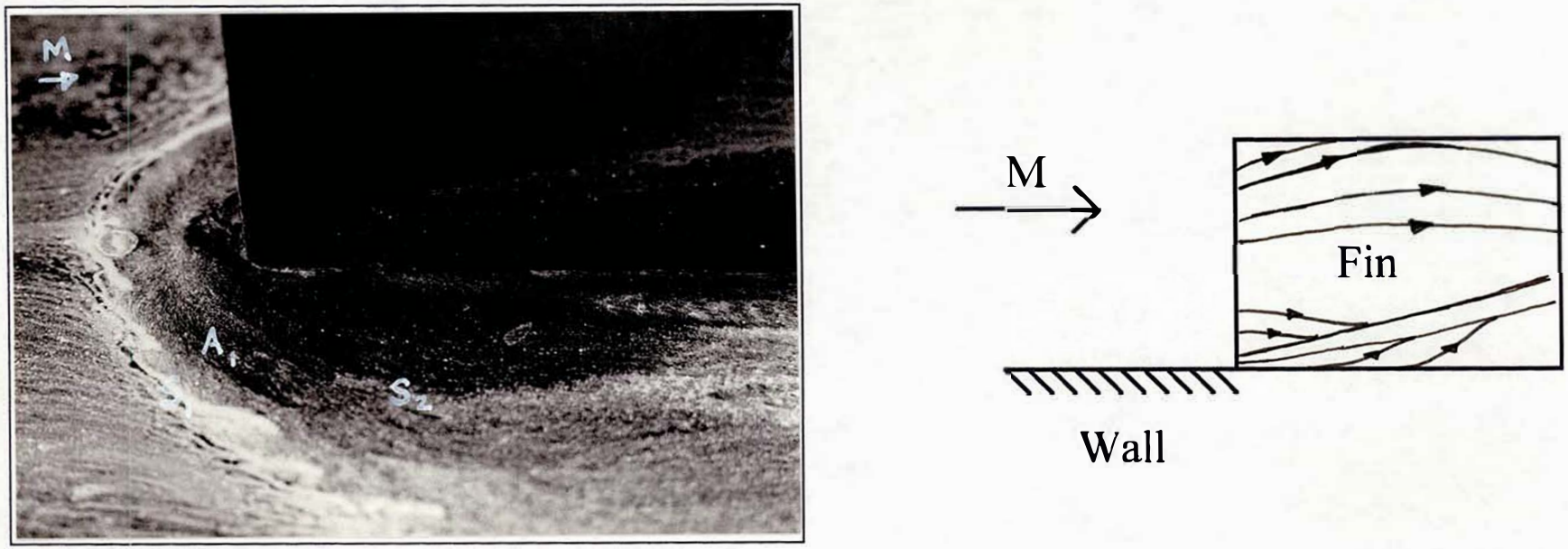
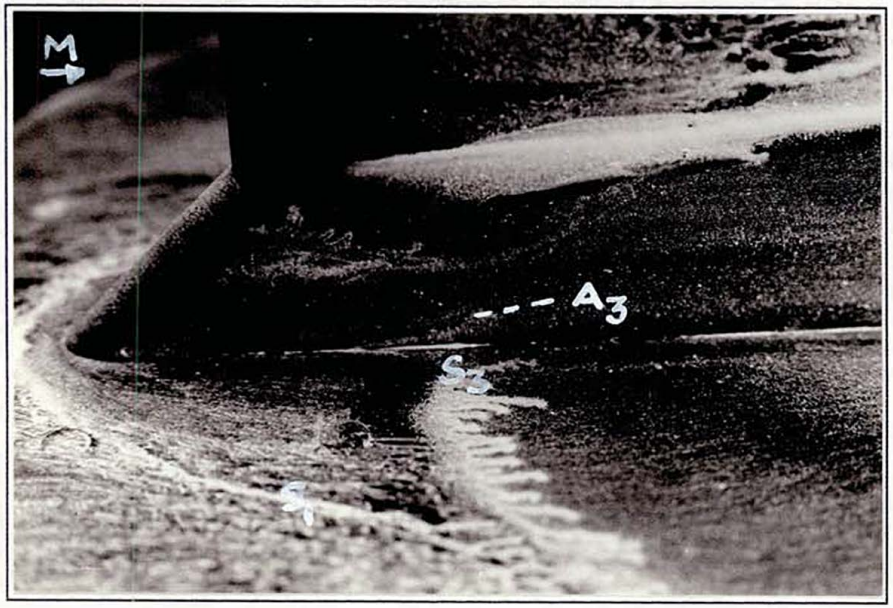


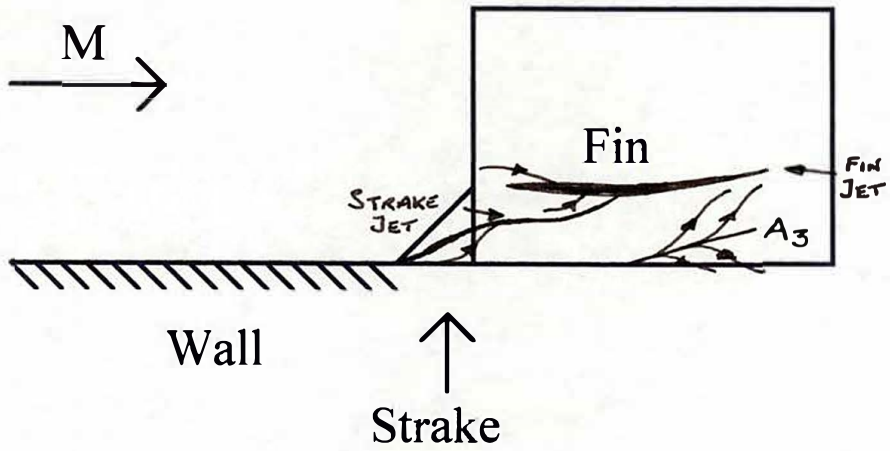
Fig. 44. Plan view oil flow photographs for the $D/\delta = 0.6$ fin with and without a blunt leading edge strake. (i) Unmodified fin (top) and (ii) with a blunt leading edge strake (bottom).



(i) Unmodified fin.

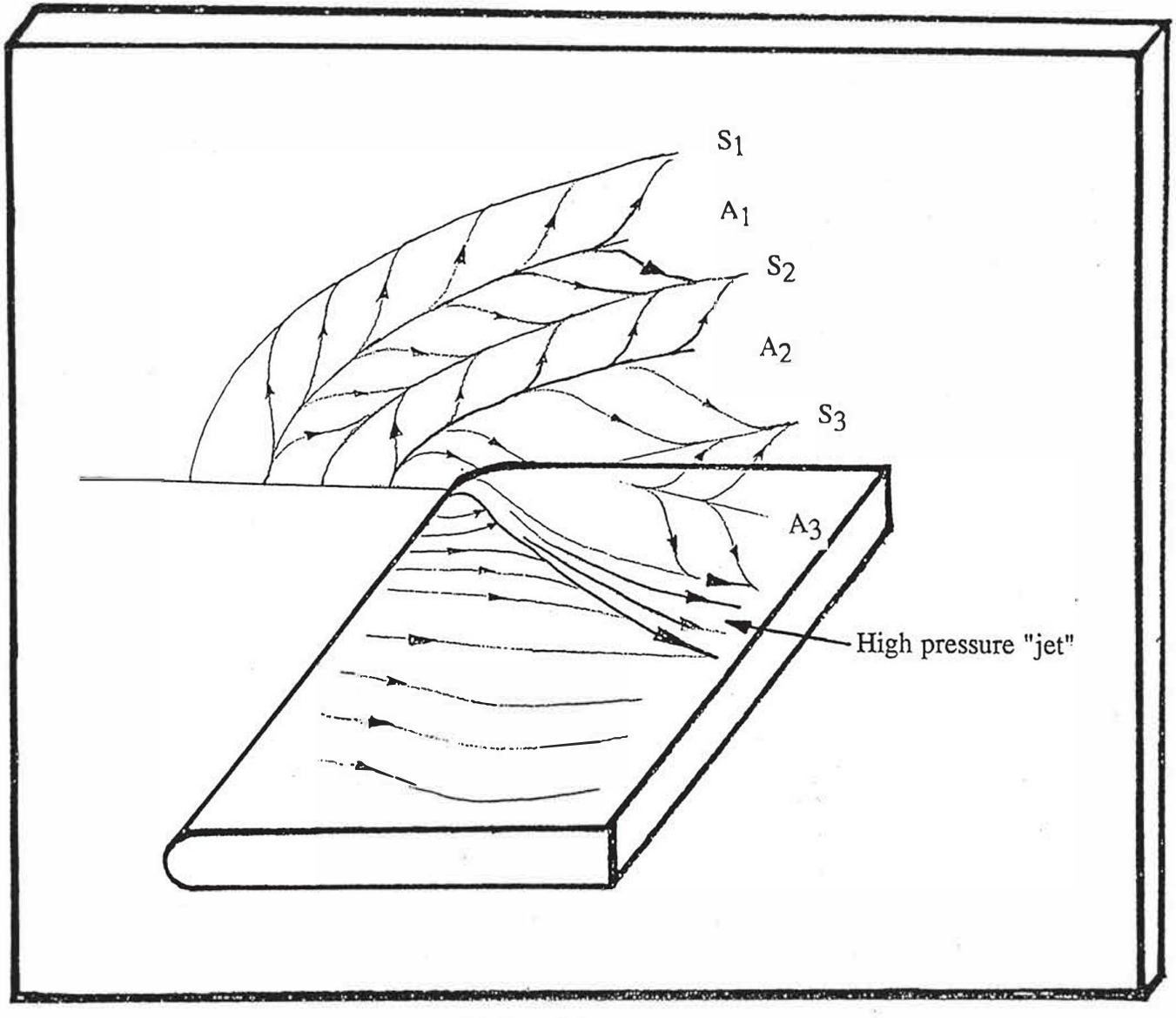
Fig. 45. Side view oil flow photographs for the $D/\delta = 0.6$ fin with and without a blunt strake.





(ii) Fin with a blunt strake.

Fig. 45. Contd. 1.



(a) Streak line pattern.

Fig. 46. Flow field model for the $D/\delta=0.6$ fin.

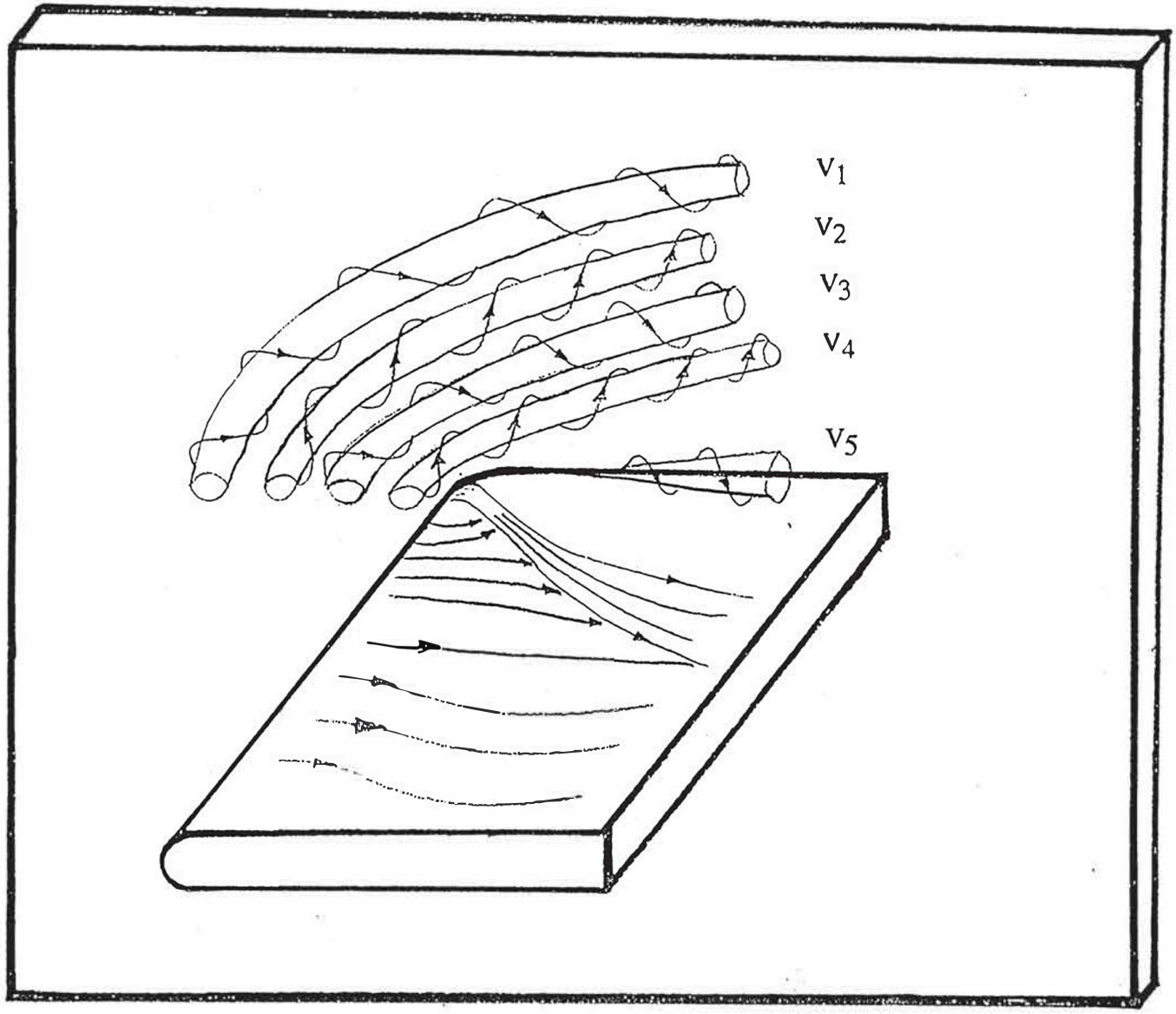


Fig. 46 (b). Vortex skeleton representation.

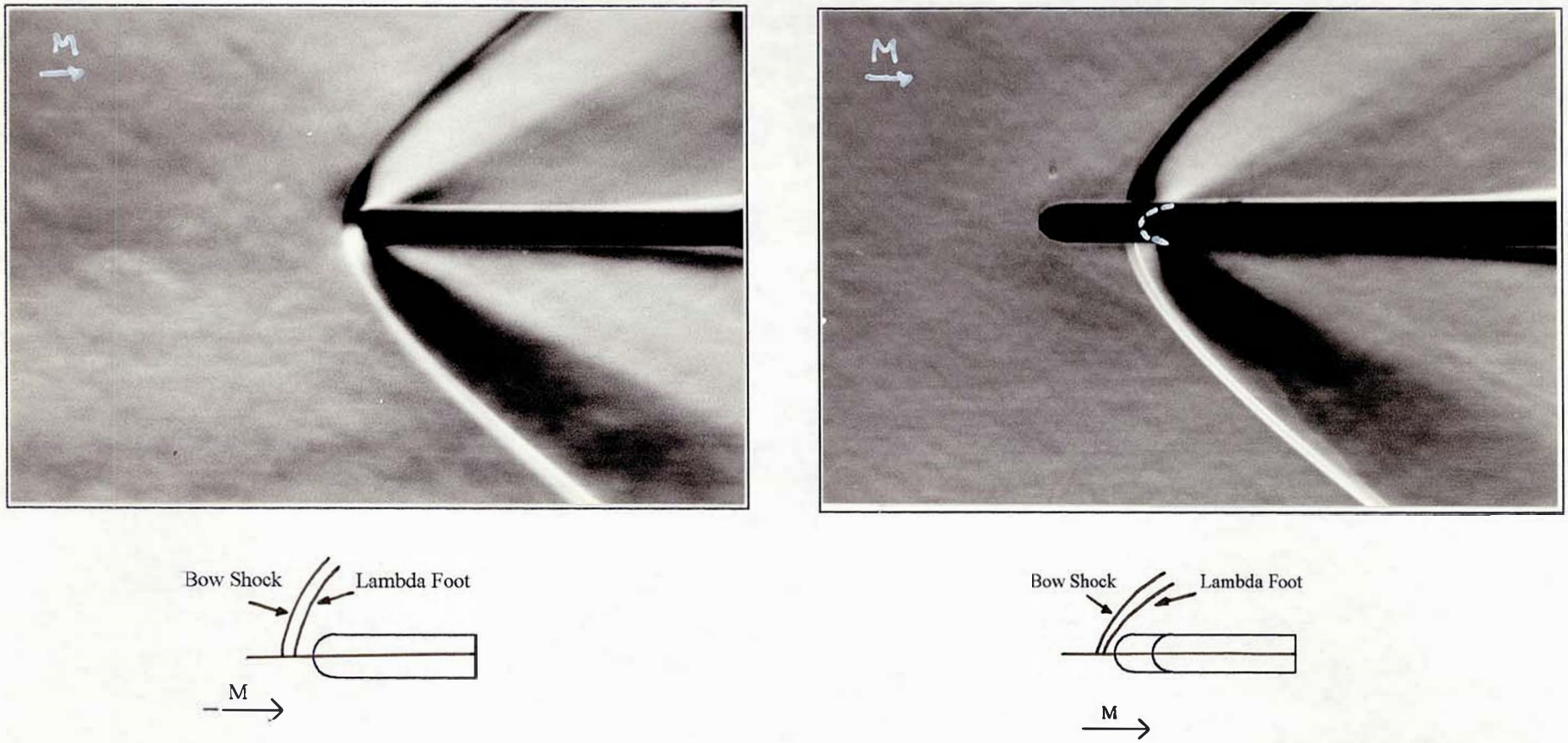
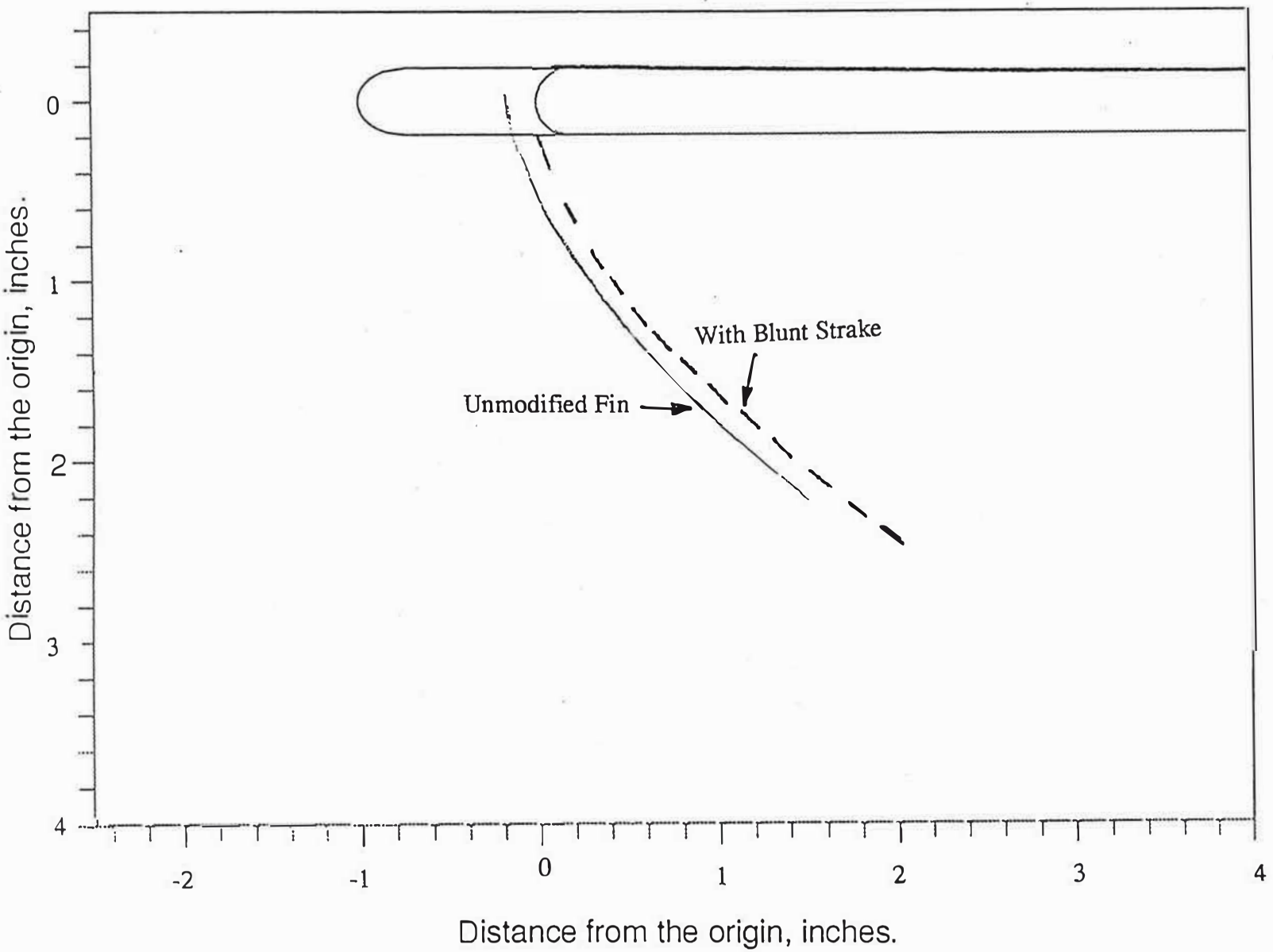
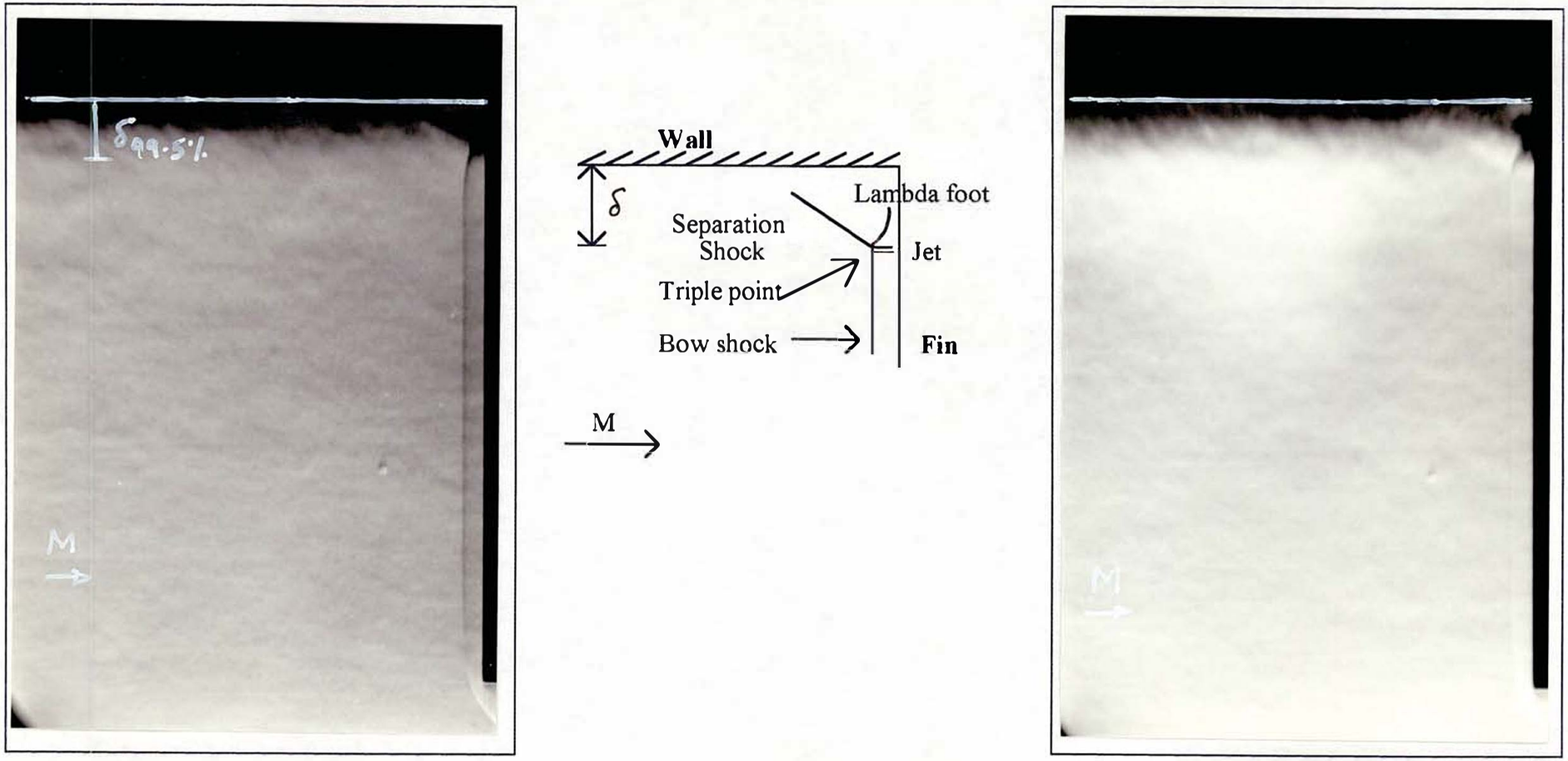


Fig. 47. Plan view schlieren images for the $D/\delta = 0.6$ fin with and without a blunt strake.
(a) Photographs of the shocks.
(i) Unmodified fin (left) and (ii) Fin with a Blunt Strake (right).

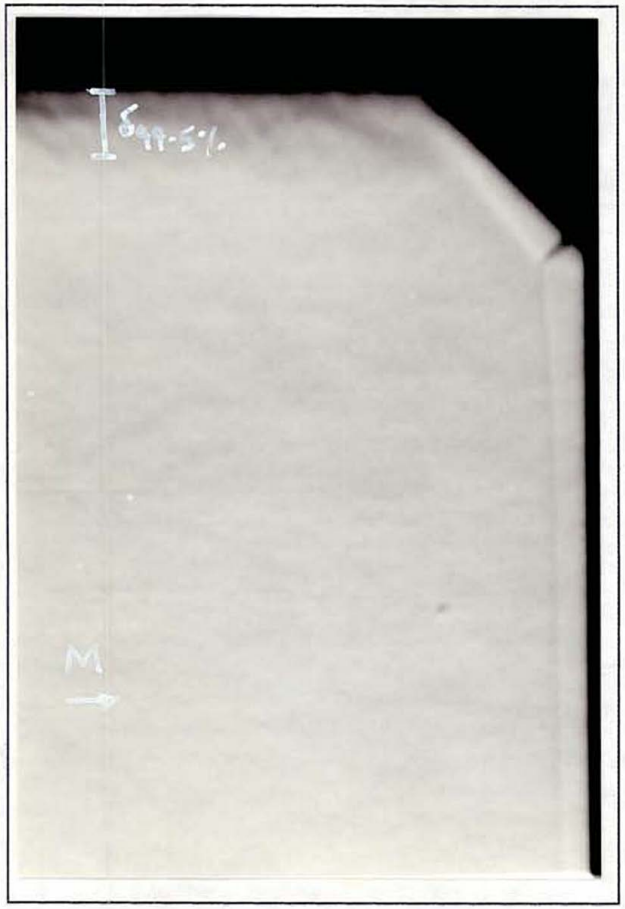
Fig. 47 (b). Comparison of the position of the bow shock waves for the $D/\delta = 0.6$ fin with and without a blunt 45° swept strake.

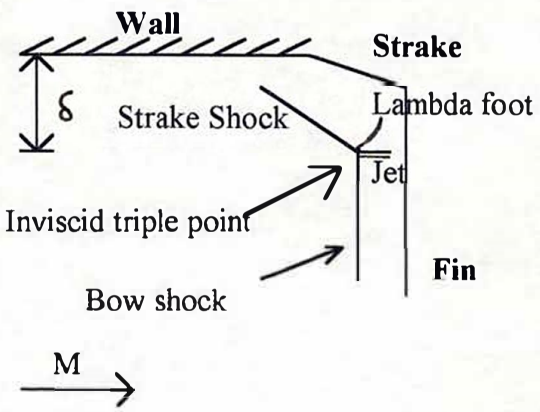


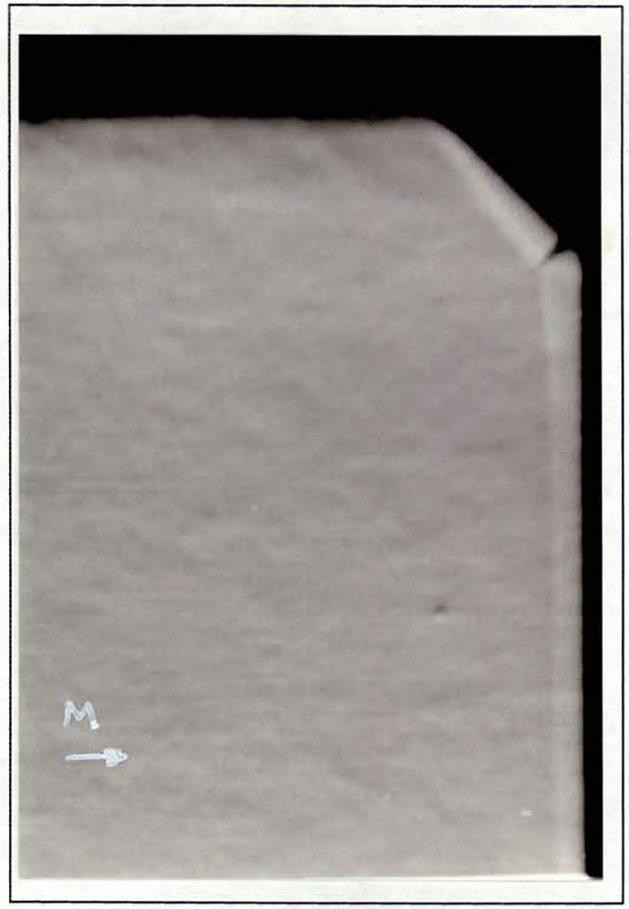


(i) Unmodified Fin

Fig. 48. Side view schlieren photographs for the straight fin of $D/\delta = 0.6$ with and without a blunt strake.

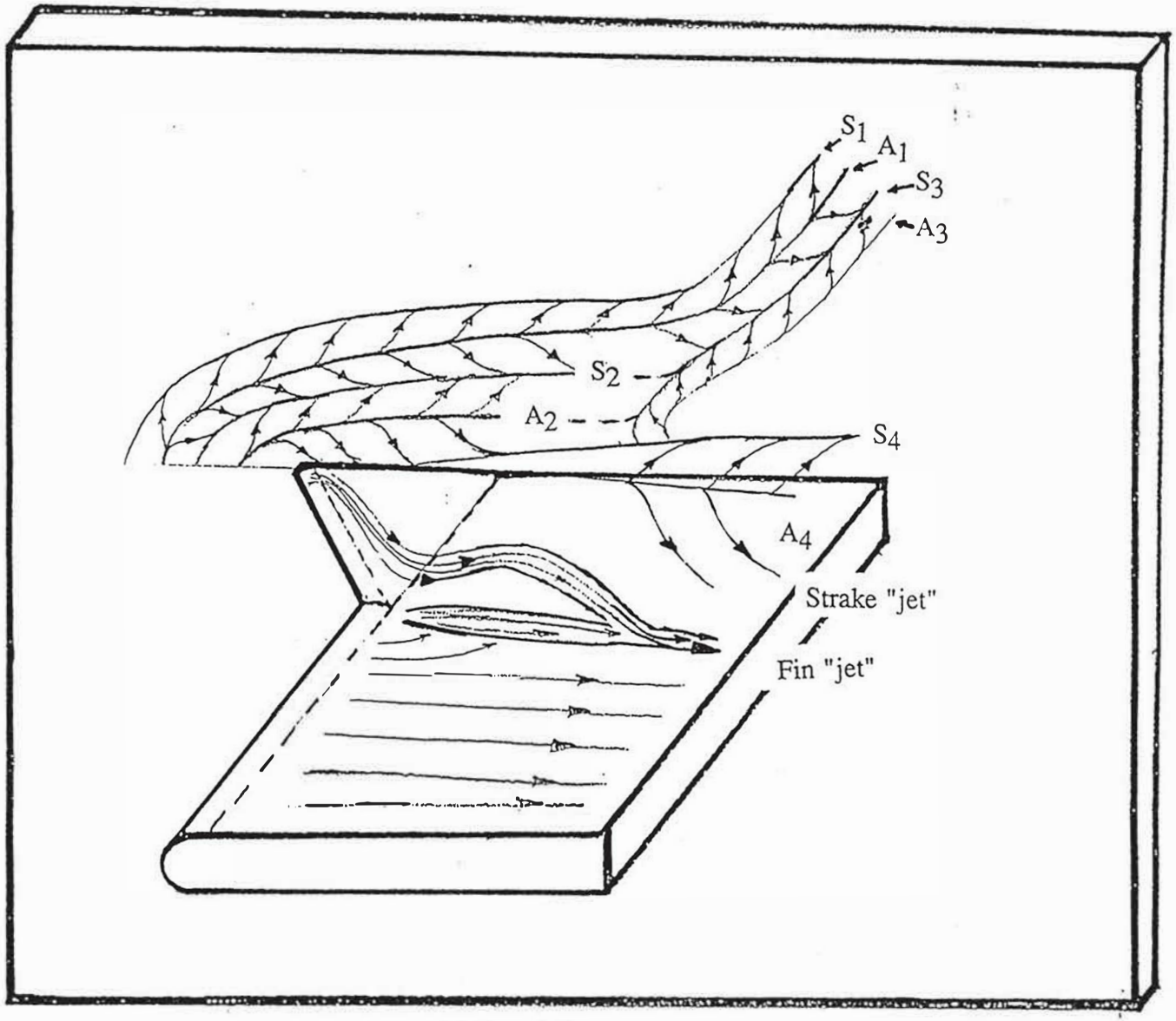






(ii) Fin with a blunt strake

Fig. 48. (Contd. 1).



(a) Streak line pattern.

Fig. 49. Flow field model for the $D/\delta=0.6$ fin with a blunt 45° swept strake.

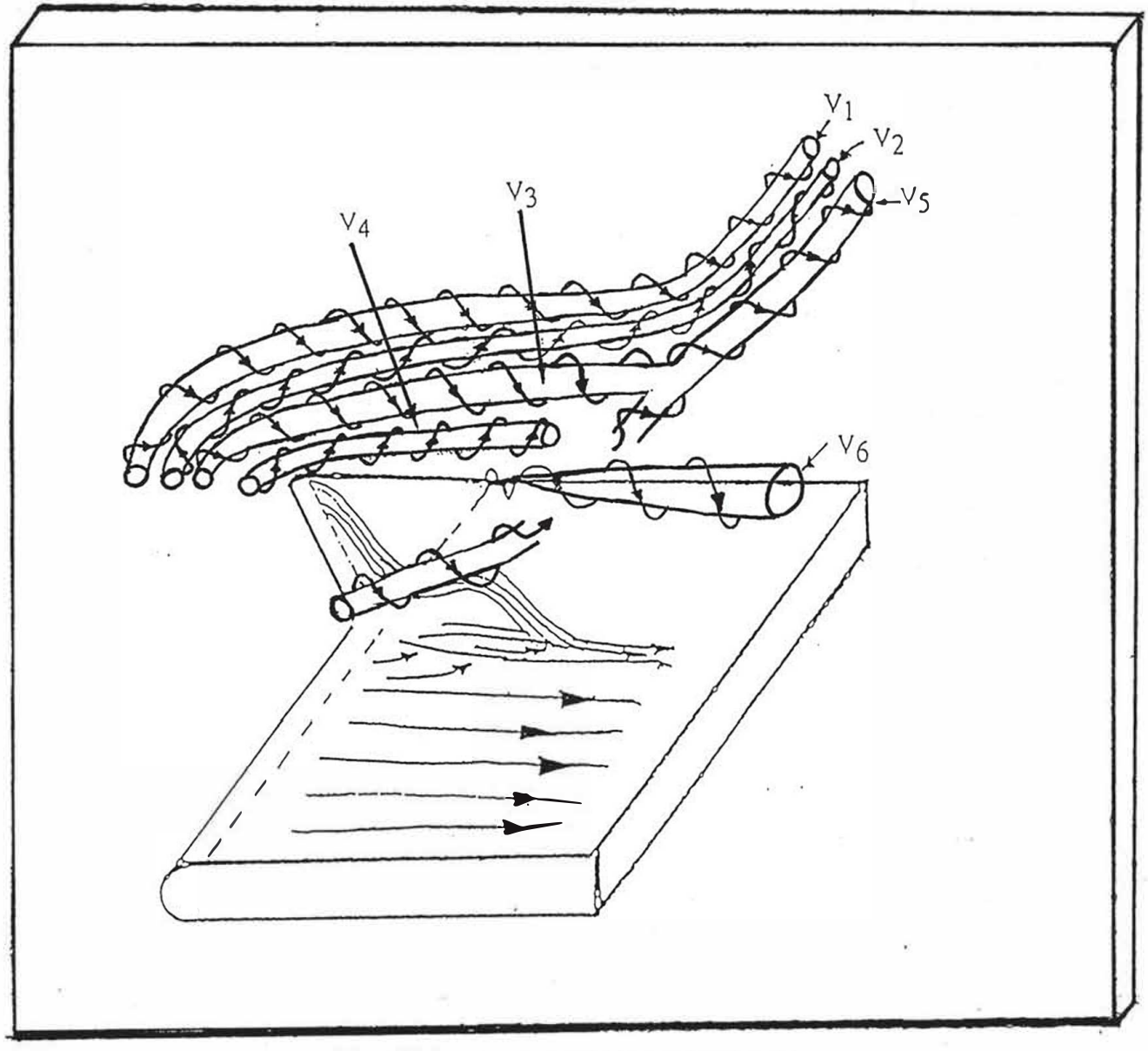
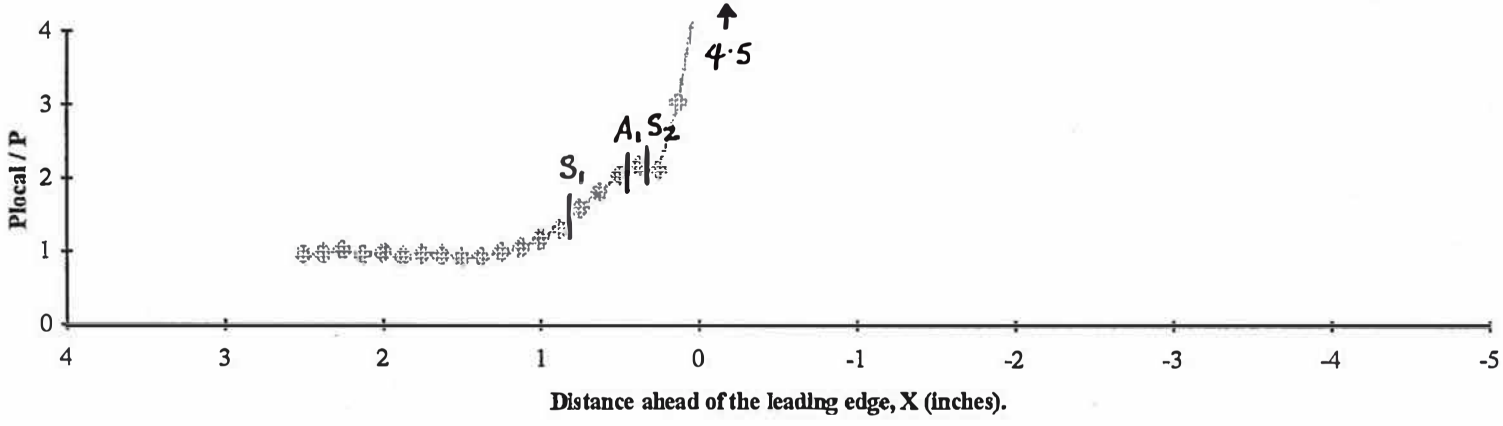
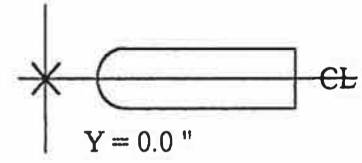


Fig. 49 (b). Vortex skeleton representation.

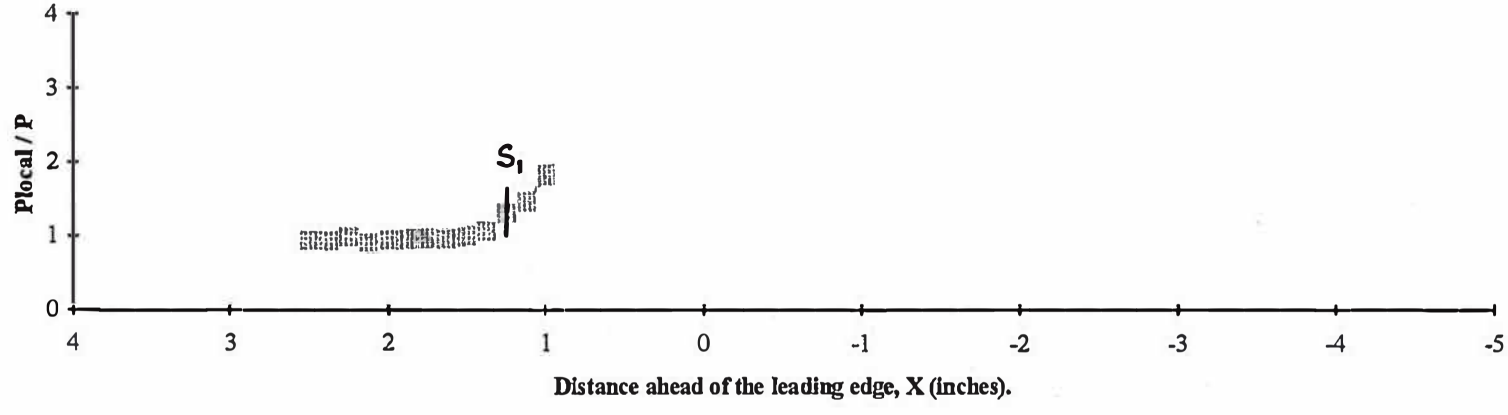
The Small Straight Fin with and without a Blunt Strake, Y = 0.0"

i. The Small Straight Fin





ii. With Blunt Strake



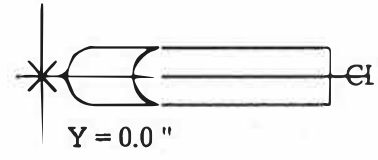
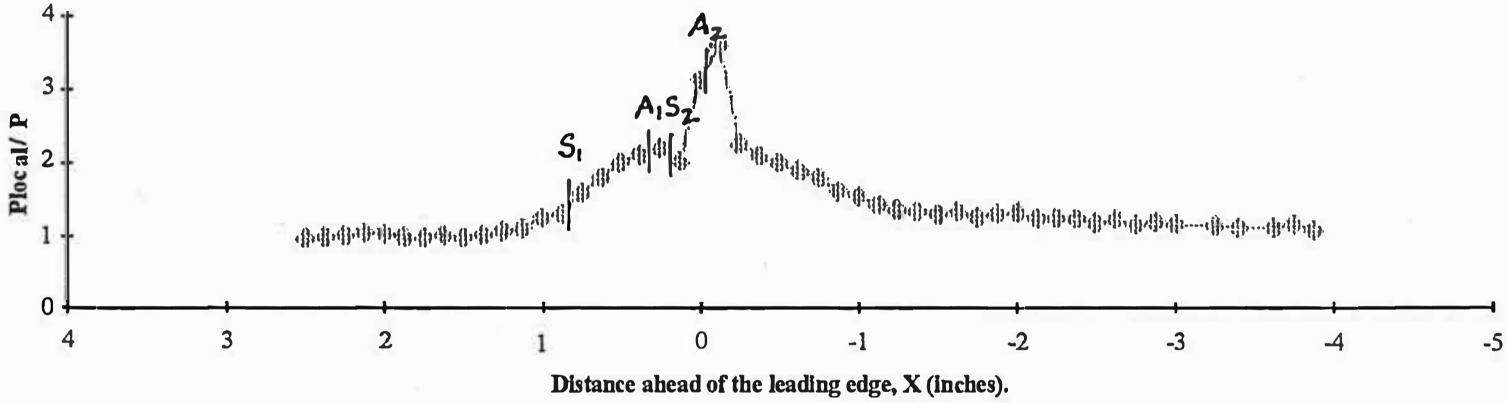
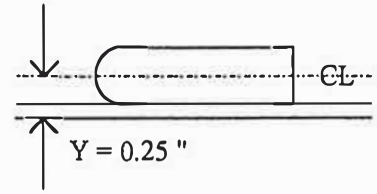


Fig. 50. Pressure plots for the fin of D/δ = 0.6 with and without a blunt leading edge strake.

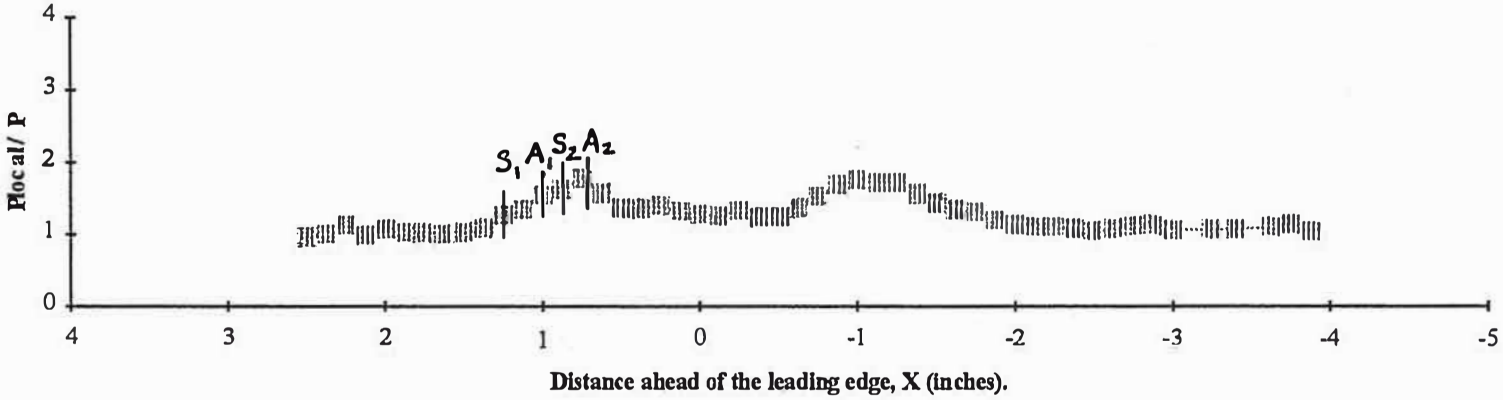
The Small Straight Fin with and without a Blunt Strake, Y = 0.25"

iii. The Small Straight Fin





iv. With Blunt Strake



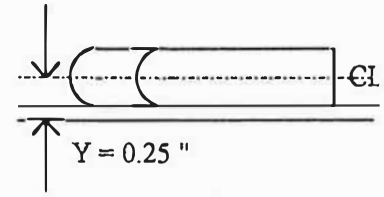
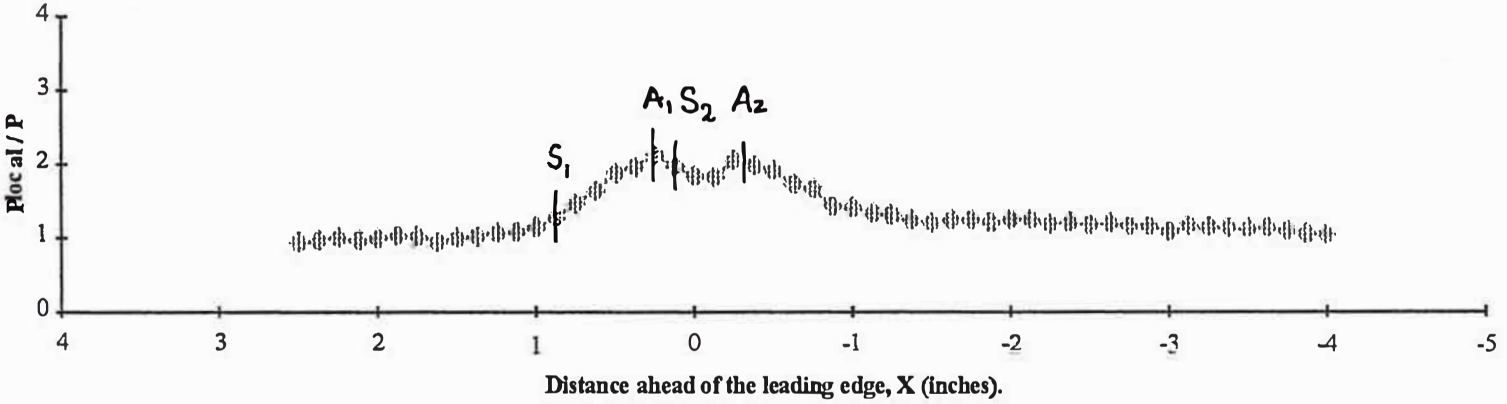
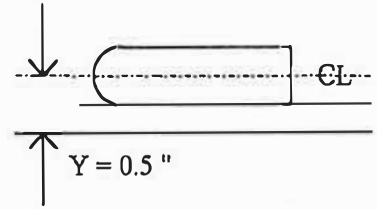


Fig. 50 (Contd. 1).

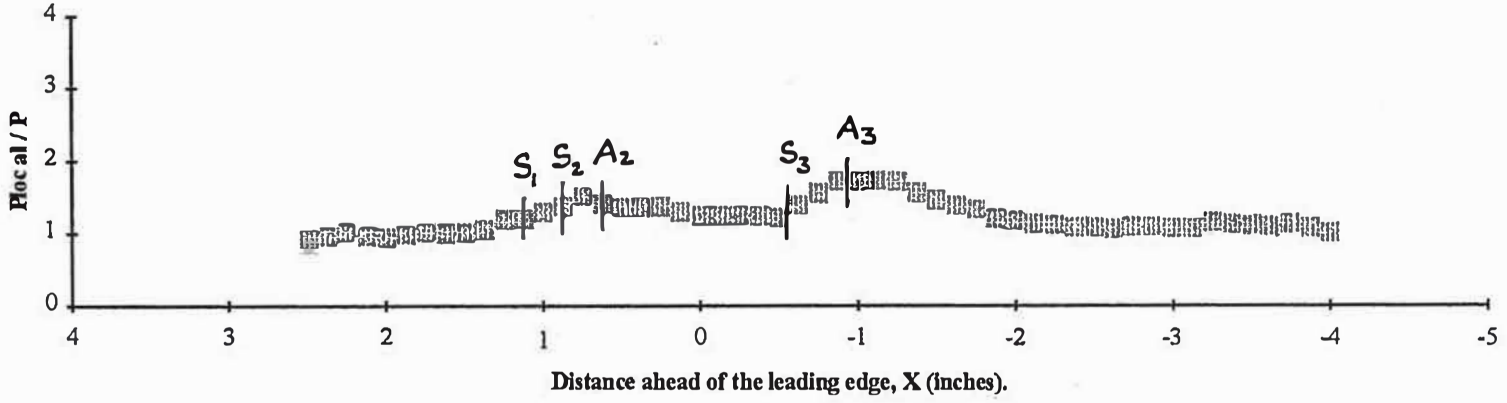
The Small Straight Fin with and without a Blunt Strake, Y = 0.5"

v. The Small Straight Fin





vi. With Blunt Strake



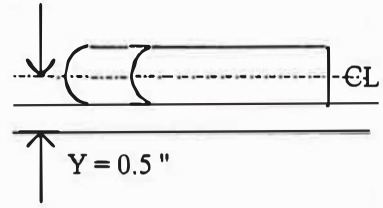
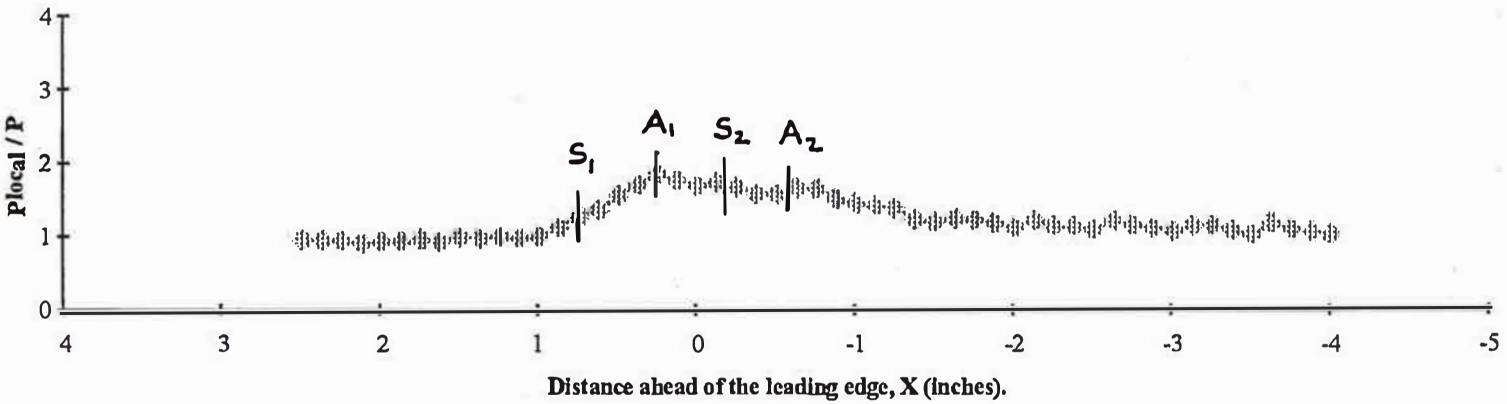
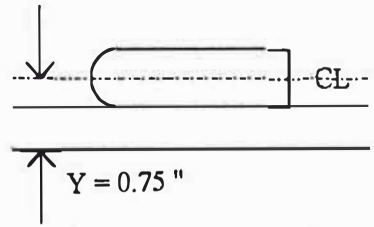


Fig. 50 (Contd. 2).

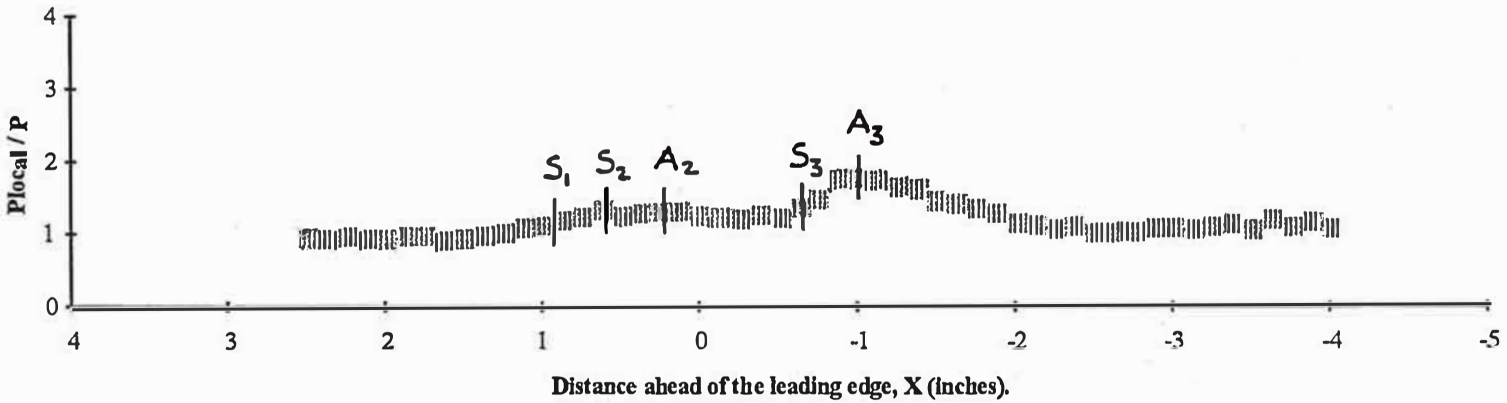
The Small Straight Fin with and without a Blunt Strake, Y = 0.75"

vii. The Small Straight Fin





viii. With Blunt Strake



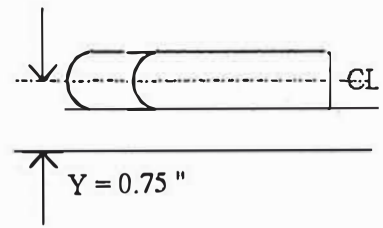
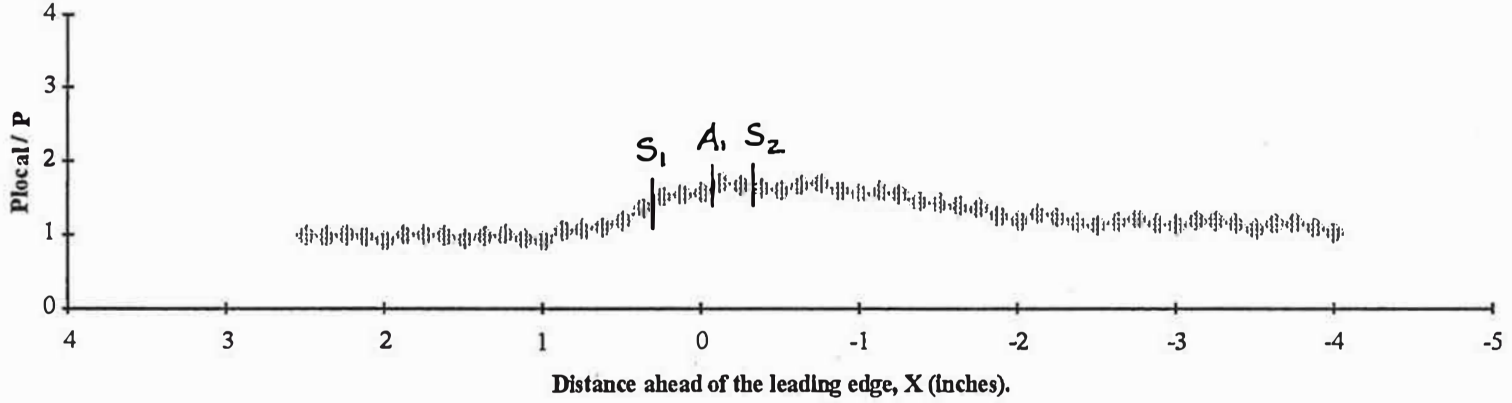
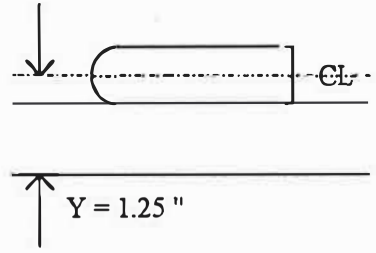


Fig. 50 (Contd. 3).

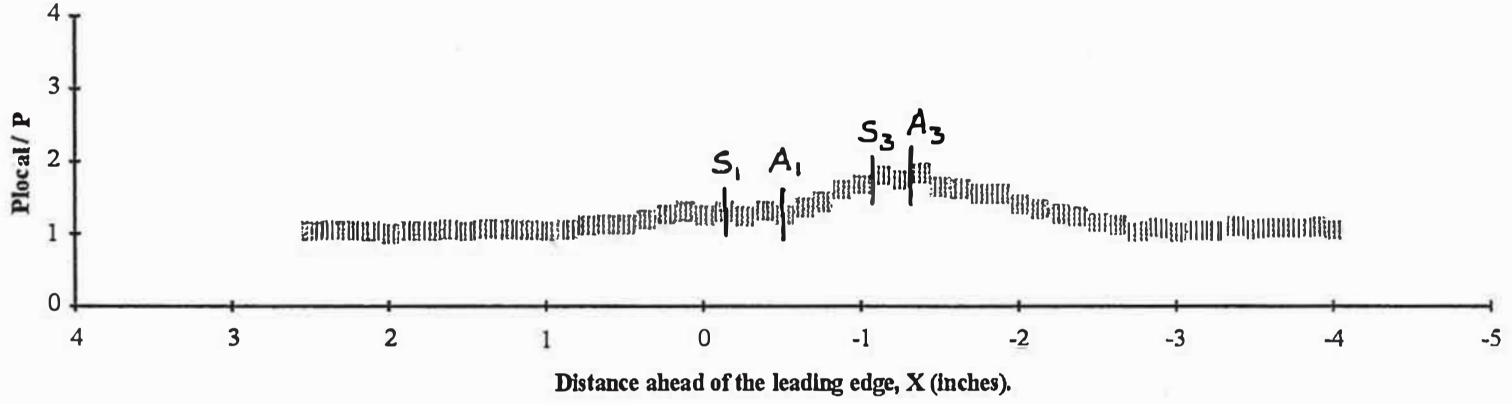
The Small Straight Fin with and without a Blunt Strake, Y = 1.25"

ix. The Small Straight Fin





x. With Blunt Strake



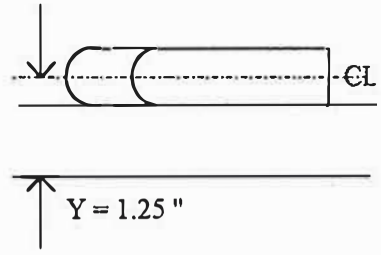
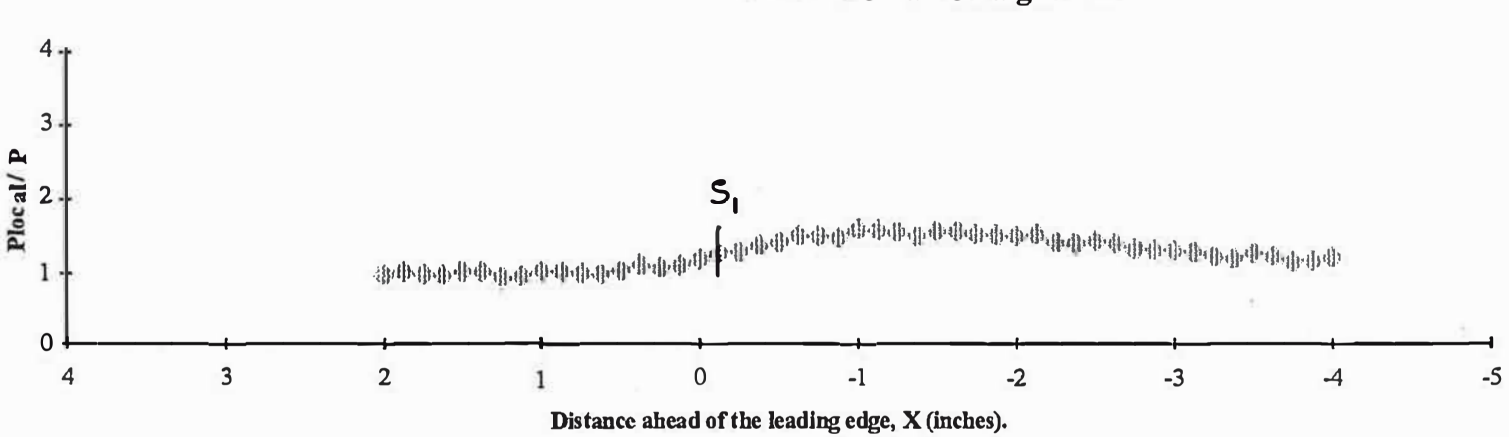
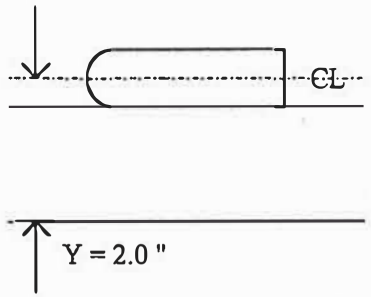


Fig. 50 (Contd. 4).

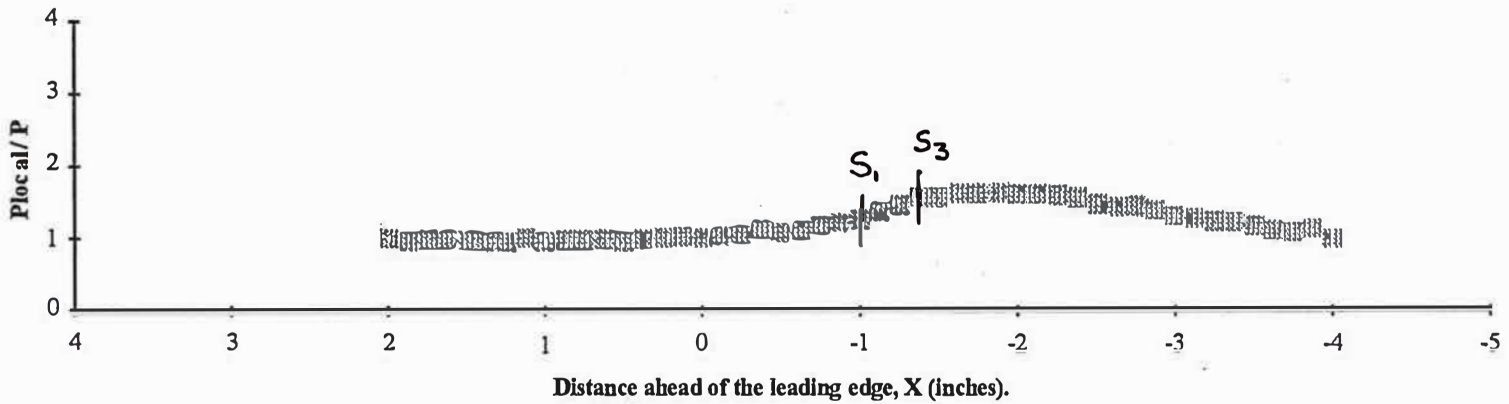
The Small Straight Fin with and without a Blunt Strake, Y = 2.0"

xi. The Small Straight Fin





xii. With Blunt Strake



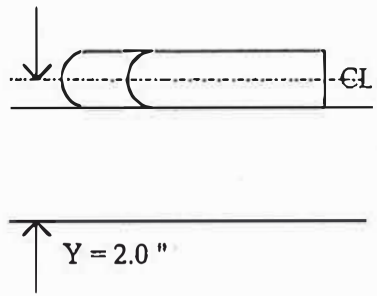
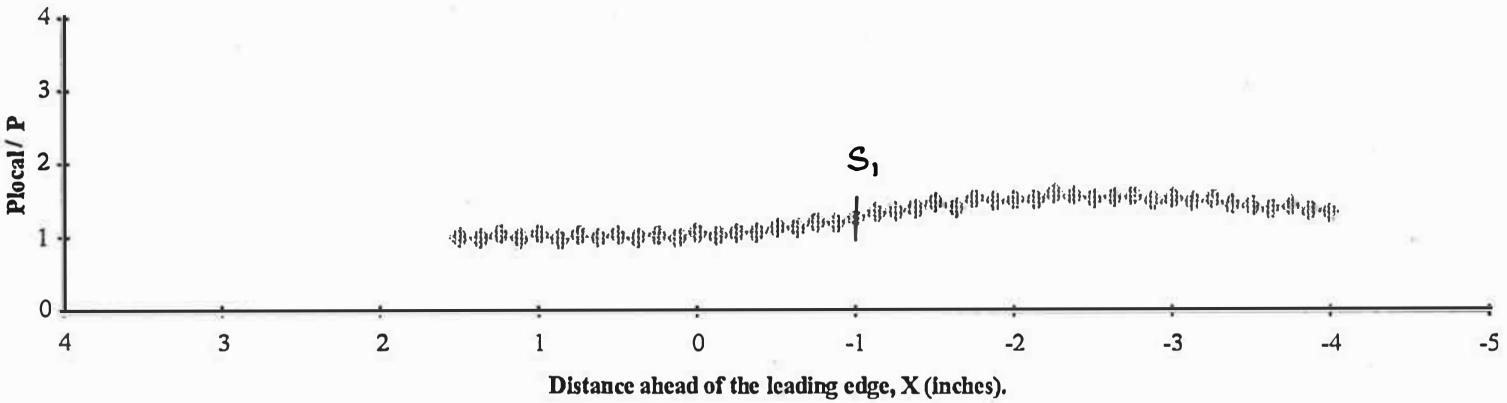
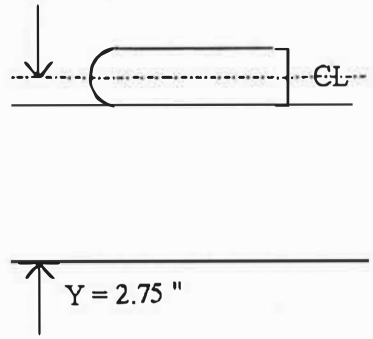


Fig. 50 (Contd. 5).

The Small Straight Fin with and without a Blunt Strake, Y = 2.75"

xiii. The Small Straight Fin





xiv. With Blunt Strake



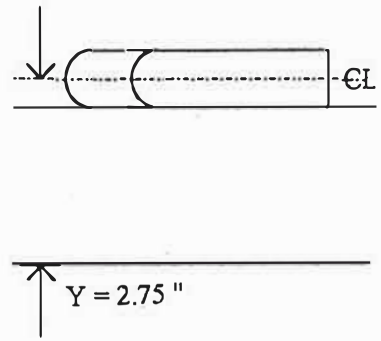
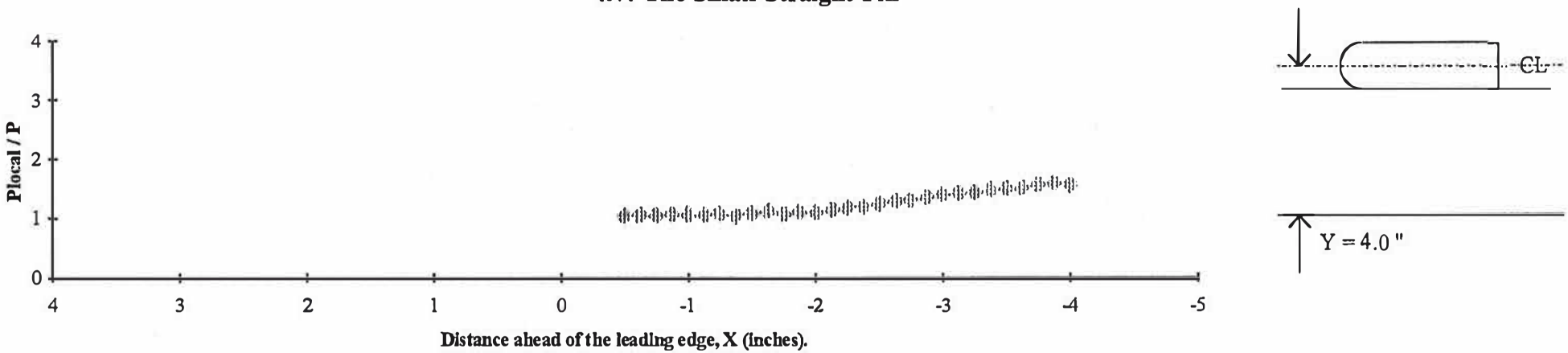


Fig. 50 (Contd. 6).

The Small Straight Fin with and without a Blunt Strake, Y = 4.0"

xv. The Small Straight Fin



xvi. With Blunt Strake

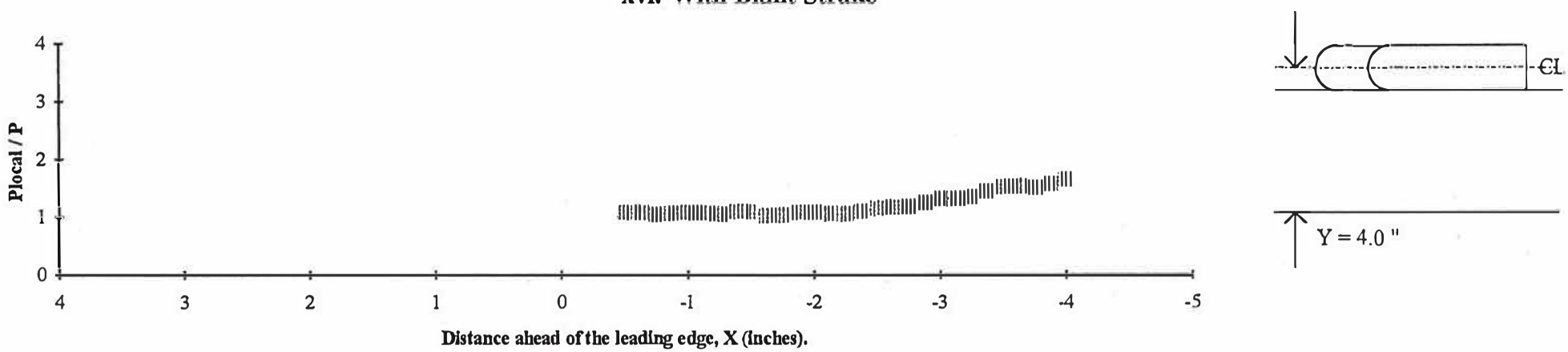


Fig. 50 (Contd. 7).

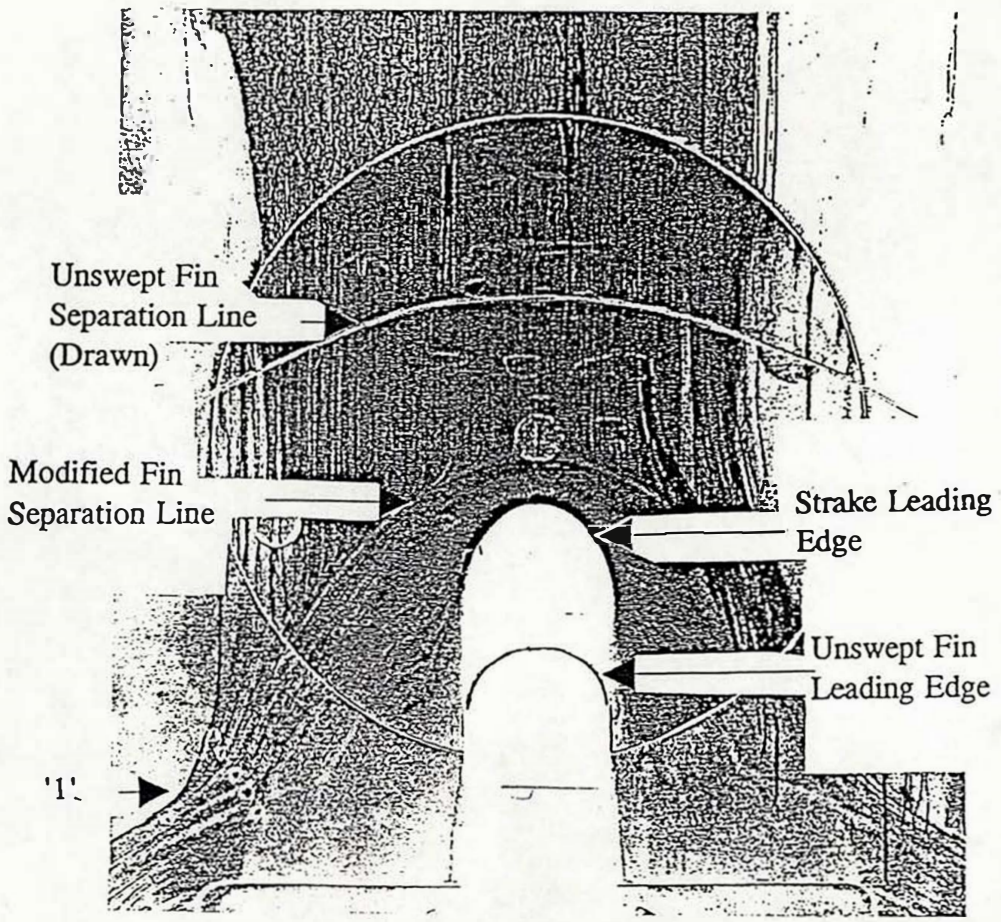
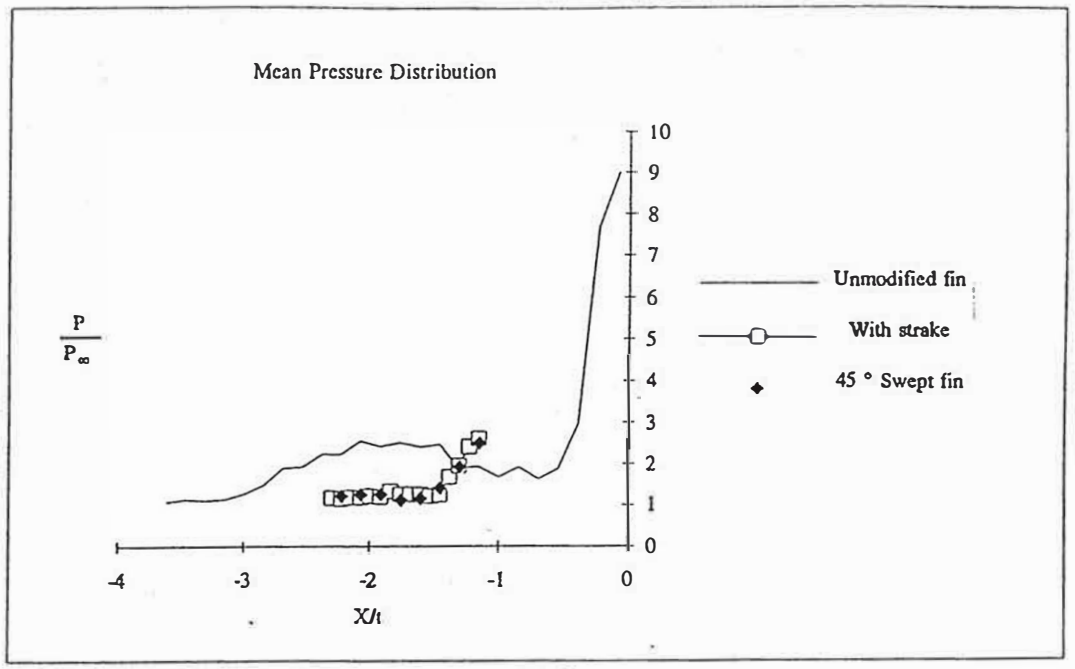
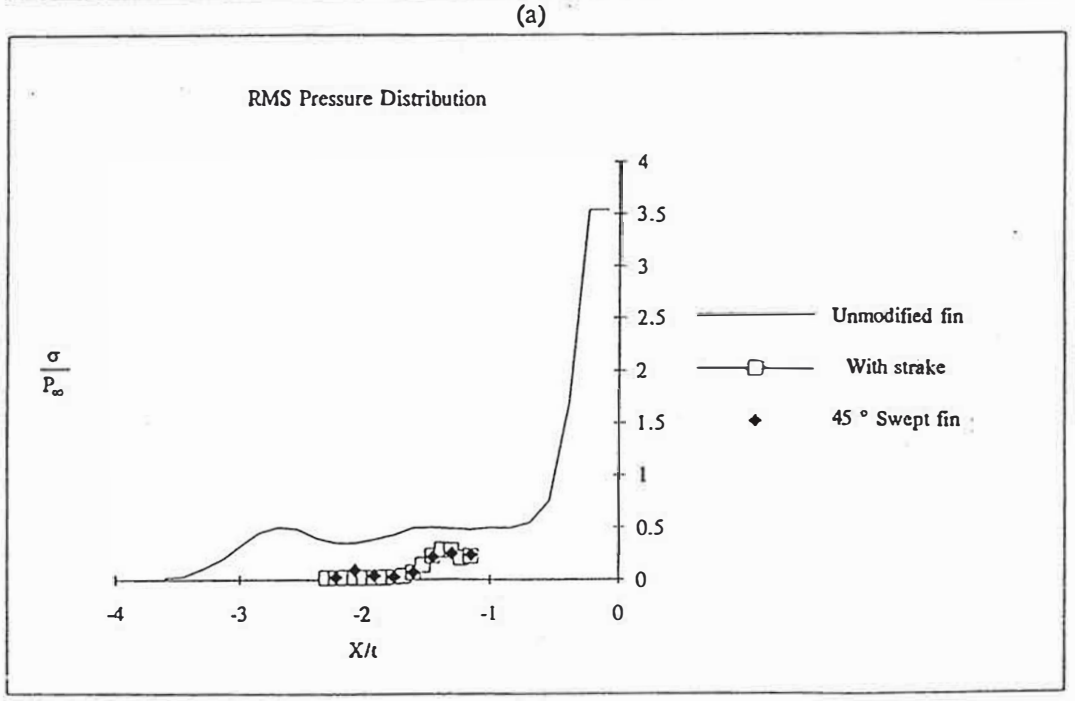


Fig. 51. Flow visualisation results for straight hemi-cylindrically blunted fin and straight fin with a blunt strake (Kleifges (1993)).



(a)



(b)

Fig. 52. Mean and RMS pressure distribution for a plain fin with and without a blunt leading edge strake (Kleifges (1993)).

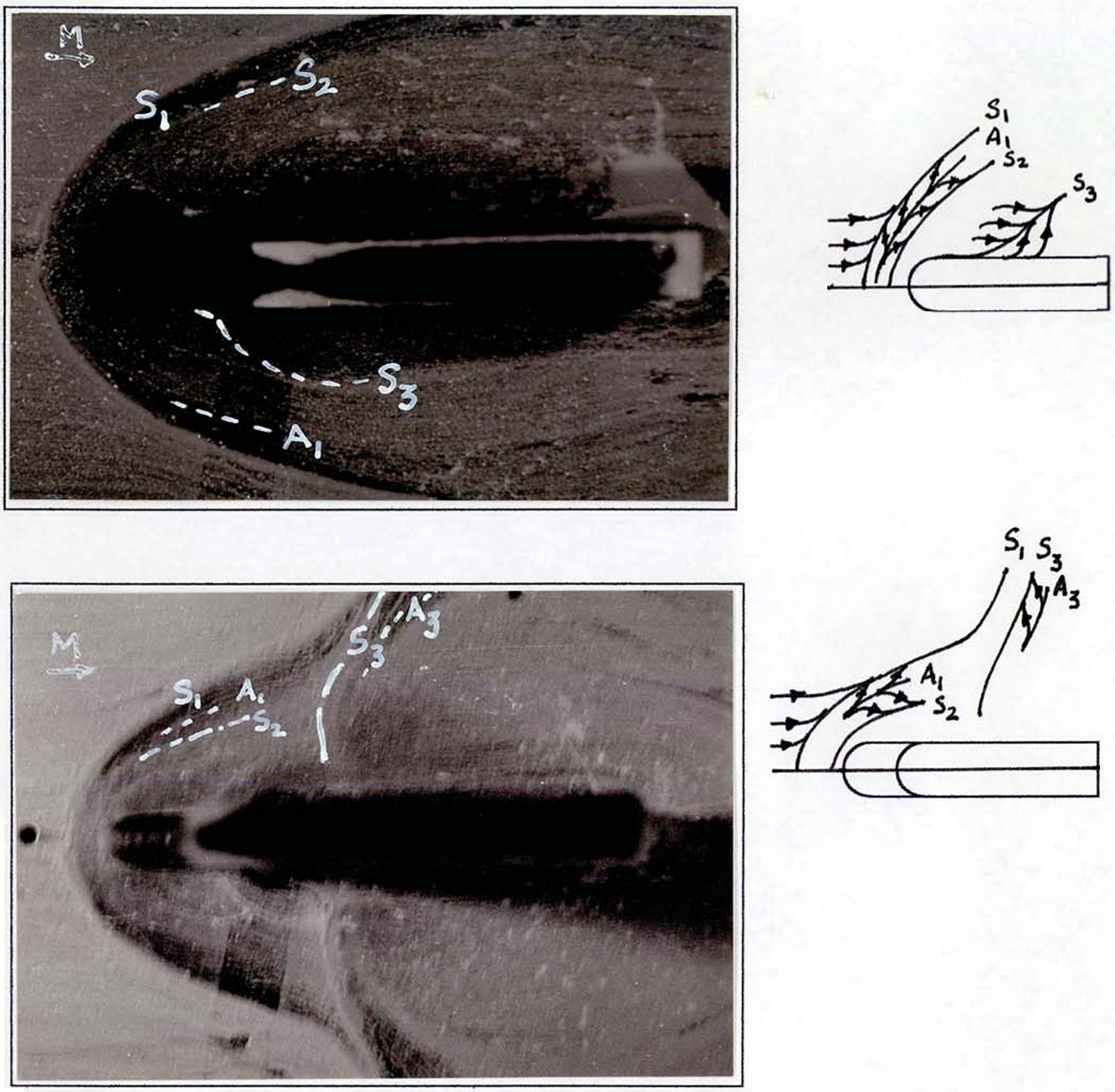
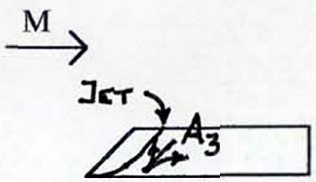
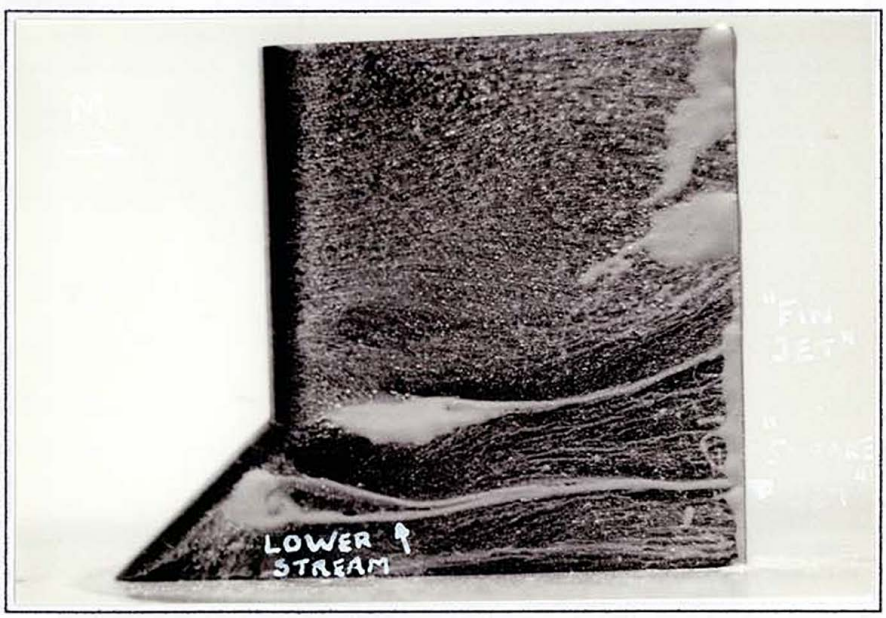


Fig. 53. Plan view oil flow photographs for the blunt 45° swept strakes of $h/\delta = 1.6$. (i) the Independent strake (top) and (ii) with the outer portion of the wing (bottom).







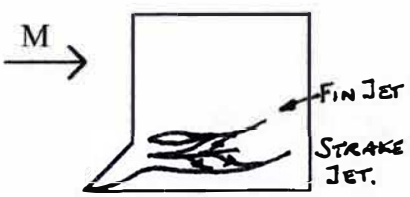


Fig. 54. Side view oil flow photographs for the blunt 45° swept strakes of $h/\delta = 1.6$.
(i) the Independent strake (top) and (ii) with the outer portion of the wing (bottom).

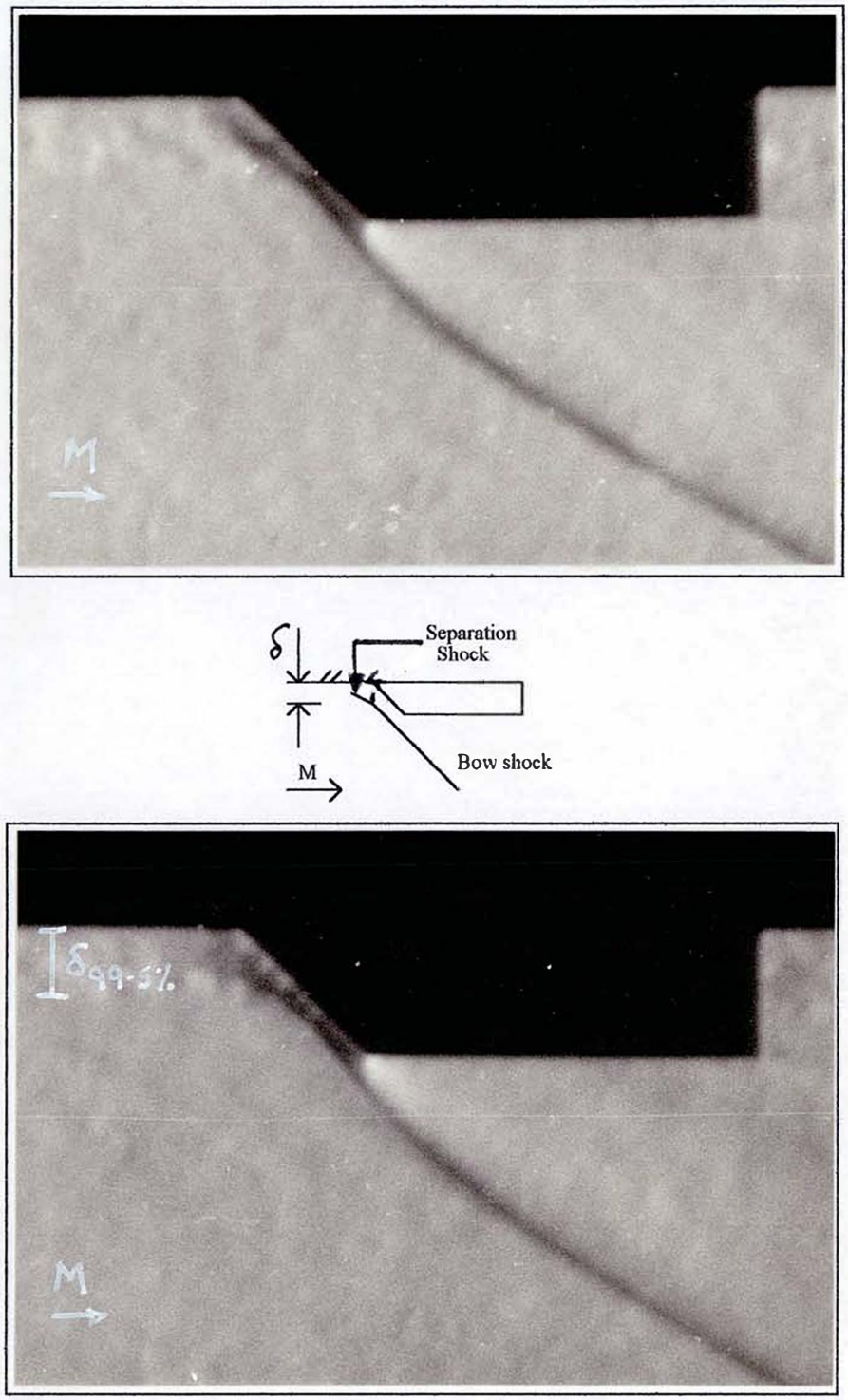
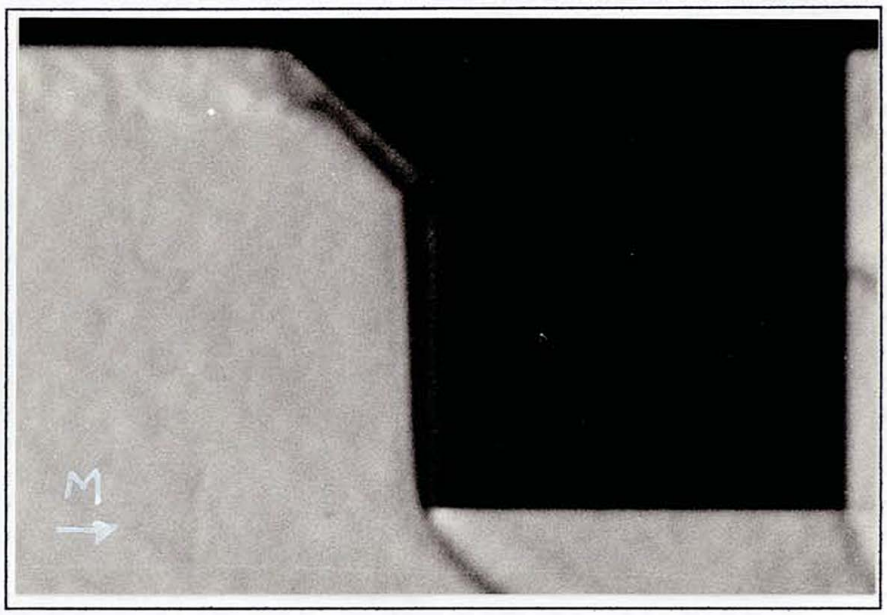
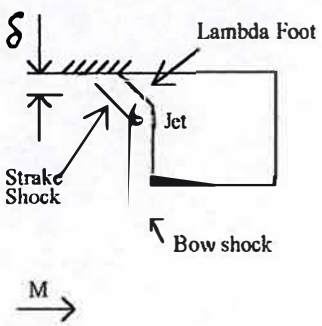


Fig. 55. Schlieren pictures for the blunt 45° swept strakes of $h/\delta = 1.6$.
(i) the Independent strake.





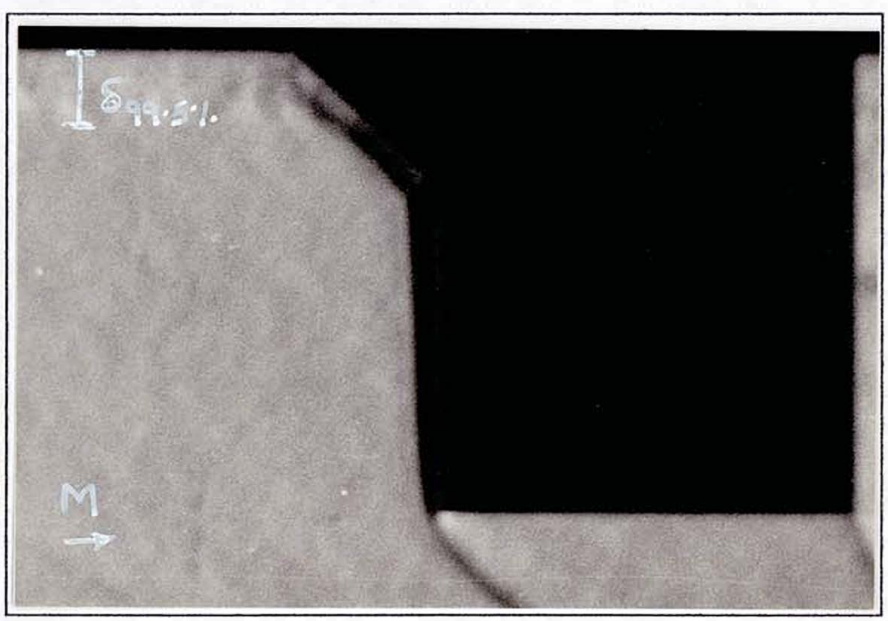
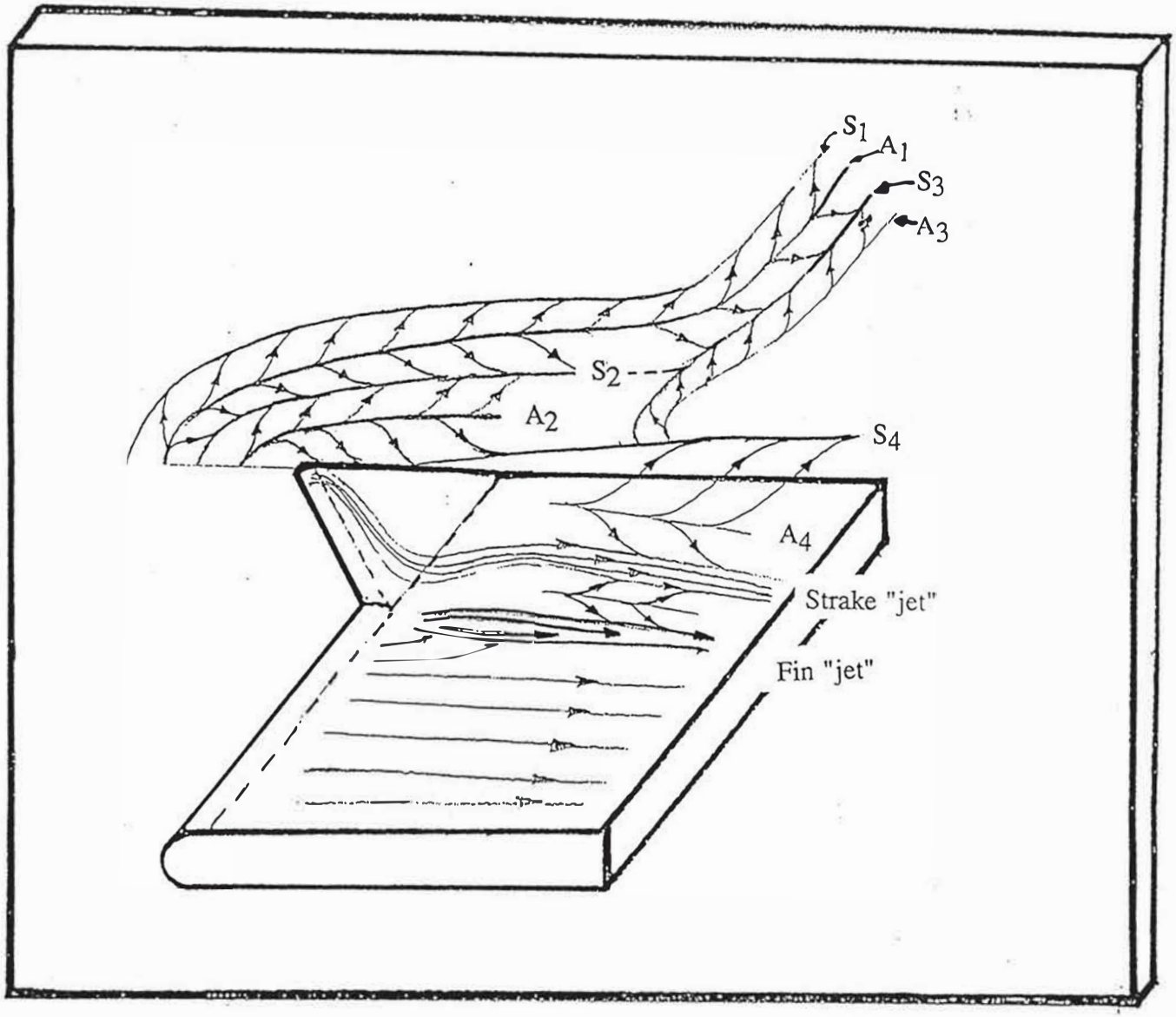


Fig. 55. Schlieren pictures for the blunt 45° swept strakes of $h/\delta = 1.6$.
(ii) with the outer portion of the wing.



(a) Streak line pattern.

Fig. 56. Flow field model for the blunt unswept fin of $D/\delta=0.682$ with a blunt 45° swept strake of $h/\delta=1.6$.

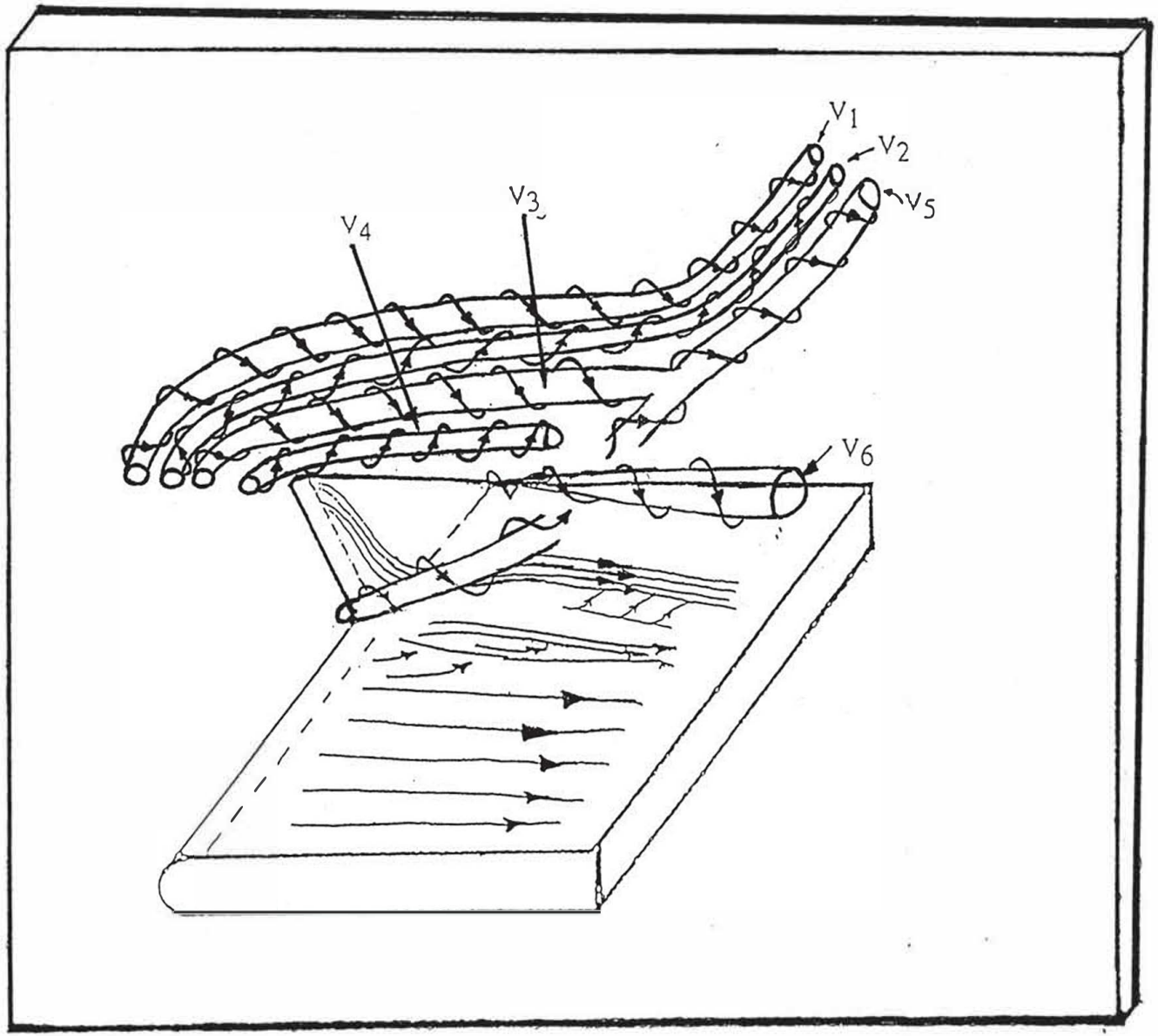
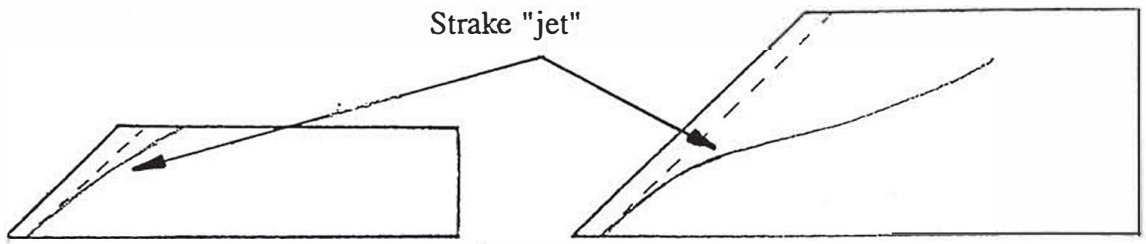
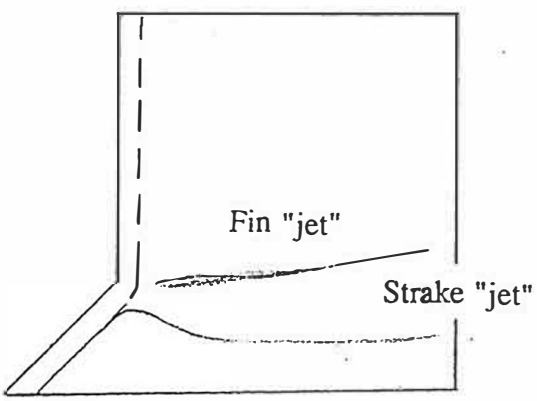


Fig. 56 (b). Vortex skeleton representation.

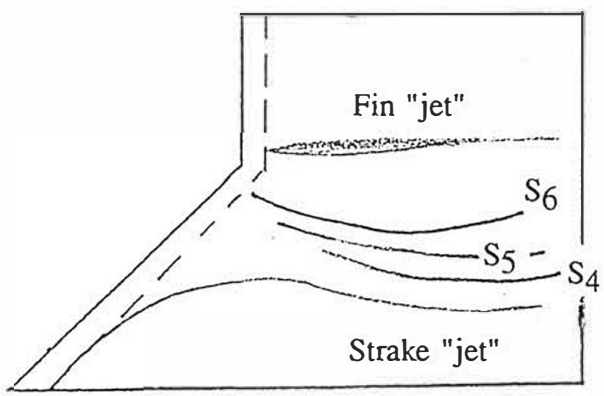


(a) The Independent Strake of $h/\delta = 1.6$.

(c) The Independent Strake of $h/\delta = 3.2$.



(b) Strake of $h/\delta = 1.6$ + the Outer Wing.



(d) Strake of $h/\delta = 3.2$ + the Outer Wing.

Fig. 57. The variation in "jet" path with increasing h/δ

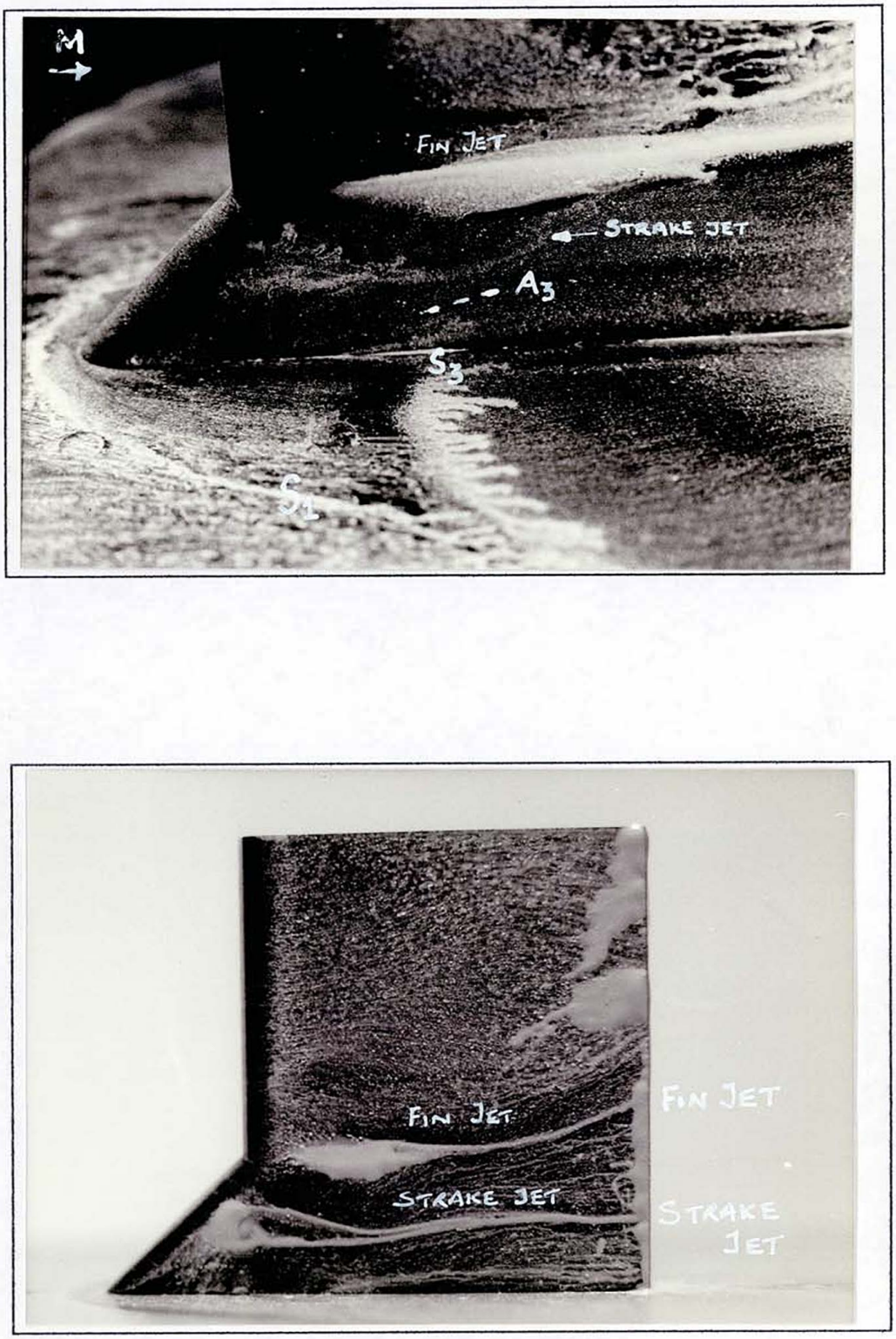


Fig. 58. A comparison of the location of the "jet" paths.
(a). Side view oil flow photographs for Cases 7 & 9.
(i) the Case 7 fin ($D/\delta = 0.6$) tested in the 9" x 9" wind tunnel (top) and,
(ii) the Case 9 fin ($D/\delta = 0.682$) tested in the 2.5" x 2.5" wind tunnel (bottom).